

3D CRUSTAL STRUCTURE MODELLING OF GARHWAL HIMALAYAS

A THESIS

*Submitted in partial fulfilment of the
requirements for the award of the degree
of
DOCTOR OF PHILOSOPHY
in
EARTHQUAKE ENGINEERING*

by

SHIPRA MALIK



G 14813
12/3/2010
[Signature]
211110

DEPARTMENT OF EARTHQUAKE ENGINEERING
INDIAN INSTITUTE OF TECHNOLOGY ROORKEE
ROORKEE - 247 667 (INDIA)

FEBRUARY, 2009

**©INDIAN INSTITUTE OF TECHNOLOGY ROORKEE, ROORKEE, 2009
ALL RIGHTS RESERVED**



INDIAN INSTITUTE OF TECHNOLOGY ROORKEE ROORKEE

CANDIDATE'S DECLARATION

I hereby certify that the work which is being presented in the thesis entitled, **3D CRUSTAL STRUCTURE MODELLING OF GARHWAL HIMALAYAS** in the partial fulfilment of the requirements for the award of the Degree of Doctor of Philosophy and submitted in the Department of Earthquake Engineering of the Indian Institute of Technology Roorkee, Roorkee, is an authentic record of my own work carried out during a period from January 2005 to February 2009 under the supervision of Prof. M. L. Sharma, Professor, Department of Earthquake Engineering, Indian Institute of Technology Roorkee, Roorkee.

The matter presented in this thesis has not been submitted by me for the award of any degree of this or any other Institute.

Shipra Malik

(SHIPRA MALIK)

This is to certify that the above statement made by the candidate is correct to the best of my knowledge.

(M. L. Sharma)
Signature of Supervisor

Date: 07 February, 2009

Signature of Chairman,
SRC/DRC

The Ph.D. Viva-Voice Examination of **Ms. Shipra Malik**, Research Scholar, has been held on

Signature of Supervisor

Signature of External Examiner

ABSTRACT

Determination of seismic velocity structure of crust and upper mantle of the earth is one of the major objectives of seismology. Accurate velocity information is necessary for a variety of purposes, including the location of earthquakes, the determination of the composition and origin of the outer layers of the earth, and the interpretation of large-scale tectonics. While lot of advancement has taken place in instrumentation and digital data acquisition has the capabilities to mark the arrivals with requisite accuracies, the velocity modeling has been lacking in the past for accurate estimation of locations and to make use of relatively more accurate phase arrival data. Taking advantage of the high rate of occurrence of microearthquakes, an attempt has been made in the present study to estimate the crustal velocity structure in Garhwal Himalaya. The main objective of the present study has been to revisit the current velocity structures available for the Garhwal Himalaya and propose a crustal velocity structure based on the earthquake data acquired from this region.

Local Earthquake Tomography (LET) technique has been used in the present study which uses simultaneous inversion for hypocenter and seismic velocity parameters to minimize the data misfit. The earth structure has been represented in 3-D by velocity at discrete points, and velocity at any intervening point is determined by linear interpolation among the surrounding eight grid points. The data acquired through a local seismological network in the Garhwal Himalaya deployed by Department of Earthquake Engineering, IIT Roorkee has been used in the present study. 1-D analyses has been carried out to estimate minimal 1-D models using *VELEST* by considering three of the 1-D velocity models from past studies carried out by

various workers for Himalayas. Based on the output of the 1-D analysis an average 1-D crustal velocity model has been proposed for Garhwal Himalaya.

The three 1-D crustal velocity models thus estimated using 1-D analyses and the proposed 1-D crustal velocity model are then used separately as minimum 1-D velocity models for estimation of 3-D crustal velocity structure for Garhwal Himalaya. The 3-D crustal velocity structure has been estimated using linearized inversion using LET. The grid point locations with respect to the center of the coordinate system have been chosen iteratively based on the earthquake locations and tectonic features in the area. The resolution matrix, derivative weighted sum (proportional to number of rays that sample each cell) and hit counts (number of rays that traverse a specific cell) shows that the profiles falling in the center of the grid and in the upper layers are well resolved. Further, the whole grid was rotated by 45° to get the grids perpendicular to the predominant direction of the seismogenic features in the Garhwal Himalaya. The comparison of resolution matrix, derivative weighted sum and hit counts shows better results in later case.

An endeavor has been made to validate the results by comparing the velocity distribution patterns observed in the estimated 3-D crustal velocity structures with the surface manifestations of the tectonic features. Velocity profiles along the grid lines have been used for matching the geological and tectonic features in the Garhwal Himalaya. Further, the traverses reported by Valdiya (1980) elucidating the lithotectonic settings have been also compared with the depth profiles obtained through 3-D crustal velocity structure analyses. The comparison reveals the depth wise behavior of surface manifestations of the geological features namely, Basul Thrust, Srinagar Thrust, Dunda Thrust, Main Boundary Thrust, Main

Central Thrust and Dunda Fault. Further, out of sequence thrust which is Srinagar thrust is found to be dipping southerly in many of the profiles.

The 3-D velocity structure reveals a variation in velocities at a depth of about 10-20 km in almost all the profiles which can be attributed to the detachment (decollement) surface as reported in earlier studies throughout the Himalayas. The transition zone at detachment surface is found to be about 10 km thick with a velocity contrast of about 5.6 km/sec at the top and about 6.0 km/sec at the bottom. The undulating pattern observed in the vertical profiles reveals that detachment surface is not an even surface and possibly participating in the tectonic process. Further, the depth sections of contemporary seismicity have been overlaid on the vertical profiles which reveal that most of the features are seismically active.

Based on the matching of the 3-D crustal velocity structure with the existing geological and tectonic features and relatively higher values of resolving parameters (KHIT, DWS and RESOLUTION) the 3-D Model IV estimated using the average 1-D velocity model (Model IV) has been proposed for Garhwal Himalaya. The 3-D crustal velocity structure estimated in the present study will be useful for accurately locating the earthquakes in the area for better seismotectonic modeling which in turn is useful in seismic hazard assessment and mitigation.

ACKNOWLEDGEMENT

A strong power has always been supporting me during the entire course of this study. I am sure this has been the force of blessings of ALMIGHTY "THE GOD", which never let me trapped in difficulties. I express my gratitude to the Almighty for this divine favor.

In a venture like the present one so many people contribute in so many ways that is quite impossible to list their names, not to mention the extent of their contribution. The taboo of conciseness does not spare the vastness, rather conveys the intensity of one's feelings in acknowledging their ineffable encouragement and indefatigable support offered all through the pursuance of this arduous task.

I have no words to express my gratitude to my supervisor **Prof. M.L. Sharma**, Department of Earthquake Engineering, IIT Roorkee, for his keen interest and liberal guidance, which I received so spontaneously and lavishly throughout the work of my thesis. With his experience, sharp and incisive intellect, maestro ability combined with astute research methodology and deep insight of the subject has unerringly steered the work on smooth and steady course. His unflagging zeal, complete dedication, constructive criticism, besides a hardworking nature and pleasant disposition, has inspired me for the successful completion of this thesis. I humbly acknowledge a life time's gratitude to him.

I am thankful to **Prof. V. N. Singh**, Department of Earth Sciences, IIT Roorkee, for his guidance, constructive comments and ingenious suggestions at every step that had made it possible for me to complete this uphill task.

I am grateful to **Prof. Ashwani Kumar**, Head and **Prof. D. K. Paul** ex Head Department of Earthquake Engineering, IIT Roorkee for extending all the departmental facilities during my study.

The data used in the present study has been acquired under the project “Seismological array around Tehri region” funded by Tehri Hydroelectric Development Corporation Ltd (THDC). Thanks are due to the Principal Investigator Prof. Ashwani Kumar and THDC for providing me the earthquake data required without which this task is impossible. The use of the programs namely **VELEST** and **SIMULPS** is greatly acknowledged.

I wish to express my deep regards and gratitude to Dr. S. C. Gupta, Dr. J. Das, Dr. A.K. Jindal, and Mr. S.K. Jain Department of Earthquake Engineering, IIT Roorkee for their immense help, esteemed guidance, constant encouragement and inspiration throughout my thesis work.

I would like to specially thank the non teaching staff Shri Rajendra Sudan, Shri Narendra Sharma, Shri R. K. Giri, Shri Manjeet Singh Shri. Laxman Singh and other staff members who had helped a lot during my entire tenure at the department.

I take this opportunity to express my gratitude and indebtedness to fellow researchers and friends, Dr. Shilpa Pal, Dr. Naveen Pareek, Dr. Anju Bhalla, Mr. Girish Chandra Joshi, Mr. Atanu Bhattacharya, Dr. Roopesh Kumar, Dr. Anupam Tyagi, Dr. Javed A. Naqash, Mr. Arup Sen, Mr. Arjun Kumar and Mr. Ratnesh Kumar for their sincere support and help during the process of this research work.

Expressions of encomium are due to my guide’s family for providing homely ambience and ardent moral support.

No words are adequate to express my indebtedness towards my beloved mummy and papa whose blessings have always shadowed me. These pages wouldn’t be sufficient to mention their enormous support, encouragement and especially invaluable untiring patience displayed. I owe my whole life to them.

I am in dearth of proper words to express my abounding feeling for my brother Mohit for his unflinching support and love to achieve this hallmark

I deeply appreciate the cooperation and deep involvement of my mother-in-law **Mrs. Shakuntla Sheoran**. Her love and affection nothing short of a miracle, served as a dynamic impetus in spurring me on to greater self-assurance. Her love always inspired me to work more than I would have otherwise. Her continuous endeavor, strive, prudence and blessings made the lucrative triumph in my academic pursuit and blooming future.

Countless images flash through my mind when I remember the hard phases of time I had been through and here my husband **Dr Kulwant Singh** deserves a special mention who made the most conspicuous contribution in making this ambition of mine, a reality. His unending love, patience, understanding and constant personal support has shown this work the light of the day. His sense of humour has always helped me to overcome the difficult phases. This thesis belongs to him as much as it does to me.

I also wish to put forth my abounding feelings for all my family members for their unending affection.

Finally, I wish to thank all those whose names have not figured above but have helped me directly or indirectly during the course of my research work. Really this thesis would not have been written without any of you.

Shipra Malik
(Shipra Malik)

CONTENTS

	Page No.
Certificate	(i)
Abstract	(iii)
Acknowledgement	(vii)
Contents	(xi)
List of Figures	(xv)
List of Tables	(xix)
Chapter 1 INTRODUCTION	1-5
1.1 Preamble	1
1.2 Crustal velocity structure	2
1.3 Objectives of the study	4
1.4 Scope of the Thesis	4
1.5 Plan of the thesis	5
Chapter 2 LITERATURE REVIEW	7-34
2.1 Introduction	7
2.2 Crustal velocity structure for Garhwal Himalaya- A review	8
2.3 Determination of Crustal velocity structure	12
2.3.1 1-D crustal velocity structure	12
2.3.2 3-D crustal velocity structure	15
2.3.3 Local earthquake tomography	16
2.3.3.1 <i>Representation of structure</i>	19
2.3.3.2 <i>Ray-path and travel time calculation</i>	22
2.3.3.3 <i>Hypocenter-velocity structure coupling</i>	24
2.3.3.4 <i>Inversion methods</i>	27
2.3.3.5 <i>Solution quality</i>	31
2.4 Summary	33

Chapter 3	GEOLOGY AND TECTONIC SETUP OF THE GARHWAL HIMALAYA	35-52
3.1	Introduction	35
3.2	Garhwal Himalaya - Study area	36
3.3	Geology and tectonic setup of the Garhwal Himalaya	38
3.4	Traverses in Garhwal Himalaya	47
3.5	Seismicity of the Garhwal Himalaya	50
3.6	Summary	52
Chapter 4	ESTIMATION OF CRUSTAL VELOCITY STRUCTURE - METHODOLOGY	53-63
4.1	Introduction	53
4.2	Simultaneous Inversion	54
4.3	3-D velocity inversion	59
4.4	Summary	62
Chapter 5	3-D CRUSTAL VELOCITY STRUCTURE FOR GARHWAL HIMALAYA	65-88
5.1	Introduction	65
5.2	Data set	66
5.3	Estimation of 1-D crustal velocity structure	68
5.3.1	1-D crustal velocity structure analysis	69
5.3.2	Average 1-D crustal velocity structure for Garhwal Himalaya	73
5.4	Estimation of 3-D crustal velocity structure	74
5.4.1	Parameters for 3-D crustal velocity structure estimation	75
5.4.2	3-D crustal velocity structure analysis for east-west gridding	76
5.4.3	3-D crustal velocity structure analysis for NE-SW gridding	82
5.5	Summary	88

Chapter 6	RESULTS AND DISCUSSIONS	89-116
6.1	Introduction	89
6.2	3-D crustal velocity structure for Garhwal Himalaya	90
6.2.1	East West gridding	92
6.2.2	NE-SW gridding	97
6.3	Matching of features with traverses	102
6.4	Seismicity plots on vertical profile	112
6.5	Summary	114
Chapter 7	CONCLUSIONS	117-120
7.1	General	117
7.2	Summary	117
7.3	Conclusions	118
7.4	Scope for the future work	120
	<i>Bibliography</i>	121-136
	<i>Appendix I</i>	137-154
	<i>Appendix II</i>	155-161
	<i>Appendix III</i>	163-220
	<i>Appendix IV</i>	221-246

LIST OF FIGURES

Figure No.	Details of Figure	Page No.
2.1	P wave velocity structure for Himalaya region	11
2.2	Overview of procedure VELEST	14
2.3	Schematic representation of the local earthquake tomography (LET)	17
2.4	Schematic indication of three approaches to discrete velocity model representation (a) constant-velocity blocks; (b) laterally varying layers; (c) a grid of nodes	20
3.1	Seismotectonic domains of NW Himalayan seismic belt (after Narula <i>et al.</i> , 2000)	37
3.2	Map showing tectonic features of the Garhwal Himalaya (after Fuchs and Sinha, 1978)	38
3.3	Geological map of Lesser Himalaya (Valdiya, 1980)	40
5.1	Location of stations and events on the tectonic map of study area	67
5.2	(a) Input Model I after Tandon and Dubey (1973) (b) 1-D modeling results for Model I	70
5.3	(a) Input Model II after Kumar <i>et al.</i> , (1994) (b) 1-D modeling results for Model II	71
5.4	(a) Input Model III after Mukhopadhyay and Kayal (2003) (b) 1-D modeling results for Model III	72
5.5	(a) 1-D velocity input models for analysis (b) Results of 1-D analysis on the three initial models	73

5.6	3-D view of the velocity model	74
5.7	Grid location with respect to the tectonic features in Garhwal Himalaya in East West direction	75
5.8	Depth Slices of 3-D Model I for east-west gridding	78
5.9	Depth Slices of 3-D Model II for east-west gridding	79
5.10	Depth Slices of 3-D Model III for east-west gridding	80
5.11	Depth Slices of 3-D Model IV for east-west gridding	81
5.12	Rotated gridding for the 3-D velocity structure analysis	82
5.13	Depth Slices of 3-D Model I for NE-SW gridding	84
5.14	Depth Slices of 3-D Model II for NE-SW gridding	85
5.15	Depth Slices of 3-D Model III for NE-SW gridding	86
5.16	Depth Slices of 3-D Model IV for NE-SW gridding	87
6.1	An example of interpretation of tectonic features on vertical profiles.	91
6.2	Tectonic features marked on vertical profiles obtained using 3-D Model I for east-west gridding.	93
6.3	Tectonic features marked on vertical profiles obtained using 3-D Model II for east-west gridding.	94
6.4	Tectonic features marked on vertical profiles obtained using 3-D Model III for east-west gridding.	95
6.5	Tectonic features marked on vertical profiles obtained using 3-D Model IV for east-west gridding.	96
6.6	Tectonic features marked on vertical profiles obtained using 3-D Model I for NE-SW gridding.	98

6.7	Tectonic features marked on vertical profiles obtained using 3-D Model II for NE-SW gridding.	99
6.8	Tectonic features marked on vertical profiles obtained using 3-D Model III for NE-SW gridding.	100
6.9	Tectonic features marked on vertical profiles obtained using 3-D Model IV for NE-SW gridding.	101
6.10	Location of traverses reported by Valdiya (1980) in Garhwal Himalayas along with the NE-SW gridding	103
6.11	Matching of traverse pp with profile 5 of 3-D Model I	104
6.12	Matching of traverse pp with profile 5 of 3-D Model II	105
6.13	Matching of traverse pp with profile 5 of 3-D Model IV	105
6.14	Matching of traverse qq with profile 6 of 3-D Model I	106
6.15	Matching of traverse qq with profile 6 of 3-D Model II	107
6.16	Matching of traverse qq with profile 6 of 3-D Model III	107
6.17	Matching of traverse qq with profile 6 of 3-D Model IV	108
6.18	Matching of traverse KK with profile 6 of 3-D Model I	109
6.19	Matching of traverse KK with profile 6 of 3-D Model II	109
6.20	Matching of traverse KK with profile 6 of 3-D Model III	110
6.21	Matching of traverse KK with profile 6 of 3-D Model IV	110
6.22	Matching of traverse ss with profile 6 of 3-D Model I	111
6.23	Seismicity laid over the vertical profiles. The tectonic features are also marked on the profiles.	113

LIST OF TABLES

Table No.	Detail of Table	Page No.
3.1	Details of Traverses reported by Valdiya (1980)	49
3.2	The historical record of the largest earthquakes in the previous century in the Himalaya region	51
5.1	Station locations of the seismological network	67
5.2	Model I used in 1-D analysis	70
5.3	Model II used in 1-D analysis	71
5.4	Model III used in 1-D analysis	72
5.5	Maximum values of the parameters KHIT, DWS and RESOLUTION for the east west gridding	77
5.6	Maximum values of the parameters KHIT, DWS and RESOLUTION for the NE-SW gridding	83
6.1	Representation of tectonic features on vertical profiles.	92

INTRODUCTION

1.1 Preamble

The ongoing continental convergence and collision between Indian and Eurasian plates since ~45-50 Ma has given rise to Himalayas stretching east-west over a length of ~2500 km. The developmental activities and urbanization in highly seismic regions like Himalayas make earthquake risk reduction a pressing societal imperative. Vulnerability of our civilization to such natural disasters is rapidly increasing. Today a single damaging earthquake with subsequent ripple effects may take up to a million of lives, cause material damage, render large region uninhabitable and can trigger a localized or regional economic depression. The precarious condition arising due to earthquakes could be avoided only by making in-depth studies to understand the physical process and use it in mitigating the disastrous effects. The seismicity, spatial as well as temporal, becomes an important input in the endeavors to assess seismic hazard and in turn, the seismic risk.

The knowledge of crustal velocity structure is of paramount importance for accurately locating the earthquakes and help in getting more precise and constrained seismicity picture of the region. While lot of advancement has taken place in instrumentation and digital data acquisition has the capabilities to mark the arrivals with requisite accuracies, crustal velocity modeling has been lacking in the past for accurate estimation of locations and to make use of relatively more accurate phase arrival data. Determination of seismic velocity structure of crust and upper mantle of the earth is one of the major objectives of seismology. Accurate velocity information is necessary for a variety of purposes,

including the location of earthquakes, the determination of the composition and origin of the outer layers of the earth, and the interpretation of large-scale tectonics. The accuracy in location of an earthquake mainly depends on the velocity structure used to compute the location. Taking advantage of the high rate of occurrence of microearthquakes in this region, a two pronged approach has been applied for estimation of velocity structure and accurate locations of earthquakes on one hand and validating and interpreting the outcome to get more precise picture in terms of the prevailing geological and tectonic setup of the area on the other hand.

1.2 Crustal Velocity Structure

The crustal velocity structure consists of the information about the layering structure of the underneath media along with the velocities of primary and secondary waves of each layer. The velocity structures range from a simple one dimensional (1-D) model of a layer over a half space to three dimensional (3-D) velocity models describing the velocities and geometry of the blocks with dipping layers. While Crosson (1976a and b) provided the basis for 1-D velocity inversions at the same time Aki and Lee (1976) published a 3-D inversion technique which was later called as *Seismic Tomography*. The first applications of tomography were made in the medical field and then in seismology. Clayton (1984) defined *Tomography* as the reconstruction of a field from the knowledge of linear path integrals through the field. In seismology, the analysis of lateral velocity variations fits this definition, if the travel time equation is perturbed about the reference velocity model. The field in this case is slowness perturbations and the observations are travel time deviations. Seismic tomography has produced many notable 3-D images of the earth interior including a global velocity distribution correlated with the geoid which can be explained by mantle dynamics, detailed configuration of subducting plates, which can be

related to tectonics, the volume and geometry of magma sources under volcanoes and geothermal areas, detailed structures of earthquake fault zones, and deep weak zones which have become easy pass for magma ascent (Iyer and Hirahara, 1993). One of the important applications of tomography is in the use of local seismological networks data to estimate the local 3-D crustal velocity structures and is generally known as *Local Earthquake Tomography* (LET). It is this technique which is being used to estimate the 3-D velocity inversions in the present thesis.

The study area selected for the present study is Garhwal Himalaya which is structurally very complex and characterized by various thrusts, faults and folds. The area has high seismicity concentrated mainly around the regional features like Main Boundary Thrust and Main Central Thrust along with other local seismogenic features present in the region. The developmental activities and urbanization in Garhwal Himalaya make it imperative to develop 3-D crustal velocity model for accurately locating the earthquakes and help in getting more precise and constrained seismicity picture of the region. Several 1-D and 3-D velocity models have been proposed by various studies covering various segments of the Himalaya (Chauhan and Singh, 1965; Kaila *et al.*, 1968; Tandon and Dubey, 1973; Verma, 1974; Chander *et al.*, 1986; Kumar *et al.*, 1987; Kumar *et al.*, 1994; Sarkar *et al.*, 2001; Kumar and Sato, 2003; Mukhopadhyay and Kayal, 2003).

The previous methods were based on surface wave dispersion and crustal phases and ignore the lateral heterogeneities which are always present in such a complex geological and tectonic setup of lesser Himalayas. Therefore, estimations using seismic tomography which may give more realistic picture of the region including lateral heterogeneities are required to be done for this region.

1.3 Objectives of the study

The main objective of the present study is to revisit the current crustal velocity structures available for the Garhwal Himalaya and propose 3-D crustal velocity structure based on the earthquake data acquired from this region. The objectives of the study are as follows:

1. Critical review of the available crustal velocity models and the prevailing tectonics in the Garhwal Himalaya,
2. Estimation of 1-D crustal velocity structure for the Garhwal Himalaya,
3. Estimation of 3-D crustal velocity structure for the Garhwal Himalaya,
4. Validation of the results and interpretation in terms of prevailing tectonics in the region.

1.4 Scope of the thesis

An attempt has been made in the present thesis to estimate the 3-D crustal velocity structure in Garhwal Himalaya. The data for the study has been obtained from the digital telemetered array deployed by Department of Earthquake Engineering, IIT Roorkee, in and around Tehri region of the northwestern Himalaya. The data contains mainly the arrival times of the seismic phases for the earthquake events recorded by the array in and around the Tehri region. The 3-D inversions have been carried out for estimation of 3-D crustal velocity structure using *Local Earthquake Tomography*. The technique comprising of finding the minimal 1-D model and then using it for simultaneous relocation of hypocenters and determination of local velocity structure using linearised inversion has been used in the present study. The results are presented in form of depth slices (horizontal) and vertical profiles in the Garhwal Himalaya. The results have been validated by the known geological and tectonic features in the region by comparing them with the velocity distributions in the vertical profiles obtained through 3-D inversions.

1.5 Plan of the Thesis

The thesis comprises seven chapters. In *Chapter 2*, brief review of the proposed crustal velocity structures by various workers in past for Himalayas is presented. The methods to estimate 1-D and 3-D crustal velocity structures have been also presented in this chapter. Specially, the methodology used in *Local Earthquake Tomography* (a type of seismic tomography) has been discussed and reviewed.

Chapter 3 describes the geological and tectonic setup of the study area. The cross sections of the traverse lines reported by Valdiya (1980) and falling in study area have been described in the chapter and are given in *Appendix I*.

Chapter 4 presents the simultaneous inversion method and *Local Earthquake Tomography* method used for estimation of 3-D crustal velocity structure in the present study.

The results of 1-D analysis and the proposed 1-D average crustal velocity structure of Garhwal Himalaya are presented in *Chapter 5*. It also contains the 3-D analyses results as depth slices for the four different models considered for 3-D inversions. The parameters KHIT, DWS and RESOLUTION used to quantify the confidence level in the final results are given in *Appendix III*. The vertical profiles for the Himalaya region are presented in *Appendix IV*.

Chapter 6 presents the validation of results in terms of comparison of velocity profiles obtained from the 3-D analysis with the existing geological and tectonic features. Further, the matching of the vertical profiles with the traverse lines reported by Valdiya (1980) has been carried out and presented in this chapter.

Finally the summary of the work and conclusions drawn along with the recommendations for further research work are highlighted in *Chapter 7* of the thesis.

LITERATURE REVIEW

2.1 Introduction

Himalaya was formed by collision of Indian and Eurasian continents wherein the buoyant crust of the Indian plate was detached from the underlying mantle and its subsequent deformation raised mountain chains. The collision also caused large-scale deformations and high seismicity of vast areas of both continents. To explain the cause of occurrence of earthquakes and to understand the seismotectonics of the Himalayan collision zone, various models have been proposed for the evolution of the Himalaya (Ni & Barazangi, 1984; Seeber *et al.*, 1981). These models based on the past seismicity patterns play an important role in the endeavors to assess seismic hazard. The seismicity patterns are recognized based on the earthquake locations estimated in terms of latitude, longitude, depth and origin times which are, in turn, the results of inversion methods by assuming a velocity model of the medium underneath. Therefore, knowledge of crustal velocity structure is of paramount importance for accurately locating the earthquakes and help in getting more precise and constrained seismicity picture of the region.

The velocity structure consists of the information about the layering structure of the underneath media along with the velocities of primary and secondary waves of each layer. Accurate velocity information is necessary for a variety of purposes, including the location of earthquakes, the determination of the composition and origin of the outer layers of the earth,

and the interpretation of large-scale tectonics. The present chapter reviews the proposed crustal velocity structure for Garhwal Himalaya in the past and the applicable methodologies to estimate the same.

2.2 Crustal velocity structure for Garhwal Himalaya- A review

Several crustal velocity models have been proposed by various studies covering various segments of the Himalaya based on surface wave dispersion and crustal phases (Chauhan & Singh, 1965; Kaila *et al.*, 1968; Tandon and Dubey, 1973; Verma, 1974; Chander *et al.*, 1986; Kumar *et al.*, 1987; Kumar *et al.*, 1994; Sarkar *et al.*, 2001; Kumar and Sato, 2003; Mukhopadhyay and Kayal, 2003).

Chauhan and Singh (1965) estimated that the depth of Mohorovicic discontinuity varies from 50 km to 60 km in the Himalayas. They give the average velocity of granitic layer in Himalayas to be 5.5 km/sec and for the basaltic layer to be 6.6 km/sec. The velocity at Moho was proposed to be as 7.8 km/sec

Kaila *et al.*, (1968) worked out the crustal structure in the Himalayan foothills area. The data used by them was travel times of different P-wave phases. The effect of the sedimentary layers was also taken into account. The crustal structure in the Himalayan foothills area of northern India consisting of sedimentary layer of thickness 6 ± 1 km with velocity as 2.7 km/sec, then the Granitic layer 8 ± 5 km thick with velocity 6.2 ± 0.1 km/sec and basaltic layer 14 ± 7 km thick with velocity 6.9 ± 0.1 km/sec giving a total crustal thickness of 28 ± 8 km was proposed by Kaila *et al.*, (1968) (Fig 2.1). The upper mantle velocity in this area was proposed as 8.2 ± 0.1 km/sec.

The body wave data was used by Tandon & Dubey (1973) from the earthquakes having epicenters over the Himalayas and recorded by the observatories situated over or very near the foothills of the mountains. A three-layer crustal model (Fig. 2.1), without the top sedimentary layer, with velocities for the P-wave group velocity in Granite I, Granite II, and the Basaltic layer as 5.48 km/sec, 6.00 km/sec, and 6.45 km/sec and for the S-wave group as 3.33 km/sec, 3.56 km/sec, and 3.90 km/sec respectively was proposed. The upper mantle velocity for the P-wave was observed to be 8.07 km/sec, and for the S-wave as 4.57 km/sec. Average thickness for the Granite I layer was computed as 22.7 km, for the Granite II layer as 16.3 km and for the Basaltic layer as 18.7 km. Crustal and subcrustal velocities indicated a lower trend under the mountain. A relatively thicker crust (nearly 58 km) was obtained beneath the Himalayas by Tandon & Dubey (1973).

Verma (1974) used the time-distance curves plotted from the first onsets of the longitudinal and transverse waves from the earthquakes originating from the foothills of Himalayas, to reveal a bi-layered crust in this region (Fig. 2.1). The total crustal thickness was investigated as 30.1 km with 13.4 km thick Granitic layer and 16.7 km thick basaltic layer. Longitudinal and transverse wave velocities in the topmost Granitic layer were found to be 5.92 ± 0.03 km/sec and 3.54 ± 0.01 km/sec, respectively, and those in the basaltic layer as 6.80 ± 0.03 km/sec and 3.92 ± 0.01 km/sec, respectively. These velocities, immediately below the crust, were reported to be 8.00 ± 0.03 km/sec and 4.54 ± 0.02 km/sec, respectively. No existence of any low velocity layer in the crust was reported.

Chander *et al.*, (1986) used the arrival times of compressional waves recorded at the stations deployed in the Garhwal region. A value of 5.2 km/sec was obtained for compressional wave velocity in the upper crust in the vicinity of the Main Central Thrust.

Kumar *et al.*, (1987) estimated the P-wave velocity as 6.0 km/sec in the second crustal layer in the Garhwal Himalaya.

Kumar *et al.*, (1994) considered the first layer upto the depth of 15 km (top of lithosphere) based on Chander *et al.*, (1986) and the second layer upto depth of 46 km based on Kumar *et al.*, (1987). The velocity below 46 km based on Tandon (1954) was used by Kumar *et al.*, (1994). In view of scientific considerations and lack knowledge of velocity structure for the Garhwal Himalaya Kumar *et al.*, (1994) considered the hybrid crustal velocity structure as described above for the use of locating the earthquakes from the data obtained through the digital telemetered array deployed in Garhwal Himalaya by Department of Earthquake Engineering, IIT Roorkee.

Kumar and Sato, (2003) obtained compressional wave velocities beneath the Garhwal Himalaya as 4.72 km/sec and 5.89 km/sec; and shear wave velocities as 2.90 km/sec and 3.39 km/sec for the upper crustal and the lower crustal layers, respectively. These estimations were made in the vicinity of Main Central Thrust. The 1-D crustal velocity structures as proposed by various workers in past have been summarized in Fig. 2.1.

Sarkar *et al.*, (2001) carried out the inversion of the body wave arrival time data to estimate seismic velocity model for the Garhwal Himalaya region. Main findings of the study included significantly lower seismic velocities within the Middle-Lesser Garhwal Himalaya, and higher seismic velocities in the interface zone between the Middle-Lesser and Higher Garhwal Himalaya. Seismic activity was observed to be mostly confined to a relatively narrow north-east dipping zone in the upper 4 km of the crust characterized by a relatively higher P-wave velocity. This active seismicity represented reverse thrusting along steep

north-easterly dipping parallel slip surfaces within this zone forming a ramp in the crystalline formations of Higher Himalaya.

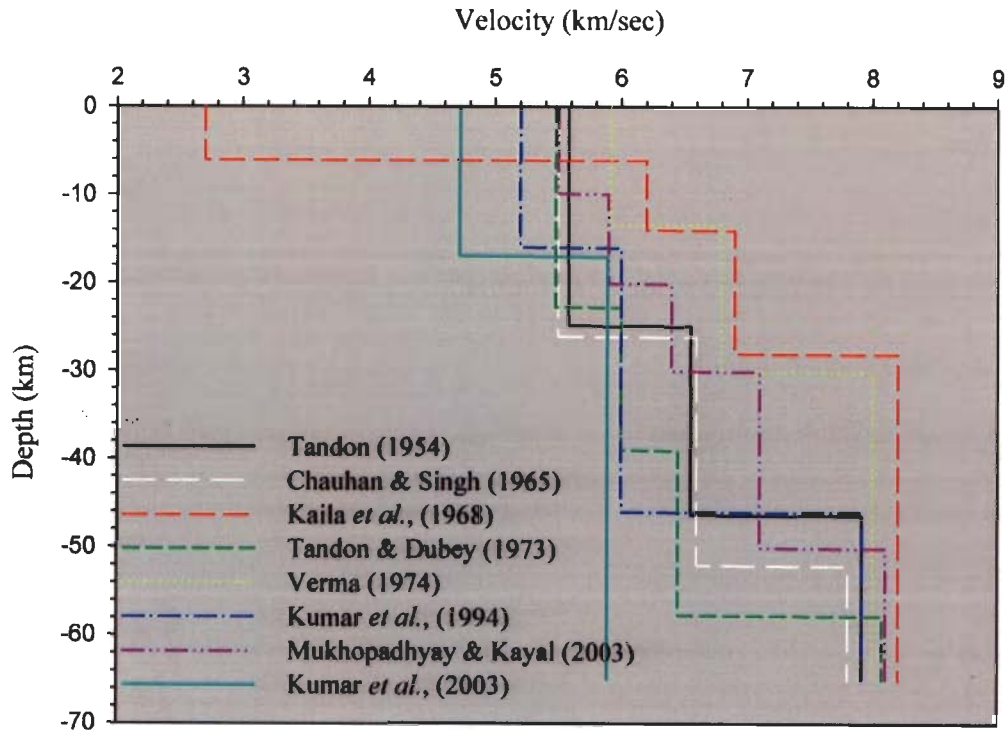


Fig. 2.1 P wave velocity structure for Himalaya region

Mukhopadhyay and Kayal (2003) carried out 3-D inversions using P- and S- arrival data of the Chamoli earthquake (29th March 1999) aftershocks. The 1-D velocity model considered by Mukhopadhyay and Kayal (2003) for 3-D inversions is shown in Fig. 2.1. The majority of well-located aftershocks occurred to the southwest of the mainshock epicenter and lie above the plane of detachment. A prominent, near-vertical, east–west–trending Low Velocity Zone (LVZ) was observed from the surface to a depth of 15 km, and was compared with the surface trace of the Alakananda fault. The LVZ was estimated to be quite broad and

heterogeneous at shallower depth (0–10); narrowed at deeper depth (12–15 km) and is well defined in the 15-km depth slice. Rajendran *et al.*, (2000) reported that an anticlinal structure close to the Chamoli area is delimited on two sides by almost vertical faults, the east–west trending major Alakananda fault in the south and a north-northwest–southsoutheast trending fault in the east.

2.3 Determination of Crustal velocity structure

2.3.1 1-D crustal velocity structure

The data collected through deployment of seismological arrays provide two types of data viz, for local earthquakes and for teleseismic events. While the local earthquake data can be used for the determination of hypocenter locations as well as the velocity structure, the teleseismic data is generally used for the velocity structure. Crosson (1976) developed a nonlinear least square modeling procedure to estimate simultaneously the hypocenter parameters and parameters for a layered velocity model by using arrival times from local earthquakes.

One of the Programs namely *VELEST* was designed to derive 1-D velocity models for earthquake location procedures which can be used as initial reference models for seismic tomography (Kissling 1988; Kissling *et al.*, 1994). Originally written in 1976 by W.L. Ellsworth and S. Roecker for seismic tomography studies (under program name *HYPO2D*, see Ellsworth 1977; Roecker, 1978) *VELEST* has been modified by R. Nowack (who also gave it its current name), C. Thurber, and R. Comer who implemented (among other things) the layered-model ray tracer (Thurber 1981). In 1984 E. Kissling and W. L. Ellsworth after modifications of the flow structure and implementation of several new options used it to calculate a 'Minimum 1-D model' (i.e., a well-suited 1-D velocity model for earthquake

location and for 3-D seismic tomography) for Long Valley area, California (Kissling *et al.*, 1984). Since then *VELEST* has been applied to local earthquake and controlled-source data from several areas in California, Alaska, Wyoming, Utah, and the Alps (Kissling 1988; Kradolfer 1989; Kissling and Lahr 1991; Maurer 1993) U. Kradolfer implemented the option to use *VELEST* as single-event-location routine and H. Maurer reintroduced the option to use both P- and S-wave data, separately or combined. The model consists of a (layered) 1-D velocity model and station corrections. The forward problem is solved by ray tracing from source to receiver, computing the direct, refracted, and (optionally) the reflected rays passing through the 1-D model. The inverse problem is solved by full inversion of the damped least squares matrix $[A^T A + L]$ (A = Jacobi matrix, A^T =transposed Jacobi matrix; L =damping matrix). Because the inverse problem is non-linear, the solution is obtained iteratively, where one iteration consists of solving both the complete forward problem and the complete inverse problem once. The overview of the 1-D estimation of velocity structure using *VELEST* program is given in Fig. 2.2.

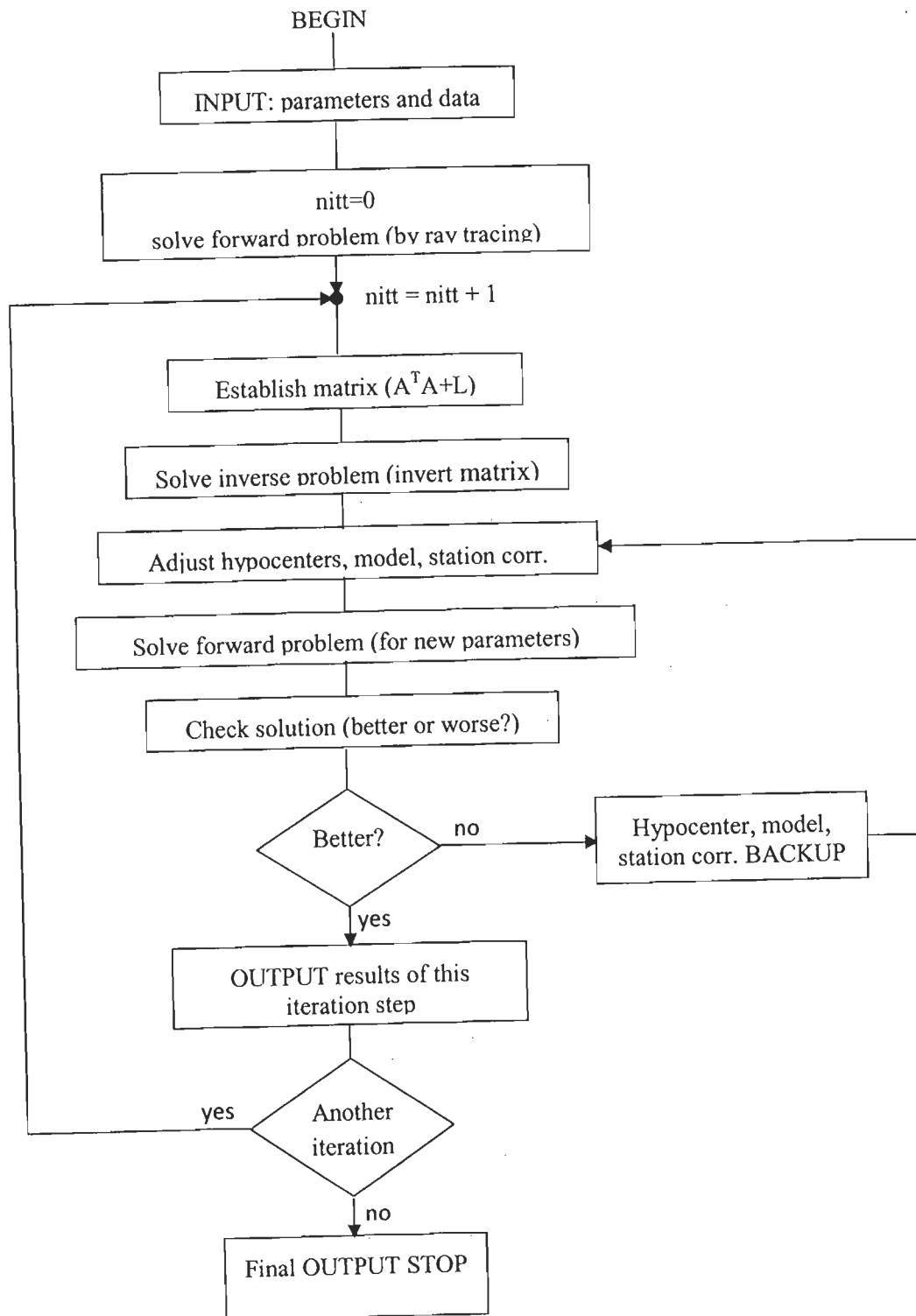


Fig. 2.2 Overview of procedure used in *VELEST*

2.3.2 3-D crustal velocity structure

While Crosson (1976) provided the basis for one dimension at the same time Aki and Lee (1976) published a 3-D inversion technique. Aki *et al.*, (1977) also produced the theory for teleseismic events for 3-D inversion. The first method for 3-D inversion was developed at NORSAR by Aki, Christoffersson and Husebye in 1974 (Iyer and Hirahara, 1993). The first result of 3-D inversion was reported by Aki *et al.*, (1974) for the earth structure beneath the San Andreas Fault using the teleseismic P-wave arrival time data obtained at the Central California Seismic Network. This method and its extension by Aki *et al.*, (1976) and Aki and Lee (1976) were then used in many studies for 3-D inversions. The name tomography was introduced to such methods when iterative matrix solvers were introduced allowing a quantum jumps in the number of model parameters (Clayton and Comer, 1983; Nolet 1985).

Clayton (1984) defined Tomography as the reconstruction of a field from the knowledge of linear path integrals through the field. In seismology, the analysis of lateral velocity variations fits this definition, if the travel time equation is perturbed about the reference velocity model. The field in this case is slowness perturbations and the observations are travel time deviations. *Tomo* is a greek word which means *slice*. The Central Slice Theorem allows construction of 2-D section from multiple one dimension (1-D) line integrals. By combining many of these 2-D slices a 3-D model of the object can be reconstructed (Iyer and Hirahara, 1993). The first applications of tomography was made in medical field and then in seismology. Seismic tomography is essentially an imaging problem that can be solved by several techniques, for example, (i) Inversion by non-linear optimization techniques, (ii)

Iterative back-projection method borrowed from radiological tomography, and (iii) Fourier or transform methods.

Seismic tomography has produced many notable 3-D images of the earth interior including a global velocity distribution correlated with the geoid which can be explained by mantle dynamics, detailed configuration of subducting plates, which can be related to tectonics, the volume and geometry of magma sources under volcanoes and geothermal areas, detailed structures of earthquake fault zones, and deep weak zones which have become easy pass for magma ascent (Iyer and Hirahara, 1993).

2.3.3 Local Earthquake Tomography

The local earthquakes used as sources for seismic arrival time tomography has advantages that they substantially excite both compressional and shear waves with 3-D spatial distribution. Compared with teleseismic tomography, *Local Earthquake Tomography* (LET) usually offer much higher spatial resolution of structure due to increased density of ray sampling, higher wave frequency, and closer station spacing. However, the depth extent of LET models is limited by the maximum earthquake focal depths in the area.

Several books and review papers have examined various aspects of the methodology of LET, and have applied the technique to geologically diverse areas. Some reviews that focus to a large extent on the LET problem include Thurber (1986), Thurber and Aki (1987), Kissling (1988), Asad (1998), Husen and Kissling (2001), Aldersons (2004) and Reidel *et al.* (2005).

Theoretically, the body wave travel time T from an earthquake i to a seismic station j is expressed using ray theory as a path integral

$$T_{ij} = \int_{source}^{receiver} u ds \quad (2.1)$$

where u is the slowness field and ds is an element of path length. The actual observations are the arrival times t_{ij} where

$$t_{ij} = \tau_i + T_{ij} \quad (2.2)$$

and τ_i is the earthquake origin time. The knowns are the receiver locations and the observed arrival times and the unknowns are the source coordinates (x_1, x_2, x_3) , origin times, ray-paths, and slowness field. The problem is shown schematically in Fig 2.3.

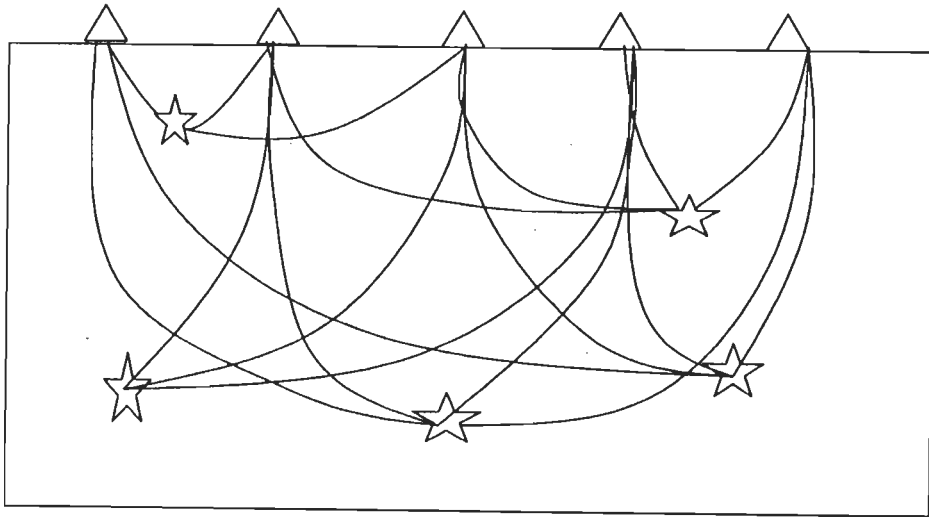


Fig. 2.3 Schematic representation of the local earthquake tomography (LET)

Given a set of arrival times t_{ij}^{obs} measured at a network of stations, the calculated arrival times t_{ij}^{cal} are determined from equations (2.1) and (2.2) using trial hypocenters and origin times and an initial model of the seismic velocity structure. The residuals r_{ij} are given as

$$r_{ij} = t_{ij}^{obs} - t_{ij}^{cal} \quad (2.3)$$

These residuals can be related to the desired perturbations to the hypocenter and velocity structure parameters by a linear approximation.

$$r_{ij} = \sum_{k=1}^3 \frac{\partial T_{ij}}{\partial x_k} \Delta x_k + \Delta \tau_i + \int_{source}^{receiver} \delta u ds \quad (2.4)$$

The hypocenter partial derivatives $\partial T_{ij}/\partial x_k$ at the source point are given as (Thurber, 1986):

$$\frac{\partial T_{ij}}{\partial x_k} = -\frac{1}{v} \left(\frac{dx_k}{ds} \right)_{source} \quad (2.5)$$

For any finite parameterization of the velocity structure, the equation (2.4) can be written as

$$r_{ij} = \sum_{k=1}^3 \frac{\partial T_{ij}}{\partial x_k} \Delta x_k + \Delta \tau_i + \sum_{l=1}^L \frac{\partial T_{ij}}{\partial m_l} \Delta m_l \quad (2.6)$$

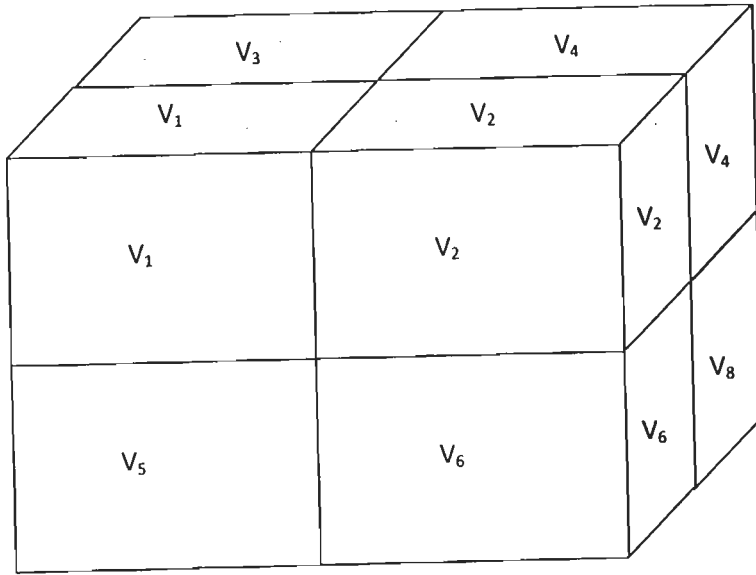
where m_l represents the L parameters of the velocity model. The velocity model partial derivatives $\partial T_{ij}/\partial m_l$ are essentially line integrals along the ray-path reflecting the relative influence of each model parameter on a given travel time datum. The main objective is to improve the estimates of the model parameters (structure and hypocenters) by perturbing them in order to minimize some measure of the misfit to the data. An iterative scheme is required for solution, as the hypocenter-velocity structure coupling inherent in equation (2.6) can lead to significant non-linearity. Various estimates of solution quality are also desired, such as the matrices of resolution and uncertainty (Menke, 1989), as well as improvement in data fit and uniqueness of the final solution.

Generally, LET methods begin with equation (2.4) and then diversify to some extent, based on differing treatments of some or all of the following aspects of the problem. These may include (i) the scheme for the representation of the velocity structure; (ii) the technique for travel time and ray-path calculations; (iii) the treatment of the hypocenter-velocity structure coupling; (iv) the method of inversion; (v) the assessment of solution quality; (vi) the use of S waves. These aspects are discussed in details as follows:

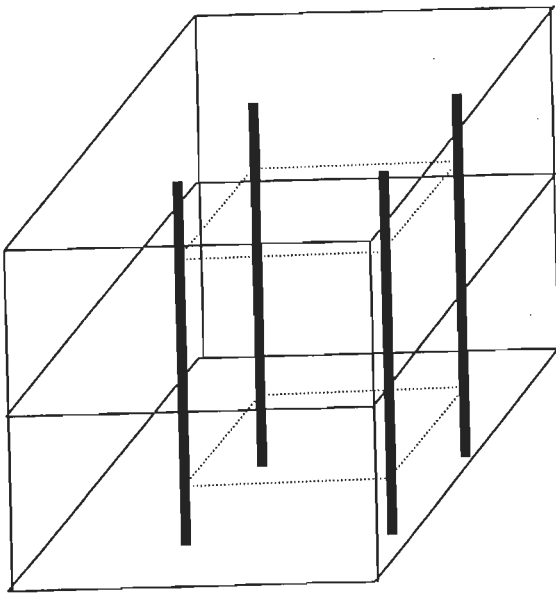
2.3.3.1 *Representation of structure*

The true 3-D structure of some portion of the Earth can be represented in a wide variety of ways. The Earth's crust (and upper mantle) has heterogeneous structure including discontinuities, faults, layering, intrusions, inclusions, zones of elevated temperature or partial melt, and random geologic heterogeneities. It also displays anisotropy. No single scheme can represent faithfully all aspects of this heterogeneity. The constant-velocity block approach of Aki and Lee (1976) treats the Earth as a set of boxes within each of which the seismic velocity is constant (Fig 2.4(a)). This approach lacks in the ability to represent heterogeneous structure faithfully, even structures as simple as slight gradients in velocity or oblique discontinuities. The constant-velocity layer approach of Crosson (1976) also suffers from such limitation. From the inverse theory point of view, the traditional block and layer methods are both over-determined (more independent data than unknowns) and under-parameterized. A slight extension of the Aki and Lee approach using thousands of small blocks mitigates this limitation by allowing gradual or rapid velocity changes from block to block to mimic gradients or discontinuities, respectively (Nakanishi, 1985; Walck and Clayton, 1987; Lees and Crosson, 1989). But, the vast number of blocks usually results in the problem being under-determined, and also imposes other computational difficulties.

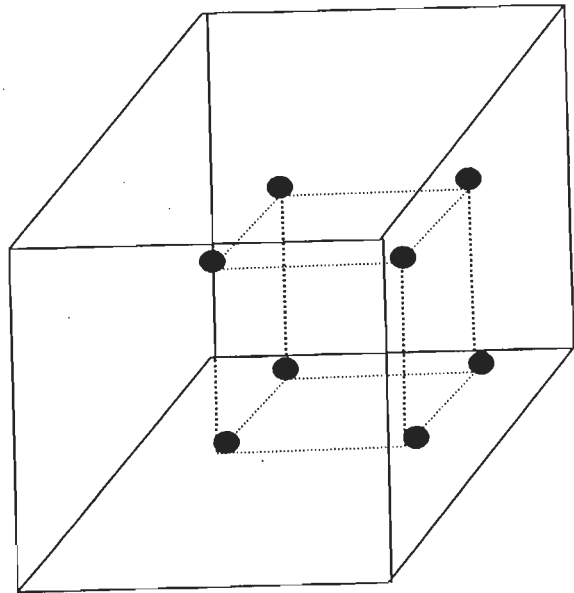
Variations on the discrete block parameterization include laterally varying layers (Hawley *et al.*, 1981) and a 3-D grid of nodes (Thurber, 1983), as illustrated in Fig 2.4(b) and (c). Hawley *et al.*, (1981) divided the model into layers in which velocity is constant in the vertical direction, but velocity is obtained by interpolation among vertical nodal lines in the horizontal directions. The spacing between nodal lines may vary from layer to layer.



(a)



(b)



(c)

Fig. 2.4 Schematic indication of three approaches to discrete velocity model representation
 (a) constant-velocity blocks; (b) laterally varying layers; and (c) a grid of nodes

Thurber (1983) used a 3-D grid approach, in which velocity varies continuously in all directions, with linear B-spline interpolation among nodes. Lin and Roecker (1990) proposed another variant of the 3-D grid theme by considering each set of four neighboring nodes as defining the vertices of a tetrahedron. The four node velocities are used to define a unique linearly varying velocity field within the tetrahedron; the velocity gradient can thus point in any direction. A functional approach to represent 3-D structure can also be adopted either with some set of basis functions or an a priori functional form.

The velocity structure can also be treated explicitly as a continuous function of the spatial coordinates. Two examples are the Backus-Gilbert approach of Chou and Booker (1979) and the 'no-block' approach of Tarantola and Nercessian (1984). In principle, these approaches allow for essentially arbitrary model solutions with no parameterization bias. In practice, however, models must be constrained in one way or another, as they are under-determined and therefore non-unique by design. The models must eventually be discretized, also, for calculation and representation by computer. Chou and Booker (1979) remove the non-uniqueness by evaluating 'ideal averaging volumes' that reflect the spatial variations in ray sampling of the structure. The idea is to view the Earth structure through the window with the maximum spatial resolution allowed by the data.

Zhao *et al.*, (1990) have incorporated boundaries within a 3-D velocity model, by generalizing the 2-D method of Horiuchi *et al.*, (1982) to 3-D, parameterizing the Conrad and Moho discontinuities in a power series in latitude and longitude. Velocities within the crustal layers are constant, though additional a priori vertical boundaries in the mantle are included to separate areas of different P_n velocity (land versus ocean). Zhao (1991) has taken the additional step of allowing laterally and vertically varying velocities within each layer.

There is an enormous variety of choices for representing Earth structure in LET but each LET application is unique, accounting in part for the diversity of methods developed to represent structure. A judicious choice of representation must be made based on the particular LET data set that is to be analyzed.

2.3.3.2 *Ray-path and travel time calculation*

One of the important aspects in LET method is the determination of the propagation path of the seismic wave between each source-receiver pair, and the wave travel time along that path. The travel time is needed in order to calculate the arrival time residual, and the path is needed for computation of the hypocenter and velocity model partial derivatives. There are as many techniques for determining ray-(or wave-) paths and travel times. The choice made for representing the 3-D structure as described above often tends to define the most appropriate method to use or vice versa. The methods can be categorized broadly as either exact or approximate, and the computational strategy involved usually can be classified as either shooting, bending, approximate, or finite-difference. The use of approximate ray-tracing methods has the advantage of computational speed. However, it introduces errors in the computation of residuals, hypocenter derivatives, and velocity model partial derivatives, because the travel time will be in error, the ray direction at the source will be in error, and the ray-path itself will not be correct, respectively.

The ray-tracing is a two-point boundary value problem (BVP) where the end-points are specified and the propagation path and time is determined. Shooting methods solve the two-point BVP by iteratively solving an initial value problem (IVP) with one fixed end-point and the initial ray trajectory varied, while bending methods solve the BVP directly by keeping the

end-points fixed and perturbing the path connecting them. Both methods suffer from the possibilities of convergence to a local rather than global travel time minimum, or determination of a global minimum ray with negligible amplitude. Some of the shooting algorithms developed for and/or applied to LET have been described by Koch (1985), Lin and Roecker (1990), and Sambridge and Kennett (1990). The latter study employed a form of dynamic ray equations to provide derivative information for perturbing the initial ray trajectory. Bending methods have been developed by Wesson (1971), Julian and Gubbins (1977), and Pereyra *et al.*, (1980), among others. The pseudo-bending method of Um and Thurber (1987) and the related method of Prothero *et al.*, (1988) are basically approximate but fairly accurate treatments of the 'exact' bending method.

Some of the LET studies have used extremely simplistic ray-tracing that limits the capabilities of the inversion. Aki and Lee (1976) used straight-line rays through a homogeneous medium to evaluate the equations for inversion, and Walck and Clayton (1987) have improved on this slightly by using an initial layered structure for tracing rays. Thurber and Ellsworth (1980) developed an approximate ray-tracing scheme that computes rays and times in a local layered average of the 3-D structure. This represented a slight improvement over straight rays or rays in a layered structure, but its application is limited to cases with modest lateral heterogeneity, here laterally refracted rays are not significant. Recognizing this limitation, Thurber (1983) developed a fast, simple, brute-force search technique that allowed for laterally refracted rays but assumed that the curvature along anyone trial ray was constant. For ray-paths of modest length (say 40 km or less), this assumption appears reasonable (Eberhart-Phillips, 1986). Two alternative approaches to the ray-tracing problem are the finite-difference method of Vidale (1990) and the network theory method of Moser

(1991). Accurate ray-tracing techniques combined with powerful computers promise to provide solutions using LET for large-scale problems.

2.3.3.3 Hypocenter-velocity structure coupling

The proper treatment of the mathematical coupling between hypocenter parameters and the velocity structure model is one of the important aspects in LET. One of the immediate concern is the large matrix represented by equation (2.6) i.e., for a data set and model of L stations, N earthquakes, and M velocity parameters, the construction of a matrix of size approximately $(L \times N)$ by $(4N + M)$ is implied. Three groups, apparently simultaneously and independently, suggested conceptually similar schemes for constructing and sequentially accumulating a system of equations involving velocity model parameters only, without sacrificing the formal mathematical coupling between hypocenter and velocity parameters (Pavlis and Booker, 1980; Spencer and Gubbins, 1980; Rodi *et al.*, 1981). The complete system of simultaneous inversion equations can be written in the (discrete) form

$$r = H\Delta h + M\Delta m \quad (2.7)$$

where r is the residual vector, H and Δh are the matrix and vector of hypocenter parameter partial derivatives and perturbations, respectively, and M and Δm are the matrix and vector of velocity parameter partial derivatives and perturbations, respectively. For the i^{th} event, set of equations can be written as

$$r_i = H_i\Delta h_i + M_i\Delta m_i \quad (2.8)$$

noting that all terms are partial vectors or matrices from equation (2.7) except for Δm .

If we consider the *QR* decomposition of H_i (Lawson and Hanson, 1974),

$$QH_i = \begin{pmatrix} r_{11} & r_{12} & r_{13} & r_{14} \\ 0 & r_{22} & r_{23} & r_{24} \\ 0 & 0 & r_{33} & r_{34} \\ 0 & 0 & 0 & r_{44} \\ 0 & 0 & 0 & 0 \\ \cdot & \cdot & \cdot & \cdot \\ \cdot & \cdot & \cdot & \cdot \\ \cdot & \cdot & \cdot & \cdot \\ 0 & 0 & 0 & 0 \end{pmatrix} \quad (2.9)$$

the partition of Q can be used below row 4, known as Q_0 , to form the equation

$$Q_0 r_i \equiv r'_i = Q_0 H_i \Delta h_i + Q_0 M_i \Delta m \equiv M'_i \Delta m \quad (2.10)$$

where the property that $Q_0 H_j = 0$ is used. Thus, a smaller system of equations containing only the velocity model parameters as unknowns can be assembled by carrying out the separation step indicated in equation (2.10) for each event and accumulating the 'reduced' set of equations $r' = M' \Delta m$. An additional step of directly accumulating the corresponding normal equations can be taken to reduce the matrix size even further (Spencer and Gubbins, 1980; Thurber, 1983).

Tomography studies generally use suitable hypocenter locations derived from a laterally homogeneous (1-D) velocity model, with or without station corrections (statics), with no explicit treatment of the hypocenter-velocity structure coupling; that is, the term $H \Delta h$ in equation (2.7) is ignored. This approximation would be perfectly acceptable in the geologically rather uninteresting case that lateral velocity fluctuations were low in amplitude and spatially random. In geologically complex areas, though, this approach will almost inevitably result in the introduction of bias in the velocity model due to systematic hypocenter mislocation, so that tomography results should be viewed with a cautious eye. Some of the other problems with the simple tomography approach are the absence of

information on the improvement to fit to the data, and the practical inability to carry out a truly iterative inversion. Note that 'iterative back-projection techniques' such as the Simultaneous Iterative Reconstruction Technique (SIRT) (Walck and Clayton, 1987) do not actually constitute an iterative solution to this non-linear problem. Rather they just derive an approximate solution of the linear matrix inversion problem using an iterative sequence of vector operations. Simultaneous inversion avoids all of these pitfalls, in principle, by directly accounting for the hypocenter-velocity structure coupling in the matrix equations and allowing an iterative solution, but normally at a significant computational cost.

Pavlis and Booker (1983) analyzed some aspects of nonlinearity in the simultaneous inversion problem for 1-D velocity structure. They used synthetic arrival time data (calculated in the 'true' model) to assess the differences between perturbation estimates from a starting (reference) model calculated by their inversion method (the linear estimate) and the theoretically best estimate possible, given the data available. The latter is given by the true perturbation smoothed by the resolution function. They called this difference the non-linear error. Their most relevant test compared the non-linear error for a particular true and reference model when the earthquakes were fixed at their true locations versus when they were first relocated in the reference model. Kissling (1988) tested the need for the parameter separation step in tomographic inversion for 3-D structure at Long Valley, California. Using synthetic arrival time data modeled on actual data set and a hypothetical velocity structure, it was observed that a tomographic inversion ignoring the hypocenter-velocity structure coupling produced a severely biased model. Including parameter separation, although computationally costly, does a far superior job of recovering the hypothetical velocity structure. A similar analysis presented by Thurber (1981) also found a significant

improvement in model fidelity when the hypocenter-velocity structure coupling was included explicitly in the inversion equations. Thurber (1981) also used synthetic simulations to show that the 'linear' range for local earthquake location is of the order of 2-3 km, while the 'linear' range for velocity perturbations is of the order of 10%.

The single-step 'tomographic' inversion underestimates velocity contrast by nearly an order of magnitude, while the 'simultaneous inversion' recovers the true structure and event location nearly exactly. Ignoring explicit hypocenter-velocity structure coupling leads to bias in the derived 'tomographic' models (Walck and Clayton, 1987; Lees and Crosson, 1989).

2.3.3.4 *Inversion methods*

The non-linear nature of the problem is one of the major difficulties with LET. Unless the level of heterogeneity is quite modest, it is essential to adopt an iterative approach in finding a solution. There are different kinds of schemes that have been employed to carry out this iterative solution. Also the LET inversion problem can become intractable due to the large size of the matrix involved. Direct solution of the equations via Singular Value Decomposition (SVD) (Lawson and Hanson, 1974) for very large problems can also be carried out. SVD breaks down the matrix composed of the coefficients of the parameter derivatives in equation (2.6) into a product of three orthogonal matrices containing the singular ('eigen') vectors of the data and model spaces and the corresponding singular values (Menke, 1989). The SVD approach would retain the key advantage of the explicit calculation of singular values and vectors, allowing direct assessment of the determinedness of the system of equations and the null space of the solution (i.e. the model parameters unconstrained by the data).

A popular alternative to SVD is to combine parameter separation with construction of the normal equations and the incorporation of damping, using the equation

$$\Delta m = [(M')^T M' + \varepsilon^2 I]^{-1} (M')^T r' \quad (2.11)$$

resulting in a matrix size fixed by the number of velocity model parameters (Spencer and Gubbins, 1980; Thurber, 1983). Therefore, this method is not subject to an increase in the size of the matrix to be inverted as the number of earthquakes included in the inversion grows. The algorithm *SIMUL3* originally developed by Thurber (1981, 1983, 1984), which uses this approach with a 3-D grid of nodes to represent the velocity structure, has been applied to many LET data sets. Some of the costs of this normal equations short cut are the loss of singular value information, the sensitivity of the solution to the choice of damping value; and squaring of the condition number of the matrix to be inverted.

Eberhart-Phillips (1986) developed a practical scheme for determining a reasonable choice for the value of damping. By constructing 'trade-off' curves comparing the data variance (residual size measure) and solution variance (model perturbation size measure) from a suite of one-step inversions with varying damping, optimum damping values below which decreased damping led to rapidly increased solution variance with little or no decrease in data variance were found.

Efforts have been made in the development and use of other approximate solution methods that do not require storage and manipulation of large matrices. Kissling (1988) made use of parameter separation and applied an Algebraic Reconstruction Technique (ART) type of approximation of equation (2.11):

$$\Delta m_j = [(M')^T]_j / [(M')^T M' + \varepsilon^2 I]_{ij} \quad (2.12)$$

where the subscripts j and jj indicate the j^{th} vector element and jj^{th} diagonal element of the corresponding vectors and matrix. Other back-projection techniques, such as the Simultaneous Iterative Reconstruction Technique (SIRT) have been used for LET, but generally in applications where the hypocenter-velocity structure coupling was not treated explicitly (Walck and Clayton, 1987). Simultaneous Iterative Reconstruction Technique also has the undesirable property that it yields a least squares solution with different weighting (scaling) than that specified by the 'user' (Van der Sluis and Van der Vorst, 1987). The conjugate gradient method, in particular the algorithm LSQR (Least Squares QR) developed by Paige and Saunders (1982), is an effective alternative to such reconstruction techniques (Nolet, 1985, 1987; Van der Sluis and Van der Vorst, 1987). Least Squares QR has been applied to the LET problem (Spakman and Nolet, 1988; Lees and Crosson, 1989), although in the later case the hypocenter-velocity structure coupling was not treated explicitly.

One of the approaches that avoids full matrix inversion is the subspace method described by Kennett and Williamson (1988) and Kennett *et al.*, (1990) and applied by Sambridge (1990). The full matrix problem is projected on to a specified set of orthonormal vectors (the subspace), which in practice is defined as the set of steepest descent directions for the various classes of parameters in the problem. Thus this represents a generalization of the parameter separation method. Parameter classes can include: earthquake origin times and earthquake locations (treated separately); crustal P, crustal S, mantle P, and mantle S velocities (again treated separately); and interface parameters. Convergence is improved in a 2-D subspace scheme (hypocenter and structure, as in the parameter separation case above) compared with simple steepest descent (all parameters treated jointly), and a 6-D subspace scheme

converges faster still, due to the higher dimensional, schemes choosing a more optimal step than those of lower dimensionality.

Many workers have used the Levenberg-Marquadt method (Gill *et al.*, 1981), also known as iterative damped least squares for iterative solution. A perturbation to the model is computed at each of the iteration using damped least squares (or a sparse-matrix approximation) and is then added to the model and the next iteration is carried out, thus allows the solution to deviate freely from the initial model. Significant exceptions to this are the approaches of Tarantola and Necessian (1984) and Sambridge (1990). Tarantola and Necessian 'anchor' their solution to the starting model, while Sambridge includes explicit second-order derivatives (the Hessian matrix) in computing the solution.

The use of a priori information has been advocated for many kinds of inverse problems (see for example Jackson, 1979). Types of a priori information include an initial model from which deviations are 'penalized' (Jackson and Matsu'ura, 1985), or an assumed form for the (spatial) covariance of the model or both (Tarantola and Necessian, 1984). Such information is valuable for improving stability and uniqueness of the solution. Tarantola and Necessian (1984) show that, in the under-determined case, this can be accomplished by minimizing the expression

$$(d_0 - d)^T (C_{d_0}^{-1} (d_0 - d) + (m_0 - m)^T C_{m_0}^{-1} (m_0 - m)) \quad (2.13)$$

subject to the condition $d=g(m)$, where d and m are the data and model, g is the non-linear vector functional representing the physical theory (the forward problem), a subscript 0 indicates the observed data or a priori model values, and C represents the a priori (data or model) covariance matrix. This expression penalizes deviations of the 'calculated data' d_0

from the observed data d (i.e. data misfit) and deviations of the perturbed model m from the a priori model m_o , in inverse proportion to the respective variances.

An expression of very similar form to equation (2.13) is to be minimized in the case that one wishes to find a 'smooth' model that fits the data. Note that this can also be thought of as using a priori information, in this case the information that a smooth model is a preferred model.

There has been no definitive study that documents and quantifies in detail the advantages and disadvantages of these diverse inversion methods. More detailed methods may permit the removal of as many approximations as possible from LET, so that results may become less dependent on the choice of inversion method.

2.3.3.5 *Solution quality*

The interpretation of complex 3-D model to the real world depends on the model's quality which may include data variance (misfit) reduction, model resolution, and model covariance (Menke, 1989). Misfit is a measure of the disagreement between the observed and predicted data, for example, the norm of the residual vector. Resolution represents the interdependence of the predicted model parameters. Covariance measures the mapping of data errors on to model parameter errors.

In the standard discrete inverse theory approach, in the course of finding the solution to the problem $Gm = d$, an inverse G^{-1} is computed. One can then directly determine the matrices of model resolution R and model covariance C_m

$$R = G^{-1}G \tag{2.14}$$

$$C_m = (G^{-1})^T C_d G^{-1}$$

given some (assumed) form for the data covariance matrix C_d (Menke, 1989). R represents the 'filter' through which the model estimate is obtained from the 'true' model, while C contains the estimated variance of individual parameters (diagonal elements) and the co-variation between pairs of parameters (off-diagonal elements).

Jackson (1979) and Nowack and Lutter (1988) show that these matrices can be generalized to the case where a priori information is included. Nowack and Lutter (1988) suggested that most algorithms yield underestimated values for covariance, as the standard approach yields model covariance values that tend to zero as the diagonal elements of the resolution matrix tend to zero (Ellsworth and Koyanagi, 1977). This suggestion is supported by the quasi-empirical testing of synthetic LET data by Thurber (1981), who showed that estimated model uncertainties generated from a suite of synthetic data were nearly a factor of 2 smaller than actual model errors, on average.

All the measures namely misfit, resolution, and covariance are inherently coupled. It is well known that increasing the number of model parameters generally will diminish the misfit. In turn, a model that is spatially finer in scale will have the ability to represent structure at a higher spatial resolution, but the resolution of the individual model parameters will be reduced, given the same set of data. The exact effect of covariance depends on how it is calculated, but it is generally the case that improved resolution comes at the cost of increased model variance. Toomey and Foulger (1989) undertook a careful examination of the effect of 'coarse' versus 'fine' model parameterization on the solution and its formal resolution in their simultaneous inversion of data from Hengill volcano, Iceland. They compared two solutions, one (fine) with half the spacing between nodes compared with the other (coarse). Although the diagonal elements of the resolution matrix were uniformly smaller in the former case (by

about a factor of 2), as expected, they found that the 'fine' case yielded a statistically significant improvement in data fit, and had a resolution matrix with a trace nearly twice that of the 'coarse' case. Thus they argued that the fine solution, although having poorer formal resolution, was indeed a better solution.

Toomey and Foulger (1989) also introduced the use of the spread function (Menke, 1989) to LET as a single parameter (rather than a full matrix) that characterizes model resolution for each parameter (node or cell).

In the tomographic approach, where direct calculation of resolution and covariance is generally not practical due to the unavailability of the full matrix and its inverse, it is common to assess resolution by examining inversions of synthetic data for models with isolated anomalies. This is equivalent to determining the point spread function for the single anomalous model cell (Humphreys and Clayton, 1988). This provides a sense of model fuzziness and streakiness at selected points. Nakanishi and Suetsugu (1986) demonstrated that it is possible to derive a resolution matrix for the tomography problem, but of course the sheer size of the matrix (number of parameters squared), which must be determined separately for each parameter, limits its usefulness. An examination of ray coverage, either directly (Walck and Clayton, 1987) or by way of the ray density tensor (Kissling, 1988), provides another qualitative perspective on the solution quality.

2.4 Summary

The 1-D and 3-D crustal velocity structure proposed for the Garhwal Himalaya have been reviewed in the present chapter. 1-D crustal velocity structures proposed by various workers have been found to be consisting mainly three layers over a half space for Himalaya region.

Two of the 3-D velocity structures proposed for the area are from Sarkar *et al.*, (2001) and Mukhopadhyay & Kayal (2003) .

The methods for determination of 1-D and 3-D velocity studies have been discussed in the present chapter. Further, the development of methodology for *Local Earthquake Tomography* (LET) has been reviewed. The steps involved in LET namely (i) Representation of structure, (ii) Ray path and travel time calculations, (iii) Hypocenter-velocity structure coupling, (iv) Inversion methods and (v) Solution quality have been discussed in details.

GEOLOGY AND TECTONIC SETUP OF GARHWAL HIMALAYA

3.1 Introduction

The Himalaya occupies the northern part of the Indian subcontinent forming about 400 km wide arcuate bend which is convex to the SSW and runs unbroken for 2400 km between the mountain peaks of Nanga Parbat in the west and Namcha Barwa in the east, each of these peaks being located where the trend of the mountains changes abruptly. It is bounded by Indo-Gangetic plains towards south and the Trans Himalaya ranges towards north. The actual northern may be taken as more or less continuous depression running parallel to the Himalaya trend and containing the valleys in which lie the upper reaches of the Indus and the Tsangpo (named Bhramputra further downstream in Assam). Within the Himalaya, the mountain ranges are arranged in various linear belts; the Trans Himalaya belt, Main Central Crystalline belt which is also called the Great or Higher Himalaya and comprises of high mountain peaks, 30 of which, including Mount Everest, have elevations in excess of 7300 m, the Lesser Himalaya which comprises mostly of the mountains with elevations upto 4500 m and the southern-most outer Tertiary Foot Hill belt with elevations upto 1300 m. The boundaries between the various belts are marked by thrusts. The Great and the lesser Himalaya have also been dissected by transverse deep valleys carrying drainage.

3.2 Garhwal Himalaya – Study area

Narula (1991) evaluated the seismotectonics of the northwest Himalaya based on tectonic set up, contemporary deformation styles interpreted on the basis of manifestations of neotectonic activity, direction of crustal shortening in the Quaternary sediments, source mechanism of discrete seismic events and seismicity patterns, and classified into five seismotectonic domains of discrete deformation styles and seismic behavior. These seismotectonic zones are the Main Himalayan Seismic Zone, High Plateau Seismic Zone, High Himalayan Seismic Zone, Kashmir Syntaxial Seismic Zone and Foot Hill Seismic Zone (Fig. 3.1). The Garhwal Himalaya falls in the Main Himalaya Seismic Zone where the seismicity is prominently due to underthrusting decollement surface. Further, based on several features like seismicity patterns, focal mechanism studies, geophysical attributes, tectonic flux studies and pattern of geothermal manifestation, Narula (1992) divided the longitudinal Himalayan Seismic Zone into discrete seismotectonic segments with well defined transverse boundaries marked by interpretative fundamental faults. These segments are the Kashmir Block, Chamba Kishtwar Block, Kangra Block, Shimla Block, Garhwal Block and Kumaun Block (Fig. 3.1). It has also been contended that the segmentation of the crust by transverse features might result in the block specific adjustment of mechanical strain and these blocks would respond to discrete stress field and thus rupture individually. These segmentation boundaries are the result of the first order interpretation and it is possible that the individual blocks could have additional sub-parallel transverse features below the metasedimentary wedge overlying the basement (Narula, 2000). Narula and Shome (1992) suggested that the transverse features have a significant role in generation and modification of source parameters. Acharya and Narula (1998) contended that segmentation boundaries might act as earthquake nucleation sites with

rupture propagation only in one direction along the longitudinal (Himalayan trend) seismic source. The area of interest *viz* Garhwal Himalaya lies in the Garhwal and Kumaun block in the Main Himalayan seismic zone. The study area sprawls around 24000 km² bounded by 29°45' N and 31° N latitudes and 77°45' E and 79°30'E longitudes and is structurally very complex and characterized by various thrusts, faults and folds (Fig. 3.2).

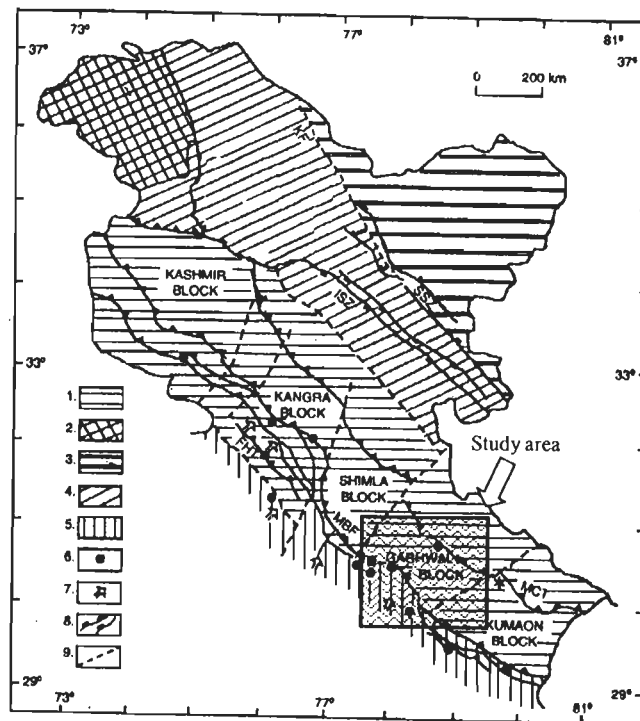


Fig. 3.1 Seismotectonic domains of NW Himalayan seismic belt. 1. Main Himalayan Seismic Zone (MHSZ); 2. Kashmir Syntaxial Seismic Zone (KSSZ); 3. High Plateau Seismic Zone (HPSZ); 4. High Himalayan Seismic Zone (HHSZ); 5. Foot Hill Seismic zone (FHSZ); 6. Specific location where neotectonic activity has been recorded; 7. Direction of crustal shortening during Quaternary; 8. Suture Zone; 9. Block boundary based on geological/geophysical/tectonic flux attributes. SSZ-Shylok Suture Zone; ISZ-Indus Suture Zone; KF-Karakoram Fault; MCT-Main Central Thrust; MBF-Main Boundary Fault; FHT-Foot Hill Thrust. (after Narula *et. al.*, 2000)

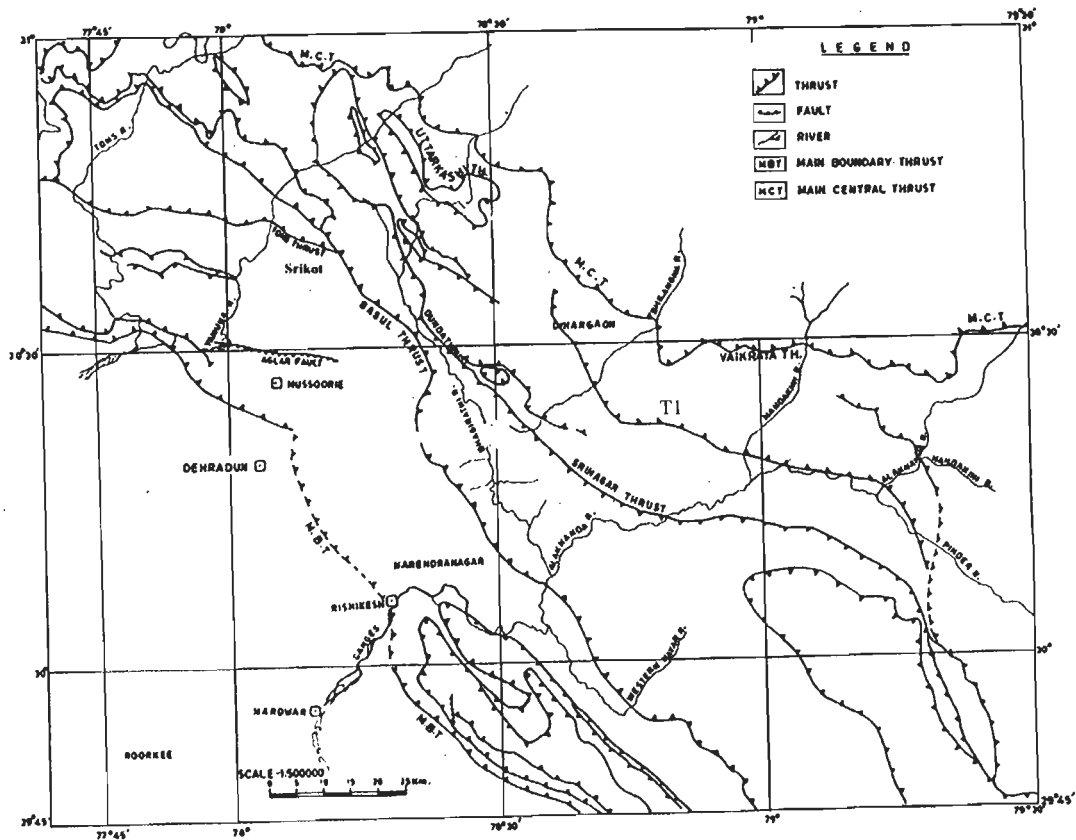


Fig 3.2. Map showing tectonic features of the Garhwal Himalaya (after Fuchs and Sinha, 1978)

3.3 Geology and tectonic setup of Garhwal Himalaya

The Garhwal Himalaya, area of interest in the present study, is a subset to Lesser Kumaun Himalaya and is demarcated by two major thrust planes. In the south the young sedimentary Siwalik realm is severed from it by *Main Boundary Thrust* (MBT) and in the north the *Main Central Thrust* (MCT) delimits the northern boundary of the Lesser Himalaya against the Precambrian high-grade metamorphics of the Great Himalaya. Between these two thrusts the sprawling Lesser Himalayan subprovince is built up of a number of thrust sheets resting on the extensive foundation of the neoautochthonous unit. Each of these tectonic units is characterized by its own lithology, structural pattern and magmatic history. The outer Lesser

Himalaya adjacent to the Siwalik subprovince, comprises a succession of three nappes piled up one over the other. The lowermost sheet is constituted of possibly Palaeozoic sedimentaries of great thickness. The tectonic sheet that succeeds comprises mildly metamorphosed early Precambrian flysch penetrated with voluminous granitic porphyroids of the Ramgarh Group. The uppermost sheet is constituted of possibly late Precambrian moderately metamorphosed sediments and augen gneisses and granite-granodiorite of trondhjemitic suite (Almora Group). The larger part of the inner Lesser Himalaya embraces the neoautochthonous Precambrian sedimentaries (Damtha and Tejam groups), covered by two thrust sheets - the lower one is constituted of quartzites and basic volcanics (Berinag Formation) and the upper unit representing the detached pieces or klippen of the crystalline nappe that caps the Dudhatoli-Ranikhet-Champawat Range of outer Lesser Himalaya. This crystalline nappe is rooted in the base of the Great Himalaya, the root being delimited by the southern Munsiri Thrust and the northern (higher) Vaikrita (Main Central) Thrust.

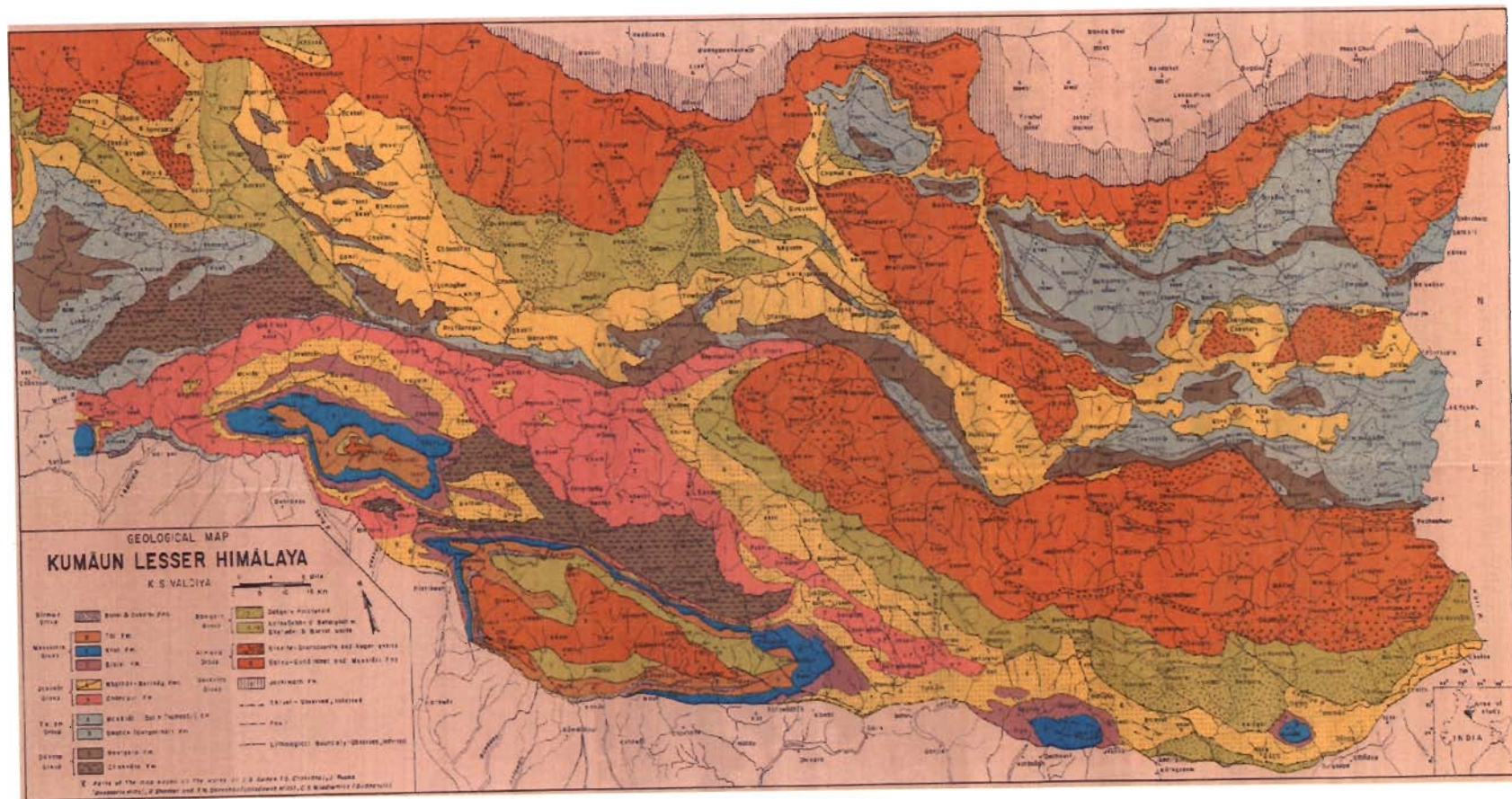


Fig. 3.3 Geological map of Lesser Himalaya (after Valdiya, 1980)

Valdiya (1980) has found that the large scale thrusts recognized in the Kumaun Lesser Himalaya are boundary thrusts defining the limits of the various lithotectonic units. A large number of local thrusts have severed the tightly folded rock formations along the axial planes and brought the older ones over the younger. Schuppen zones have developed where this phenomenon is closely repetitive in space. The tectonics of the region along with its geology (Fig. 3.3) has been well described by Valdiya (1980) and is summarized as given below.

The Almora Thrust defines the tectonic base of the great Almora Nappe built up of medium grade metamorphics and granitoids constituting a major tectonic element of the structural framework of Kumaun. Heim and Gansser (1939) have named the two flanks of this asymmetrically synformal thrust as North Almora Thrust and South Almora Thrust, respectively. The North Almora Thrust is indeed the northern flank of the synclinally folded South Almora Thrust (Valdiya, 1980). The North Almora Thrust does not extend northwestward to join up with the Srinagar Thrust that delimits the Chandpur against the sedimentaries, as asserted by Mehdi *et al.*, (1972), Kumar *et al.*, (1974), Ghose (1973) and Ghose *et al.*, (1974). On the contrary, it bends round to join up with the South Almora Thrust in the Paithani-Musagali area (Valdiya, 1980).

The Munsiri Thrust, which Heim and Gansser (1939) had called the Main Central Thrust separates the crystallines of the Munsiri formation at the base of the Central crystalline zone of the Great Himalaya. It is the root of the Almora Thrust and its extension defining the base of klippen. The abrupt and pronounced contrast of the lithologies across the North Almora Thrust and the violent folding and cataclastic deformation to which the sediments of the underlying Rautgara formation have been subjected, bear unquestionable testimony to its existence.

The low-angled tectonic boundary between the sedimentaries of the Berinag or Mandhali Formation and crystallines of the Munsiri formation at the base of the Great Himalaya has been designated Main Central Thrust by Heim and Gansser (1939). Munsiri Thrust would be a better name for it (Valdiya, 1980). The Munsiri represents the root of the Almora Group forming the nappe in the Lesser Himalaya, so that the Munsiri Thrust is the extension of the Almora Thrust in its root. Recent fieldwork has demonstrated beyond doubt that the Munsiri Thrust joins up with the Jutogh Thrust of Himachal Pradesh (Valdiya, 1964). However, it certainly is not the 'Main Central Thrust' identified by Bordet (1973) and Hashimoto *et al.*, (1973) in Western Nepal. The Main Central Thrust of these workers constitutes the boundary between the equivalents of the Munsiri and overlying Joshimath units and is indeed the extension of the Vaikrita Thrust. This low angled thrust is the root of the Almora Thrust and its klippen-bounding thrusts.

The plane that separates the epizonal succession of sericite-chlorite-biotite schists, micaceous quartzites, amphibolites and lenticular marble with granites and augen gneisses of the Munsiri Formation from the high-grade metamorphics (kyanite-sillimanite-garnet psammitic gneiss, granulites and migmatites) of the Vaikrita Group building the bulk of the Great Himalaya, is postulated as a thrust (Valdiya 1973a, 1978). Heim and Gansser (1939) not only did not perceive any break between the mesozonal and high-grade metamorphics but also emphasized the progressive increase in the grade of metamorphism upwards (Gansser, 1964). It is conceded that there is no structural discordance indicating existence of a thrust plane, nor are there geomorphic expressions of the weak zone associated with the thrust. But there is an abrupt, dramatic change in the grade of metamorphism and the constitution of lithologies.

The abruptly dramatic change in the grade of metamorphism from the epizonal schists and quartzites (with augen- and para-gneisses and porphyritic granites) belonging to greenschist facies or locally lower amphibolite facies of the Munsiri formation to the high-grade metamorphics of the granulite facies represented by the kyanite-sillimanite-garnet-bearing two-mica psammitic gneiss and schist, the garnet-quartz-mica granulite and the calc-silicate rock of the Vaikrita Group is indicative of a break, even though the succession seems to be continuous. The Vaikrita Group within its range shows gradual upward decrease of metamorphism, but only above the Vaikrita Thrust. Below the thrust plane the Munsiri succession does evince slight fall in the grade of metamorphism downwards - from biotite grade to chlorite grade. But this is a consequence of retrograde metamorphism along the base of the formation.

The Vaikrita Thrust demarcates the northern boundary of the Lesser Himalaya. In other words, the Munsiri Formation at the base of the Great Himalaya is really a Lesser Himalayan formation, and not a part of what is called the "Central Crystalline Axis" (Valdiya, 1980). The Vaikrita Thrust has moderate to low (30-45°) inclination due NNE in eastern and central and NE in western Kumaun and ENE to E in the Satluj valley in Himachal. Some of the hot springs of the Great Himalaya seems to be related in some way with the Vaikrita Thrust, or the sympathetic faults associated with it, for they sprout hot water in its close proximity. Perhaps the high seismicity of the belt may be attributed to the movement along this thrust. The seismic plane that Kaila and Narain (1976) recognized from the analysis of profiles giving a dip of 40° NE in Nepal and Kumaun corresponds more to the 30-45° dipping Vaikrita Thrust than with the Munsiri Thrust which has the inclination of 5-20°.

The thrust which has brought the Ramgarh group of rocks, over the Nagthat formation of the Krol belt has been designated the Ramgarh Thrust (Figs. 3.3). It is quite obvious that the Ramgarh Thrust is a major plane of tectonic separation and movement.

Below the Munsiri Thrust (the root of the Almora Thrust) the metasedimentaries have been split up into imbricate thrust sheets forming schuppen zone between the Alaknanda and Bhagirathi and then northwest of the Bhagirathi. The Ramgarh Thrust is usually a low-angled feature, but may locally become quite steep as seen between Ramgarh and Bhawali, where it is liable to be mistaken for a reverse fault (Merh et al., 1971). It is a regional thrust of the first order which has brought a huge succession of porphyroid-implanted weakly metamorphic sedimentaries over the rocks of the Krol Belt from their root below the Munsiri Thrust. Parts of the root as revealed in the Alaknanda-Bhagirathi triangle and in the Purola area are split up into schuppen. The Ramgarh thrust sheet being imbricatedly overridden by still vaster and thicker sheet of the crystallines, only its frontal part is visible, so that the Ramgarh Thrust describes only a semi-ellipse. As already emphasized, the Ramgarh Thrust is analogous to the Chail Thrust, so that the Ramgarh unit represents the extension of the Chail Nappe. The Bijni and Saklana units of the Lansdowne and Mussoorie Hills are the klippen of this nappe-its detached far-travelled frontal parts.

In Himachal Auden (1934) designated the sharply defined thrust plane at the base of the Krol succession (Infra Krol-Krol) as the Krol Thrust. This thrust has brought various lithostratigraphic units of the Krol unit (namely Mandhali, Chandpur, Nagthat, Blaini, Krol and Tal) over one or the other of the three Tertiary formations, namely Subathu, Dagshai and Kasauli, or on the Siwalik. In the Kumaun Himalaya, excepting the short stretch west of Yamuna where a narrow horizon of the Subathu intervenes, everywhere the Siwalik is

overridden by one or the other of the six units of the Krol Belt (Fig. 3.3). In a way thus there is a thrust which serves as the boundary of the Siwalik subprovince. This fact has led most of the workers, including Heim and Gansser (1939); Misra and Valdiya, 1961; Valdiya 1962a and Rupke (1974), to refer the Krol Thrust as the Main Boundary Thrust. Beyond Yamuna throughout Kumaun the Krol Thrust has overlapped and concealed the Main Boundary Thrust completely (Valdiya, 1980).

The northern flank of the synclinally folded Jaunsar Group in the Chakrata region is defined at the base by normally steep, south or southwestward dipping thrust, named Tons Thrust by Auden (1934).

The Krol Thrust is manifest in the sharp boundary between the Siwalik molasse and much older Himalayan rock-formations. The thrust is traceable along extraordinarily wide and straight valleys, with their slopes scarred by landslide and the courses of the streams deflected by fans and cones of landslide debris. In the northeastern flank likewise, movement along the Tons Thrust has caused tremendous crushing and deformation. Pronounced discordance of dip of the rocks on the two sides of the thrust plane is noticeable in many areas. Perhaps no other Lesser Himalayan thrust has cut off or truncated as many lithostratigraphic units as the Krol Thrust. The Tons Thrust has likewise placed the Mandhali and Chandpur of the Krol belt over different rock formations of the north. As already mentioned, between the Tons and a little southeast of Thana-Lakhapokhri the Subathu mantling the Chakrata formation has been thrust over. The Krol Thrust is very steep and the Tons Thrust is still steeper almost throughout their extent. The steepness of the Krol Thrust is attributable to later tectonic movement along it which has compressed the folded thrust plane still further. The Krol Thrust shows signs of recent tectonic activity. The wide valleys along

which the thrust is traceable are in many places ridden with landslide debris, occurring as huge cones and fans (e.g. in the Balia, NW of Ranibagh).

In the southern part of the inner sedimentary belt the Berinag Thrust is traceable from Chhera through Dashainthan, Ganai, Bhadar Gad, past Sisakhani and Girichhina, and through Dhular and Lakhmari to Lod-Dungri where it turns around to frame the North Almora Thrust and is thus traceable through the vicinity of Ranman to Takula whence it vanishes under the Almora crystallines. The Berinag formation is synclinally folded, particularly east of the Saryu River like the formations above and below it. The northern flank of the Berinag Thrust discernible at Chhera can be traced along the Kalapani Gad through Patalbhubaneshwar and Rain-Agar the Bhadar Gad valley to the vicinity of Dataut (Valdiya, 1980). It then turns back eastward passing past Kanda, Pokhri to 5 km south of Berinag, and then crosses the Ramganga at Muwani to be discernible all along the tract, a little north of Dewalthat-Kanalichhina-Shangri and Panthsera in the Kali valley. The northern flank keeps close to the Askot-Baijnath thrusts, and like them is very steeply inclined. The thrust that defines the base of the Berinag at the foot of the Great Himalaya maintains a very close proximity and parallelism with the Munsiri Thrust. East of Girgaon until Darma river it vanishes under the overthrust crystallines.

By and large the Berinag Thrust is described by Valdiya (1980) as a bedding plane thrust. Higher up the succession in the Chamoli and Purola regions the Berinag thrust sheet is overlain by packs of imbricate tectonic scales or minor sheets, comprising various formations, including the Berinag itself. The development of these thrusts over the Berinag sheet, and paralleling it, coupled with the fact that the Berinag itself is involved in the imbrications. It has been pointed out that west of the Pabar River the Berinag Thrust becomes

what Pilgrim and West (1928) showed as the Jaunsar Thrust. The Jaunsar Thrust describes a huge parabola around the Chaur massif in southeastern Himachal. However, in the southeast towards the Chandpur mountain the thrust seems to die out into the Chandpur-Nagthat contact, which is locally a disconformity. According to Auden (1934) in southern part of the Jaunsar syncline the Nagthat rests on the truncated Mandhali-Chandpur contact and thus there is a marked unconformity between the Chandpur and the Nagthat. It is just as well likely that what has been interpreted as an unconformity, may in actuality be a thrust plane-representing the extension of the Berinag Thrust. Significantly, in the northern flank of the syncline along the Dharasu-Mussoorie bridle path, Jain (1971) noticed a 50-m wide crushed zone of extremely powdered friable and deformed quartz schists of the basal Nagthat at its contact with the Chandpur. He has therefore postulated a thrust at the Chandpur-Nagthat contact, and named it Basul Thrust. But this has to be just a local feature, for over vast region in the Krol Belt there is perfect transition between the Chandpur and Nagthat.

3.4 Traverses in Garhwal Himalaya

A number of traverses mainly consisting of the cross sections describing lithotectonic setting of the area being traversed have been reported by Valdiya (1980) from Lesser Kumaun Himalaya. These cross sections may be useful in finding the depth-wise extension of the lithotectonic units when inferred along with the 3-D crustal velocity models of the medium beneath the traverses. The traverses reported by Valdiya (1980) for Garhwal Himalaya have been used here for validation of results and interpretation of the 3-D velocity model in terms of location and geometry of the tectonic features.

Traverses falling in the study area are given in *Appendix I*. The lithological succession and

structural setting of the inner Lesser Himalaya in northwestern Almora and adjacent southern Chamoli district are given by traverses namely *Yj*, *hh*, and *ii*. The lithological and structural design of the inner Lesser Himalayan belt in southern and eastern Chamoli district are given by the traverses namely, *jj*, *kk*, and *ll*. Geology of the western Chamoli district in the inner Lesser Himalaya is described using the traverses *nn*, *mm*, and *oo*. Lithotectonic setting of the inner Lesser Himalaya in northwestern Tehri are described by traverses *pp*, *qq* and *rr*. Cross sections of the inner Lesser Himalaya in eastern Uttarkashi district are given by traverses *ss*, *Yq*, *Yz* and *Yr*. Structure and lithological setting of the outer Lesser Himalaya in Pauri and southern Tehri districts are described using traverses *LL*, *KK*, and *JJ*. The traverses are given in *Appendix I* along with the map showing the location of the traverses in the Lesser Kumaun Himalaya. The direction, location, length and the names of the traverses used in the present study have been summarized in Table 3.1.

Table 3.1 Details of Traverses reported by Valdiya (1980) for Lesser Kumaun Himalaya

S. No.	Traverse Name	Location	Length (km)	Direction
1	<i>Yj</i>	Akhora-Manwadevi-Niuni Gwaldam-Manmati-Kilbara	19.5 36.5	S55°W- N55°E S18°W-N18°E
2	<i>hh</i>	Rampur-Khansar-Tharali-Ghes- Chovelia	51.8	S53°W- N80°E
3	<i>ii</i>	Pajaina(S of Gairsen)-Ganpurgarh- Narayanbagar-Ala	46.6	SW-NE
4	<i>jj</i>	Ali(Adibadri)-Gauna-Kunwarikhal	56.8	SW-NE
5	<i>kk</i>	Karanprayag-Nandprayag- Pipalkoti-Hilang	36.6	S52°W- N40°E
6	<i>ll</i>	Dobri-Gauchar-Pokhri-Kimotha- Tungnath	32.6	S35°W- N6°E
7	<i>nn</i>	Khairi-Lameri—Syupuri Rudraprayag-Sandar Bhimli-Bhatwari-Ukhimath	8.0 6.0 32.5	S-N S-N S-N
8	<i>oo</i>	Shrinagar-Chirpatiakhil-Jakhwari	41.0	S13°W-N13°E
9	<i>mm</i>	Utyasu-Rudraprayag-Karnaprayag	42.8	S65°W- S60°E
10	<i>pp</i>	Gohar-Ghansali-Ghuttu	33.0	S5°E-N29°E
11	<i>qq</i>	Jakhand-Tankhand Gadolia-Ghonti-Budhakedar	12.3 24.2	S50°W-N50°E S40°W-N32°E
12	<i>rr</i>	Dabra-Lamgaon-Kammand	21.3	S27°W-N27°E
13	<i>ss</i>	Barkot-Dhanari-Netala	27.2	S35°W-N35°E
14	<i>Yq</i>	Dichligad Uttarkashi-Bhakoli	5.7 15.3	SW-NE S10°W-N10°E
15	<i>Yz</i>	Chgajjula(Bangaon)-Sartali- Nakuri	16.1	S60°W-N75°E
16	<i>Yr</i>	Dharasu-Dunda-Panjala	27.0	S15°W-N15°E
17	<i>LL</i>	Rajpur-Suakholi-Dewalsari- Chapra-Dharasu	37.3	S15°W-N55°E
18	<i>KK</i>	W by Rishikesh-Agrakhal- Chamba-Pratapnagar	35.2	S28°W-N40°E
19	<i>JJ</i>	N by Kotdwar-Pali-Satpuli- Suharkhal(Khirsu)-Pohri- Chantikhal	34.2	SW-N6°E

3.5 Seismicity of the Garhwal Himalaya

The Himalaya tectonic zone, being a collision plate boundary, is manifested with a number of north dipping thrusts that are exposed at the surface. These thrusts originate at a decollement surface dipping 15° towards north at depths ranging from about 12 to 20 km (Seeber *et al.*, 1981). Fault plane solutions of moderate sized earthquakes depict upthrusting from the north along shallow dipping planes (e.g. Ni and Barazangi, 1984). The seismicity belt is mostly confined in between MCT in the north and MBT in the south, though closer to MCT. The Himalayan arc zone, a collision plate boundary, has most recently ruptured in the western sector (1905 Kangra earthquake), in the central sector (1934 Bihar -Nepal earthquake and 1988 Bihar earthquake), and in the eastern sector (Assam earthquake of 1897 and 1950) relieving the accumulated stresses in these sectors. Some of the notable earthquakes in the Himalaya region are listed in Table 3.2.

More recently, damaging earthquakes of magnitude 6.6 (Uttarkashi earthquake) and 6.8 (Chamoli earthquake) occurred in the Garhwal Kumaun Himalaya region on Oct. 20, 1991 and March 29, 1999 respectively. These earthquakes caused widespread damage to poorly constructed buildings killing about 800 persons in Uttarkashi earthquake and 103 in Chamoli earthquake. The epicenter of the Uttarkashi earthquake was determined as 30.75° N and 78.86° E and focal depth as 12km. The earthquake was felt at very far distances including Delhi and maximum ground acceleration of 0.3g was recorded at Bhatwari. The earthquake was followed by a large number of aftershocks and a maximum intensity of VIII+ was observed. The Chamoli earthquake also occurred on Main Central Thrust zone in the east of Uttarkashi. The motion is again thrust type with focal depth of about 20km.

The spatial distributions of epicenters of microearthquakes (MEQ) in Garhwal Himalaya

recorded by different small aperture local seismic networks show the existence of a seismic belt, about 150 km long and 30-50 km wide running almost parallel to the surface trace of MCT lying between Yamuna and Alaknanda valleys (Gaur et al., 1985; Khattri *et al.*, 1989; Jain and Chander, 1991). The subsequent observations of more than 400 microearthquakes by a MEQ network deployed after the Uttarkashi earthquake have shown that the overall microearthquake activity is concentrated in the region between Budhakedar, Bhatwari and Manpur close to the MCT (Wason, 1996; Wason *et al.*, 1999).



Table 3.2 Historical record of the largest earthquakes in the previous century in Himalayas

Year	Month	Day	Lon(°E)	Lat(°N)	Mag
1720	7	15	77.1	28.37	6.5
1816	5	26	80	30	6.5
1833	5	30	80.1	29.4	7.5
1905	4	4	76	33	8.5
1916	8	28	81	30	7.7
1945	6	4	80	30.3	6.5
1956	10	10	77.67	28.15	6.7
1958	12	28	79.94	30.01	6.3
1964	9	26	80.7	30.1	6.2
1975	1	19	78.43	32.46	6.8
1991	10	20	78.77	30.78	6.6
1999	3	29	79.4	30.51	6.8

The seismicity observed in Garhwal and Kumaun Himalaya defines a 50 km wide NW-SE trending belt in the vicinity of the surface trace of MCT. The seismicity defined by local networks operated intermittently between 1979 and 1988 by University of Roorkee show location of earthquakes south of MCT in Barkot-Bhatwari sector, north of MCT in Bhatwari and Okhimath sector, and on both sides of MCT in Okhimath-Gopeshwar sector (Khattri, 1992). Wason *et al.*, (1999) reported the concentration of micro earthquake activity between Budhakedar, Bhatwari and Manpur close to MCT. Sharma and Wason (1994) concluded that the relative low stress drops of the events at shallow depths show that the rock mass constituting the upper crust in Garhwal Himalaya has low strength for accumulation of strength and the rocks undergo brittle fractures and adjustments by analysing the data recorded by telemetered digital seismic array.

3.6 Summary

The geology and tectonic setup of the Garhwal Himalaya has been described in the present chapter. The study area lies in the Garhwal and Kumaun block in the Main Himalayan seismic zone. Various tectonic features namely MBT, MCT, Basul thrust, Srinagar Thrust, Dunda Thrust, Thrust T1, Tons thrust, Uttarkashi thrust encompasses the area having a very complex geological and tectonic setup. The tectonic features have been described in details along with their geology. The traverses as given by Valdiya (1980) consisting mainly the cross sections describing lithotectonic setting have been discussed and shown in *Appendix I*. The seismicity of the area mostly lies in between MCT and MBT.

ESTIMATION OF CRUSTAL VELOCITY STRUCTURE - METHODOLOGY

4.1 Introduction

The hypocenter parameters of each event are independent, yet they do depend on the velocity model used to calculate travel times for all events. Since the parameters used to describe the model are common to all events, the ensemble of arrival times from the collection of discrete events carries information on local velocity structure. The difference of observed and calculated arrival times (residuals) for a number of individual earthquakes reflect model inaccuracies and may provide information used to correct or improve the velocity model. Crosson and Peters (1970) and Peters (1973) attempted to apply classical least squares estimation to the velocity-hypocenter problem. There are several methods for obtaining the crustal structure information for example, surface wave studies for the shallow velocity structure, seismic tomography, receiver functions etc. In the present study the type of seismic tomography used is based on simultaneous inversion of earthquake hypocentral parameters and velocity structure from local earthquakes and the method is known by the name *Local Earthquake Tomography* (LET). This chapter contains the detailed discussions on simultaneous inversions and the methodology used for 3-D inversion of velocity structure.

4.2 Simultaneous Inversion

One of the important aspects of seismic tomography is the simultaneous inversion of hypocentral parameters and velocity structure. The problem may be formulated by generalizing Geiger's method of determining hypocenter parameters. The theory is well documented by Lee and Stewarts (1981) and Iyer and Hirahara (1993) and the same is described in brief here.

A set of first P-arrival times observed at m stations from a set of n earthquakes along with the P-velocity structure underneath the stations is given to determine the hypocenter parameters. Let τ_{jk} is first P-arrival time at the k^{th} station for the j^{th} earthquake along the ray path Γ_{jk} . As there are n earthquakes so the total number of hypocenter parameters to be determined will be $4n$. Let the hypocenter for j^{th} earthquake be $(t_j^0, x_j^0, y_j^0, z_j^0)$, where t_j^0 is the origin time and x_j^0, y_j^0 and z_j^0 are the hypocenter coordinates for the j^{th} earthquake. Thus, all the hypocenter parameters for n earthquakes may be considered as components of a vector in a Euclidean space of $4n$ dimensions i.e., $(t_1^0, x_1^0, y_1^0, z_1^0, t_2^0, x_2^0, y_2^0, z_2^0, \dots, t_n^0, x_n^0, y_n^0, z_n^0)^T$, where the superscript T denotes the transpose.

The Earth underneath the stations is divided into a total of L rectangular blocks with sides parallel to the $x, y,$ and z -axes of the Cartesian coordinate system. Let each block is characterized by a P-velocity denoted as v . If l is the index for the blocks, then the velocity of the l^{th} block is $v_l, l = 1, 2, \dots, L$. It is assumed that the set of n earthquakes and the set of m stations are contained within the block model. Thus the velocity structure underneath the stations is represented by L parameters of block velocity. These L velocity parameters may

be considered as components of a vector in a Euclidean space of L dimensions, i.e., $(v_1, v_2, \dots, v_L)^T$.

It is assumed that every block of the velocity model is penetrated by at least one ray path. Then, the total number of parameters to be determined in the simultaneous inversion problem is $(4n + L)$. These hypocenter and velocity parameters may also be considered as components of a vector ξ in a Euclidean space of $(4n + L)$ dimensions, i.e.,

$$\xi = (t_1^0, x_1^0, y_1^0, z_1^0, t_2^0, x_2^0, y_2^0, z_2^0, \dots, t_n^0, x_n^0, y_n^0, z_n^0, v_1, v_2, \dots, v_L)^T \quad (4.1)$$

Let ξ^* be the assumed trial parameter vector given by

$$\xi^* = (t_1^*, x_1^*, y_1^*, z_1^*, t_2^*, x_2^*, y_2^*, z_2^*, \dots, t_n^*, x_n^*, y_n^*, z_n^*, v_1^*, v_2^*, \dots, v_L^*)^T \quad (4.2)$$

The arrival time residual at the k^{th} station for the j^{th} earthquake may be defined as

$$\begin{aligned} r_{jk}(\xi^*) &= \tau_{jk} - T_{jk}(\xi^*) - t_j^* \\ k &= 1, 2, \dots, m; j = 1, 2, \dots, n \end{aligned} \quad (4.3)$$

where τ_{jk} is the first P-arrival time observed at the k^{th} station for the j^{th} earthquake, $T_{jk}(\xi^*)$ is the corresponding theoretical travel time from the trial hypocenter (x_j^*, y_j^*, z_j^*) of the j^{th} earthquake, and t_j^* is the trial origin time of the j^{th} earthquake. The objective is to adjust the trial hypocenter and velocity parameters (ξ^*) simultaneously such that the sum of the squares of the arrival time residuals is minimized.

The objective function for the least-squares minimization applied to the simultaneous inversion is

$$F(\xi^*) = \sum_{j=1}^n \sum_{k=1}^m [r_{jk}(\xi^*)]^2 \quad (4.4)$$

where $r_{jk}(\xi^*)$ is given by Eq. (4.3). The set of arrival time residuals $r_{jk}(\xi^*)$, for $k=1,2,\dots, m$, and $j=1,2,\dots, n$, as components of a vector r in a Euclidean space of mn dimensions, i.e.,

$$r = (r_{11}, r_{12}, \dots, r_{1m}, r_{21}, r_{22}, \dots, r_{2m}, \dots, r_{n1}, r_{n2}, \dots, r_{nm})^T \quad (4.5)$$

The adjustment vector will be

$$\delta\xi = (\delta t_1, \delta x_1, \delta y_1, \delta z_1, \delta t_2, \delta x_2, \delta y_2, \delta z_2, \dots, \delta t_n, \delta x_n, \delta y_n, \delta z_n, \delta v_1, \delta v_2, \dots, \delta v_L)^T \quad (4.6)$$

and it is determined from a set of linear equations. After this the trial parameter ξ^* is replaced by $(\xi^* + \delta\xi)$ and the iteration is repeated until some cutoff criteria is met.

A set of linear equations is to be solved for the adjustment vector $\delta\xi$ at each iteration step to apply the Gauss-Newton method to the simultaneous inversion problem. In the generalized form it can be written as

$$B\delta\xi = -r \quad (4.7)$$

where B is the Jacobian matrix generalized to include a set of n earthquakes and a set of L velocity parameters, i.e.,

$$B = \left(\begin{array}{cccc|c} A_1 & 0 & 0 & \dots & 0 & \\ 0 & A_2 & 0 & \dots & 0 & C \\ & & & \vdots & & \\ 0 & 0 & 0 & \dots & A_n & \end{array} \right) \quad (4.8)$$

where the O 's are $m \times 4$ matrices with zero elements, the A 's are $m \times 4$ Jacobian matrices given as,

$$A_j = \begin{pmatrix} 1 & \partial T_{j1} / \partial x & \partial T_{j1} / \partial y & \partial T_{j1} / \partial z \\ 1 & \partial T_{j2} / \partial x & \partial T_{j2} / \partial y & \partial T_{j2} / \partial z \\ \vdots & \vdots & \vdots & \vdots \\ 1 & \partial T_{jm} / \partial x & \partial T_{jm} / \partial y & \partial T_{jm} / \partial z \end{pmatrix}_{|_{\xi}} \quad (4.9)$$

and C is a $mn \times L$ matrix. Each row of the velocity coefficient matrix C has L elements and describes the sampling of the velocity blocks of a particular ray path. If Γ_{jk} is the ray path connecting the k^{th} station and the j^{th} earthquake, then the elements of the i^{th} row [where $i = k + (j-1)m$] of C are given by

$$C_{il} = -\Pi_{jkl} (\partial T_{jk} / \partial v_l) |_{\xi} \quad \text{for } l=1,2,\dots,L \quad (4.10)$$

where Π_{jkl} is defined by

$$\Pi_{jkl} = \begin{cases} 1 & \text{if the } l^{\text{th}} \text{ block is penetrated by} \\ 0 & \text{otherwise} \end{cases} \quad (4.11)$$

if u_l is the slowness in the l^{th} block defined by

$$u_l = 1/v_l \quad (4.12)$$

then we have

$$\delta u_l = -\delta v_l / v_l^2 \quad (4.13)$$

To approximate $\partial T_{jk} / \partial v_l$ in Eq. (4.10) to first order accuracy, it is noted that $\partial T_{jk} / \partial u_l \approx \partial T_{jkl} / \partial u_l$, where T_{jkl} is the travel time spent by the ray Γ_{jk} in the l^{th} block. Also, $T_{jkl} = u_l S_{jkl}$, where S_{jkl} is the length of the ray path Γ_{jk} in the l^{th} block. Assuming that the dependence of S_{jkl} on u_l is of second order, $\partial T_{jkl} / \partial u_l \approx S_{jkl} = v_l T_{jkl}$. Hence Eq. (4.10) becomes

$$C_{il} = \Pi_{jkl} T_{jkl} (\xi^*) / v_l^* \quad \text{for } l = 1, 2, \dots, L \quad (4.14)$$

because $(\partial T_{jk} / \partial v_l) \delta v_l = (\partial T_{jk} / \partial u_l) \delta u_l$ and using Eq. (4.13)

Since each ray path samples only a small number of blocks, most elements of matrix C are zero. Therefore, the matrix B as given by Eq. (4.8) is sparse, with most of its elements being zero.

Equation (4.7) is a set of mn equations written in matrix form, and by Eqs. (4.5), (4.6), (4.8), (4.9), and (4.14), it may be written as

$$\delta x_j + \frac{\partial T_{jk}}{\partial x} \Big|_{\xi} \delta x_j + \frac{\partial T_{jk}}{\partial y} \Big|_{\xi} \delta y_j + \frac{\partial T_{jk}}{\partial z} \Big|_{\xi} \delta z_j - \sum_{l=1}^L \frac{\Pi_{jkl} T_{jkl}}{v_l^*} \delta v_l = r_{jk}(\xi^*) \quad (4.15)$$

$$\text{for } k = 1, 2, \dots, m, \quad j = 1, 2, \dots, n$$

Equation (4.15) is a generalization of Geiger's method for the simultaneous inversion problem.

4.3 3-D velocity inversion

Several tomographic techniques have been proposed to analyse arrival time data from body waves. In this study the linearized inversion comprising the following stages is used

1. Finding the minimal 1-D model using *VELEST* (Kissling *et al.*, 1994)
2. Simultaneous relocation of hypocenters and determination of local velocity structure (Thurber, 1983; Eberhart-Phillips, 1990)

Minimum 1-D model estimation by VELEST: Kissling *et al.*, (1994) define the minimum 1-D model as the 1-D velocity model that itself represents the least square solution to the coupled hypocenter velocity model relation equation. In this model the layer velocities are approximately equal to the average velocity in the 3-D tomographic solution within the same depth range. The various steps involved in this method are given in the flowchart as shown in Fig. 2.2

Linearized 3-D inversion: Thurber's (1983) method of iterative simultaneous inversion for 3-D velocity structure and hypocenter parameters using travel-time residuals from local earthquakes has been used in the present study. Key features of this method which allow the problem to be computationally feasible are parameter separation and approximate ray tracing. The ray theoretical approach taken in nearly all LET studies has its limitations also. The method makes use of the arrival times of observed first arriving waves. It is implicitly assumed that these observed waves are the 'direct' ray theoretical arrivals. As Chou and Booker (1979) point out, seismic energy propagates through some finite volume surrounding a 'ray', not along an infinitesimal line. Thus, the structure that is 'sampled' by an observed arrival corresponds roughly to the Fresnel volume about the ray. Furthermore, finite-frequency diffracted arrivals may exist in reality that are not modeled by ray theory, as

discussed by Wielandt (1987). A particularly important example would be a diffraction around a low-velocity region, which would be expected to arrive before the 'direct' arrival that passed through it. Alternatively, a ray-theoretical arrival could be of insignificant amplitude and, therefore, not correspond to the observed 'first arrival'. One must be aware of these limitations when assessing the results of an inversion.

The method by Thurber (1983) make use of an approximate ray-tracing technique (ART) to compute the theoretical first arrival time from source to receiver through a 3-D medium. The ray path is broken into very small segments and then integrates travel time over each of these segments, a high frequency approximation approach to solving the complete wave equation valid for small high frequency local earthquakes. The output of such method is generally complex because travel time is calculated over small segments of the ray path while velocities are iteratively updated to better minimize observed theoretical data misfit. Um and Thurber (1987) updated the ART ray tracing technique by allowing pseudo-bending (PB) ray perturbations to accurately model the first arrival ray path which in turn decreased computation time, and ART-PB is now the ray-tracing currently utilized in the widely available *SIMULPS* algorithm (Evans *et al.*, 1994) which is used in the present study. ARTPB approximates the first arrival time more poorly at large distances (Um and Thurber, 1987; Eberhart-Phillips, 1990). For an optimally parameterized inversion, however, differences between ART-PB and more complete 3-D ray tracing techniques lead to very small changes in the final velocity solution at greater distances (Haslinger and Kissling, 2001; Kissling *et al.*, 2001; Husen and Kissling, 2001). Previous local earthquake tomography studies using ART-PB ray tracing techniques maintain high resolution across the network (i.e., Reyners *et al.*, 1999; Eberhart-Phillips and Reyners, 2001; Husen *et al.*, 2000).

Using a minimum 1-D velocity model (using *VELEST*) as the initial starting model for 3-D local earthquake tomography significantly improves the stability of the initial inversion perturbation (Kissling *et al.*, 1994). The minimum 1-D model represents the layer averaged velocity structure sampled by the same dataset when calculated using identical data to the 3-D inversion. Progressive iterations starting from a 1-D velocity model and moving to a coarsely spaced 3-D model then a more finely spaced 3-D model have been shown to yield smoother velocity models with fewer single point velocity artifacts and more realistic model variance (Kissling *et al.*, 1994; Eberhart-Phillips and Reyners, 1999; Reyners *et al.*, 1999; Husen *et al.*, 2000, 2003). Station spacing, data distribution, and inversion parameterization, including choice of damping parameters and grid node spacing, ultimately limit the resolution of the 3-D inversion (Kissling *et al.*, 2001). In order to decrease the amount of velocity smearing between grid nodes, rays should cross from multiple directions and angles. Earthquakes should be evenly distributed throughout a model, or grid spacing are to be adjusted so that ray coverage across nodes does not vary (e.g., Eberhart-Phillips, 1990; Evans *et al.*, 1994). Outer nodes will always be relatively poorly resolved because in order to ensure accurate earthquake relocation, only events with a greatest P-wave azimuthal separation can be used for inversion; this limits the ray coverage to within the network boundaries. Damping of velocity and station parameters affects both the resulting velocity model and resolution estimates (Kissling *et al.*, 2001). The correct choice of damping parameters ensures a smoothly varying model with a significant decrease in data variance.

The parameters used to quantify the error in the 3-D analysis are hit counts (KHIT), derivative weighted sum (DWS) and resolution matrix (RESOLUTION). KHIT is the numbers of rays traversing the specific cell. The DWS takes into account the number of rays

that sample each cell. The DWS considers the normalized length of each ray within the cell and an observational weight for that specific ray. The DWS is defined as

$$DWS = N \sum_i \sum_j [\int_{p^{ij}} \omega_n(H) dS] \quad (4.16)$$

where N is the normalization factor that takes into account the volume influenced, i and j are the event and station indices, p^{ij} is the ray-path between i and j and ω is the weight used in the linear interpolation and depends on coordinate position. A large DWS indicates that the velocity at the grid point is based on a large body of data. The RESOLUTION describes the extent to which data can be resolved.

The 3-D inversions using LET has provided high-resolution images of individual seismogenic zones and better interpretation of seismotectonic setup in many regions (e.g., Nishizawa *et al.*, 1990; Hino *et al.*, 1996; Eberhart-Phillips and Reyners, 1999; Husen *et al.*, 1999, 2000, 2002; Shinohara *et al.*, 1999; Obana *et al.*, 2003).

The methodology described above has been used in the present study to estimate the 3-D crustal velocity structure beneath Garhwal Himalaya. The data on local earthquake acquired through deployment of the digital telemetered array in Garhwal Himalaya has been used in the present study.

4.4 Summary

The methodology adopted to estimate the 3-D crustal velocity structure has been described in this chapter. In the present study *Local Earthquake Tomography* (LET) which carries out simultaneous inversion of earthquake hypocentral parameters and velocity structure for local earthquakes has been used. The theory of simultaneous inversion is described in details.

Specifically, linearized inversion techniques comprising of (i) finding minimal 1-D model using *VELEST* and (ii) simultaneous relocation of hypocenters and determination of local velocity structure has been used. The effect of input parameters such as station spacing, data distribution, inversion parameterization including damping, and grid node spacing on resolution in 3-D inversion has been discussed. The program *SIMULPS* has been used for the purpose. The parameter KHIT, DWS and RESOLUTION have been used to quantify the errors in the final product.

3-D CRUSTAL VELOCITY STRUCTURE FOR GARHWAL HIMALAYA

5.1 Introduction

The 3-D velocity inversions have been carried out to estimate the 3-D crustal velocity structure for the Garhwal Himalaya using the methodology as described in Chapter 4. The steps include estimation of minimum 1-D velocity model and then simultaneous relocation of hypocenters and determination of local velocity structure using linearized inversion (Thurber, 1983; Eberhart-Phillips, 1990). The minimum 1-D velocity model is defined as the 1-D velocity model that itself represents the least squares solution to the coupled hypocenter velocity model relation equation. In this model the layer velocities are approximately equal to the average velocity in the 3-D tomographic solution within the same depth range. To start with, the initial 1-D crustal velocity structure has been estimated using the earlier models proposed for the region and generally consists of three layers over half space as given in Chapter 2. These models have been considered along with data recently acquired from local earthquake events through digital telemetry array in Garhwal Himalaya. Simultaneous Inversion technique has been used to compute minimal 1-D velocity model (as described in section 4.2) using *VELEST* (Kissling *et al.*, 1994)

The output of 1-D analysis has been used for estimating the 3-D crustal velocity structure of Garhwal Himalaya. The same set of earthquake data has been used for 3-D crustal velocity

structure estimation. The present chapter contains the information on the estimation of 1-D and 3-D crustal velocity structure of Garhwal Himalaya.

5.2 Data set

The data set in the present study consists of the arrival times of the P and S phases of the local events acquired through the digital telemetered seismological network deployed by Department of Earthquake Engineering, IIT Roorkee in the Garhwal Himalayan region as shown in Fig. 5.1. The network comprises of seven remote seismological stations namely, Ayarchali (AYR), Chandrabadni (CHN), Dhargaon (DHR), New Tehri Town (NTT), Chaurangikhal (CKL), Srikot (SRT) and Surkanda (SUR) radio linked to a central recording station (CRS) located at New Tehri Town. The location of stations is given in Table 5.1 and shown in Fig. 5.1. Each of the stations is equipped with short period seismometer (Natural period 1 Hz), digitizer and a transmitter. The signals from the seismometers are digitized and modulated over a carrier frequency and transmitted to the central receiving and recording station at New Tehri Town (Fig. 5.1).

The data recorded on local earthquake events occurring in the study area during the period from April 1995 to December 2007 has been used in the present study. Out of 519 events only 164 events have been selected for the study with depth ranging between 1.3 to 45.4 km and $s-p$ times ranging between 2 to 15 seconds. The errors in locations are constrained between 0.1 and 0.9. The numbers of stations of records include 83 events recorded at 4 stations, 61 events recorded at 5 stations and 20 events recorded at 6 stations. The location of the earthquakes events are given in *Appendix II* and plotted in Fig. 5.1.

Table 5.1 Station locations of the seismological network

S.No.	Station Name	Location		Elevation (meters)
		Latitude (°N)	Longitude(°E)	
1	Ayarchali	30°-18.22'	78°-25.91'	2000
2	Chandrabadni Temple	30°-18.30'	78°-37.23'	2250
3	Chaurangikhal	30°-38.80'	78°-29.50'	1680
4	Dhargaon	30°-31.58'	78°-45.44'	1680
5	New Tehri Town	30°-22.60'	78°-25.89'	1850
6	Srikot	30°-36.97'	78°-17.41'	1800
7	Surkunda Temple	30°-24.65'	78°-17.34'	2720

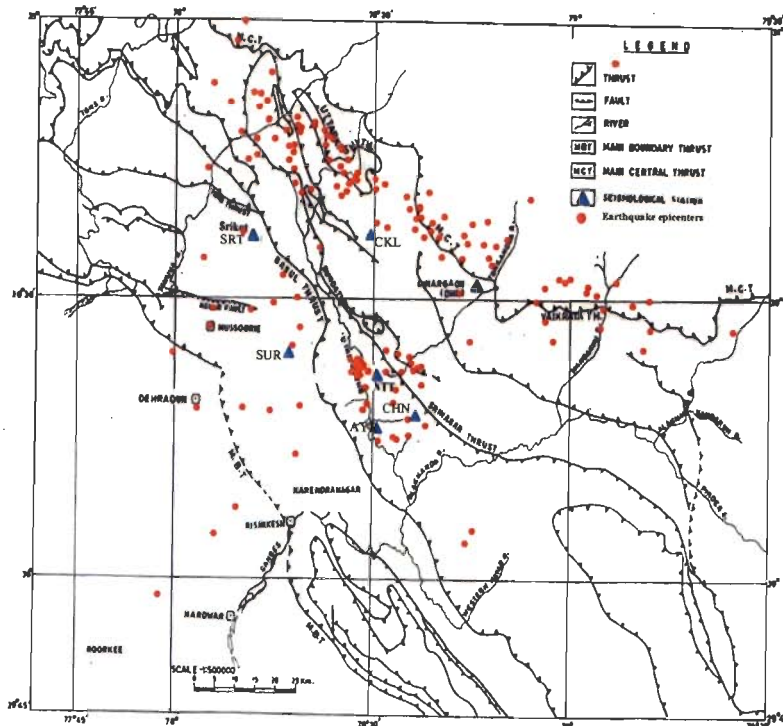


Fig. 5.1 Location of stations and events on the tectonic map of study area

5.3 Estimation of 1-D crustal velocity structure

Several velocity models have been proposed by various studies covering various segments of the Himalaya based on surface wave dispersion and crustal phases as described in Chapter 2. To start with three models proposed by Tandon and Dubey (1973), Kumar *et al.*, (1994) and Mukhopadhyay and Kayal (2003) have been considered in the present study.

The first model used in the present study is from Tandon and Dubey (1973) (as given in Table 5.2). In the study by Tandon & Dubey (1973) body wave data was used from the earthquakes having epicenters over the Himalayas and recorded by the observatories situated over, or very near the foothills of the mountains. A three-layer crustal model (Fig. 5.2) without the top sedimentary layer, with velocities for the P-wave group velocity in Granite I, Granite II, and the Basaltic layer as 5.48 km/sec, 6.00 km/sec, and 6.45 km/sec and for the S-wave group as 3.33 km/sec, 3.56 km/sec, and 3.90 km/sec respectively was proposed. The upper mantle velocity for the P-wave was observed to be 8.07 km/sec, and for the S-wave as 4.57 km/sec. Average thickness for the Granite I layer was computed as 22.7 km, for the Granite II layer as 16.3 km and for the Basaltic layer as 18.7 km. Crustal and subcrustal velocities indicated a lower trend under the mountain. A relatively thicker crust (nearly 58 km) was obtained beneath the Himalayas by Tandon & Dubey (1973).

The second model used as initial model for our studies is based on Kumar *et al.*, (1994). Kumar *et al.*, (1994) considered the first layer upto the depth of 15 km (top of lithosphere) based on Chander *et al.*, (1986) and the second layer upto depth of 46 km based on Kumar *et al.*, (1987). The velocity below 46 km was proposed based on Tandon (1954). In view of scientific considerations made by Kumar *et al.*, (1994) and lack knowledge of velocity structure for the region under study, the velocity model employed by Kumar *et al.*, (1994)

has been used here as one of the initial model namely Kumar *et al.*, (1994) as shown in Fig. 5.3(a) and given in Table 5.3.

The third model has been considered from Mukhopadhyay and Kayal (2003). This model was initially used by Mukhopadhyay and Kayal (2003) as 1-D initial model for 3-D inversions and was estimated using the aftershocks of Chamoli earthquake (March 29, 1999). The Moho upto the depth of 50 km with the velocity of 8.1 km/sec was considered by Mukhopadhyay and Kayal (2003). Above Moho, four layers were considered of thickness 10 km each with the velocity of 5.5 km/sec, 5.9 km/sec, 6.4 km/sec and 7.1 km/sec starting from the surface respectively. The model is shown in Fig. 5.4(a) and given in Table 5.4.

5.3.1 1-D crustal velocity structure analysis

The 1-D crustal velocity structure analysis has been carried out using simultaneous inversion technique and the program *VELEST* has been used for the purpose. The flow chart for the methodology used in *VELEST* is described in Fig. 2.2 of Chapter 2. Simultaneous Inversion has been carried out for estimation of hypocentral location and 1-D velocity structure. The estimates for velocity structure were obtained by fixing the hypocenter locations during alternate iterations of the simultaneous inversion. To get more precise velocity model, the thickness of the layers were fragmented into 2 km bins with their respective velocities in the input models. The output of the 1-D analyses using three assumed input 1-D models are shown in Figs 5.2(b), 5.3(b) and 5.4(b).

Table 5.2 Model I used in 1-D analysis

S. No.	Depth (km)	Initial V_p (km/sec)	Final V_p (km/sec)
1	-3	5.48	4.40
2	2	5.48	5.18
3	4	5.48	5.19
4	6	5.48	5.32
5	10	5.48	5.47
6	12	5.48	5.49
7	16	5.48	5.57
8	18	5.48	5.59
9	22	6.00	5.81
10	24	6.00	5.87
11	26	6.00	6.38
12	28	6.00	6.57
13	40	6.45	6.62
14	44	6.45	6.63
15	46	6.45	6.65
16	58	8.07	8.07

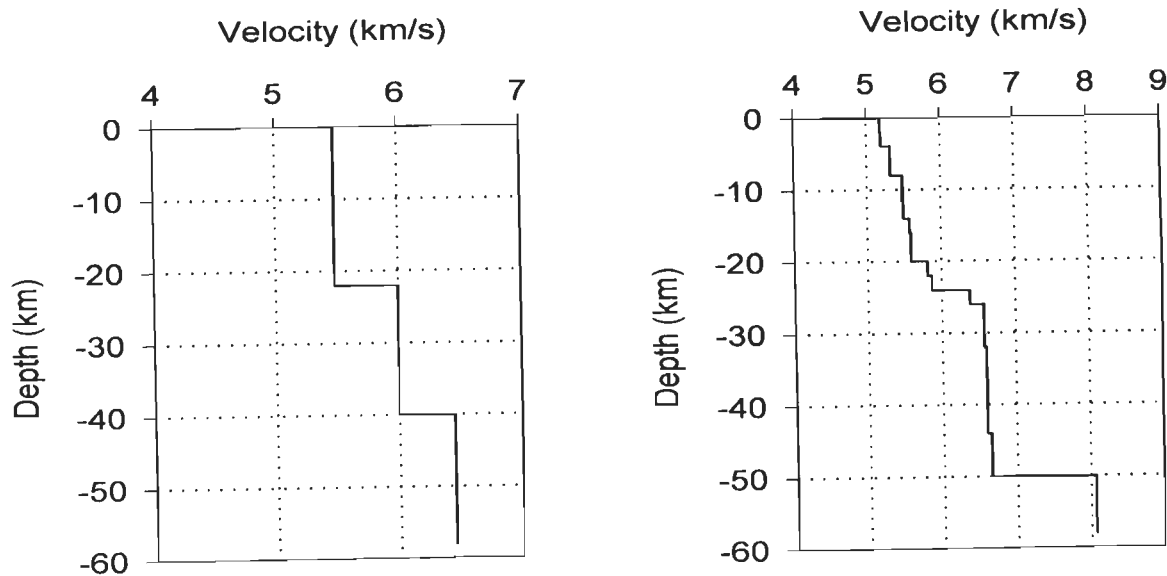


Fig. 5.2 (a) Input Model I after Tandon & Dubey (1973) (b) 1-D modeling results for Model I

Table 5.3 Model II used in 1-D analysis

S. No.	Depth (km)	Initial V_p (km/sec)	Final V_p (km/sec)
1	-3	5.2	4.26
2	2	5.2	5.10
3	4	5.2	5.27
4	12	5.2	5.28
5	14	5.2	5.58
6	16	6	5.73
7	20	6	5.74
8	24	6	5.83
9	26	6	6.17
10	46	7.91	7.79
11	50	7.91	7.91

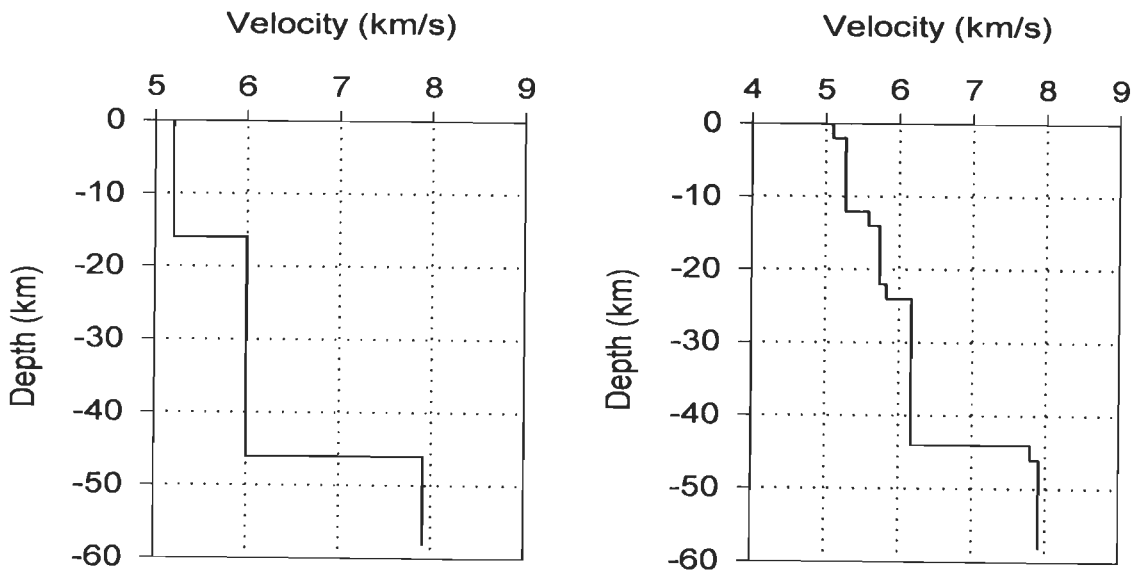


Fig. 5.3 (a) Input Model II after Kumar *et al.*, (1994) (b) 1-D modeling results for Model II

Table 5.4 Model III used in 1-D analysis

S. No.	Depth (km)	Initial V_p (km/sec)	Final V_p (km/sec)
1	-3	5.5	4.47
2	2	5.5	5.01
3	4	5.5	5.26
4	6	5.5	5.27
5	8	5.5	5.45
6	12	5.9	5.54
7	14	5.9	5.55
8	16	5.9	5.79
9	20	6.4	5.80
10	22	6.4	6.02
11	26	6.4	6.26
12	28	6.4	6.33
13	30	7.1	6.67
14	32	7.1	7.23
15	46	7.1	7.24
16	50	8.1	8.1

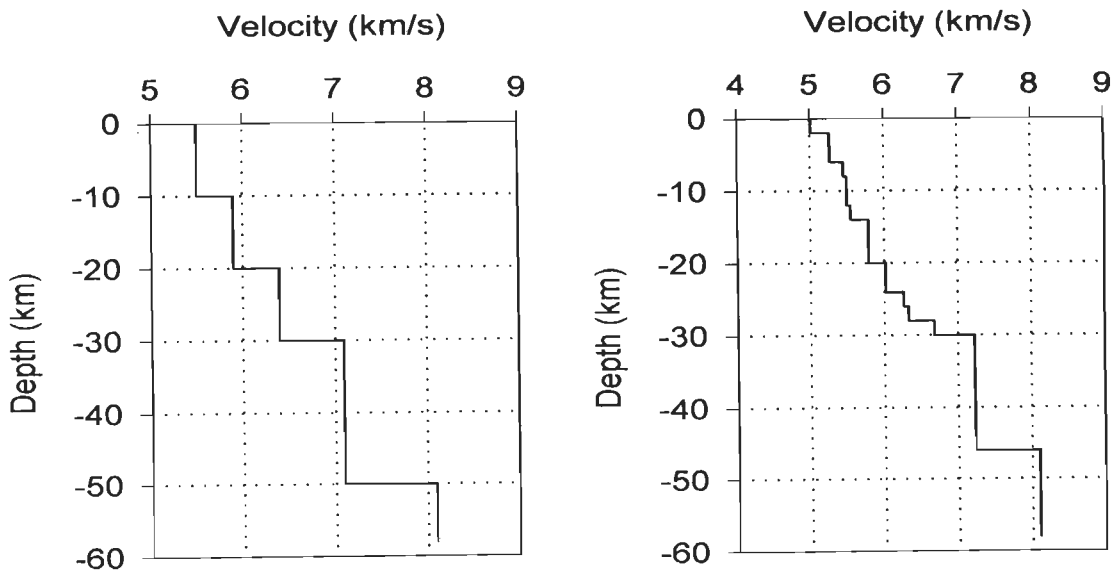


Fig. 5.4 (a) Input Model III after Mukhopadhyay and Kayal (2003) (b) 1-D modeling results for Model III

5.3.2 Average 1-D crustal velocity structure for Garhwal Himalaya

Initially, the 1-D crustal velocity structures from Tandon & Dubey (1973), Kumar *et al.*, (1994) and Mukhopadhyay and Kayal (2003) were considered as trial models for 1-D inversions and the outcome of the same, as shown in Fig.5.2, Fig. 5.3 and Fig. 5.4 has been used as input to the 3-D velocity inversion. An average of the three velocity models obtained from 1-D analysis consisting of three layer structure over half space with average velocities as 5.32 km/sec, 5.80 km/sec, and 6.48 km/sec at depths of 16 km, 26 km and 46 km with the half space having velocity of 7.60 km/sec is proposed for this region and is also used further for 3-D crustal velocity structure estimation as one of the input models. The inputs for the three models are summarized in the Fig 5.5 (a) and the output of the simultaneous inversion for the three models is summarized in Fig. 5.5 (b) along with the average of these three models which is called as Model IV. The 3-D analyses has been carried out using these four 1-D crustal velocity structures and named as Model I, Model II, Model III and Model IV.

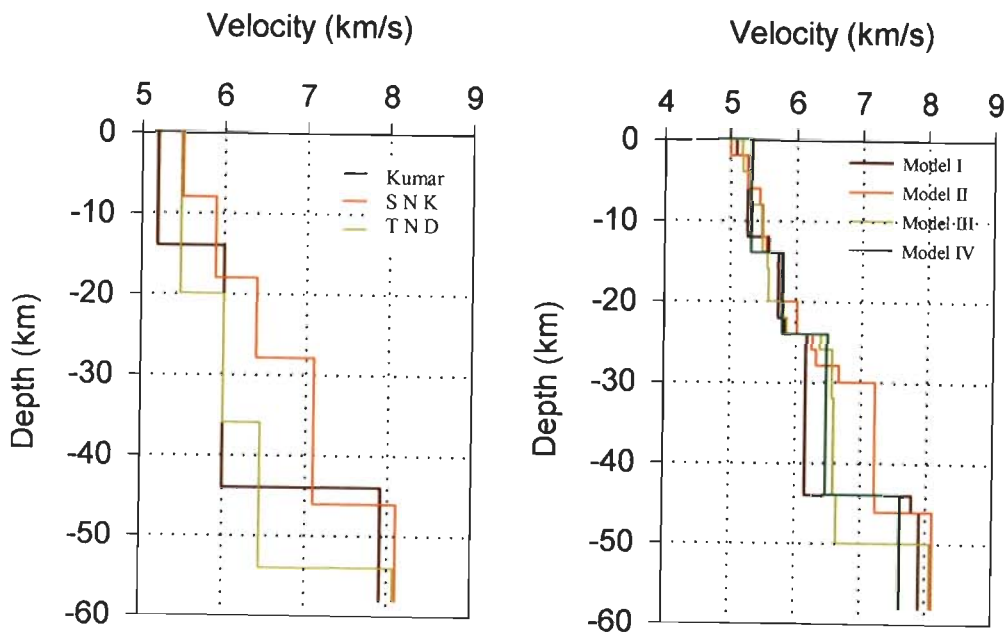


Fig 5.5 (a) 1-D velocity input models for analysis (b) results of 1-D analysis on the three initial models

5.4 Estimation of 3-D crustal velocity structure

The 3-D crustal velocity structure has been estimated based on the output of the 1-D crustal velocity structure analysis. The four models as estimated based on 1-D analysis have been used as input to the 3-D crustal velocity structure analyses. The program *SIMULPS* has been used for the computation of 3-D crustal velocity structure. The various parameters selected for the analysis are given in Section 5.4.1. The gridding has been carried out by considering the area to encompass the earthquake events and the area under study. The grid point locations with respect to the center of the coordinate system have been chosen iteratively based on the earthquake locations and tectonic features in the area. The final grid has been chosen as -90, -80, -70, -60, -50, -40, -30, -20, -15, -10, 0, 10, 20, 30, 40, 50, 60 km in East West direction, and -60, -50, -25, -20, -15, -10, 0, 10, 15, 20, 25, 30, 35, 40, 45, 50, 60 km in North South direction. Depth wise grid locations were chosen as 2, 4, 6, 8, 12, 16, 20, 22, 24, 26, 28, 30, 32, 44, 46 and 48 km. The 3-D view of the velocity model is shown in Fig. 5.6 and the grid locations on the tectonic map is shown in fig 5.7.

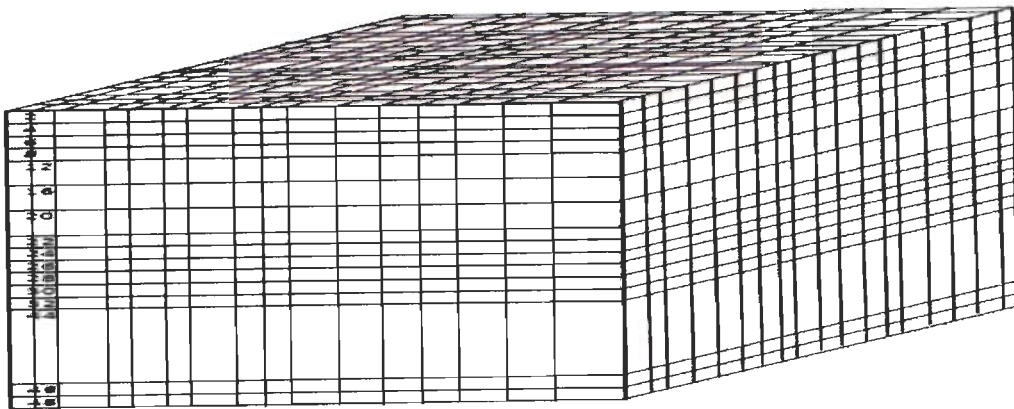


Fig. 5.6 3-D view of the velocity model

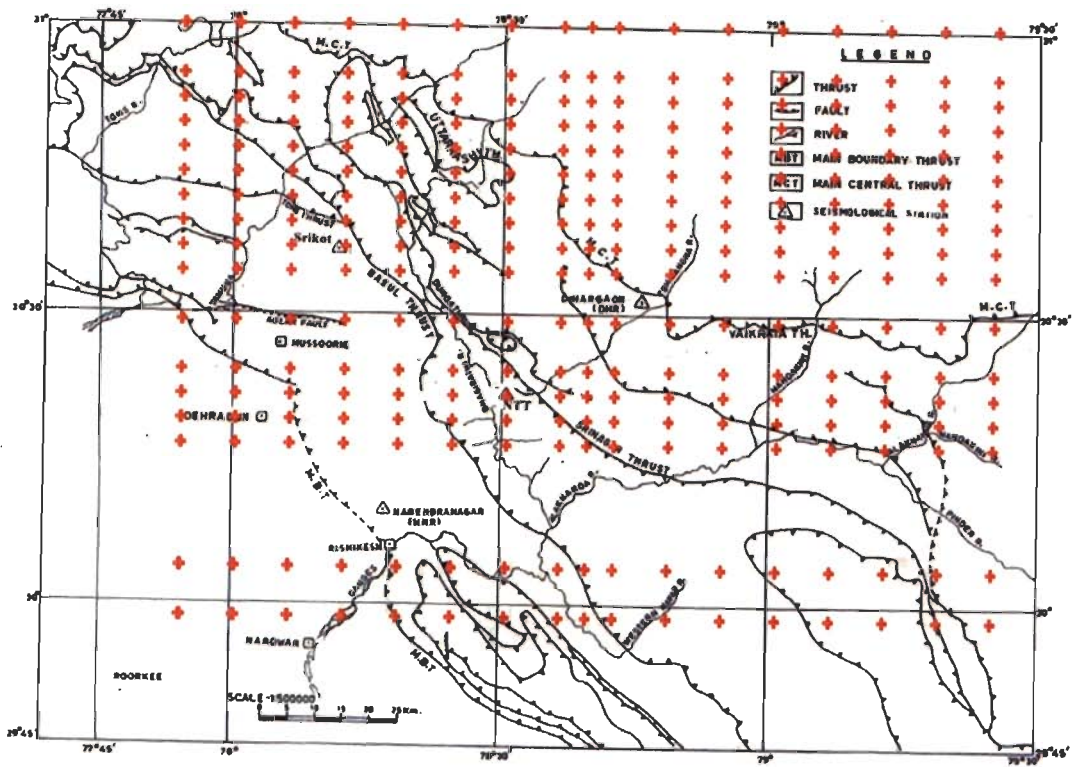


Fig. 5.7 Grid location with respect to the tectonic features in Garhwal Himalaya in East West direction

5.4.1 Parameters for 3-D crustal velocity structure estimation

The 3-D crustal velocity structure analysis has been carried out using 164 earthquakes with maximum horizontal hypocentral adjustment allowed in each hypocenter iteration taken as 10 km. The travel time reading/picking error is assumed to be 0.01 sec. While minimum derivative weighted sum (DWS) for a parameter to be included in the inversion is considered as 5, single V_p adjustment is allowed per iteration. The step length of 0.005 km has been used for calculation of partial derivatives along the ray path with 0.005 as cutoff value for solution

norm. The controls weighting as a function of residual res1, res2 and res3 are taken as 0.3, 1.0 and 2.0 respectively. Nine rotation angles of the plane of the ray have been used in the search for the fastest travel time.

5.4.2 3-D crustal velocity structure analysis for east-west gridding

The following sections describe the results of the 3-D analyses for the four 1-D crustal velocity structures considered as input. The 3-D crustal velocity model estimated using Model 1 as initial 1-D minimum model is named as 3-D Model I. Similarly, the 3-D models estimated using initially Model II, Model III and Model IV are referred as 3-D Model II, 3-D Model III and 3-D Model IV.

The errors in hypocentral locations of the events in the 3-D simultaneous inversion in terms of coordinates of hypocentres and origin time along with their residuals are given in *Appendix III*. The parameters KHIT, DWS and RESOLUTION are given in *Appendix III*. The parameters KHIT, DWS and RESOLUTION are one of the important parameters defining the confidence in the results obtained through 3-D velocity inversions. These parameters give an idea about the quality of the results obtained. The maximum value of KHIT, DWS and RESOLUTION are summarized in Table 5.5 for the east west gridding. The vertical profiles obtained by the 3-D analysis for east west gridding are given in *Appendix IV*. The depth slices obtained from the analyses using 3-D Model I, 3-D Model II, 3-D Model III and 3-D Model IV have been shown in Fig 5.8, Fig. 5.9, Fig. 5.10 and Fig. 5.11, respectively.

Table 5.5 Maximum values of the parameters KHIT, DWS and RESOLUTION for the east-west gridding

S. No.	Depth (km)	KHIT				DWS				RESOLUTION			
		M1	M2	M3	M4	M1	M2	M3	M4	M1	M2	M3	M4
1	2	96	97	96	97	2366	2307	1379	3045	0.62	0.63	0.45	0.65
2	4	89	93	73	79	1708	1859	833	1562	0.51	0.57	0.31	0.48
3	6	76	78	61	62	1783	1540	669	1173	0.51	0.45	0.26	0.41
4	8	64	69	46	53	1456	1376	628	956	0.54	0.48	0.34	0.37
5	12	45	61	31	47	789	967	389	651	0.38	0.33	0.24	0.29
6	14	17	37	18	28	536	523	196	325	0.20	0.26	0.16	0.17
7	16	14	29	15	21	644	1700	577	1183	0.14	0.26	0.29	0.24
8	20	10	13	11	13	171	279	180	276	0.13	0.12	0.11	0.12
9	22	7	8	6	9	168	92	133	94	0.07	0.04	0.25	0.06
10	24	7	5	5	7	100	147	123	128	0.05	0.06	0.03	0.04
11	26	6	4	3	6	135	151	96	152	0.07	0.09	0.03	0.10
12	28	6	4	3	6	150	150	62	168	0.08	0.05	0.04	0.04
13	30	2	2	4	2	80	65	52	82	0.02	0.01	0.03	0.02
14	32	2	3	4	3	107	124	134	137	0.02	0.09	0.09	0.03
15	44	1	3	3	2	109	122	103	129	0.00	0.11	0.07	0.07
16	46	0	2	2	2	2	65	64	66	0.00	0.03	0.02	0.03
17	48	-	2	2	2	-	70	61	29	-	0.05	0.26	0.03

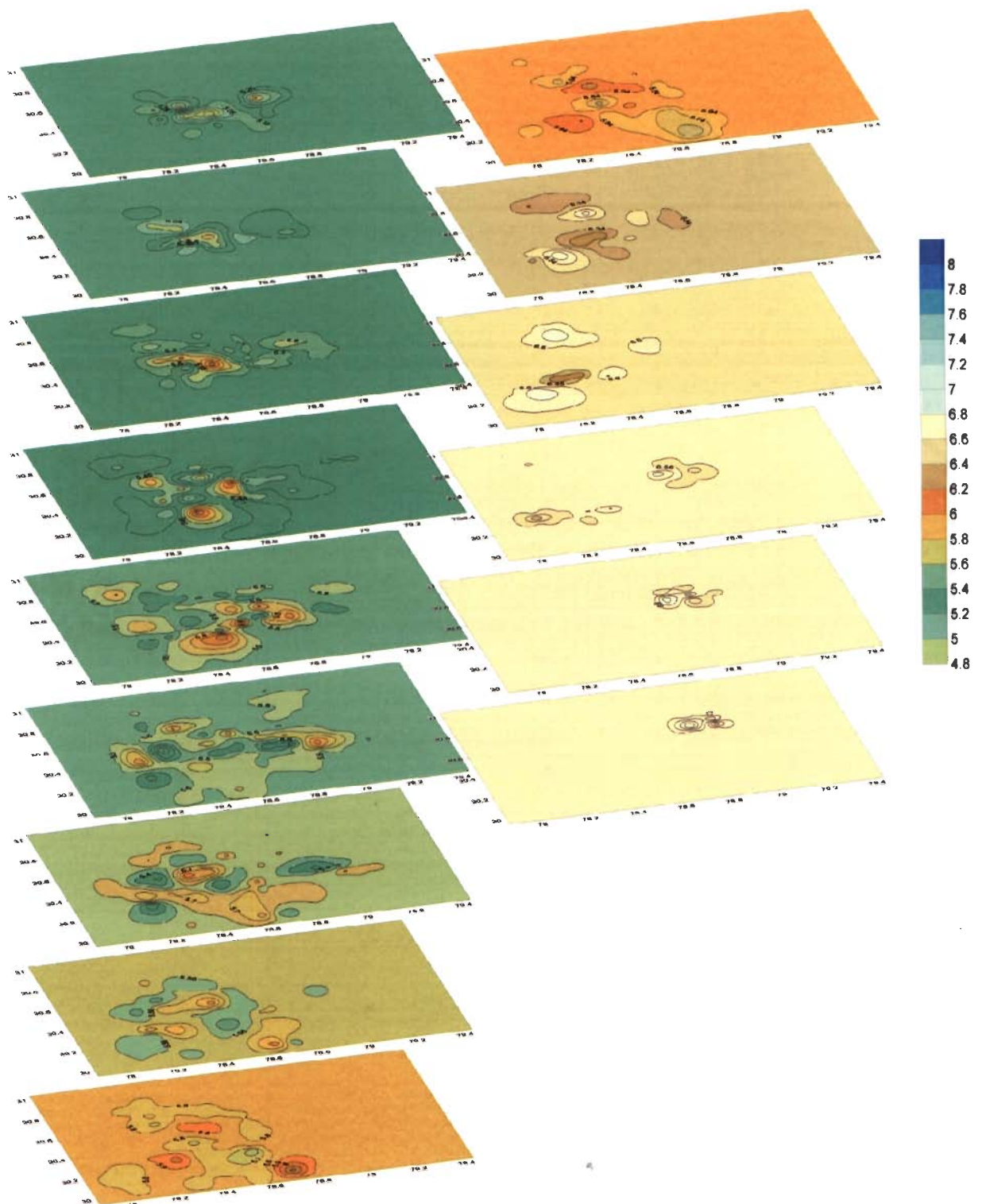


Fig. 5.8 Depth slices of 3-D Model I for east-west gridding

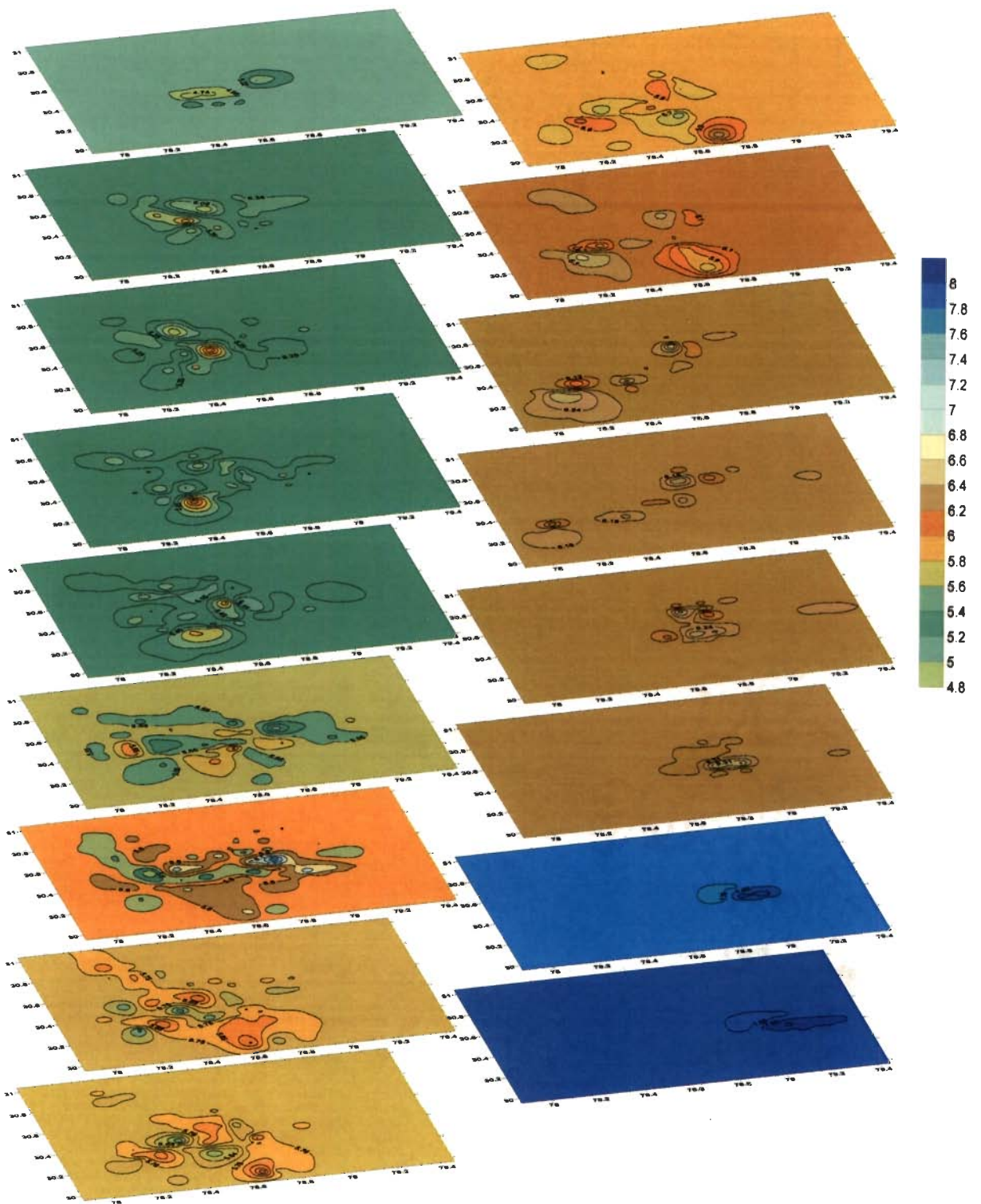


Fig. 5.9 Depth slices of 3-D Model II for east-west gridding

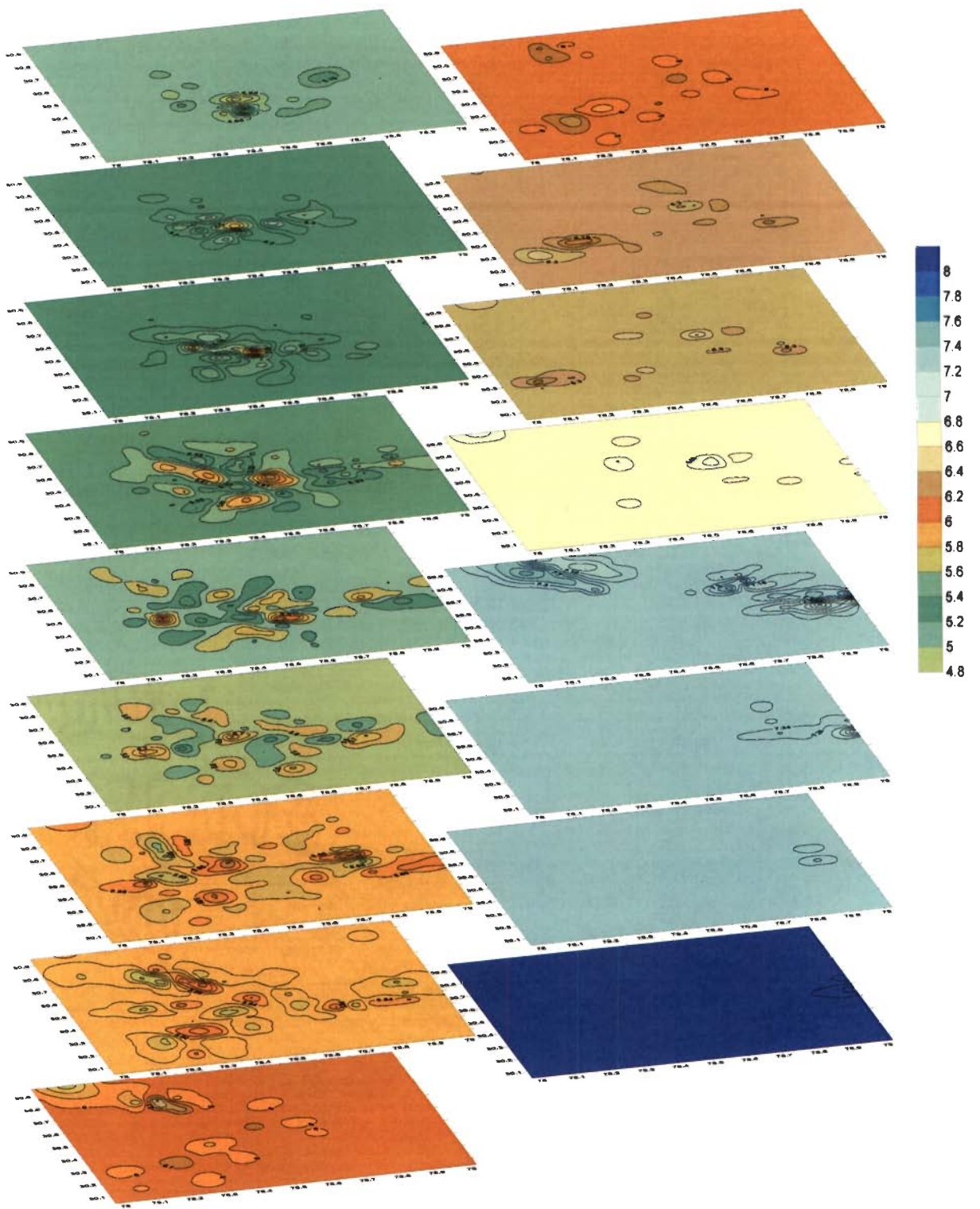


Fig. 5.10 Depth slices of 3-D Model III for east-west gridding

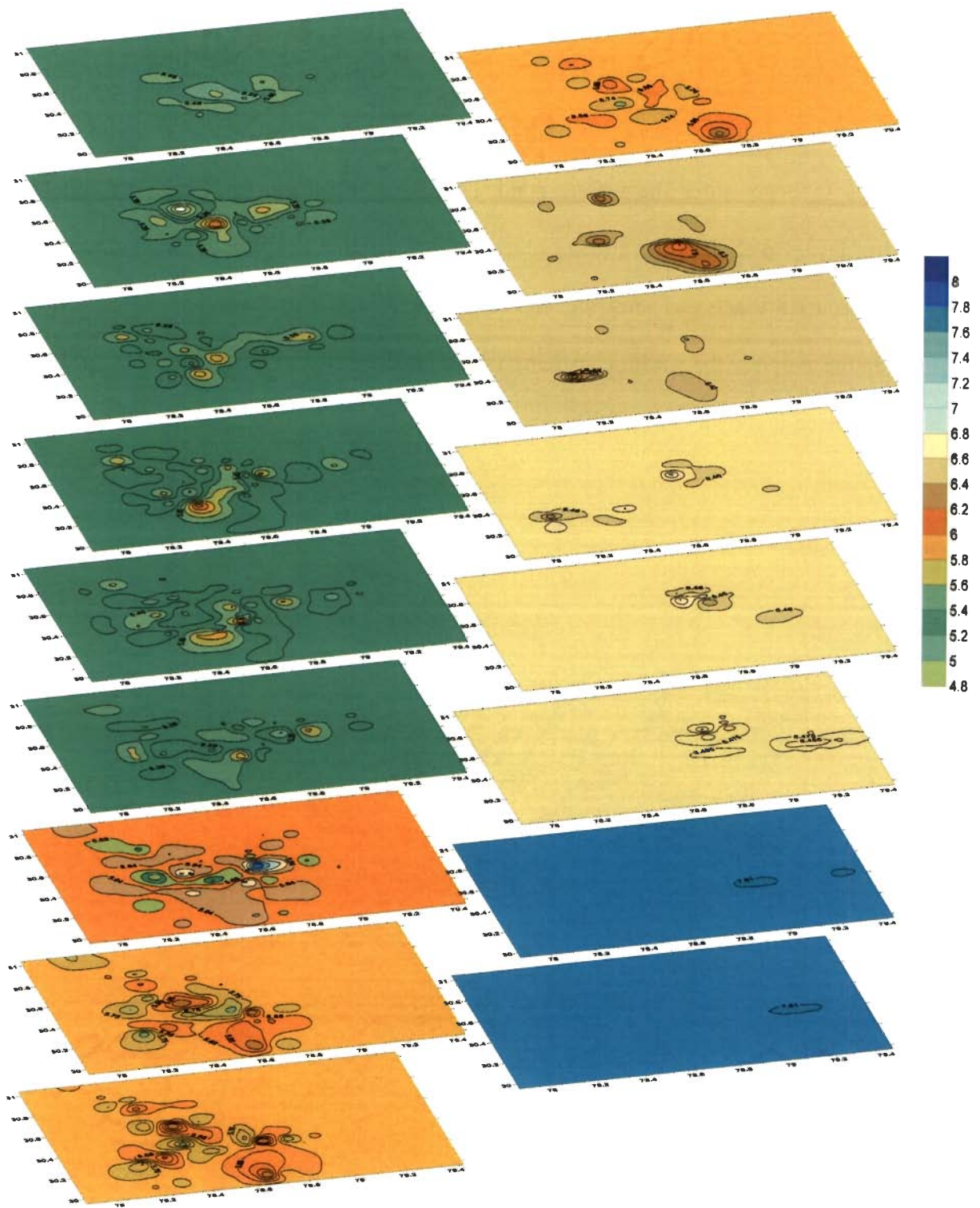


Fig. 5.11 Depth slices of 3-D Model IV for east-west gridding

5.4.3 3-D crustal velocity structure analysis for NE-SW gridding

The prevalent tectonic setting in the region shows the general trend as NE-SW. The results obtained in section 5.4.2 has encouraged to use a grid perpendicular to the regional features so as to better infer the underground anomalies in velocity structure beneath Garhwal Himalaya. Rotation of the grid coordinate system parallel to strike of the dominant structure can reduce artifacts and smearing, and equal spacing along structure can aid in interpretation. For the purpose the gridding pattern was rotated by 45° to the north. The gridding thus considered is shown in Fig. 5.12

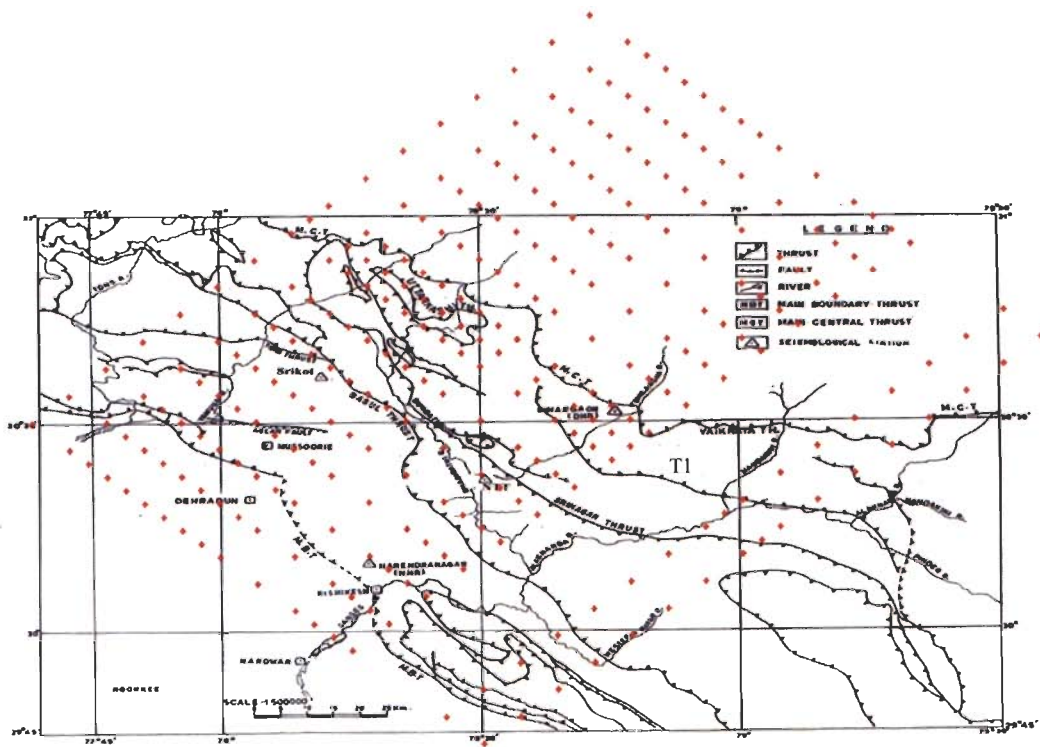


Fig. 5.12 Rotated gridding for the 3-D crustal velocity structure

The errors in hypocentral locations of the events in the 3-D simultaneous inversion in terms of coordinates of hypocentres and origin time along with their residuals for NE-SW gridding are given in *Appendix III*. For NE-SW gridding, the parameters KHIT, DWS and RESOLUTION are given in *Appendix III*. The maximum values of KHIT, DWS and RESOLUTION are summarized in Table 5.6 for the NE-SW gridding. The vertical profiles obtained by the 3-D analyses for NE-SW are given in *Appendix IV*. The depth slices obtained from the analysis using 3-D Model I, 3-D Model II, 3-D Model III and 3-D Model IV were given in Fig 5.13, Fig. 5.14 Fig. 5.15 and Fig. 5.16, respectively.

Table 5.6 Maximum values of the parameters KHIT, DWS and RESOLUTION for the NE-SW gridding

S. No.	Depth (km)	KHIT				DWS				RESOLUTION			
		M1	M2	M3	M4	M1	M2	M3	M4	M1	M2	M3	M4
1	2	97	97	96	98	2363	2189	1611	3416	0.58	0.58	0.44	0.65
2	4	91	93	71	85	2219	2394	897	1739	0.55	0.54	0.36	0.59
3	6	87	90	58	73	1570	1527	620	957	0.54	0.50	0.30	0.37
4	8	69	77	48	62	1329	1073	637	815	0.51	0.43	0.28	0.36
5	12	44	59	31	46	889	948	479	638	0.33	0.34	0.21	0.30
6	14	16	43	20	31	595	565	202	466	0.14	0.21	0.18	0.14
7	16	15	28	15	21	820	2073	663	1405	0.14	0.22	0.24	0.24
8	20	8	11	11	13	196	237	249	244	0.13	0.10	0.11	0.17
9	22	6	5	6	9	180	159	123	159	0.08	0.04	0.11	0.04
10	24	6	5	6	8	121	154	141	134	0.11	0.07	0.04	0.06
11	26	6	4	3	6	186	234	114	222	0.07	0.16	0.04	0.13
12	28	6	3	3	6	199	112	73	146	0.08	0.02	0.02	0.05
13	30	2	2	3	3	76	72	58	76	0.02	0.02	0.03	0.02
14	32	2	2	4	3	118	115	128	121	0.05	0.07	0.21	0.06
15	44	1	3	3	3	99	92	207	115	0.01	0.06	0.03	0.05
16	46	0	2	2	2	2	59	40	51	0.00	0.03	0.01	0.02
17	48	-	2	2	2	-	114	94	41	-	0.04	0.05	0.02

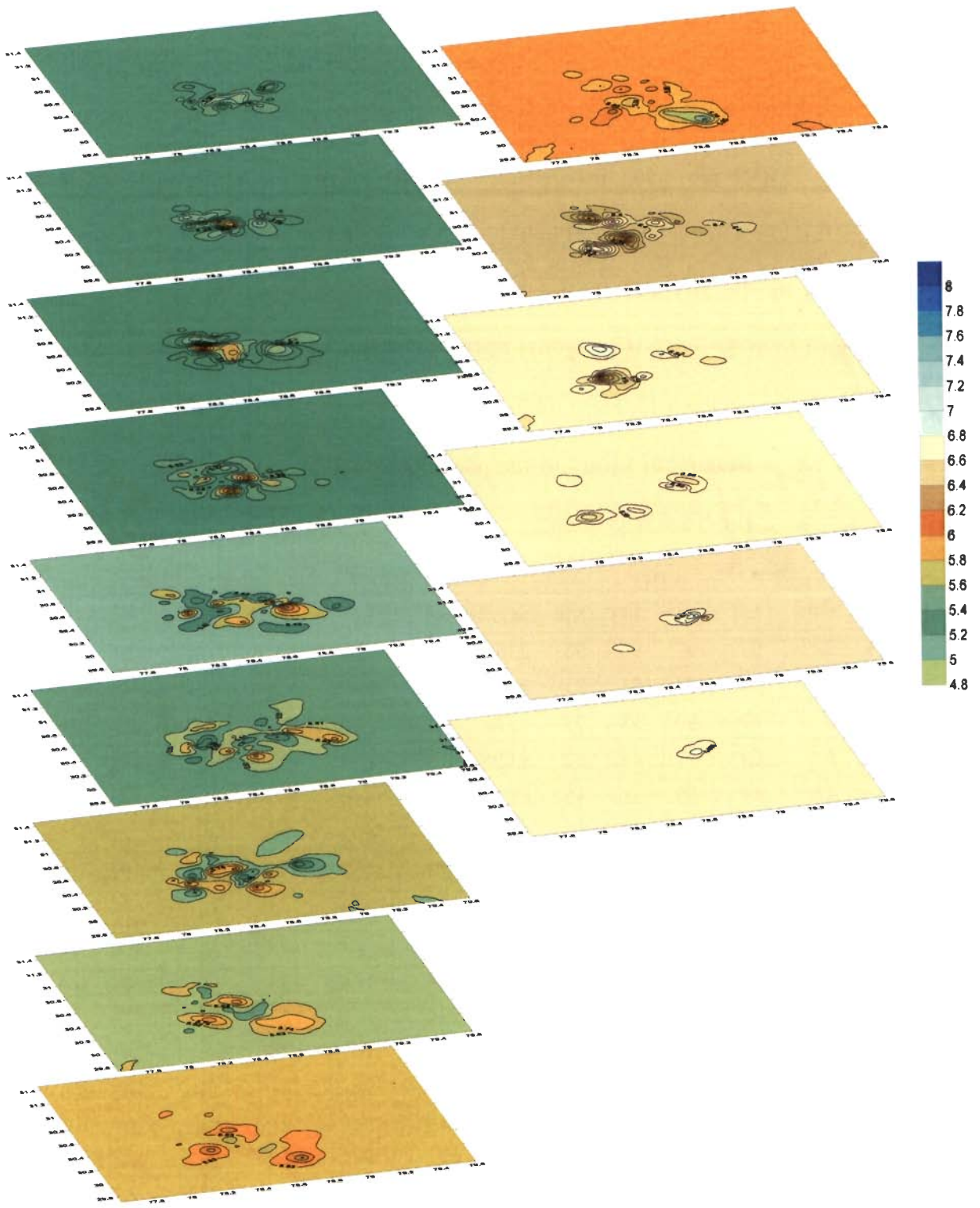


Fig. 5.13 Depth slices of 3-D Model I for NE-SW gridding

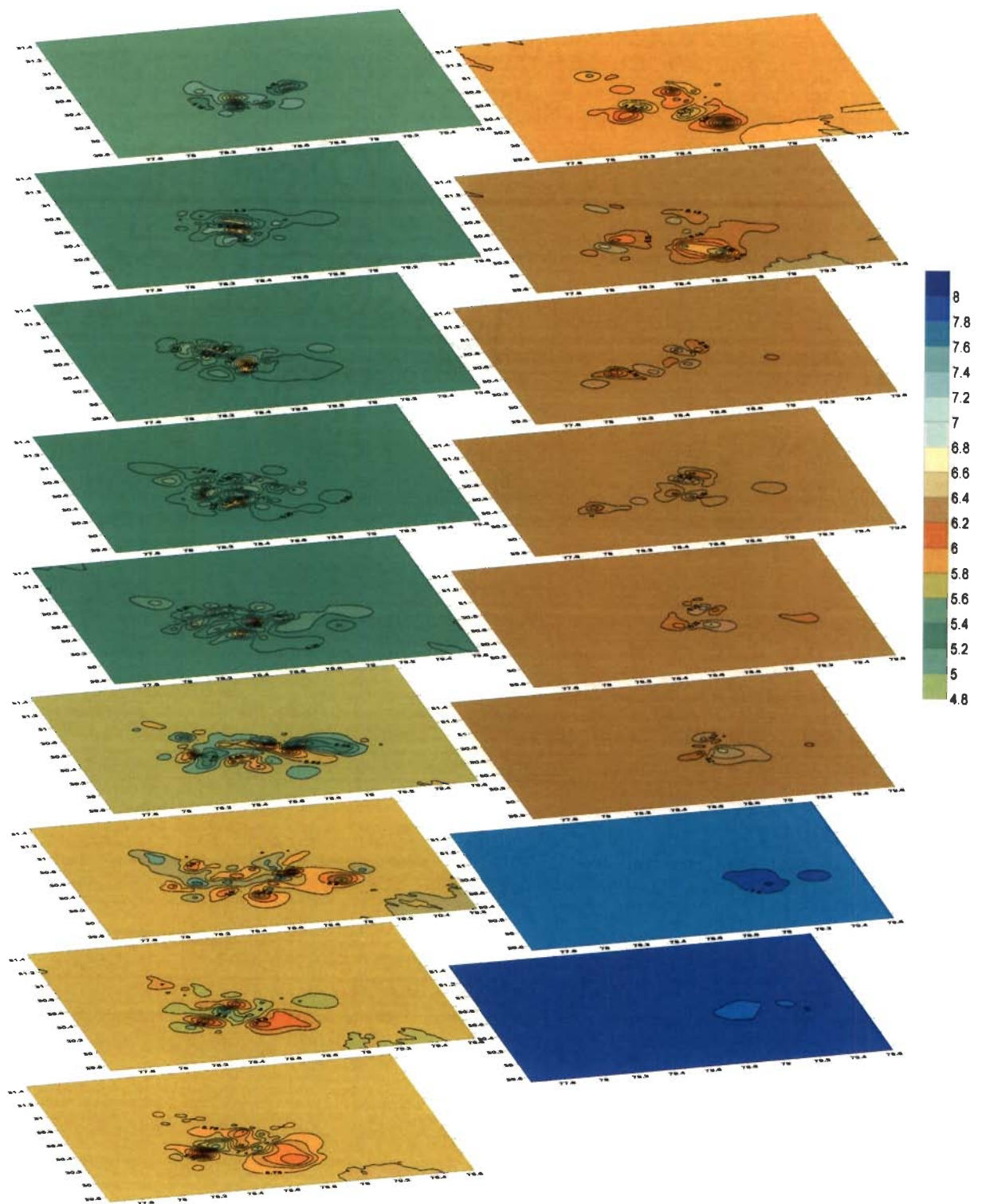


Fig. 5.14 Depth slices of 3-D Model II for NE-SW gridding

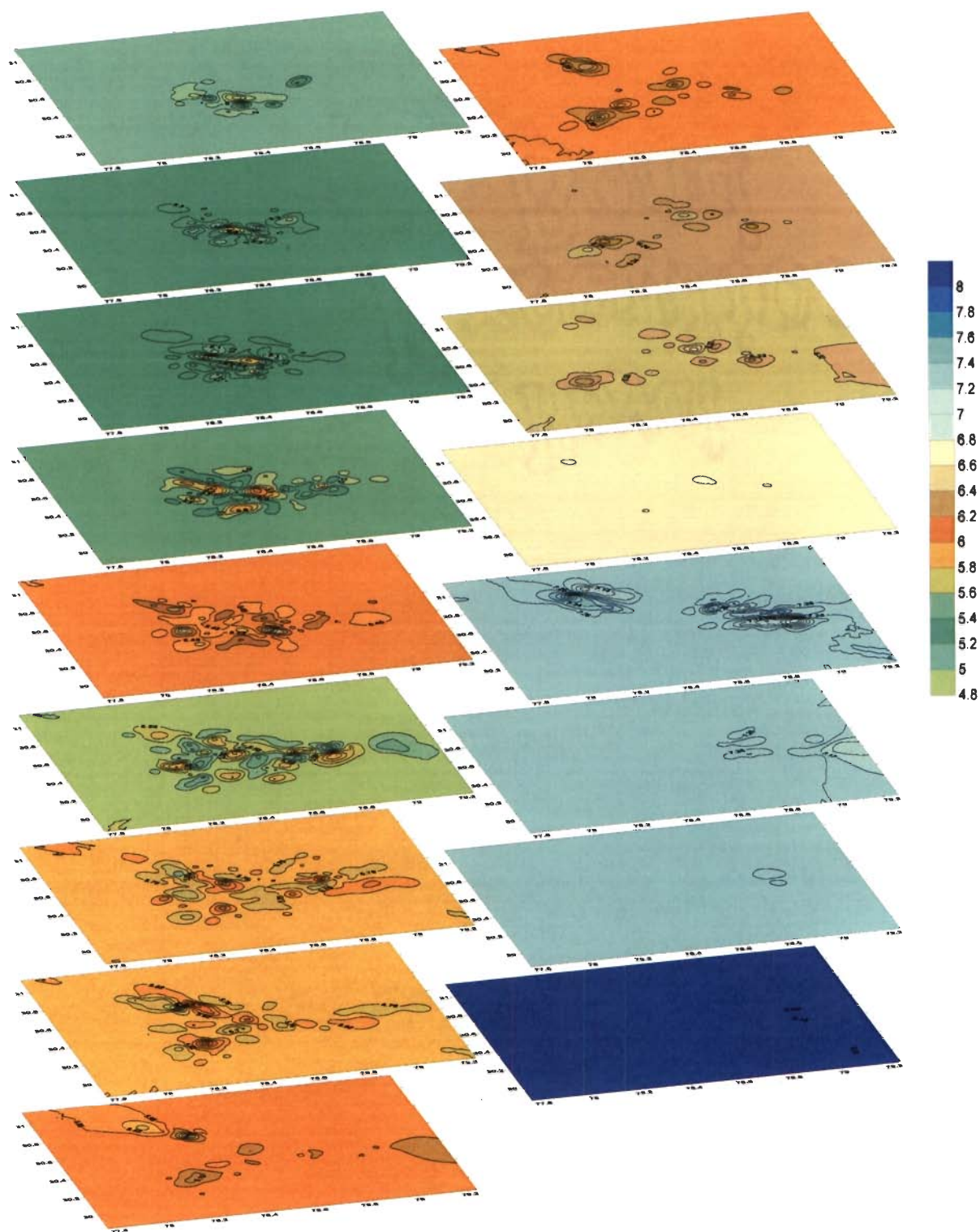


Fig. 5.15 Depth slices of 3-D Model III for NE-SW gridding

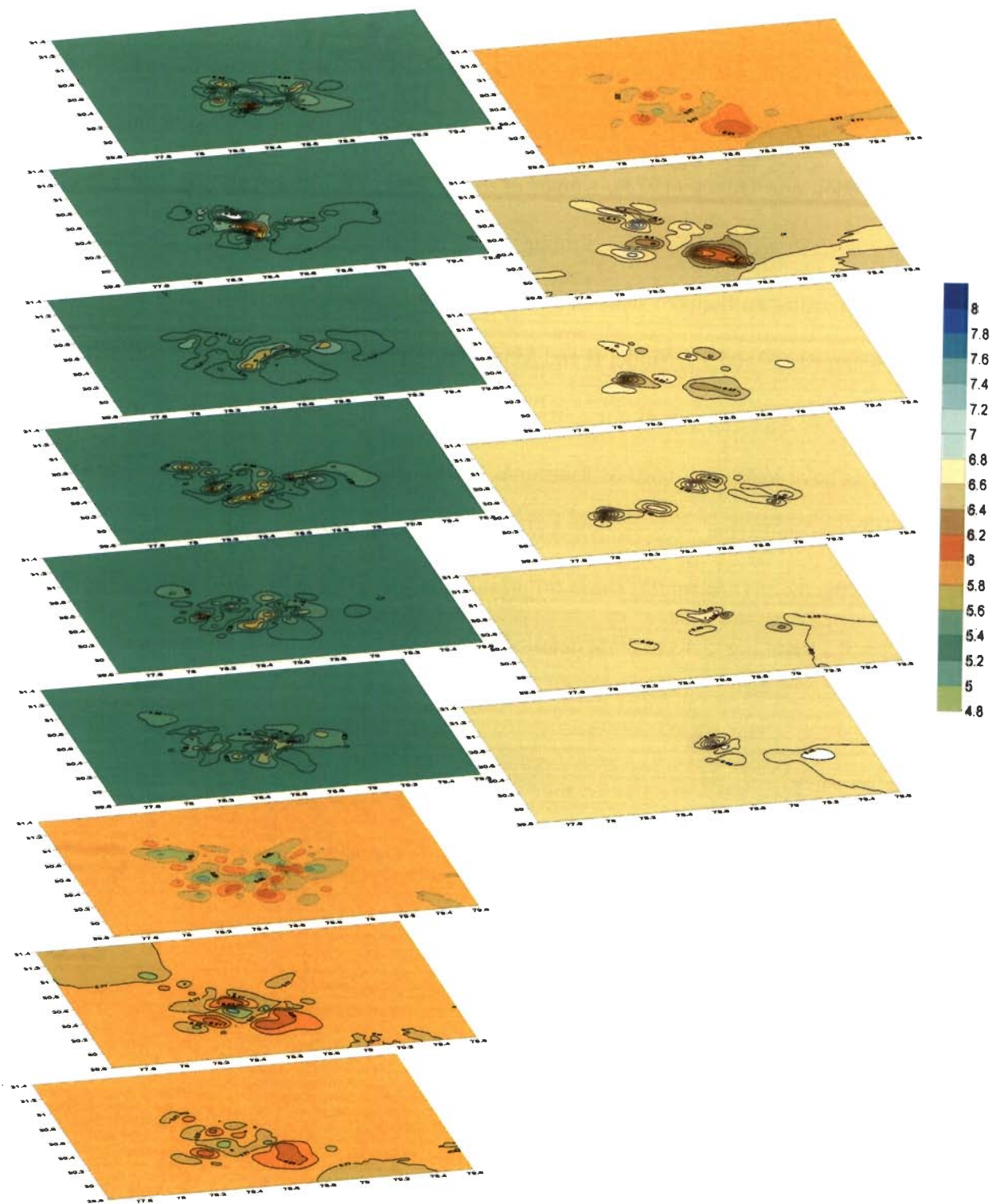


Fig. 5.16 Depth slices of 3-D Model IV for NE-SW gridding

5.5 Summary

The 3-D crustal velocity structure for Garhwal Himalaya has been estimated using 3-D velocity inversion technique namely *Local Earthquake Tomography*. Three models proposed by Tandon and Dubey (1973), Kumar *et al.*, (1994) and Mukhopadhyay and Kayal (2003) have been considered for 1-D simultaneous inversion using *VELEST*. The output of 1-D analysis using earthquake data acquired through digital telemetered array in Garhwal has been named as Model I, Model II and Model III. The average 1-D model based on these three models has been proposed for Garhwal Himalaya and named as Model IV. These four models have been then used as minimum 1-D models for 3-D inversions. Using two of the gridding namely east west and NE-SW, the 3-D crustal velocity structure has been estimated. While the depth (horizontal) slices for all the four models and two gridding are shown in Fig. 5.8 to 5.11 and Fig. 5.13 to 5.16, detailed vertical profiles are given in *Appendix IV*.

RESULTS AND DISCUSSIONS

6.1 Introduction

The 3-D inversions made using *Local Earthquake Tomography* (LET) has produced high resolution images of individual seismogenic zones and better interpretation of seismotectonic setup of many areas in past (Nishizawa *et al.*, 1990; Hino *et al.*, 1996; Eberhart-Phillips and Reyners, 1999; Husen *et al.*, 1999, 2000, 2002; Shinohara *et al.*, 1999; Obana *et al.*, 2003). In the present study LET has been used to estimate the 3-D crustal velocity structure of the Garhwal Himalaya. The present chapter describes the results obtained and their validation and interpretation in terms of prevailing tectonics of the region. The validation of results is generally carried out by its comparison to the real world. In the present case also the surface manifestations of the geological discontinuities due to tectonic movements have been considered for matching with the velocity distribution obtained in form of 3-D crustal velocity structure beneath the study area.

The geology and tectonics of the Garhwal Himalaya has been described in Chapter 3. Specifically, surface evidences of the geological features and the traverses given by Valdiya (1980) have been used to validate and interpret the results.

6.2 3-D crustal velocity structures for Garhwal Himalaya

The KHIT, DWS and the RESOLUTION are the three parameters which have been used to identify the vertical profiles which have to be further used to interpret the results in form of the prevailing tectonics of the region. While KHIT is the number of hit counts in a specific cell, DWS takes into account the number of rays that samples each cell and considers the normalized length of each ray within the cell and an observational weight for that specific ray. A large DWS indicates that velocity at the grid point is based on large body of data. RESOLUTION describes the extent to which the data can be resolved. The values of these parameters have been summarized in Table 5.5 and 5.6 in Chapter 5 for the maximum values obtained from east-west gridding and NE-SW gridding, respectively. *Appendix III* contains the plots of the parameters KHIT, DWS, RESOLUTION for depth slices obtained using east-west and NE-SW gridding.

An endeavor has been made to match the surface manifestations of the tectonic features with the 3-D velocity anomalies as estimated using 3-D velocity inversions and plotted as vertical profiles. The tectonic features as marked in Fig. 5.7 for east west gridding and in Fig. 5.12 for NE-SW gridding have been used for the interpretations. For example, Basul Thrust and Dunda Thrust have been matched with the velocity distribution patterns in the vertical profile obtained for the east-west gridding for *Profile 7* using 3-D Model IV as shown in Fig. 6.1.

The following section describes the validations of the 3-D inversion results by way of matching the various tectonic features on the vertical profiles from different models and the two gridding considered for 3-D velocity inversions.

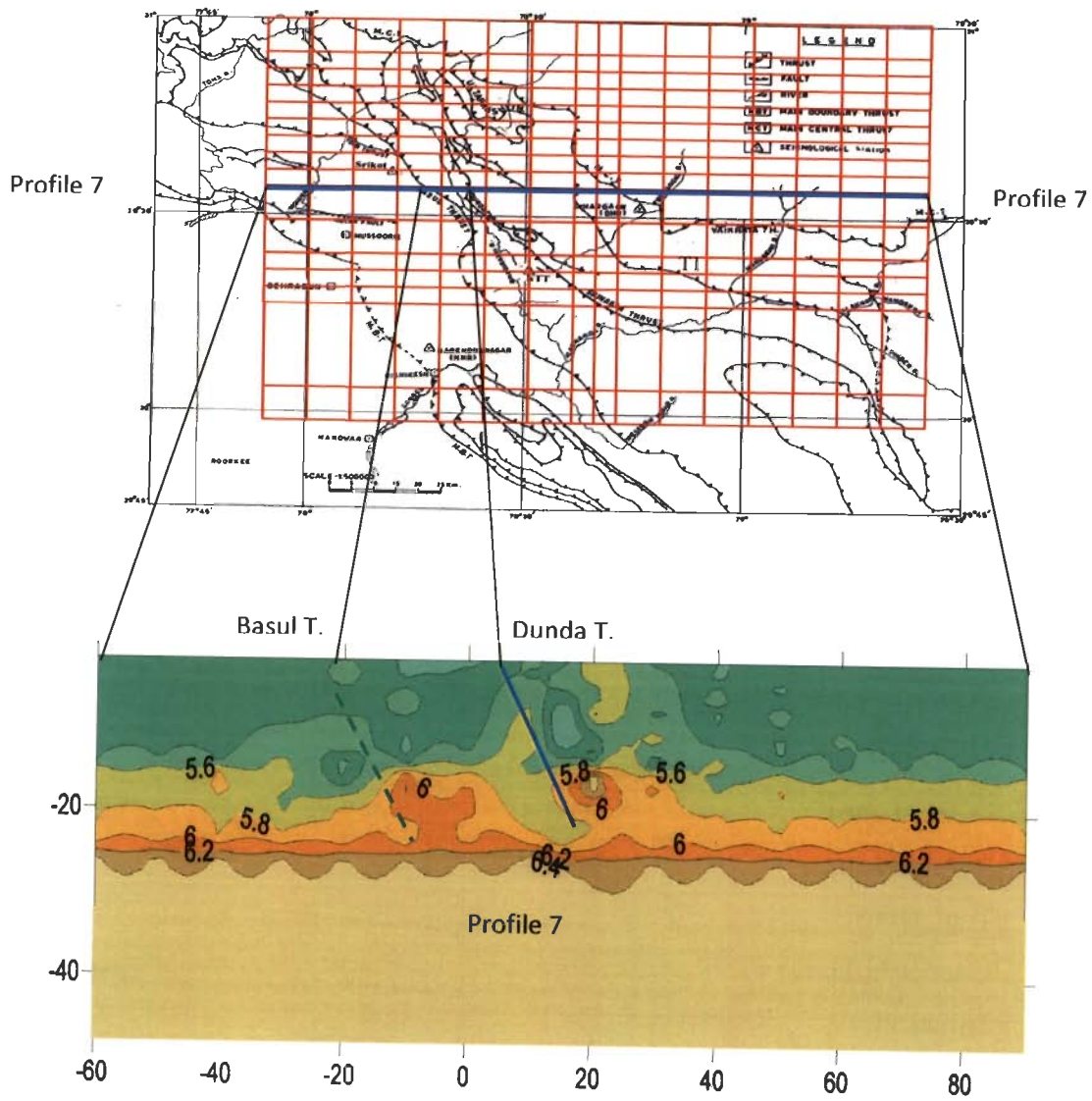











Fig. 6.1 An example of interpretation of tectonic features on vertical profiles.

6.2.1 East-West gridding

The vertical profiles as given in *Appendix IV* are the results of the 3-D inversions based on four models considered as initial minimum 1-D velocity models for 3-D inversions. The tectonic features which encompass the gridded area include Main Boundary Thrust, Main Central Thrust, Srinagar Thrust, Dunda Thrust, Basul Thrust, Tons Thrust, Thrust T1, Uttarkashi Thrust and Dunda Fault. The representation and color coding for these tectonic features used for marking on vertical profiles is given in Table 6.1.

Table 6.1 Representation of tectonic features on vertical profiles.

Sl. No	Tectonic features	Representation on vertical profiles
1	Main Boundary Thrust (MBT)	
2	Main Central Thrust (MCT)	
3	Srinagar Thrust	
4	Dunda Thrust	
5	Basul Thrust	
6	Tons Thrust	
7	Uttarkashi Thrust	
8	Thrust T1	
9	Dunda Fault	

The surface manifestations of the geological and tectonic features have been matched with the velocity distributions using 3-D Model I as shown in Fig. 6.2. As the outer nodes are less resolved, the actual representation of the medium is diminishing with distance from the center of the gridding on either side. The *Profiles 1 to 5* could not attain any results. Before

proceeding further, it may be noted that the interpretations are qualitative in terms of the matching of the surface manifestations and their down dip extensions in form of velocity distributions. The intrusion of relatively high velocity material can be seen near to the surface manifestations of Srinagar and Basul Thrusts in the *Profile 6*. Similarly, MCT could be marked on *Profile 7* at distance of about 60 km and on *Profile 8* at a distance of about 20 km from the center towards east. However, the high velocity material intrusion at a distance of 40 km towards west from the center in *Profile 6* could not be correlated to any of the geological or tectonic features. It may be noted that MBT is also present on the western side of the profile.

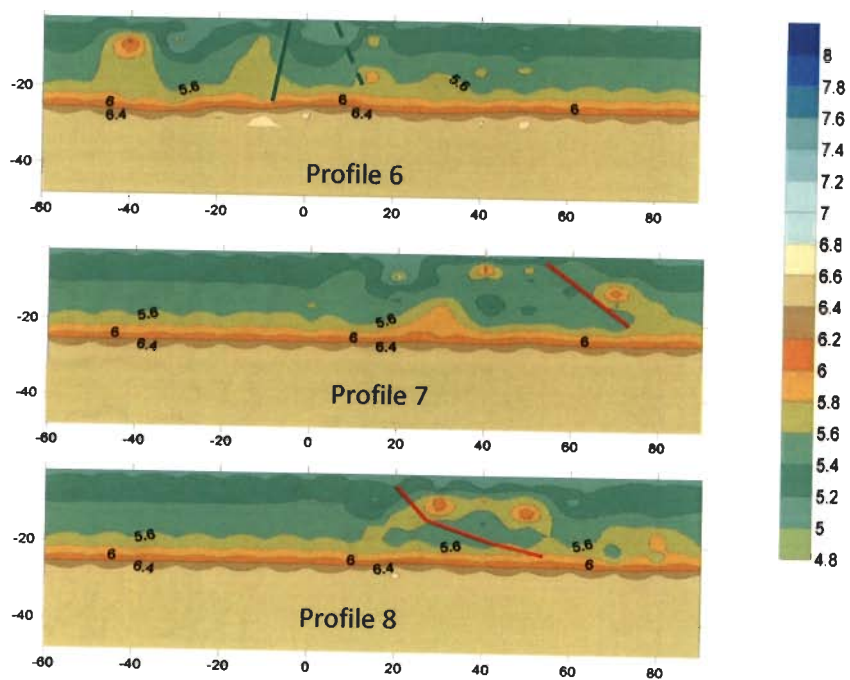


Fig. 6.2 Tectonic features marked on vertical profiles obtained using 3-D Model I for east-west gridding

The 3-D crustal velocity structure obtained using Model II as minimum 1-D velocity model has usable KHIT, DWS and resolution values upto a depth of 28 km (which is almost same for all the vertical profiles). In *Profile 6*, Srinagar Thrust and Basul Thrust were observed at a distance of 5 km on either side of the centre. While Srinagar Thrust is dipping southwardly, Basul Thrust was found to be dipping northwardly. The Dunda Thrust could be marked on *Profile 7* at a distance of 20 km from the centre. MCT was observed on *Profile 7* and *8*.

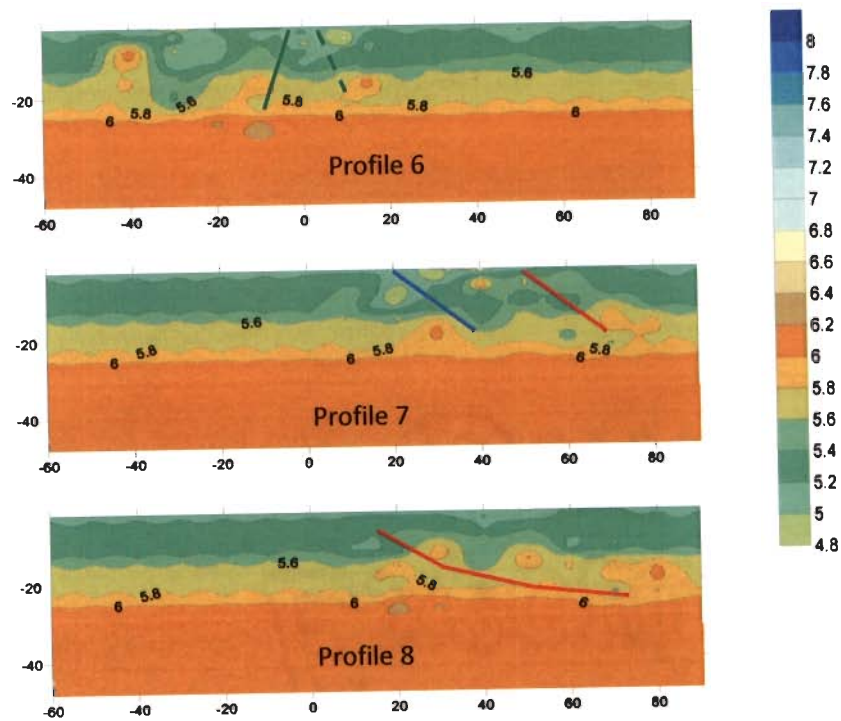


Fig. 6.3 Tectonic features marked on vertical profiles obtained using 3-D Model II for east-west gridding.

In case of the 3-D Model III, the vertical *Profiles 6, 7 and 8* as shown in Fig. 6.4 have been used for inferring about the tectonic features. Srinagar Thrust could be marked only on *Profile 6*. The pattern of velocity distribution in *Profile 7* revealed the location of MCT at a distance of 20 km from the centre in the east. The velocity distributions in *Profile 8* could not be interpreted in terms of location of any of the tectonic features falling in this profile as given in Fig. 6.4.

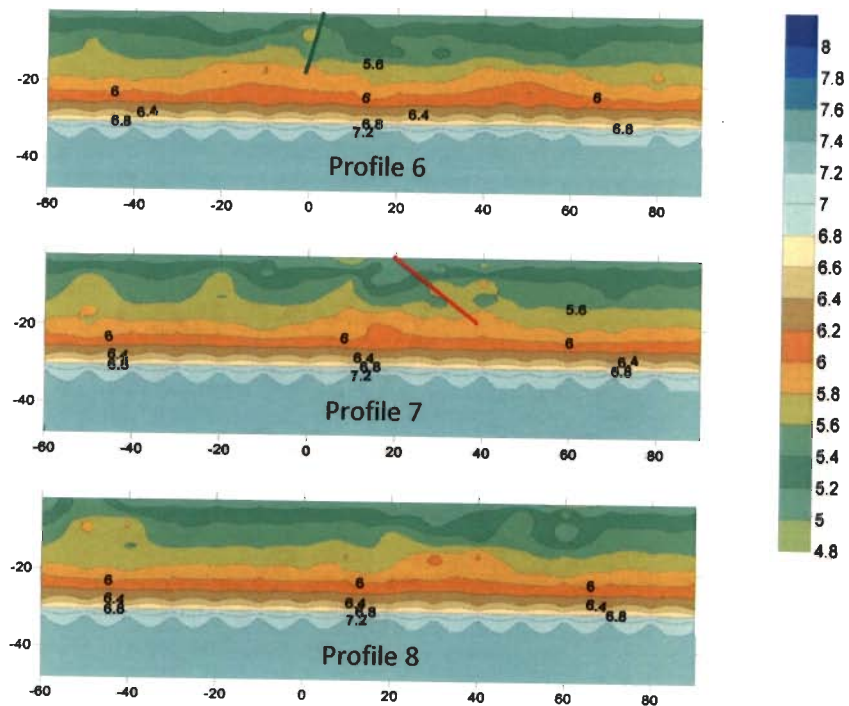


Fig. 6.4 Tectonic features marked on vertical profiles obtained using 3-D Model III for east-west gridding.

Basul Thrust is one of the features which has been observed in most of the profiles using different initial minimum 1-D velocity models. In case of 3-D Model IV, Basul Thrust has

been observed in *Profiles 3, 5, 6 and 7*. While Srinagar Thrust could be marked on *Profile 6*, Dunda Thrust can be seen on *Profile 7* at a distance of 5 km from the centre.

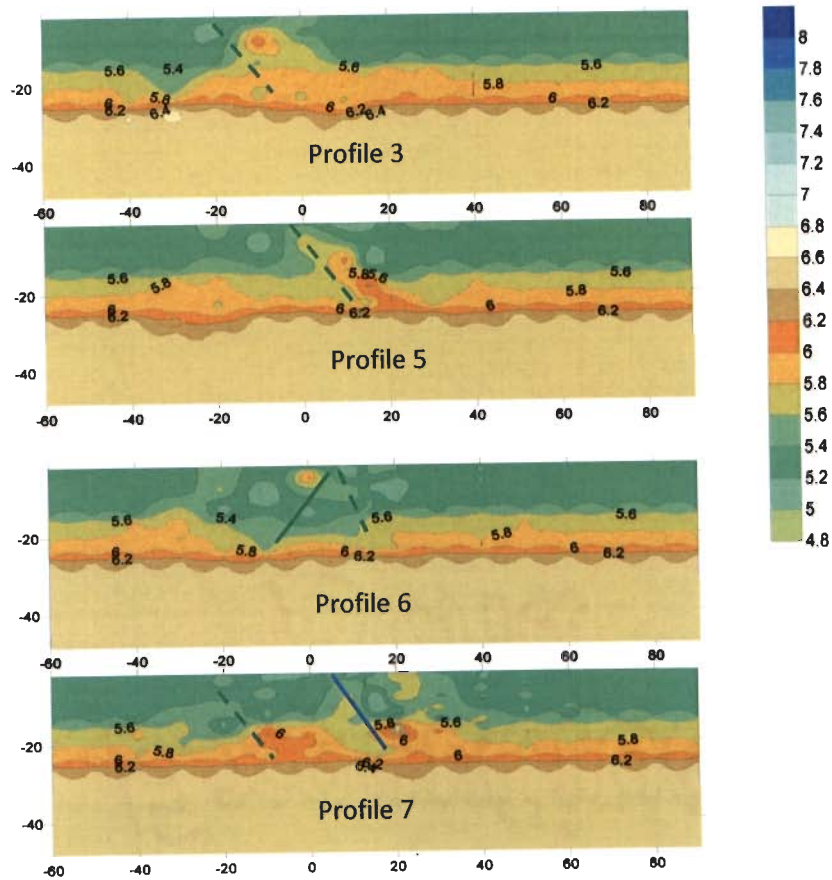


Fig. 6.5 Tectonic features marked on vertical profiles obtained using 3-D Model IV for east-west gridding.

One of the conspicuous features in Himalaya is the presence of detachment surface (Seeber *et al.*, 1981; Ni and Barazangi, 1984; Acharya and Narula, 1998). This detachment surface is present at a depth of about 15 km and is almost horizontal with a gentle dip of about 10-15°. The changes in the velocities at depth between 10 to 20 km match with this feature. Similar pattern in all the profiles reveals the presence of detachment surface. This seems to be a zone

of about 10-15 km thick with a velocity of about 5.6 km/sec at the top and about 6.0 km/sec at the bottom. The undulating pattern observed in the vertical profiles reveals that detachment surface is not an even surface and possibly participating in the tectonic process.

6.2.2 NE-SW gridding

The NE-SW gridding was obtained by rotating the east-west gridding by 45° so that profiles perpendicular to the general strike of the features in this region were obtained. Obviously, the velocity contrast in the dip direction is expected to be more using NE-SW gridding. The Srinagar Thrust could be marked even on *Profiles 3, 5, 6, 7 and 9* as shown in Fig. 6.6 using 3-D Model I. While Basul Thrust could be marked in *Profiles 3, 5, 6 and 8*, Dunda Thrust which is near to Basul Thrust could be marked only on *Profile 7*. Since the MBT position lies away from the centre in most of the profiles it could not be marked on any of the profiles. In *Profile 9*, Dunda Fault could be marked (Please see section 6.3). One of the thrust namely Thrust T1 (see Fig. 6.1) between MCT and Dunda Thrust was also observed on *Profile 4*.

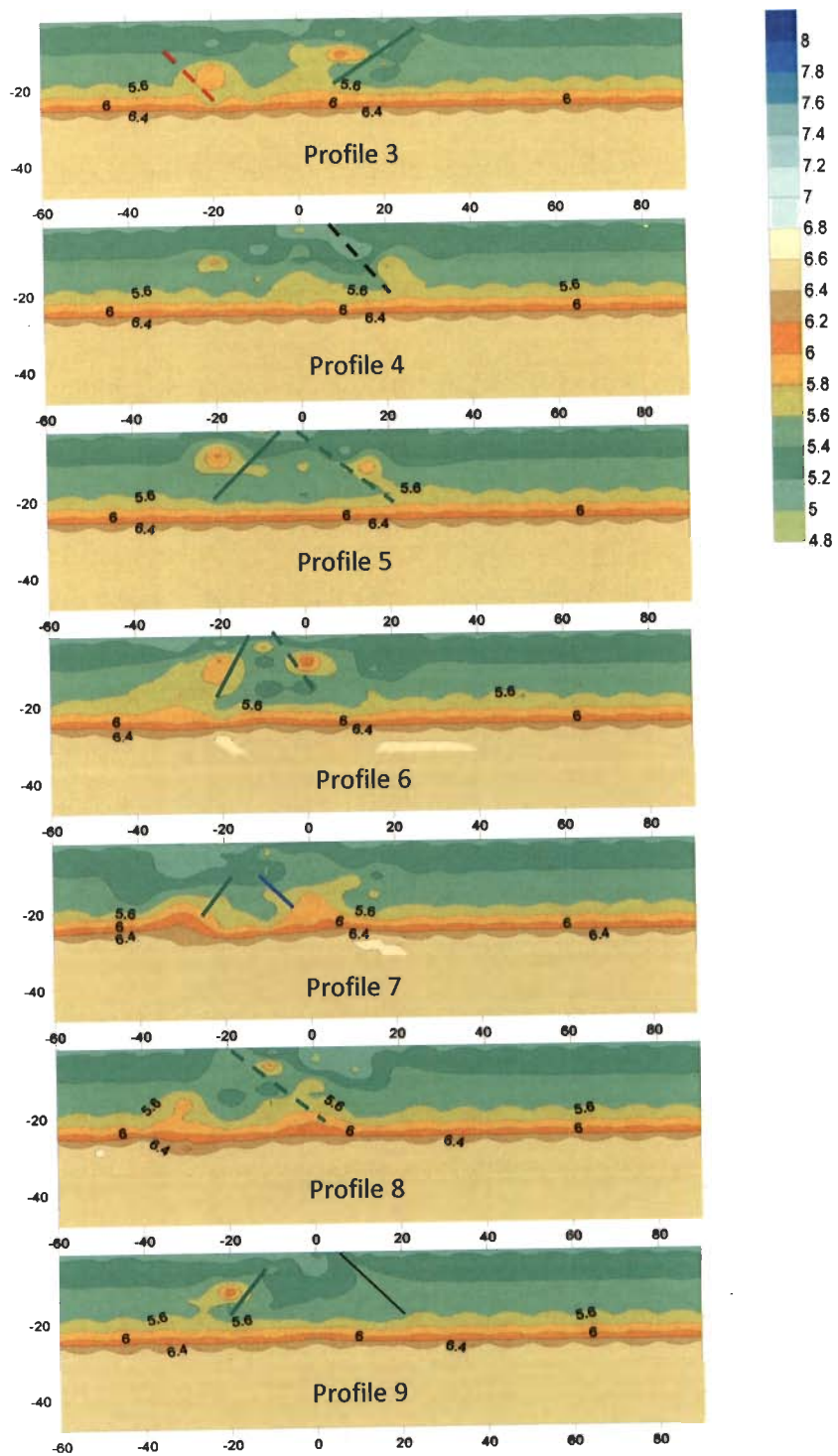


Fig. 6.6 Tectonic features marked on vertical profiles obtained using 3-D Model I for NE-SW gridding.

Using Model II as initial minimum 1-D model for 3-D inversions, tectonic features could be marked on *Profiles 4 to 8*. Thrust T1 could be seen on *Profile 4* at a distance of 5 km from centre towards east. In *Profiles 5, 6 and 8*, Basul Thrust was observed as given in Fig. 6.7. One of the profiles namely *Profile 6* could revealed the location of out of sequence thrust namely Srinagar Thrust. Dunda Thrust was marked on *Profile 7*.

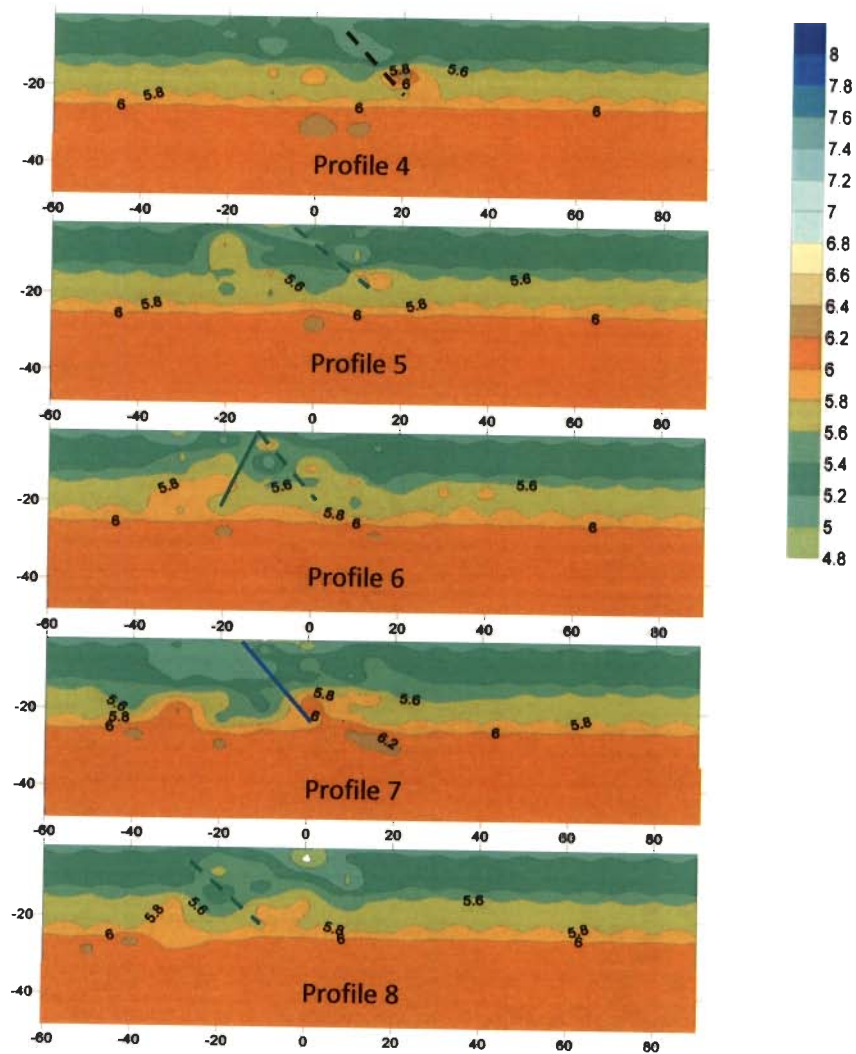


Fig. 6.7 Tectonic features marked on vertical profiles obtained using 3-D Model II for NE-SW gridding.

The velocity distributions estimated using Model III as the initial minimum 1-D model revealed the location of Dunda Thrust as marked on *Profiles 7, 8, 9 and 11*, Basul Thrust on *Profile 6 and 10* and Srinagar Thrust on *Profile 6 and 11* (Fig 6.8).

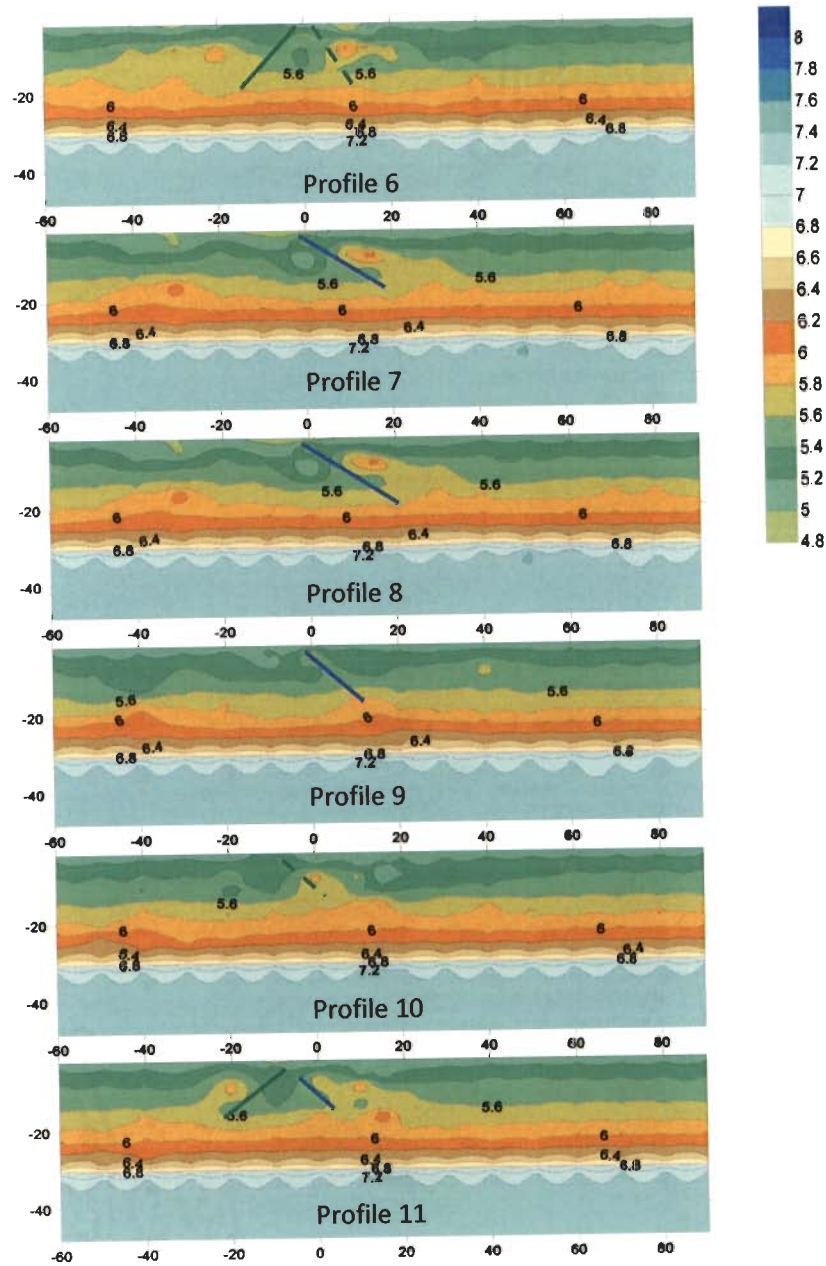


Fig. 6.8 Tectonic features marked on vertical profiles obtained using 3-D Model III for NE-SW gridding.

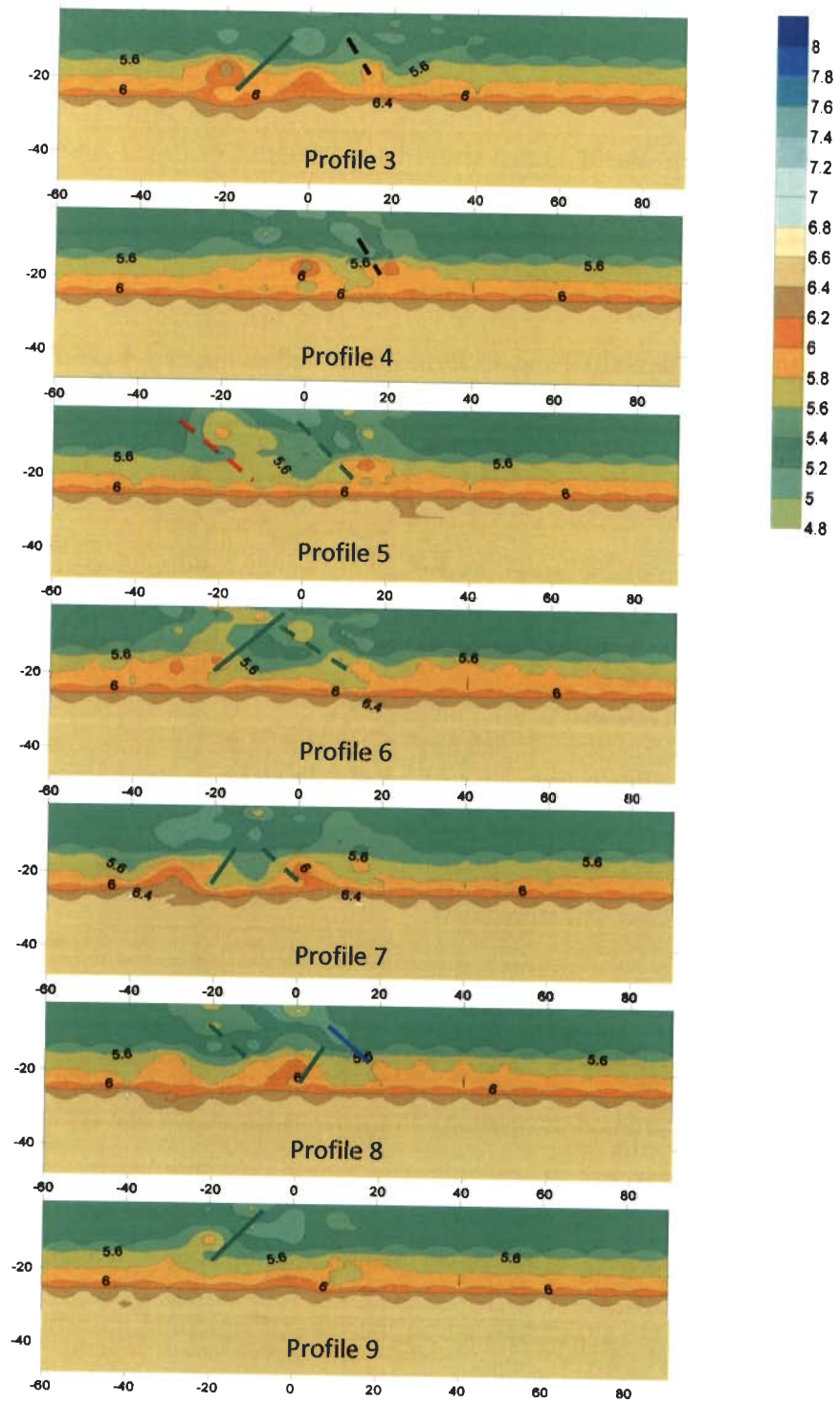


Fig. 6.9 Tectonic features marked on vertical profiles obtained using 3-D Model IV for NE-SW gridding..

In case of Model IV being used as initial minimum 1-D model for 3-D inversions, the *Profiles 3 to 9* obtained could be used for inferences made for the tectonic features as given in Fig 6.9. While the Basul Thrust could be marked on *Profile 5 to 8*, Srinagar Thrust was observed and marked on *Profile 3, 6, 7, 8 and 9*. Thrust T1 has been observed in *Profile 3 and 4*. In *Profile 5*, Main Boundary Thrust could be marked.

Similar patterns at depth of 10 to 15 km as observed in the east-west profiles have been also found in NE-SW profiles supporting the presence of detachment surface. The comparison of the tectonic features marked in Fig 6.2 to 6.9 using east-west gridding and NE-SW gridding supports the rotation of the gridding. Relatively better results have been obtained using the profiles which are drawn perpendicular to the strike direction of the tectonic features in Garhwal Himalaya. Based on the matching of the 3-D crustal velocity structure with the existing geological and tectonic features and relatively higher values of KHIT, DWS and RESOLUTION the 3-D Model IV estimated using the average 1-D velocity model (Model IV) is proposed for Garhwal Himalaya.

6.3 Matching of features with traverses

Valdiya (1980) has studied the geology in Garhwal Himalaya and reported many traverses in this region elucidating the lithotectonic settings. These traverses have been marked on the map and the cross sections of the traverses falling in the study area are shown in *Appendix I*. All these traverses are superimposed on the NE-SW gridding and shown in Fig. 6.10. An attempt has been made in this section to compare these cross sections with the vertical profiles obtained through 3-D crustal velocity structure analyses.

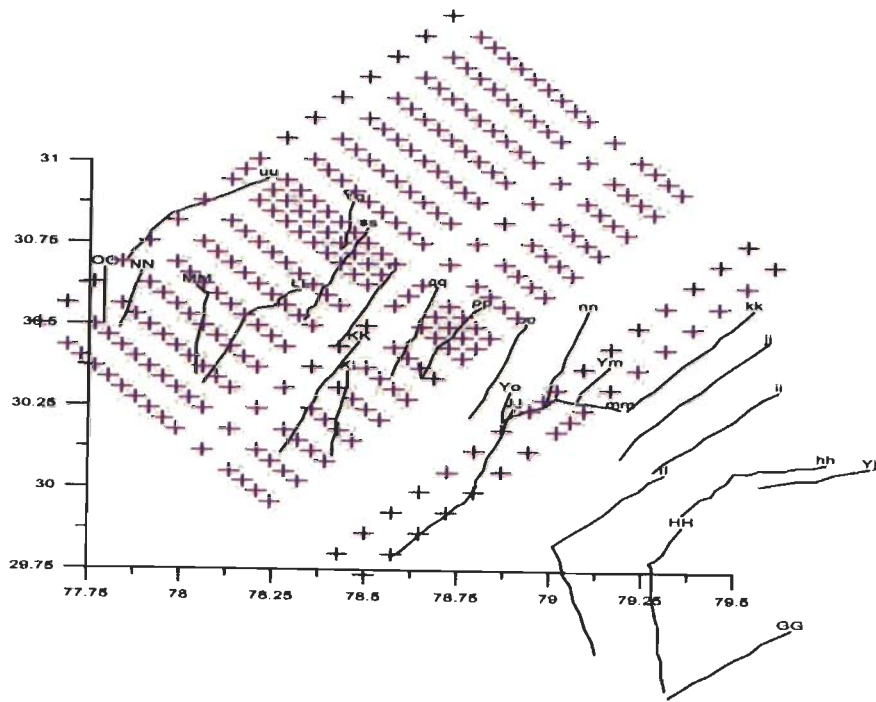


Fig. 6.10 Location of traverses reported by Valdiya (1980) in Garhwal Himalayas along with the NE-SW gridding

The traverse namely, *GG, HH, Yj, HH, ll, ii, jj, kk* are falling outside the grid being taken in the present study. Further the traverses *uu, OO, NN, mm, Ym, JJ, Yo, nn* and *oo* are falling in the areas which are less resolvable as evident from the low values of *KHIT, DWS* and *RESOLUTION* parameters. Therefore, all these traverses have not been considered for comparison with the vertical profiles obtained through 3-D inversion in the present study. The traverses *pp, qq, KK* and *ss* were only used to match the features in the vertical profiles namely *Profile 5, 6* and *9*.

The traverse *pp* reported by Valdiya (1980) runs from Gadolia to Ghuttu for about 33 km in the direction $S5^{\circ}E$ to $N29^{\circ}E$. This traverse approximately matches with *Profile 5* of NE-SW gridding considered in the present study and mainly encompasses Srinagar Thrust in the

starting, then Berinag Thrust, Bhatwari Thrust and Munsiri Thrust (Please see *Appendix I*). On regional basis, as given in Fig. 5.6 the profile encompasses MBT, Basul Thrust, Srinagar Thrust, Thrust T1 and MCT. Fig. 6.11 shows the portion of the traverse *pp* falling on *Profile 5* of 3-D Model I. The figure reveals the location of Basul Thrust which probably represents Berinag Thrust in the traverse *pp*. Srinagar Thrust is falling towards left of the profile and is given in Fig 6.11. The location of Basul Thrust could be marked on *Profile 5* of 3-D Model II and IV as shown in Fig. 6.12 and 6.13, respectively.

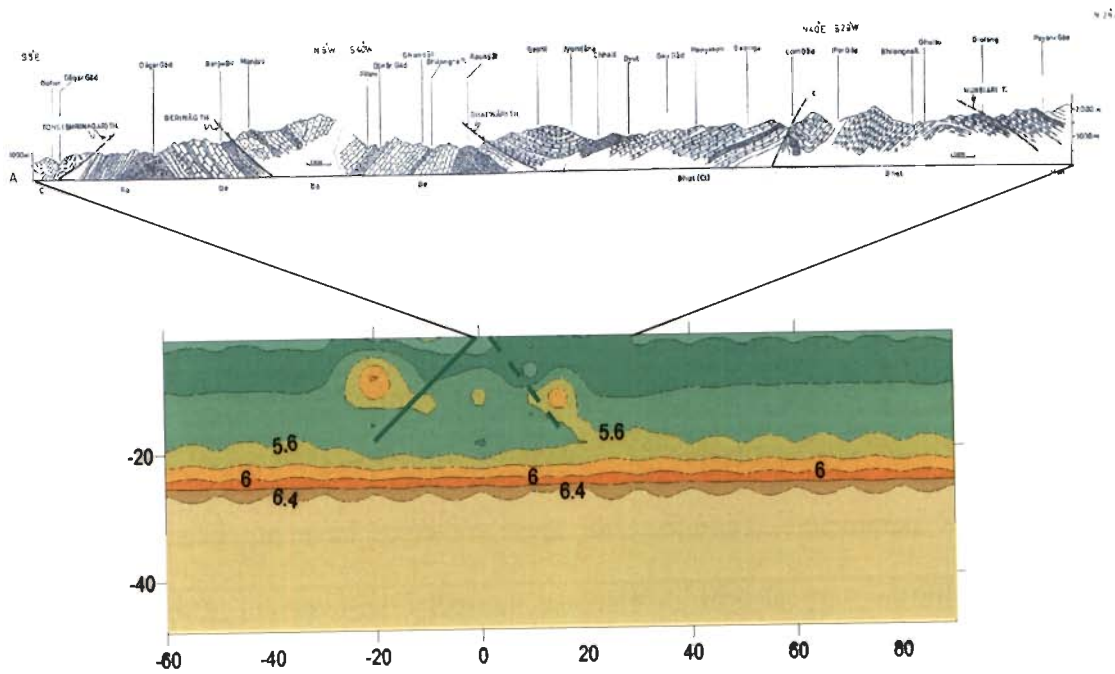


Fig. 6.11 Matching of traverse *pp* with profile 5 of 3-D Model I

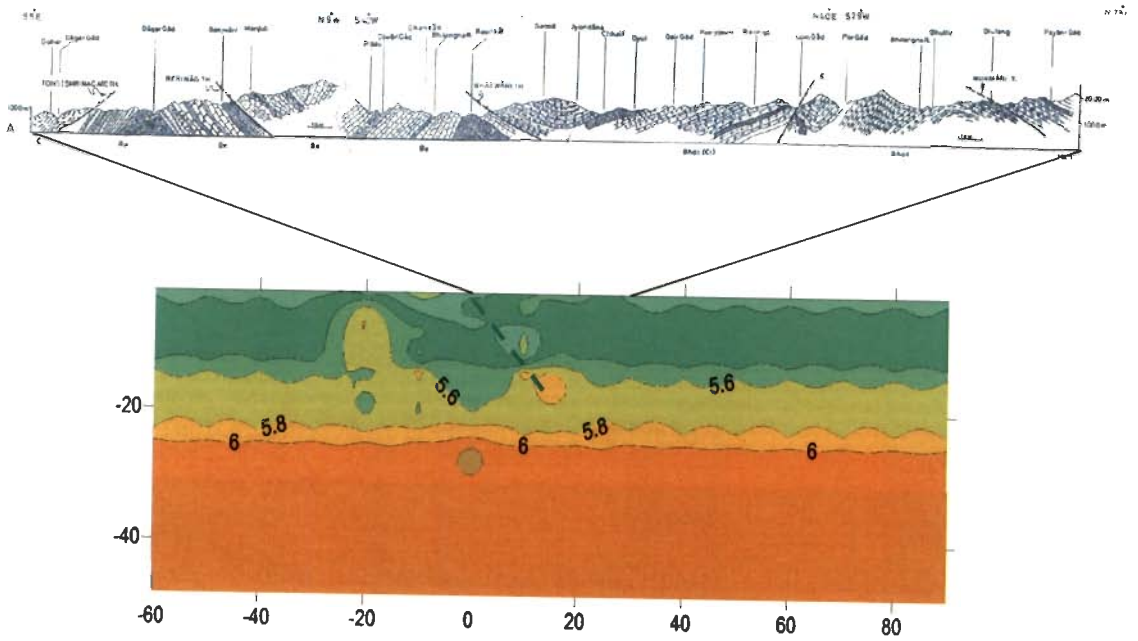


Fig. 6.12 Matching of traverse *pp* with profile 5 of 3-D Model II

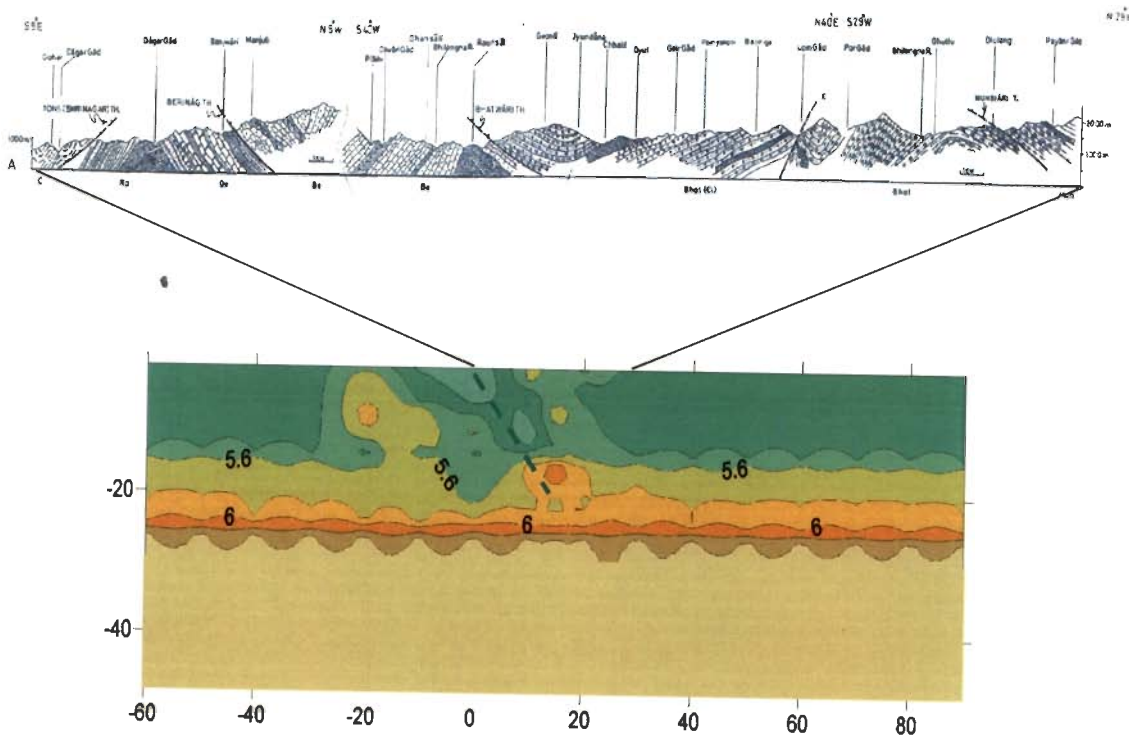


Fig. 6.13 Matching of traverse *pp* with profile 5 of 3-D Model IV

Two of the traverses reported by Valdiya (1980) between Jakhand to Tankhand and Gadolia to Budhakedar in the Bhilangana valley have been represented as traverse *qq* (see *Appendix I*). First section between Jakhand to Tankhand matches with a section of *Profile 6* of NE-SW gridding in the present study. The traverse has been drawn in the direction S50°W to N50°E. This section mainly encompasses the Srinagar Thrust, Berinag Thrust and Bhatwari Thrust. Both the thrust namely Srinagar Thrust and Berinag Thrust matches with the velocity distribution of *Profile 6* of 3-D Model I as shown in Fig. 6.14. Same pattern can be observed in *Profile 6* of 3-D Model II (Fig. 6.15). However, Srinagar Thrust could not be seen in *Profile 6* of 3-D Model III but Basul Thrust (Berinag Thrust) could be marked as shown in Fig. 6.16. A good matching of these thrust was also found with *Profile 6* of 3-D Model IV as shown in Fig. 6.17. It may be noted that Srinagar Thrust is dipping southwardly in the traverse *qq* as well as *Profile 6* of 3-D Model I, II and IV.

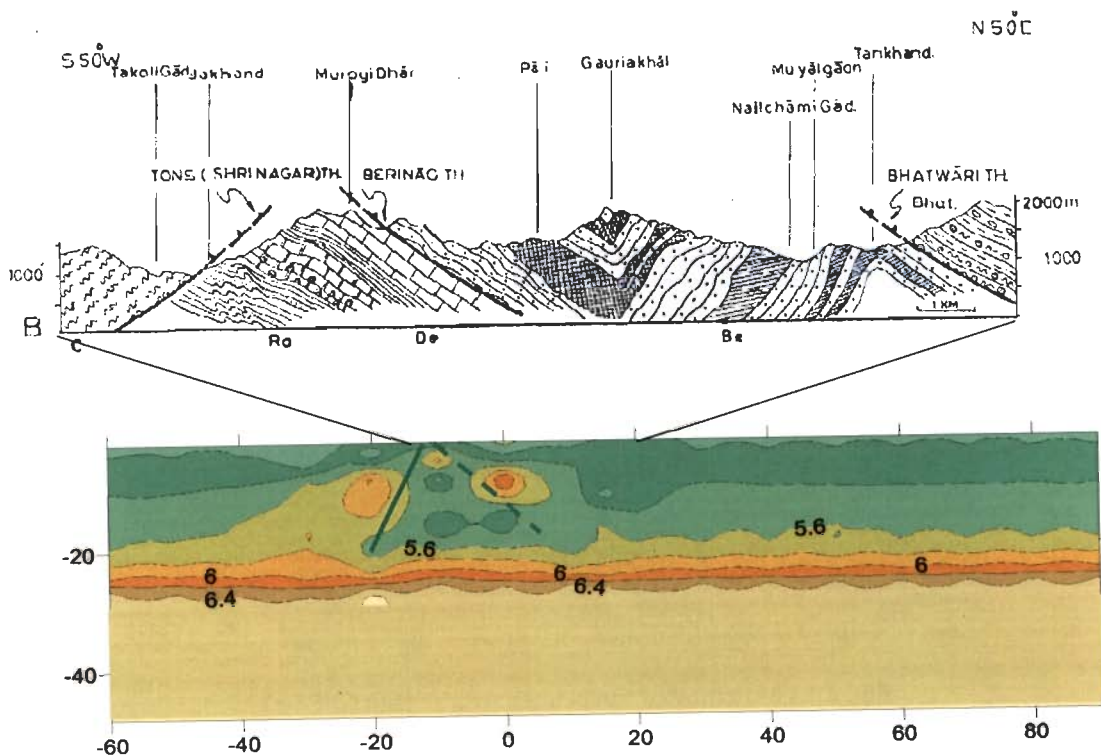


Fig. 6.14 Matching of traverse *qq* with *Profile 6* of 3-D Model I

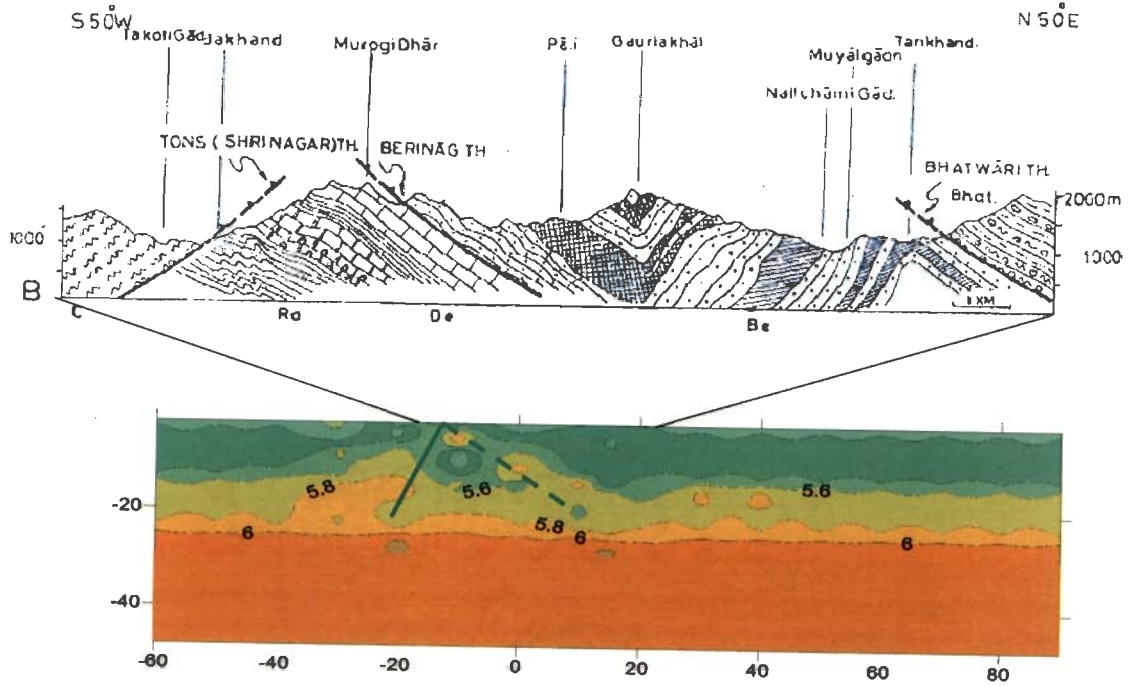


Fig. 6.15 Matching of traverse *qq* with Profile 6 of 3-D Model II

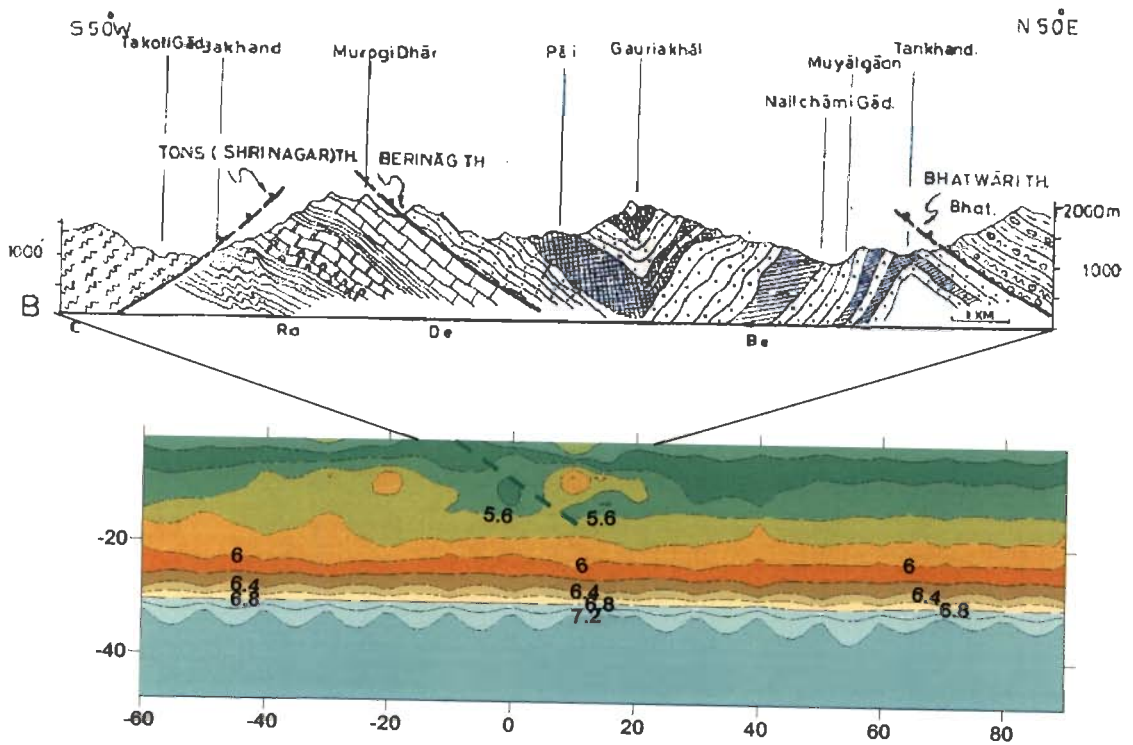


Fig. 6.16 Matching of traverse *qq* with Profile 6 of 3-D Model III

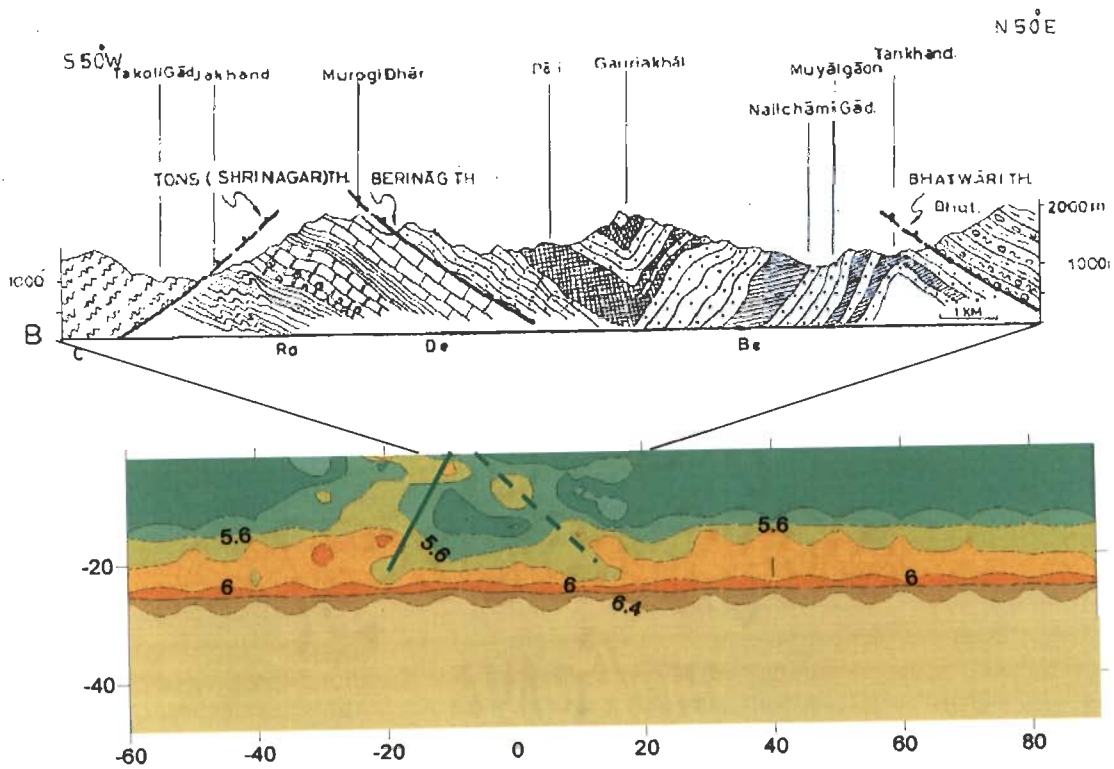


Fig. 6.17 Matching of traverse *qq* with *Profile 6* of 3-D Model IV

The traverse *KK* reported by Valdiya (1980) consists of two sections of about 18 km each running $S28^{\circ}W$ to $N28^{\circ}E$ and $S40^{\circ}W$ to $N40^{\circ}E$. This traverse matches with *Profile 6* of the present study. This traverse mainly encompasses Krol Thrust to the south with some part of Tons Thrust in the north. Only the Tons Thrust (matching with the location of Srinagar Thrust) could be observed in *Profile 6* of 3-D Model I and II as shown in Fig. 6.18 and Fig 6.19, respectively. This thrust was not clearly seen in *Profile 6* of 3-D Model III and 3-D Model IV as shown in Fig. 6.20 and Fig. 6.21, respectively.

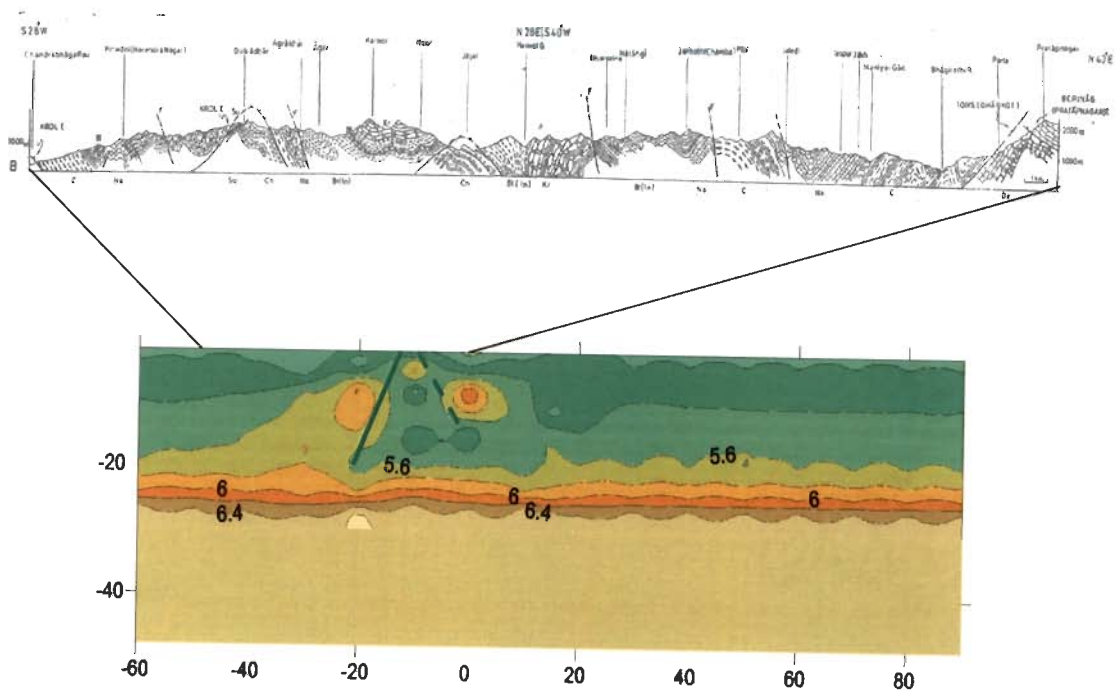


Fig. 6.18 Matching of traverse *KK* with *Profile 6* of 3-D Model I

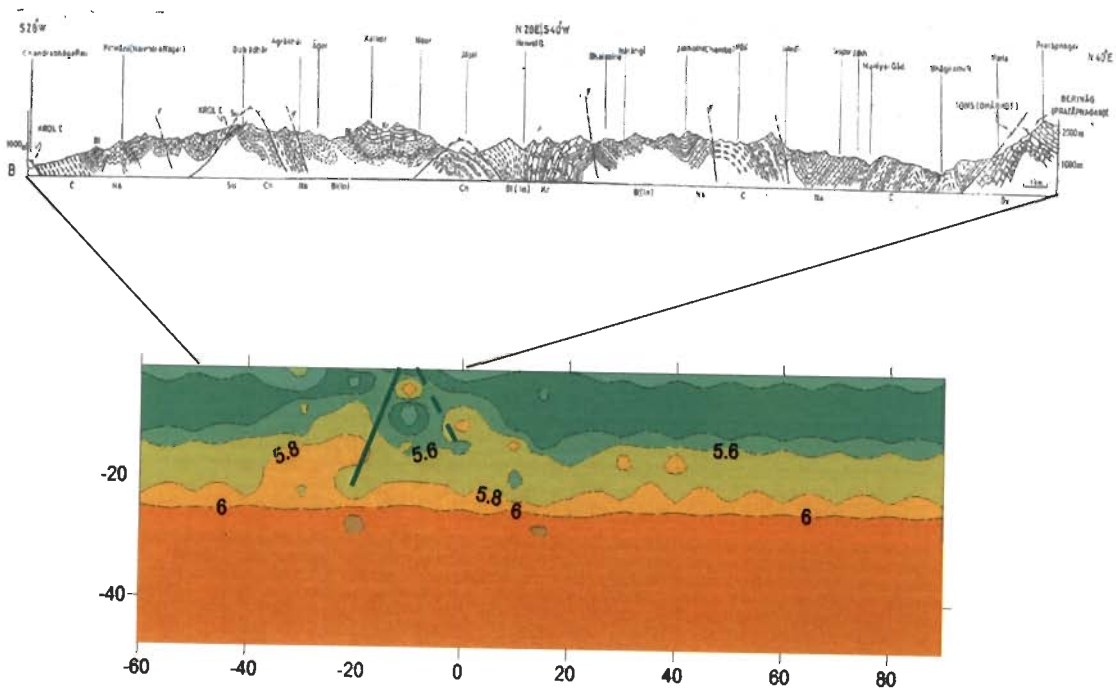


Fig. 6.19 Matching of traverse *KK* with profile 6 of 3-D Model II

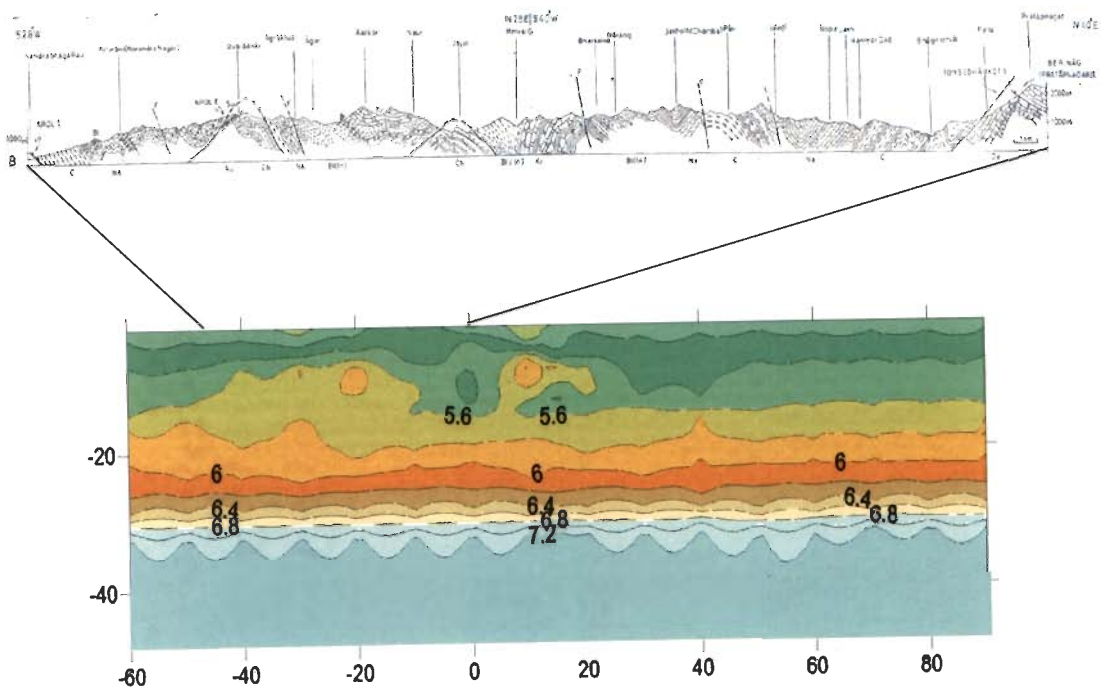


Fig. 6.20 Matching of traverse *KK* with profile 6 of 3-D Model III

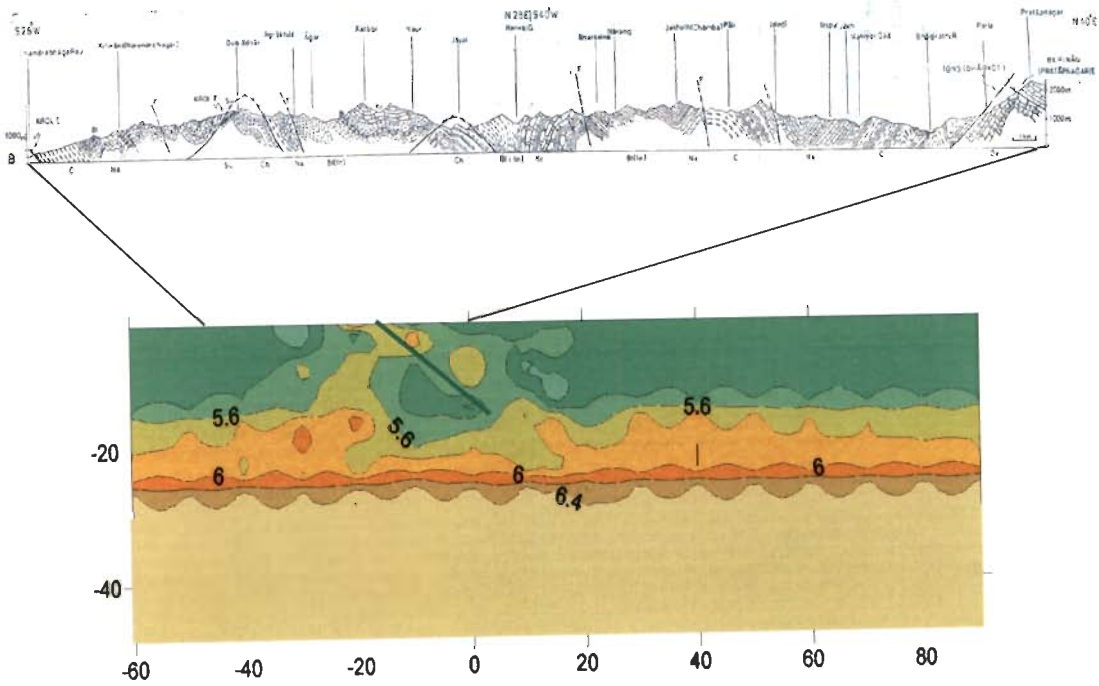


Fig. 6.21 Matching of traverse *KK* with profile 6 of 3-D Model IV

One of traverse namely *ss* of about 28 km match with *Profile 9* and runs between S35°W to N35°E. Dunda Fault could be observed on the *Profile 9* of 3-D Model I and the traverse *ss* as seen in Fig. 6.22. Similar patterns were also seen in other 3-D models. Described as a thrust by Jain (1971) the Dunda Fault is a steeply dipping reverse to almost vertical fault traceable from 3 km N of Gangani (Yamuna) through Dunda (Bhagirathi) to Bausari (Jalkur) for more than 50 km in the Uttarkashi area. Since its hade is variable and as it crosses an extremely rugged terrain, in the map it is as curvaceous as a thrust (Valdiya, 1980). Agarwal and Kumar (1973) have also identified it as a fault.

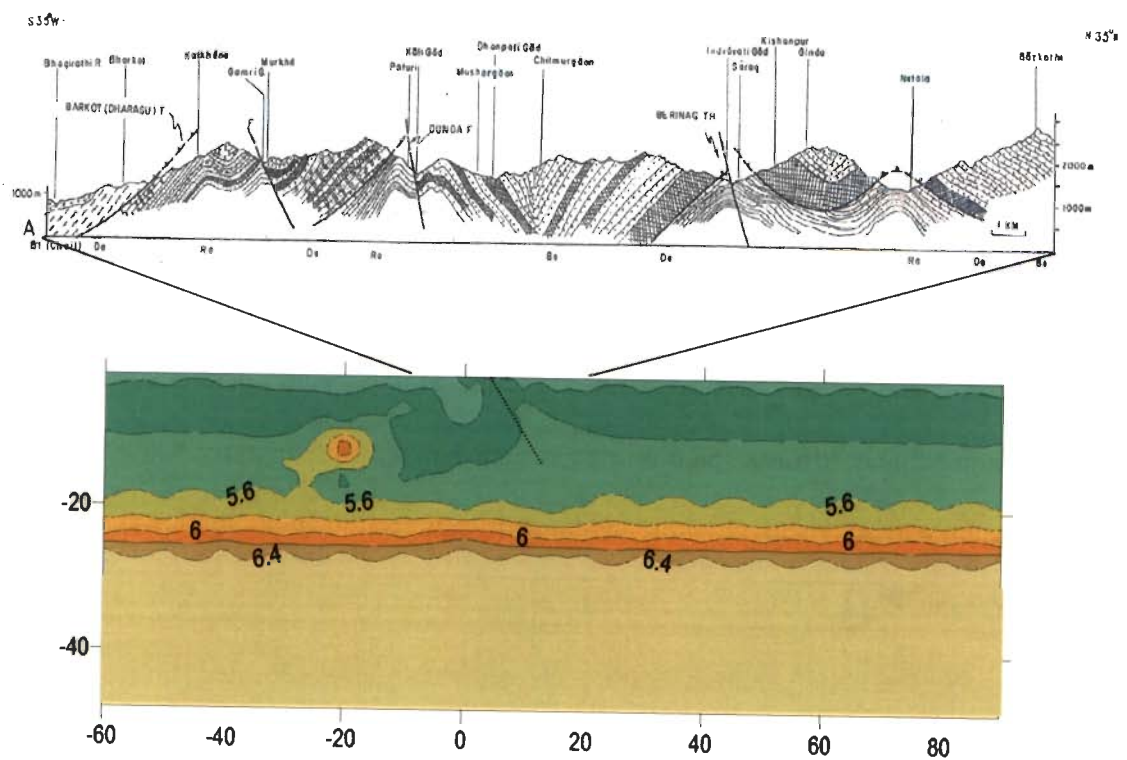


Fig. 6.22 Matching of traverse *ss* with profile 6 of 3-D Model I

Based on the matching of traverses with the different models the 3-D crustal velocity structure namely 3-D Model IV is proposed for the Garhwal Himalaya.

6.4 Seismicity plots on vertical profiles

To look into the seismic activity of the tectonic features during the period of recording the hypocenters of the earthquakes have been overlaid on the vertical profiles obtained from NE-SW gridding for 3-D Model IV which is proposed as 3-D crustal velocity structure for Garhwal Himalaya. Figure 6.23 shows an example of the *Profiles 3 to 9* of the NE-SW gridding of 3-D Model IV on which the hypocenters have been plotted. The clustering of hypocenters has been found in the vicinity of Thrust T1 as marked in *Profile 3 and 4*. Kumar *et al.*, (1998) has reported earthquake swarm activity from the same region in 1996. The clustering of hypocenters is observed between Main Boundary Thrust and Basul Thrust in *Profile 5* showing these thrusts to be active during this time. While *Profile 6, 7 and 8* shows the clustering of earthquake hypocenters around the marked tectonic features namely, Srinagar Thrust and Basul Thrust. A diffused picture of hypocenter locations can be seen in *Profile 8 and 9*. This diffused picture may be attributed to the activity shown by various tectonic features in this relatively more geologically and tectonically complex area pertaining to *Profiles 8 and 9*.

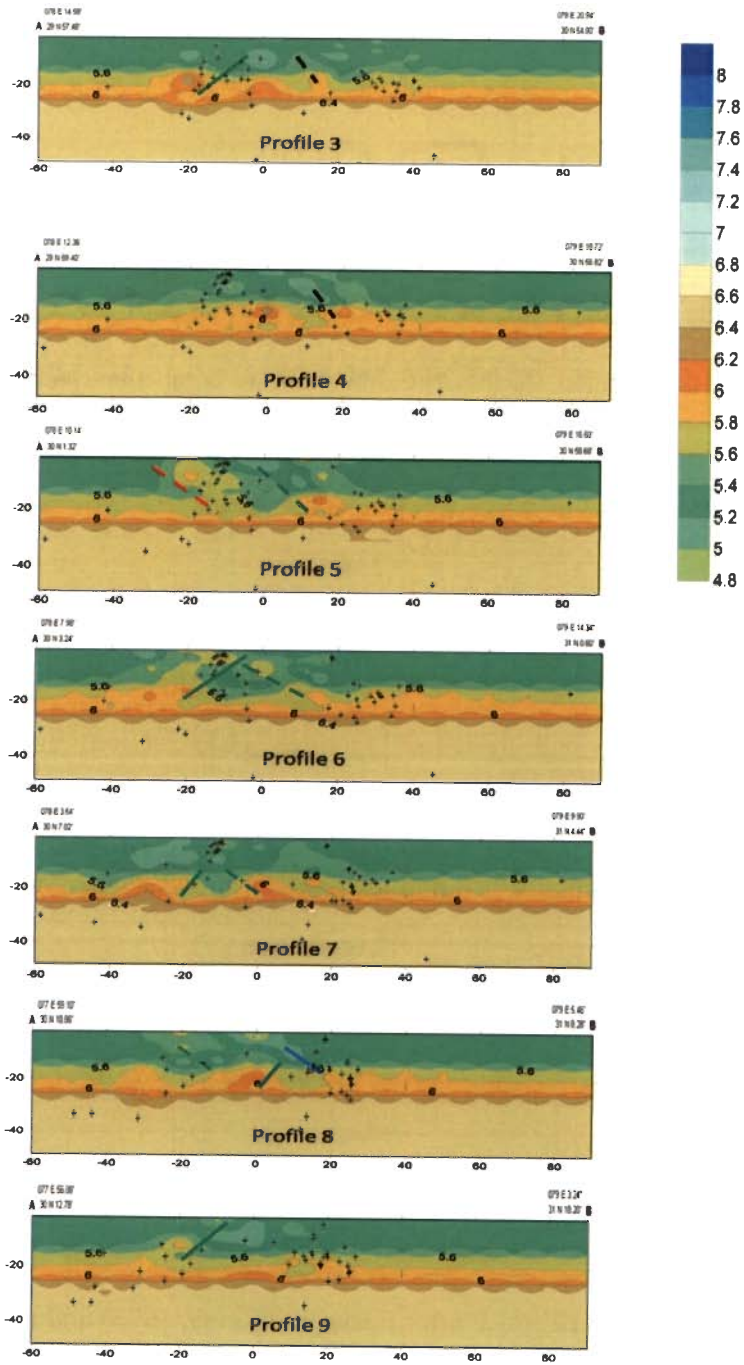


Fig. 6.23 Seismicity laid over the vertical profiles. The tectonic features are also marked on the profiles.

The spatial distributions of epicentres of microearthquakes (MEQ) recorded by different small aperture local seismic networks show the existence of a seismic belt, about 150 km long and 30-50 km wide running almost parallel to the surface trace of MCT lying between Yamuna and Alaknanda valleys (Gaur et al., 1985; Khattri *et al.*, 1989; Jain and Chander, 1991). The subsequent observations of more than 400 microearthquakes by a MEQ network deployed after the Uttarkashi earthquake have shown that the overall microearthquake activity is concentrated in the region between Budhakedar, Bhatwari and Manpur close to the MCT (Wason, 1996; Wason *et al.*, 1999). The main seismic activity has been reported in the past to be within a zone between MBT and MCT (Kumar *et al.*, 1998). Most of the workers have associated the seismicity with MBT or MCT but none of the workers have reported the association of the seismicity with these local features. The seismicity overlaid on the profiles shows a good match with these features such as Thrust T1, Basul Thrust and Srinagar Thrust. A detailed study of the seismicity is required to model the seismotectonics of the region by considering these features also.

6.5 Summary

The 3-D crustal velocity structures as obtained through 3-D inversions have been validated by comparing it with the prevailing geological and tectonic features in the study area. The geological and tectonic map (Fig. 3.2 after Fuchs and Sinha, 1978) and the traverses given by Valdiya (1980) were used for comparing the surface manifestations of the features with velocity distributions in various vertical profiles.

The following are the features which could be marked on various vertical profiles obtained from 3-D inversions obtained in the present study with the help of the geological and tectonic map and the traverses from the area.

- (i) MBT could be marked only in *Profile 3* of 3-D Model I and *Profile 5* of 3-D Model IV for NE-SW gridding
- (ii) MCT has been observed in *Profile no 7* and *8* of east-west gridding from 3-D Model I and 3-D Model II and in *Profile 7* from 3-D Model III. For NE-SW gridding it could not be marked.
- (iii) Basul Thrust was observed in *Profile 6* of 3-D Model I and II for east-west gridding. It was also observed on *Profiles 3, 5, 6* and *7* of 3-D Model IV. For NE-SW gridding, this thrust was observed in *Profiles 5, 6* and *8* of 3-D Model I and 3-D Model II and in *Profile 5* to *8* in 3-D Model IV. It could be marked on *Profiles 6* and *10* of 3-D Model III.
- (iv) Srinagar Thrust was observed in *Profile 6* obtained from all the four models for east-west gridding. For NE-SW gridding, it was seen in *Profiles 3, 5, 6, 7* and *9* of the 3-D Model I; *Profile 6* of 3-D Model II. Srinagar Thrust could be marked on *Profiles 6* and *11* obtained from 3-D Model III. For 3-D Model IV it is marked in *Profile 3, 6, 7, 8* and *9*.
- (v) For east-west gridding, Dunda Thrust could be marked on *Profile 7* obtained using 3-D Model II and 3-D Model IV. While for NE-SW gridding, it was observed on *Profile 7* obtained using 3-D Model I and 3-D Model II. It could also be marked in *Profiles 7, 8, 9, 11* for 3-D Model III and in *Profile 8* for 3-D Model IV.

- (vi) In *Profile 4* of 3-D Model I and II for NE-SW gridding, Thrust T1 could be marked. For 3-D Model IV it was marked in *Profile 3* and *4*.
- (vii) Dunda Fault has been marked on *Profile 9* of 3-D Model I for NE-SW gridding.

The detachment surface was found to be matching with the pattern of velocity distribution at a depth between 10-20 km. Similar patterns in all the profiles reveals the presence of detachment surface. This seems to be a zone of about 10-15 km thick. The undulating pattern observed in the vertical profiles reveals that detachment surface is not an even surface and possibly participating in the tectonic process. Further, the clustering of the hypocenters along the tectonic features shows that these features are active. The diffused seismicity observed in the north-east part of the study area can be attributed to the relatively more complex geological and tectonic setup of the area.

Based on the matching of the 3-D crustal velocity structure with the existing geological and tectonic features and relatively higher values of KHIT, DWS and RESOLUTION the 3-D Model IV estimated using the average 1-D velocity model (Model IV) is proposed for Garhwal Himalaya. A good match of the seismicity has also been found with 3-D Model IV.

CONCLUSIONS

7.1 General

Determination of seismic velocity structure of crust and upper mantle of the earth, one of the major objectives of seismology, is necessary for a variety of purposes, including the location of earthquakes, the determination of the composition and origin of the outer layers of the earth, and the interpretation of large-scale tectonics. An attempt has been made in the present study to estimate the 3-D crustal velocity structure in Garhwal Himalaya. While lot of advancement has taken place in instrumentation and digital data acquisition has the capabilities to mark the arrivals with requisite accuracies, the velocity modeling has been lacking in the past for accurate estimation of locations and to make use of relatively more accurate phase arrival data. Taking advantage of the high rate of occurrence of microearthquakes in this region estimation of 3-D crustal velocity structure has been carried out which is validated using prevailing geological and tectonic setup of the area.

7.2 Summary

The main objective of the thesis is to estimate 3-D crustal velocity structure beneath Garhwal Himalaya. *Local Earthquake Tomography* (LET) has been used for the purpose. The data from digital telemetered seismological array deployed by Department of Earthquake Engineering, IIT Roorkee in Garhwal Himalaya has been used in the present study. The steps in estimation of 3-D crustal velocity structure included estimation of minimum 1-D velocity

model and then simultaneous relocation of hypocenters and determination of local crustal velocity structure using linearized inversion (Thurber 1983, Eberhart-Phillips 1990). Three 1-D velocity models from past studies have been chosen to estimate minimal 1-D models using *VELEST*. Based on the output of the 1-D analysis an average 1-D velocity model has been proposed for Garhwal Himalaya. The outputs of 1-D analyses (computed using program *VELEST*) have been used as input to the 3-D inversions. The program *SIMULPS* has been used for the estimation of 3-D crustal velocity structure. Two gridding patterns namely east-west gridding and NE-SW gridding have been used to discretize the area beneath Garhwal Himalaya.

The results of the 3-D inversions have been validated by comparing the velocity distribution with the surface manifestations of the geological and tectonic features in the area. Further, traverses from Valdiya (1980) have been also used to interpret the results. The features namely, Main Boundary Thrust, Main Central Thrust, Basul Thrust, Dunda Thrust, Srinagar Thrust, Thrust T1 and Dunda Fault match well with the results of the 3-D inversions.

Based on the matching of the 3-D crustal velocity structure with the existing geological and tectonic features and relatively higher values of resolving parameters (KHIT, DWS and RESOLUTION) the 3-D Model IV estimated using the average 1-D velocity model (Model IV) is proposed for Garhwal Himalaya.

7.3 Conclusions

The following conclusions have been drawn based on the present study:

1. Based on earlier velocity models and recent data acquired from the region and using simultaneous inversion 1-D crustal velocity structure for Garhwal Himalaya

has been proposed. It consists of three layer structure over half space with velocities as 5.32 km/sec, 5.80 km/sec, and 6.48 km/sec at depths 16, 26 and 46 km, respectively with a half space having velocity of 7.60 km/sec.

2. A 3-D crustal velocity structure has been estimated and proposed for the Garhwal Himalaya namely 3-D Model IV.
3. The 3-D crustal velocity structure has been validated using local geological features present in the area and following have been observed:
 - a. The detachment surface is found to be at depth of about 15 km and the transition zone at detachment surface is found to be about 10 km thick. The velocity contrast is found to be about 5.6 km/sec at the top and about 6.0 km/sec at the bottom.
 - b. The strong velocity variations in the vicinity of detachment surface indicate that it is not an even surface and possibly participating in the tectonic process.
 - c. Out of sequence thrust which is Srinagar thrust is found to be dipping southerly in many of the profiles.
4. The depth sections of contemporary seismicity have been overlaid on the vertical profiles which reveal that most of the features are seismically active.
5. The proposed 3-D crustal velocity structure will be useful for accurately locating the earthquakes in the area for better seismotectonic modeling which in turn is useful in seismic hazard assessment and mitigation

7.4 Scope for future work

A more sophisticated analysis involving waveform modeling of some form would be required since the ray theoretical approach has its limitations. The ray theoretical approach makes use of the arrival times of observed first arriving waves with the assumption that these observed waves are the 'direct' ray theoretical arrivals. In such case seismic energy propagates through some finite volume surrounding a 'ray', not along an infinitesimal line. Thus, the structure that is 'sampled' by an observed arrival corresponds roughly to the Fresnel volume about the ray. Furthermore, finite-frequency diffracted arrivals may exist in reality, which are not modeled by ray theory. Alternatively, a ray-theoretical arrival could be of insignificant amplitude and, therefore, not correspond to the observed 'first arrival'.

The resolution of the results depend on the volume of data used for the study and for more detailed estimates of the crustal velocity structure with more resolution a bigger data set with more number of recording stations should be used.

More detailed traverses along grid lines are required to be done for validation of the estimated crustal velocity structure using 3-D inversion using more ground check points. Similarly, estimation of crustal velocity structure of the study area should be done using different methods such as receiver function analysis, surface wave dispersion analysis etc. for comparison and more realistic 3-D crustal velocity structure.

BIBLIOGRAPHY

1. Acharyya, S.K. and Narula, P.L., (1998) Seismotectonic Scenario of Himalaya and its Recent Developments XIth Symposium on Earthquake Engineering, Roorkee, pp 3-20.
2. Agarwal, N.C. and Kumar, G., (1973) Geology of the upper Bhagirathi and Yamuna valleys, Uttarkashi District, Kumaun Himalaya. *Himalayan Geology*, 3, 1-23.
3. Aki, K., Christoffersson, A. and Husebye, E.S. et al., (1974) Three dimensional seismic velocity anomalies in the crust and upper mantle under the U.S.G.S. California seismic array (abstract) *Eos. Trans. Am. Geophys. Union*, 56, 1145.
4. Aki, K. and Lee, W.H.K., (1976) Determination of three-dimensional velocity anomalies under a seismic array using first P arrival times from local earthquakes, 1, A homogeneous initial model, *J. Geophys. Res.*, V.81, p.4381-4399.
5. Aki, K., Christoffersson, A., and Husebye, E.S., (1976) Three-dimensional Seismic Structure of the Lithosphere under Montana LASA, *Bull. Seism. Soc. Am.* 66, 501-524.
6. Aki, K., Christoffersson, A., and Husebye, E.S., (1977) Determination of the 3-dimensional Seismic Structure of the Lithosphere, *J. Geophys. Res.* 82, 277-296.
7. Aldersons, F., (2004) Toward a three-dimensional crustal structure of the Dead Sea region from local earthquake tomography. Ph.D. Thesis, Senate of Tel-Aviv University 130 pp.
8. Asad, A.M., (1998) Linearized and nonlinear travel time tomography for upper crustal velocity structure of the western Great Basin, Ph.D. Thesis, University of Nevada, Reno,
9. Auden, J.B., (1934) The geology of the Krol Belt. *Rec. Geol. Surv. India*, 67, 357-454.
10. Auden, J.B., (1937) The structure of the Himalaya in Garhwal. *Rec. Geol. Surv. India*, 71, 407-433.

11. Bordet, P., (1973) On the position of the Himalayan Main Central Thrust within Nepal. Proc. Seminar Geodyn. Himalayan Region, National Geophysical Research Institute, Hyderabad, 148-155.
12. Catlos, E.J., Dubey, C.S., Marston, R.A., Harrison, M., (2006) Deformation within the Main Central Thrust shear zone, Bhagirathi River (NW India): Implications for Himalayan Tectonics in Convergent Margin Terranes and Associated Regions: A Tribute to W.G. Ernst (edited by M. Cloos, W.D. Carlson, M.C. Gilbert, J.G. Liou, and S.S. Sorenson) Geological Society of America, *Ernsfest Volume, Special Paper*, 419, (accepted in *Bull. Geol. Soc. of America*) p. 1-43
13. Chakravorthy, K.C. and Ghosh, D.P., (1960) Seismological study of the crustal layers in Indian region from the data of near earthquakes. Proc. World Conference on earthquake Engineering, Tokyo, p1633-1642.
14. Chander, R., Sarkar, I., Khattri, K.N., and Gaur, V.K., (1986) Upper crustal compressional wave velocity in the Garhwal Himalaya, *Tectonophysics*, V. 124 p.133-140
15. Chauhan, R.K.S. and Singh, R.N., (1965) Crustal studies in Himalayan region., *J. Ind. Geophys. Un. II*, V1, p51-57.
16. Chou, C.W. and Booker, J.R., (1979) A Backus-Gilbert approach to the inversion of travel time data for three dimensional velocity structure. *Geophys. J.R. Astron. Soc.*, 59, 325-44.
17. Clayton, R.W. and Comer, R.P., (1983) A tomographic analysis of mantle heterogeneities from body wave travel time (abstract) *Eos. Trans. Am. Geophys. Union*, 64, 776.
18. Clayton, R.W., (1984) Seismic Tomography (abstract). *Eos, Trans. Am. Geophys. Union*, 65, 236.
19. Crosson R.S. and Peters D.C., (1970) Crustal structure inversion of local array data, *Geological Society of America*,
20. Crosson, R.S., (1976a) Crustal structure modeling of earthquake data. Part I. Simultaneous least squares estimation of hypocenter and velocity parameters. *J. Geophys. Res.* 81, 3036-3046.
21. Crosson, R.S., (1976b) Crustal structure modeling of earthquake data. Part II. Velocity structure of the Puget Sound region, Washington. *J. Geophys. Res.* 81, 3047-3053.

22. Eberhart-Phillips, D., (1986) Three-dimensional velocity structure in northern California Coast Range from inversion of local earthquake arrival times, *Bull. Seismol. Soc. Am.*, 76, 1025– 1052.
23. Eberhart-Phillips, D., (1990) Three-dimensional P and S velocity structure in the Coalinga region, California, *J. Geo-phys. Res.*, 95, 15,343-15,363.
24. Eberhart-Phillips, D. and Reyners, M., (1997) Continental subduction and three-dimensional crustal structure: The northern South Island, New Zealand. *Journal of Geophysical Research* 102(B6): doi: 10.1029/96JB03555. issn: 0148-0227.
25. Eberhart-Phillips, D. and Reyners, M., (1999) Plate interface properties in the northeast Hikurangi subduction zone, New Zealand, from converted seismic waves. *Geophysical Research Letters* 26(16): doi: 10.1029/1999GL900567. issn: 0094-8276.
26. Eberhart-Phillips, D. and Reyners, M., (2001) A complex, young subduction zone imaged by 3-D seismic velocity, Fiordland, New Zealand, *Geophys. J. Int.*, 146,731-746.
27. Ellsworth, W.L., (1977) Three-dimensional structure of the crust and mantle beneath the island of Hawaii. Ph D thesis, MIT, Massachusetts, USA.
28. Ellsworth, W.L. and Koyanagi, R.Y., (1977) Three-dimensional crust and mantle structure of Kilauea Volcano, Hawaii. *J. Geophys. Res.*, 82, 5379-94.
29. Evans, J.R., Eberhart-Phillips, D., and Thurber, C.H., (1994) User's manual for SIMULPS 12 for imaging V_p and V_p/V_s : A derivative of the "Thurber" tomographic inversion SIMUL3 for local earthquakes and explosions, U.S. Geol Surv. Open-File Rept. 94-431, 101 pp.
30. Fuchs, G. and Sinha, A.K., (1978) The tectonics of the Garhwal Kumaon Lesser Himalaya, *Sonderdruck Jahrb. Geol. Bundesanst. (Austria)*, 121 (2), 219-241.
31. Gansser, A., (1964) *Geology of the Himalayas*, Interscience Publishers, London, 289p.
32. Gansser, A., (1977) The great suture zone between Himalaya and Tibet, a preliminary account. *Sci. Terre Himalaya, CNRS*, 268, 181-192
33. Gaur V.K., Chander R., Sarkar I., Khattri K.N. and Sinval H., (1985) Seismicity and state of stress from investigations of local earthquakes in the Kumaun Himalaya, *Tectonophysics*, 118, 243-251.

34. Geiger, L., (1912) Probability method for the determination of earthquake epicenters from the arrival time only. *Bull. St. Louis Univ.* 8, 60-71.
35. Ghose, A., (1973) Tectonic evolution of Lesser Himalaya of Kumaun, Uttar Pradesh. *Proceed. Seminar Geodyn. Himalayan Region. National Geophysical Research Institute, Hyderabad.* 136-147
36. Ghose, A., Chakrabarti, B. and Singh, R.K., (1974) Structural and metamorphic history of the Almora Group, Kumaun Himalaya, U.P. *Himalayan Geology*, 4, 171-194.
37. Gill, P.E., Murray, W. and Wright, M.H., (1981) *Practical Optimization*, Academic Press, New York.
38. GSI, (1993) Bihar-Nepal Earthquake, August 20, 1988, *Geol. Surv. India. Sp.Pub.* 31, ed.
39. GSI, (2000) *Seismotectonic Atlas of India and its Environs.* Geological Survey of India.
40. Hashimoto, S., Ohta, Y and Akiba, C., (Eds), (1973) *Geology of the Nepal Himalayas*, Himalayan Comm., Hokkaido Univ., Sappora (Japan), 286p
41. Haslinger, F. and Kissling, E., (2001) Investigating effects of 3-D ray tracing methods in Local Earthquake Tomography. *Physics of The Earth and Planetary Interiors*, 123, 103-114.
42. Hawley, B.W., Zandt, G. and Smith, R.B., (1981) Simultaneous inversion for hypocenters and lateral velocity variations: an iterative solution with a layered model. *J. Geophys. Res.* 86, 7073-76.
43. Heim, A. and Gansser, A., (1939) Central Himalaya, Geological Observation of the Swiss Expedition in 1936. *Mem. Soc. Helv. Sci. Nat.*, 73, 1-245.
44. Hino, R., Kanazawa, T. and Hasegawa, A., (1996) Interplate seismic activity near the northern Japan Trench deduced from ocean bottom and land-based seismic observations, *Phys. Earth Planet. Inter.*, 93, 37- 52.
45. Hodges, K.V., Parrish, R.R., Housh, T.B., Lux, D.R., Burchfiel, B.C., Royden, L.H. and Chen, Z., (1992) Simultaneous Miocene extension and shortening in the Himalayan Orogen. *Science*, 258, 1466-1469.
46. Horiuchi, S., Ishii, H. and Takagi, A., (1982) Two-dimensional depth structure of the crust beneath the Tohoku District, 1. Method and Conrad Discontinuity. *1. Phys. Earth*, 30, 47-69.

47. Humphreys, E. and Clayton, R.W., (1988) Adaptation of back projection tomography to seismic travel time problems. I. *Geophys. Res.*, 93, 1073-85.
48. Husen, S., Kissling, E., Flueh, E.R. and Asch, G., (1999) Accurate hypocenter determination in the seismogenic zone of the subducting Nazca Plate in northern Chile using a combined on-/offshore network, *Geophys. J. Int.*, 138, 687-701.
49. Husen, S., Kissling E., and Flueh, E.R., (2000) Local earthquake tomography of shallow subduction in north Chile: A combined onshore and offshore study, *J. Geophys. Res.*, 105, 28,183.
50. Husen, S. and Kissling, E., (2001) Local Earthquake Tomography between rays and waves: Fat Ray Tomography, *Phys. Earth Planet. Int.*, 123, 129-149.
51. Husen, S., Kissling, E. and Quintero, R., (2002) Tomographic evidence for a subducted seamount beneath the Gulf of Nicoya, Costa Rica: The cause of the 1990 Mw = 7.0 Gulf of Nicoya earthquake, *Geophys. Res. Lett.*, 29(8), 1238, doi:10.1029/2001GL014045.
52. Husen, S., Kissling, E., Deichmann, N., Wiemer, S., Giardini, D., and Baer, M., (2003) Probabilistic earthquake location in complex three-dimensional velocity models: Application to Switzerland, *J. Geophys. Res.*, 108(B2), doi: 10.1029/2002JB001778.
53. Husen, S., Quintero, R., Kissling, E., and Hacker, B., (2003) Subduction-zone structure and magmatic processes beneath Costa Rica constrained by local earthquake tomography and petrological modelling, *Geophys. J. Int.*, 155, 11-32.
54. Iyer, H.M. and Hirahara, K., (1993) "Seismic tomography: theory and practice", Chapman&Hall.
55. Jackson, D.D., (1979) The use of a priori data to resolve non-uniqueness in linear inversion. *Geophys. J.R. Astron. Soc.*, 57, 137-57.
56. Jackson, D.D. and Matsu'ura, M., (1985) A Bayesian approach to nonlinear inversion. I. *Geophys. Res.*, 90, 581-91.
57. Jain, A.K., (1971) Stratigraphy and tectonics of Lesser Himalayan region of Uttarkashi, Garhwal Himalaya, *Himalayan Geology*, 2, 188-205.
58. Jain, A. K. and Chander, R., (1991) Geodynamic models for the Uttarkashi earthquake of October 20, 1991, *Mem. GSI*, 30, 225-233.

59. Julian, B.R. and Gubbins, D., (1977) Three-dimensional seismic ray tracing. *J. Geophys.*, 43, 95-113
60. Kaila, K.L., Reddy, R.P. and Narain, H., (1968) Crustal structure in the Himalayan foot hills area of north India from P wave data of shallow earthquakes. *Bull. Seismol. Soc. Am.*, 58, 597-612.
61. Kaila, K.L. and Narain, H., (1976) Evolution of the Himalaya based on seismotectonics and deep seismic soundings, New Delhi Seminar on Him. Geol. (September), Sp. Publ. of N.G.R.I., Hyderabad, 30p.
62. Kamble, V.P., Verma, R.K., Choudhary, H.M., (1974) Crustal studies in the Himalayan region. Part I. Dalhousie-Mandi section. *Ind. J. Met. Geophys.* 25, 229-238.
63. Kayal, J.R., (2001) Microearthquake activity in some parts of the Himalaya and the tectonic model, *Tectonophysics*, 339, 331-351.
64. Kayal, J.R., Singh, O.P., Chakraborty, P.K., and Karunakaran, G., (2003) Aftershock sequence of the March 1999 Chamoli earthquake and the seismotectonic structure of the Garhwal Himalaya, *Bull. Seism. Soc. Am.* 93, 109-117.
65. Kaynia, A.M., (1999) Recent trends in geotechnical earthquake engineering. International Conference on Seismology and Earthquake Engineering, 3. Tehran, Iran 1999. Proceedings, pp. 27-42.
66. Kennett, B.L.N. and Williamson, P.R., (1988) Subspace methods for large-scale nonlinear inversion, in *Mathematical Geophysics*, (eds N.J. Vlaar, G. Nolet, M.J.R. Wortel, et al.), Reidel Hingham, MA, pp. 139-54.
67. Kennett, B.L.N., Sambridge, M.S. and Williamson, P.R., (1990) Subspace methods for large inverse problems with multiple parameter classes. *Geophys. J. Int.*, 94, 237-47.
68. Khattri, K.N., Chander, R., Gaur, V.K., Sarkar, I. and Kumar, S., (1989) New seismological results on the tectonics of the Garhwal Himalaya. *Proc. Indian Acad. Sci. (Earth Planet. Sci.)*, 98, 91-109.
69. Khattri, K.N., (1992) Local seismic investigations in the Garhwal-Kumaoun Himalaya, *Mem. Geol. Soc. of India*, No. 23, 45-66.
70. Kissling, E., Ellsworth, W.L., and Cockerham, R., (1984) Three-dimensional structure of the Long Valley Caldera, California, region by geotomography. *U.S. Geol. Surv. Open File Rep.* 84-939, 188-220.

71. Kissling, E., (1988) Geotomography with local earthquake data, Rev. of Geophysics.
72. Kissling, E., and Lahr, J., (1991) Tomographic image of the Pacific slab under southern Alaska. *Eclogae Geol. Helv.*, 84, 297-315.
73. Kissling, E., Ellsworth, W.L., Eberhart-Phillips, D., and Kradolfer, U., (1994) Initial reference models in local earthquake tomography, *J. Geophys. Res.*, 99, 19'635-19'646.
74. Kissling, E., Husen, S. & Haslinger, F., (2001) Model parameterization in seismic tomography: a choice of consequences for the solution quality, *Phys. Earth planet. Inter.*, 123, 89-101.
75. Koch, M., (1985) Nonlinear inversion of local seismic travel times for the simultaneous determination of the 3D-velocity structure and hypocenters - application to the seismic zone Vrancea. *J Geophys.*, 56, 160-73.
76. Kradolfer, U., (1989) Seismische Tomographie in der Schweiz Mittels Lokaler Erdbeben, Ph.D. Thesis, Eidgen"ossischen Technischen Hochschule Z"urich, Switzerland, 109 p.
77. Kumar, A., Pandey, A.D., Sharma, M.L., Gupta, S.C., Kumar, A., Gupta, B.K., (1994) Preliminary processing and interpretation of digital data obtained from digital seismic array in Garhwal Himalaya, Proc. Xth Symposium of Earthquake Engineering, Roorkee, Nov. 16-18, Vol I, pp 141-152.
78. Kumar, A., Pandey, A.D., Sharma, M.L., Gupta, S.C., Jindal, A.K. and Jain, S.K., (1997) Contemporary local seismicity in the Garhwal Himalaya, Proc. Workshop on Earthquake Disaster Preparedness, Roorkee, Oct 13-14, 1997, pp 39-48.
79. Kumar, A., Pandey, A.D., Sharma, M.L., Gupta, S.C., Jindal, A.K. and Jain, S.K., (1998) Pattern of two earthquake swarms in the Garhwal Himalaya, XIth Symposium on Earthquake Engineering, Roorkee, pp 67-74.
80. Kumar, G., Gyan Prakash and Singh, K.N., (1974) Geology of the Deoprayag-Dwarahat area, Garhwal, Chamoli and Almora district, Kumaun Himalaya, *U.P. Him. Geol.*, 3, 1-23.
81. Kumar, G., Prakash, G. and Singh, K.N., (1974) Geology of the Deoprayag-Dwarahat area, Garhwal Himalaya, *U.P. Himalayan Geology*. 4, 323-347.

82. Kumar, S., Chander, R. and Khattri, K.N., (1987) Compressional wave speed in the second crustal layer in Garhwal Himalaya., *J. Assoc. Expl. Geophys.*, Vol VIII, No. 4, 219-225.
83. Kumar, S and Sato, T., (2003) Compressional and shear wave velocities in the crust beneath the Garhwal Himalaya, North India. *Himalayan Geology*, Vol. 24 (2), 77-85.
84. Lawson, C.L. and Hanson, R.J., (eds) (1974) *Solving Least Squares Problems*, Prentice -Hall, Englewood Cliffs, NJ.
85. Lee, W.H.K. and Lahr, J.C., (1995) Hypo71 (revised): a computer program for determining hypocenter, magnitude and first motion pattern of local earthquakes. *US Geol. Surv. Open-File Rep.*, 75-311: 1-16.
86. Lee, W.H.K. and Stewart, S.W., (1981) *Principles and Applications of Microearthquake Networks*, Academic, New York, 293 pp.
87. Lees, J.M. and Crosson, R.S., (1989) Tomographic inversion for three dimensional velocity structure at Mount St. Helens using earthquake data. *J. Geophys. Res.*, 94, 5716-28.
88. Lin, C.H. and Roecker, S.W., (1990) Determination of earthquake hypocenters, focal mechanisms, and velocity structure in the Morgan Hill area through 3-D circular ray tracing. *Eos, Trans, Am. Geophys. Union*, 71, 1445.
89. Maurer, H., (1993) *Seismotectonics and upper crustal structure in the western Swiss Alps*. Ph D thesis, ETH Zuerich, Switzerland.
90. Mehdi, H.S., Kumar, G. and Prakash, G., (1972) Tectonic evolution of eastern Kumaun Himalaya: a new approach. *Himalayan Geology*. 2, 481-501.
91. Menke, W., (1989) *Geophysical data analysis: Discrete inverse theory*, *Int. Geophys. Ser.*, 45, 285 pp., Academic, San Diego, California.
92. Merh, S.S., Vashi, N.M. and Patel. J.P., (1971) On the nature of the Ramgarh thrust in Kumaun Himalayas. *Jour. Geol. Soc. Int.* 11, 380-382.
93. Misra, R.C. and Valdiya, K.S., (1961) The Calc zone of Pithoragarh, with special reference to the occurrence of stromatolites. *Jour. Geol. Soc. Ind.*, 2, 78-90.
94. Mitchell, A.H.G., (1981) Phanerozoic plate boundaries in mainland SE Asia, the Himalayas and Tibet, *Geol. Soc. London Jour.*, v. 138, 109-122.

95. Moser, T.J., (1991) Shortest path calculation of seismic rays. *Geophysics*, 56, 59-67. Gill, P.E., Murray, W. and Wright, M.H. (1981). *Practical Optimization*, Academic Press, London.
96. Mukherjee, S.M., (1942) *Proc. Ind. Acad. Sci.* V.16, p167-175
97. Mukhopadhyay, S. and Kayal, J.R., (2003) Seismic tomography structure of the 1999 Chamoli earthquake source area in the Garhwal Himalaya. *Bull. Seismol. Soc. Am.* 93, 1854-1861.
98. Nakanishi, I., (1985) Three-dimensional structure beneath the Hokkaido-Tohoku region as derived from a tomographic inversion of P-arrival times. *J. Phys. Earth*, 33, 241-256.
99. Nakanishi, I. and Suetsugu, D., (1986) Resolution matrix calculated by a tomographic inversion method. *J. Phys. Earth*, 34, 95-99.
100. Nandy, D.R., Choudhary, A.K., Chakraborty, C., and Narula, P.L., (1993) Geological Survey of India, Bihar-Nepal earthquake, August 20, 1988, GSI Special Publication 31, Eds.
101. Narula, P.L., (1991) Seismotectonic evolution of northwest Himalaya. Unp. GSI Report.
102. Narula, P.L., (1992) Neotectonic activity, seismicity and related contemporary deformations in the NW Himalaya, *Symp. On Himalayan Geology*, Japan, 33-36.
103. Narula, P.L. and Shome, S.K., (1992) Macroseismic studies of recent earthquakes in NW Himalaya, *Current Science*, V. 62, No. 1-2, 24-33.
104. Ni, J. and Barazangi, M., (1984) Seismotectonics of the Himalayan collision zone: Geometry of the underthrusting Indian Plate beneath the Himalayas. *J. Geophys. Res.*, 89, 1147-1163.
105. Nishizawa, A., Kono, T., Hasegawa, A., Hirasawa, T., Kanazawa, T., and Iwasaki, T., (1990) Spatial distribution of earthquakes off Sanriku, northeastern Japan, in 1989 determined by ocean-bottom and land-based observation, *J. Phys. Earth*, 38, 347-360.
106. Nolet, G., (1985) Solving or resolving inadequate and noisy tomographic systems. *J. Comput. Phys.*, 61, 463-482.
107. Nolet, G., (1987) Seismic wave propagation and seismic tomography, in *Seismic Tomography* (ed.G. Nolet), Reidel, Hingham, MA, pp. 1-23.
108. Nowack, R.L. and Lutter, W.J., (1988) A note on the calculation of covariance

- and resolution. *Geophys. J.*, 95, 205-7.
109. Obana, K., Kodaira, S., Kaneda, Y., Mochizuki, K., Shinohara, M., and Suyehiro, K., (2003) Microseismicity at the seaward updip limit of the western Nankai Trough seismogenic zone, *J. Geophys. Res.*, 108(B10), 2459, doi:10.1029/2002JB002370.
 110. Paige, C.C. and Saunders, M.A., (1982) LSQR: An Algorithm for Sparse Linear Equations and Sparse Least Squares *ACM Transactions on Mathematical Software (TOMS) Volume 8(Issue 1)*, 43-71.
 111. Pandey, A.C., Dubey, Chandra S., (2002) Structural Analysis of Lineaments using Remote Sensing techniques in a part of Lesser Garhwal Himalayas, Tehri Uttarkashi District. *IAPRS and SIS Vol.34 No.7* p.173-176.
 112. Pandey, A.C., Dubey, Chandra S., (2002) Terrain mapping and Evaluation in Himalayas using Remote sensing and GIS Techniques-A Case Study from Tehri Dam and its Environs. *IAPRS and SIS Vol.34 No.7* p.105-108.
 113. Pandey, A.C., Saklani, P.S. and Dubey, C.S., (2005) Geological and morphotectonic studies using Satellite Images Techniques of Tehri, Uttarkashi, a part of Garhwal Himalayas, in *Himalaya (Geological Aspects)*, Vol. III p.153-171, (P.S. Saklani Edn. Delhi, Satish Serial Publication, 2005, 341p. ISBN 81-89304-04-6).
 114. Pandey, M.R., Tandukar, R.P., Avouac, J.P., Lave, L., and Massot, J.P., (1995) Evidence for recent interseismic strain accumulation on a mid-crustal ramp in the Central Himalayas of Nepal, *Geophys. Res. Lett.*, 22, 751-758.
 115. Paul, A., Wason, H.R., Sharma, M.L., Pant, C.C., A. Nirwan and Tripathi, H. B., (2004) Seismotectonic implications of data recorded by DTSN in the Kumaun region of Himalaya, *Jour. Geol. Society of India*, Vol. 64, 43-51.
 116. Pavlis, G., and Booker, J.R., (1983) Progressive multiple event location (PMEL), *Bull. Seism. Soc. Am.*, vol. 73, 1753-1777.
 117. Pavlis, G.L. and Booker, J.R., (1983) A study of the importance of nonlinearity in the inversion of earthquake arrival time data for velocity structure. *J. Geophys. Res.*, 88, 5047-55.
 118. Pereyra, V., Lee, W.H.K. and Keller, H.B., (1980) Solving two-point seismic ray-tracing problems in heterogeneous medium, Pt. 1. A general adaptive finite difference method. *Bull. Seismol. Soc. Am.*, 70, 79-99.

119. Peters, D.C. and Crosson, R.S., (1972) Application of prediction analysis to hypocenter determination using a local array. *Bull. Seismol. Soc. Am.* 62, 775-788.
120. Peters D.C., (1973) Hypocenter location and crustal structure inversion of seismic array travel times, Ph.D. Thesis, University of Washington, Seattle.
121. Pilgrim, G.E. and West, W.D., (1928) The structure and correlation of the Simla rocks. *Mem. Geol. Surv. Ind.*, 53, 1-140.
122. Prothero, W.A., Taylor, W.J. and Eickemeyer, J.A., (1988) A fast, two-point, three-dimensional ray tracing algorithm using a simple step search method. *Bull. Seismol. Soc. Am.*, 78, 1190-8.
123. Raina, B.N., (1978) A review of the stratigraphy and structure of Lesser Himalaya of Uttar Pradesh and Himachal Pradesh. *Tectonic Geology of the Himalaya* (ed, P.S. Saklani), Today and Tomorrow's Printers and Publishers, New Delhi, 79-112.
124. Rajendran, K., Rajendran, C.P., Jain, S.K., Murthy, C.V.R. and Arlekar, J.N., (2000) The Chamoli earthquake, Garhwal Himalaya: field observations and implications for seismic hazard, *Curr. Sci.* 78, 45-51.
125. Ranga Rao, A., (1968) On the Krol Nappe hypothesis. *Jour. Geol. Soc. India*, 9, 153-158.
126. Reidel, C., Tryggvason, A., Dahm, T., Stefanson, R., Bodvarson, R. and Gudmundsson, G.B., (2005) The seismic velocity structure north of Iceland from joint inversion of local earthquake data. *J. of Seismology*, 9, 383-404.
127. Reyners, M., Eberhart-Phillips, D., and Stuart, G., (1999) A three-dimensional image of shallow subduction Crustal structure of the Raukumara Peninsula, New Zealand, *Geophys. J. Int.*, 137, 873-890.
128. Rodi, W.L., Jordan, T.H., Masso, J.F., et al., (1981) Determination of the three-dimensional structure of eastern Washington from the joint inversion of gravity and earthquake data. *Systems Science and Software Report SSS-R-SO-4516*, La Jolla.
129. Roecker, S.W., (1977) Seismicity and tectonics of the Pamir-Hindu Kush region of central Asia. Ph D thesis, MIT, Massachusetts, USA.
130. Roecker, S.W. and Ellsworth, W.L., (1978) VELEST Fortran program, U.S. Geological Survey, Menlo Park, California.
131. Roy, S.C., (1939) *Mem. Geol. Surv. Ind.* V. 73, p49-74.

132. Rupke, J., (1974) Stratigraphic and structural evolution of the Kumaun Lesser Himalaya. *Sedimentary Geology*, 11, 81-265.
133. Saklani, P.S., (1971) Structure and tectonics of the Pratapgarh area, Garhwal Himalaya. *Him. Geol.*, 1, 75-91.
134. Sambridge, M.S., (1990) Non-linear arrival time inversion: Constraining velocity anomalies by seeking smooth models in 3-D. *Geophys. J. Int.*, 94, 653-77.
135. Sambridge, M.S. and Kennett, B.L.N., (1990) Boundary value ray tracing in a heterogeneous medium: a simple and versatile algorithm. *Geophys. J. Int.*, 101, 157-68.
136. Sarkar, I., Jain, R. and Khattri, K.N., (2001) Mapping of shallow three dimensional variations of P-wave velocity in Garhwal Himalaya. *J. of Asian Earth Sciences*, 19, 155-163.
137. Searle, M.P., (1996) Geological evidence against large scale pre-Holocene offsets along the Karakoram fault: Implications for the limited extrusion of the Tibetan plateau. *Tectonics*, 15, 171-186.
138. Seeber, L., Armbruster, J.G. and Quittmeyer, R., (1981) Seismicity and continental subduction in the Himalaya arc, In *Zagros, Hindu Kush, Himalaya, Geodynamic Evolution*, *Geodyn. Ser. Vol.3*, Ed. H.K. Gupta and F.M. Delany, pp. 215-242.
139. Shanker, R. and Ganessan, T.M., (1973) A note on the Garhwal Nappe. *Himalayan Geology*, 3, 72-83.
140. Sharma, K.K., (1991) Tectonomagmatic and sedimentation history of Ladakh collision zone: a synthesis. *Phys. Chem. Earth*, 17, 115-132.
141. Sharma, M.L., (1992) Sample telemetered digital seismic array in Garhwal Himalaya -Software and data management, *Himalayan Seismicity Memoir No. 23*, *Geo. Soc. of India*, pp 67-80.
142. Sharma, M.L. and Wason, H.R., (1994) Occurrence of low stress drop earthquakes in the Garhwal Himalaya region. *Physics of Earth and Planetary Interiors*, 85, 265-272.
143. Sharma, M.L. and Wason, H.R., (1995) Seismic moment-magnitude relationship for the Garhwal Himalaya Region, *Bull. Ind. Soc. Earthq. Tech.*, Vol. 32, No. 3, pp 85-95.
144. Shinohara, M., Yoshizawa, T., Hino, R., Aoyagi, Y., Nishino, M., Sato, T.,

- Shiobara, H., Mochizuki, K., and Suyehiro, K., (1999) Hypocenter distribution of plate boundary zone off Fukushima, Japan, derived from ocean bottom seismometer data, *Eos Trans. AGU*, 80(46), Fall Meet. Suppl., F724.
145. Spakman, W. and Nolet, G., (1988) Imaging algorithms, accuracy, and resolution in delay time tomography, in *Mathematical Geophysics*, (eds N.J. Vlaar, G. Nolet, M.J.R. Wortel, et al.), Reidel, Hingham, MA, pp. 155-87.
 146. Spencer, C. and Gubbins, D., (1980) Travel-time inversion for simultaneous earthquake location and velocity structure determination in lateral varying media. *Geophys. J. R. Astron. Soc.*, 63, 95-116.
 147. Srikantia, S.V. and Sharma, R.P., (1976) Geology of the Shali belt and the adjoining areas. In: *The stratigraphy and structure of parts of the Simla Himalaya*. Mem. Geol. Surv. India, 106(1), 69-77.
 148. Srikantia, S.V., (1988) Himalayan thrusts and structural belts. *Jour. Geol. Soc. India*, 31, 210-229.
 149. Srikantia, S.V. and Bhargava, O.N., (1998) Geology of Himachal Pradesh. *Geol. Soc. India*, pp. 406.
 150. Tandon, A.N., (1954) Study of the Great Assam Earthquake of August 1950 and its aftershocks, *Ind. J. Met. Geophys.*, V5, p95-137.
 151. Tandon, A.N. and Dubey, R.K., (1973) A study of crustal structure beneath the Himalaya from body waves. *Pure & Appl. Geophys.*, 111, 2207-2216.
 152. Tarantola, A. and Nercessian, A., (1984) Three-dimensional inversion without blocks. *Geophys. J. R. Astron. Soc.*, 76, 299-306.
 153. Thakur, V.C., (1992) *Geology of western Himalaya*. Pergamon Press, Oxford, 366p.
 154. Thurber, C.H. and Ellsworth, W.L., (1980) Rapid solution of ray tracing problems in heterogeneous media. *Bull. Seismol. Soc. Am.*, 70, 1137-1148.
 155. Thurber, C.H., (1981) Earth structure and earthquake locations in the Coyote Lake area, central California, Ph.D. Thesis, Massachusetts Institute of Technology, Cambridge, Massachusetts, 332 pp
 156. Thurber, C.H., (1983) Earthquake locations and three dimensional crustal structure in the Coyote Lake area, Central California, *J. Geophys. Rec.*, V.88, p.8226-8236.
 157. Thurber, C.H., (1984) Seismic detection of the summit magma complex of Kilauea volcano, Hawaii. *Science*, 223, 165-167.

158. Thurber, C.H., (1986) Analysis methods for kinematic data from local earthquakes. *Rev. Geophys.*, 24, 793-805.
159. Thurber, C.H. and Aki, K., (1987) Three-Dimensional Seismic Imaging. *Annual Review of Earth and Planetary Sciences* Vol. 15: 115-139.
160. Thurber, C.H., (1992) Hypocenter-velocity structure coupling in local earthquake Tomography, *Phys. Earth Planet. Int.*, 75, 55-62.
161. Thurber, C.H., (1993) Local earthquake tomography: velocities and V_p/V_s —theory, in: *Seismic Tomography: Theory and Practice*, eds. H. M. Iyer and K. Hirahara, Chapman and Hall, London, 563-583.
162. Toomey, D.R. and Foulger, G.R., (1989) Tomographic inversion of local earthquake data from the Hengill-Grensdalur central volcano complex, Iceland. *J. Geophys. Res.*, 94, 17497-510.
163. Um, J. and Thurber, C.H., (1987) A fast algorithm for two-point seismic ray tracing, *Bull. Seismol. Soc. Am.*, 77, 972-986.
164. Upadhyay, R. and Sinha, A.K., (1998) Tectonic evolution of Himalayan Tethys and subsequent Indian plate subduction along Indus Suture zone. *Proc. Indian National Science Academy*, 64A, 659-683.
165. Valdiya, K.S., (1962a) A study of the Champawat Granodiorite and associated metamorphic of the Lohaghat subdivision, District Almora U.P., with special reference to petrography and petrogenesis. *Indian Mineralogist*, 3, 6-37.
166. Valdiya, K.S., (1964a) The unfossiliferous formation of the Lesser Himalaya and their correlation. Report 22nd Int. Geol. Congr., 11, 15-36.
167. Valdiya, K.S., (1964b) A note o the tectonic history and evolution of the Himalaya. Report 22nd Int. Geol. Congr., 11, 269-282.
168. Valdiya, K.S., (1964c) The tectonic design of the Himalaya: a survey of structures between Indus and Brahmaputra andtheir comparison with the Alpine structures. Report 22nd Int. Geol. Congr., 11, 283-315.
169. Valdiya, K.S., (1973a) Lithological subdivision and tectonics of the "Central Crystalline Zone" of Kumaun Himalaya, (Abstract). *Proc. Sem. Geodyn. Himalayan Region*, N.G.R.I., Hyderabad, 204-205.
170. Valdiya, K.S., (1978) Extension and analogues of the Chail Nappe in Kumaun Himalaya. *Ind. Jour. Earth. Sci.*, 5, 1-19.
171. Valdiya, K.S., (1978) Outline of the structure of Kumaun Himalaya. *Tectonic Geology of the Himalaya* (ed, P.S. Saklani), Today and Tomorrow's Printers

- and Publishers, New Delhi, 1-14.
172. Valdiya, K.S., (1980) Geology of Kumaun Lesser Himalaya. Wadia Institute of Himalayan Geology, Dehra Dun, p291.
 173. Van der Sluis, A. and Van der Vorst, H.A., (1987) Numerical solution of large, sparse linear algebraic systems arising from tomographic problems, in Seismic Tomography (ed. G. Nolet), Reidel, Hingham, MA, 49-83.
 174. Verma, G.S., (1974) Structure of the foothills of the Himalaya. Pure & Appl. Geophys., 112, 18-26.
 175. Vidale, J.E., (1990) Finite-difference calculation of traveltimes in three dimensions. Geophys, 55,521-6.
 176. Viridi, N.S., Thakur, V.C. and Azmi, R.J., (1978) Discovery and significance of Permian microfossils in the Tso Morari Crystallines of Ladakh, J & K, India. Himalayan Geology, 8, 993-1000.
 177. Wadia, D.N., (1966) Geology of India. Macmillan and Company Limited.
 178. Walck, M.C. and Clayton, R.W., (1987) P wave velocity variations in the Coso region, California, derived from local earthquake travel times. Journal of Geophysical Research, Volume 92, Issue B1, p. 393-405.
 179. Wason, H.R., (1996) Final report on present seismic status and earthquake process model of Garhwal Himalaya region, DST, New Delhi.
 180. Wason, H.R., Sharma, M.L., Gupta, A.K. and Kapoor K., (1998) A preliminary analysis of broad band data in the Garhwal Himalaya region, XIth Symposium on Earthquake Engineering, Roorkee, pp 85-100.
 181. Wason, H.R., Kumar, J. and Walia, S.K., (1999) Local seismicity of the Garhwal Himalaya subsequent to the Uttarkashi earthquake of October 20, 1991. In Geodynamics of the NW Himalaya (ed. A. K. Jain and R. M. Manickavasagam), Gondwana Research Group Memoir, 6, 335-340.
 182. Wason, H.R. and Sharma, M.L., (2000) Source parameter studies of local earthquakes in the Garhwal Himalaya region based on the digital broad band data, 12th World conference on Earthquake Engineering, New Zealand, 1776 / 4 / A, pp 1-8.
 183. Wason, H.R., Sharma, M.L. and Nandini, D., (2001) Aftershock activity of the Chamoli earthquake of march 29, 1999 recorded by broadband seismograph stations, Proc. Workshop on recent earthquakes of Chamoli and Bhuj, May 24-26, Roorkee, Vol. I, pp29-39.

184. Wason, H.R., Goel, O.P., Tripathi, H.B., Khan, P.K., Paul, A., and Kapoor, K., (2002) Analysis of Aftershock Events of the Chamoli Earthquake Recorded by Kumaun Digital Telemetry Seismic Network, *Journal of Himalayan Geology*, 23, 19-23.
185. Wason, H.R., Sharma, M.L., Khan, P.K., Kapoor, K., Nandini, D. and Kara, V., (2002) Analysis of aftershocks of the Chamoli Earthquake of March 29, 1999 using broadband seismic data, *Journal of Himalayan Geology*, 23, 7-18.
186. Weilandt, E., (1987) On the validity of the ray approximation for interpreting delay times in Seismic Tomography, (ed. G. Nolet) Reidel, Hingham, MA, pp. 85-98.
187. Wesson, R.L., (1971) Travel-time inversion for laterally inhomogeneous crustal velocity models. *Bull. Seismol. Soc. Am.*, 61, 729-46.
188. Zhao, D., Horiuchi, S. and Hasegawa, A., (1990) 3-D seismic velocity structure of the crust and the uppermost mantle in the northeastern Japan Arc. *Tectonophysics*. 181, 135-49.
189. Zhao, D., (1991) A Tomographic Study of seismic velocity structure in the Japanese Islands. Ph.D. Thesis, Tohoku Univ., 301pp.

APPENDIX I

This appendix contains the map (Valdiya, 1980) showing the large number of transverse and oblique north to south traverses reported by Valdiya (1980) followed by the cross sections describing lithotectonic setting of the traverses falling in study area. The traverses are marked on the map as given in the appendix.

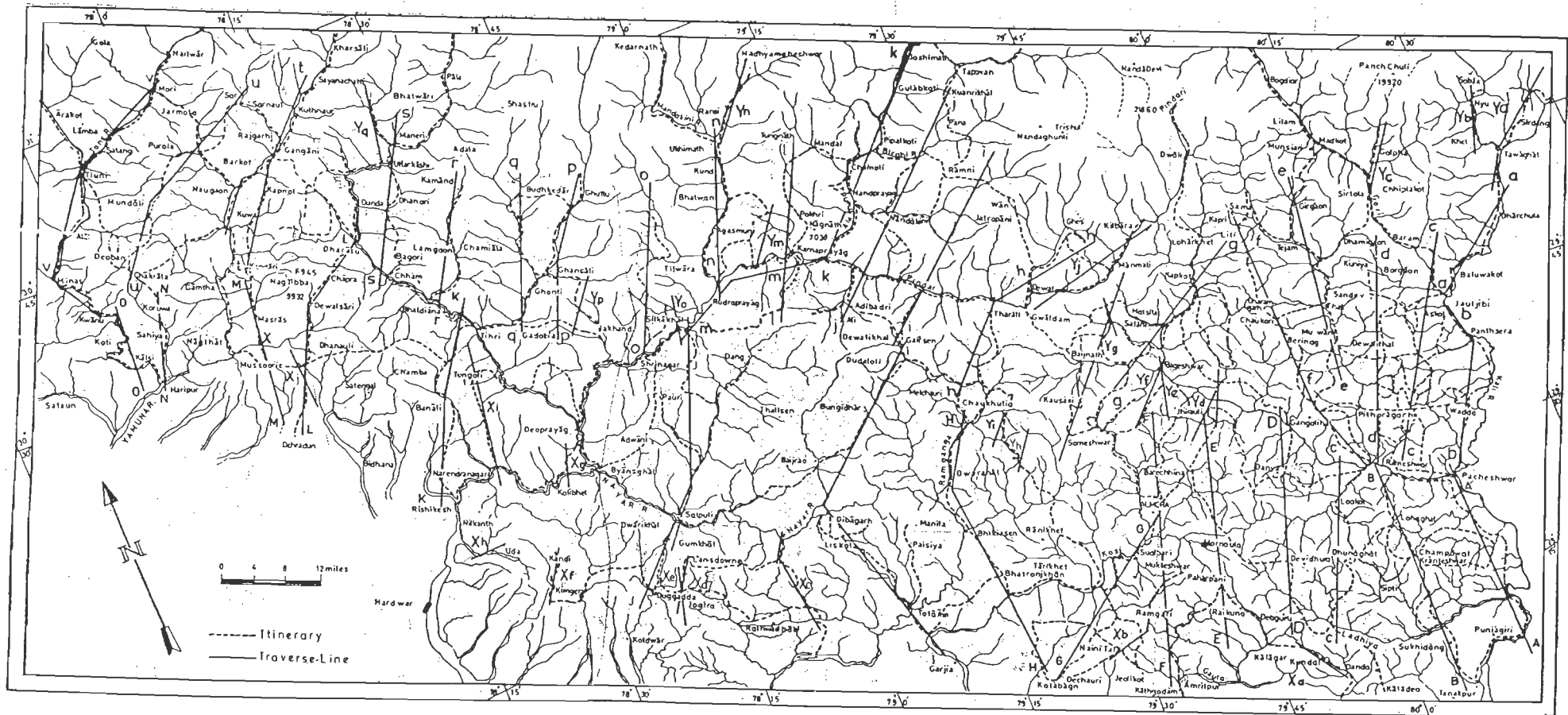
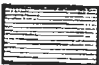

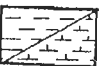
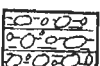
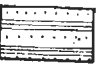
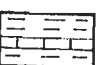
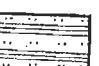
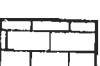
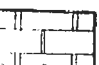

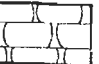
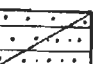
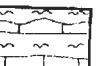
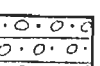



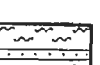
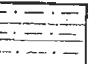
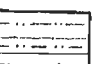

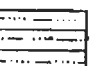
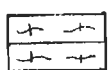


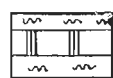
Fig. A1.1 Traverse lines as reported by Valdiya (1980)

KEY TO THE ORNAMENTATIONS USED IN SECTIONS

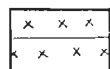
	Olive green, grey, purple and red shales-slates		Greywackes, siltstones and slates of turbidite-flysch
	Carbonaceous black slates/ pyritous black slates		Pebbly or conglomeratic mudstone/ slate (diamictite)
	Medium-grained sublitharenite, quartzwackes of fawn, brown, olivegreen, and purple colours, alternating with slates		Slates, marlite and argillaceous limestone alternation
	Alternating subgreywacke and maroon mudstone/ siltstone		Limestone of blue, black, and grey colours; marble
	Deoban dolomite and highly dolomitic limestone; with stromatolite		Crystalline magnesite within dolomite sequence
	Krol limestone and dolomite		Quartzarenite of Berinag/Nagthat Formation
	Alternation of purplewhite and light green marble /violet limonitic phyllite and pink,		Pebbly conglomerate quartzarenite
	Amphibolite/ chlorite schist (metatuffe)		Amygdaloidal and vesicular basalt
	Dolerite and epidiorite		Phyllite, interbedded with metasiltstone or very fine-grained metagreywacke
	Sercite-chlorite-biotite-schist, fine grained mica schist		Garnetiferous fine grained mica schist
	Kyanite-bearing fine grained mica schist		Garnetiferous mica schist with graphitic lenses.



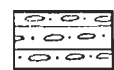
Coarse-grained kyanite-garnet-muscovite-biotite psammitic gneiss



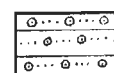
Sillimanite-kyanite-garnet-biotite muscovite-calcisilicate rock within schists and psammitic gneiss



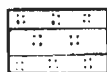
Granite-granodiorite



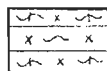
Augen gneiss/mylonitised porphyritic granite-gneiss



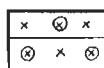
Porphyroblastic quartz-sericite schist



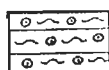
Garnet-biotite-muscovite-quartzite with occasional kyanite in interbeds of coarse-grained mica schist



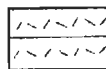
Migmatite



Granite porphyry (gneissose)



Mylonitized quartz-porphyry



Leucocratic aplogranite and adamellite

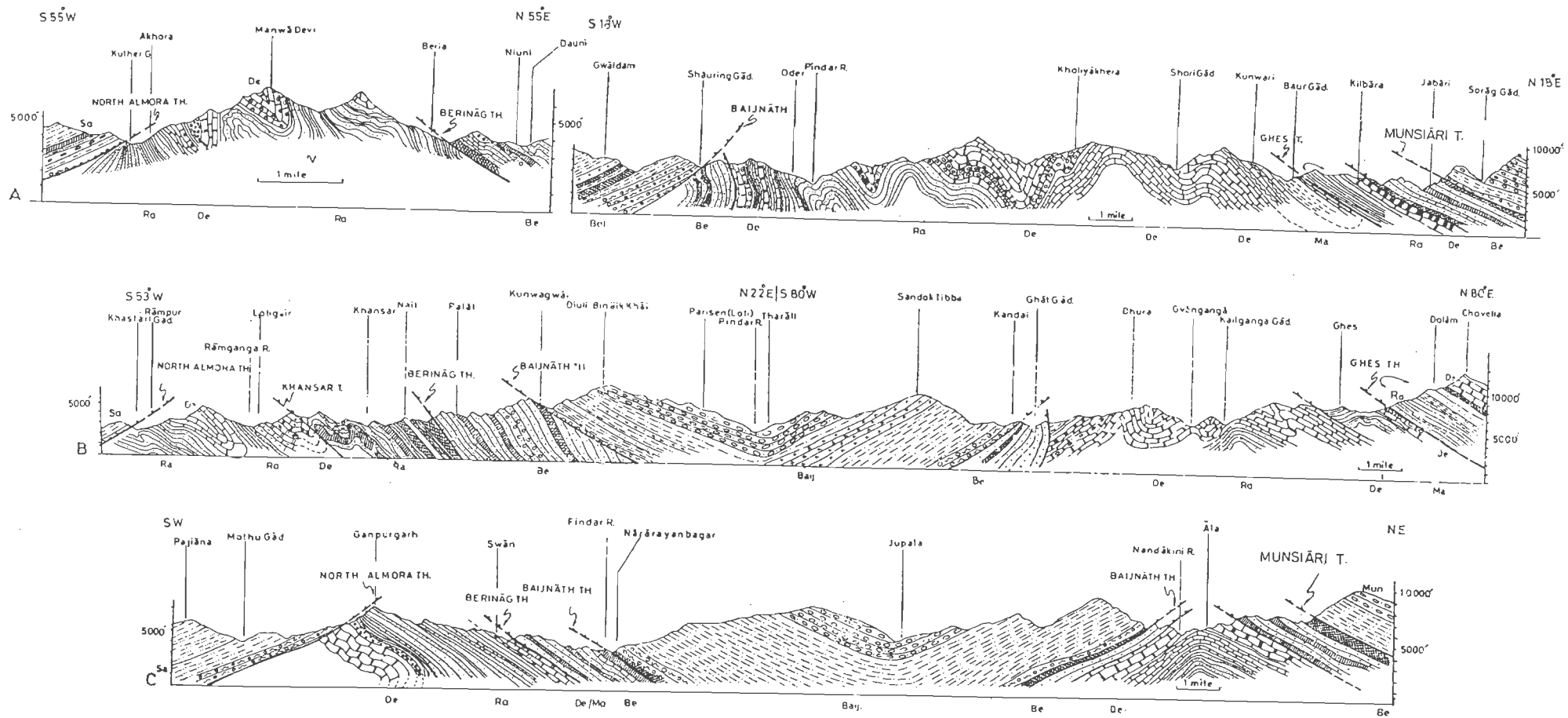


Fig. A1.2 Lithological succession and structural setting of the inner Lesser Himalaya in northwestern Almora and adjacent southern Chamoli district. Yj: Akhora-Manwadevi-Niuni and Gwaldam-Manmati-Kilbara (Pindar valley) hh: Rampur-Khansar-Tharali-Ghes-Chovelvia section ii: Pajana (S of Gairsen)-Ganpurgarh-Narayanbagar-Ala sections

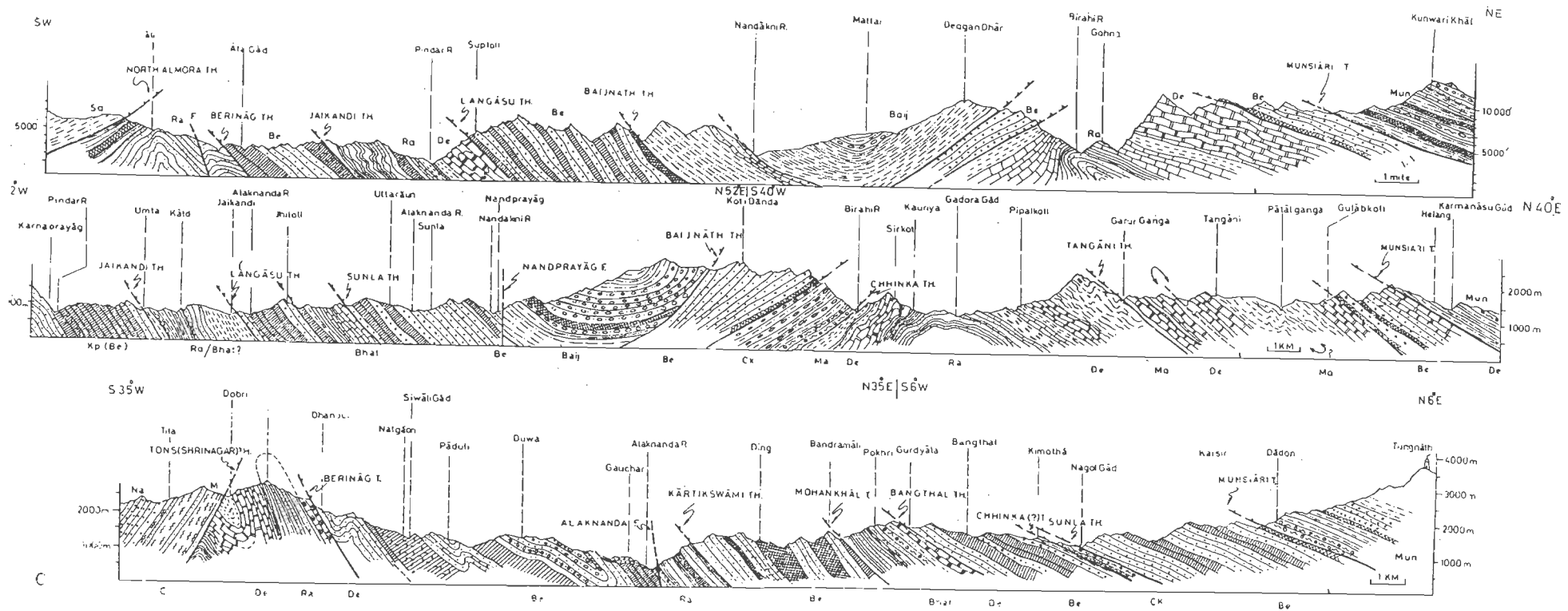


Fig. A1.3 Lithological and structural design of the inner Lesser Himalayan belt in southern and eastern Chamoli district
 jī. Ali (Adibadri)-Gauna-Kunwarikhal section
 kk: Karanprayag-Nandprayag-Pipalkoti-Hilang section
 ll: Dobri-Gauchar-Pokhri-Kimotha-Tungnath section

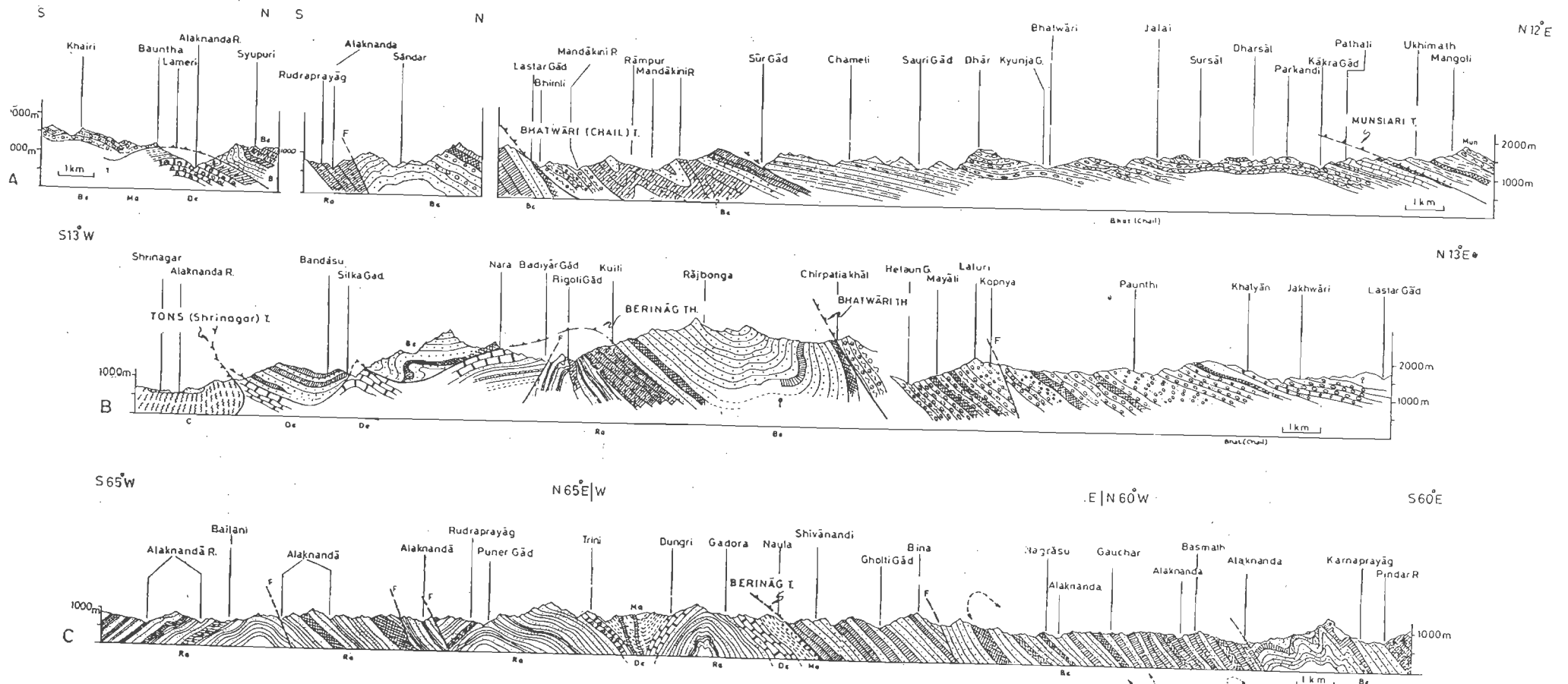


Fig. A1.4 Geology of the western Chamoli district in the inner Lesser Himalaya. nn: Khairi-Lameri-Syupuri, Rudraprayag-Sandar and Bhimli-Bhatwari-Ukhimath sections. oo: Shrinagar-Chirpatiakhali-Jakhwari section mm: Utyasu-Rudraprayag-Karnaprayag section along the Alaknanda river.

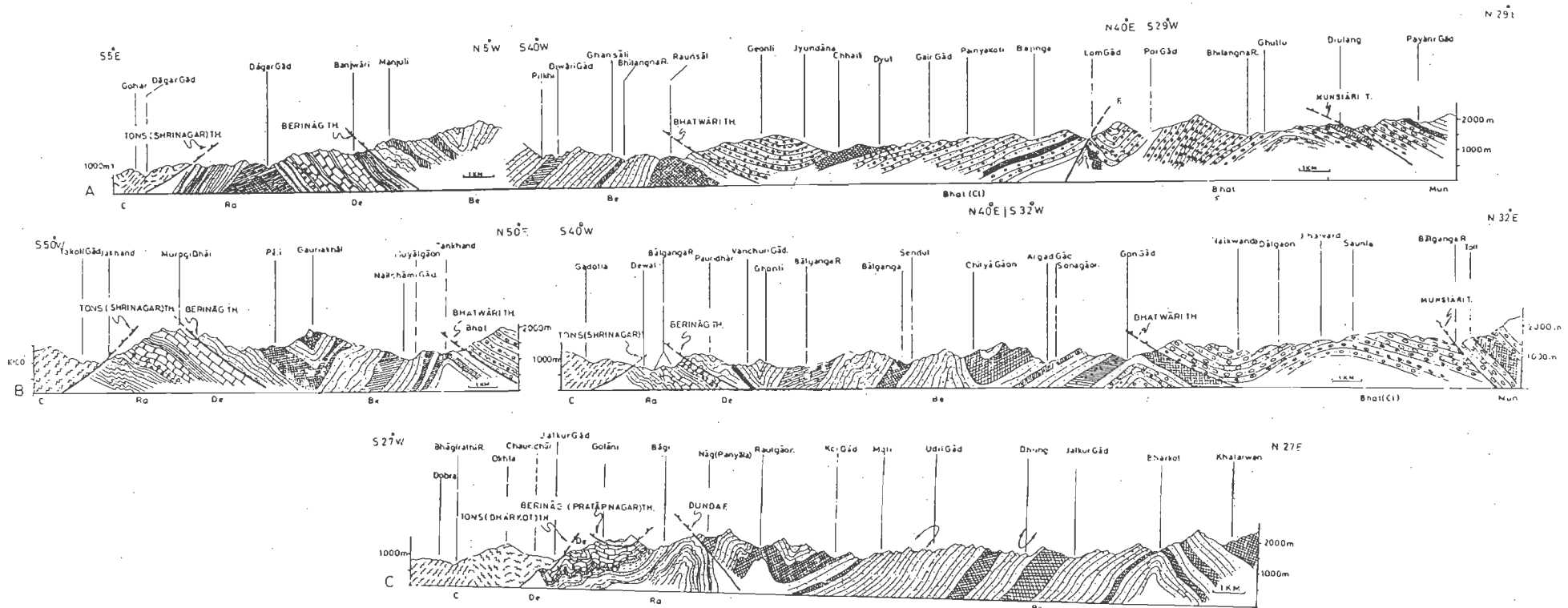


Fig. A1.5 Lithotectonic setting of the inner Lesser Himalaya in northwestern Tehri. pp: Gohar-Ghansali-Ghuttu section qq: Jakhand-Tankhand and Gadolia-Ghonti-Budhakedar sections in the Bhilangana-Balganga valleys rr: Dabra-Lamgaon-Kammand section along the Jalkur River

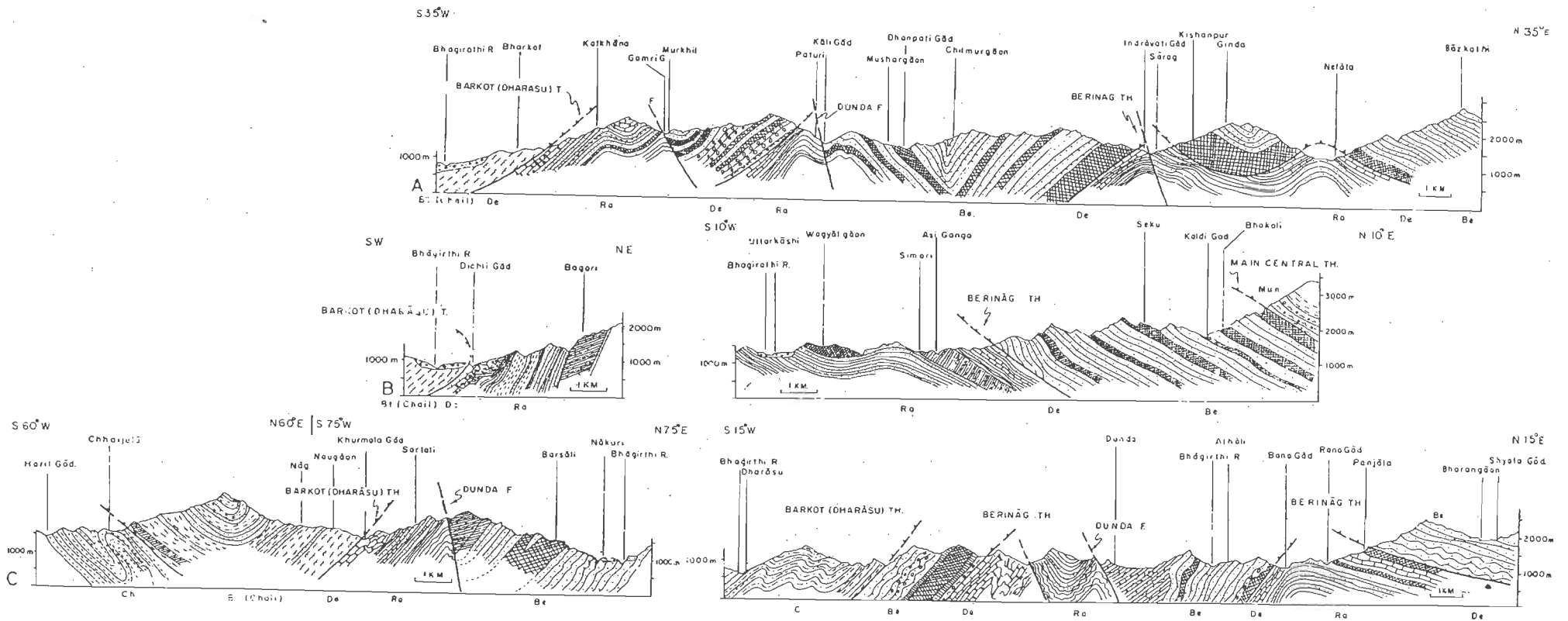


Fig. A1.6 Cross section of the inner Lesser Himalaya in eastern Uttarkashi district. ss: Barkot-Dhanari-Netala section
 Yq: Dichligad and Uttarkashi-Bhakoli sections. Yz: Chhajula (Bangaon)-Sartali-Nakuri sections Yr: Dharasu-
 Dunda-Panjala sections.

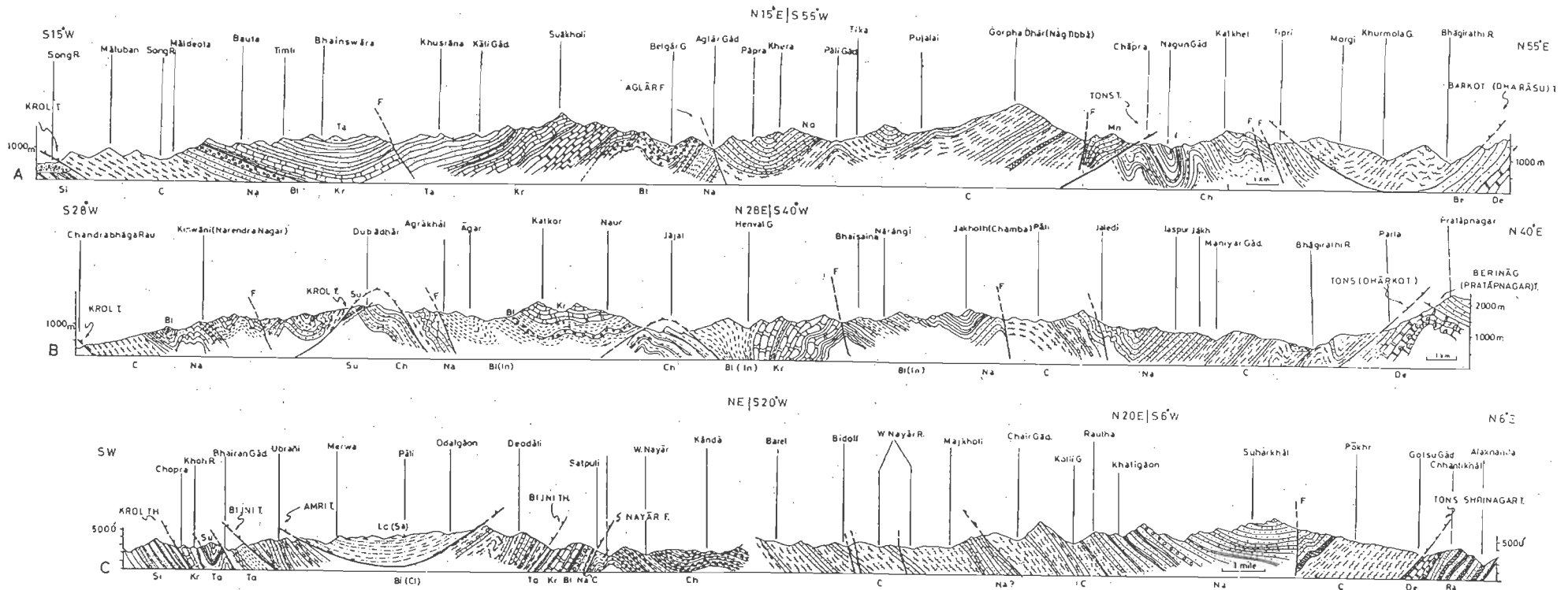


Fig. A1.7 Structure and lithological setting of the outer Lesser Himalaya in Pauri and southern Tehri districts. LL: Rajpur-Suakholi-Dewalsari-Chapra-Dharasu section. KK: W by Rishikesh-Agrakhal-Chamba-Pratapnagar section JJ: N by Kotdwar-Pali-Satpulu-Suharkhal (Khirsu)-Pokhri-Chhantikhāl section.

APPENDIX II

Appendix II contains the location of the earthquake events in the Garhwal Himalaya, which were used in the present study.

Earthquake events in the Garhwal Himalaya (used in present study)

Sl. No.	Origin -time						Latitude (° N)	Longitude (° E)	Depth (km)
	Y	M	D	Hr	Min	Sec			
1	1995	04	15	09	13	24.60	30.617	78.732	12.40
2	1995	04	19	21	57	45.80	30.698	78.508	9.60
3	1996	04	03	03	12	36.40	30.627	78.608	1.90
4	1996	04	14	21	03	35.00	30.077	78.106	29.60
5	1996	05	10	18	25	57.10	30.377	78.475	9.50
6	1996	05	18	18	35	11.00	30.370	78.449	4.50
7	1996	05	31	13	42	7.10	30.383	78.480	5.00
8	1996	07	12	14	27	48.10	30.381	78.459	4.40
9	1996	07	18	10	26	42.90	30.789	78.251	28.10
10	1996	07	18	12	34	18.90	30.735	78.300	19.70
11	1996	07	27	19	05	49.40	30.390	78.466	5.40
12	1996	07	28	14	45	8.90	30.387	78.462	3.80
13	1996	07	30	08	01	28.70	30.613	78.631	1.30
14	1996	08	20	13	28	12.60	30.370	78.465	6.60
15	1996	08	25	13	30	6.50	30.393	78.466	4.50
16	1996	08	28	14	56	5.30	30.379	78.468	4.10
17	1996	09	05	11	07	56.40	30.804	78.280	13.70
18	1996	09	13	15	53	8.70	30.687	78.420	9.40
19	1996	09	14	01	34	59.00	30.728	78.426	1.30
20	1996	09	14	07	34	16.30	30.709	78.439	11.20
21	1996	09	14	08	10	9.30	30.714	78.447	11.00
22	1996	09	14	12	31	14.90	30.695	78.433	8.90
23	1996	09	14	18	59	42.20	30.393	78.447	4.20
24	1996	09	15	01	10	57.20	30.630	78.538	26.90
25	1996	09	15	07	08	46.00	30.714	78.460	9.90
26	1996	09	15	09	49	17.10	30.709	78.303	18.90
27	1996	09	16	13	26	55.80	30.770	78.420	16.60
28	1996	09	16	13	35	4.10	30.752	78.436	14.10
29	1996	09	16	21	07	49.10	30.650	78.682	22.70
30	1996	09	18	02	55	36.10	30.727	78.462	10.60
31	1996	09	23	19	35	20.40	30.384	78.459	1.70
32	1996	09	26	13	51	57.90	30.313	78.490	27.70
33	1996	10	04	14	29	50.40	30.415	79.187	14.50
34	1996	10	07	09	14	48.60	30.379	78.480	8.60

Sl. No.	Origin -time						Latitude (° N)	Longitude (° E)	Depth (km)
	Y	M	D	Hr	Min	Sec			
35	1996	10	31	14	42	15.20	30.342	78.485	5.00
36	1996	12	19	23	29	18.10	30.613	78.669	6.40
37	1998	03	16	02	05	58.00	30.347	78.627	9.50
38	1998	03	17	23	08	32.60	30.514	78.722	16.40
39	1998	03	22	21	11	12.70	30.417	78.300	8.50
40	1998	03	22	22	08	19.50	30.721	78.456	14.50
41	1998	04	15	07	10	38.30	30.371	78.492	1.80
42	1998	04	20	07	18	43.70	30.387	78.474	6.50
43	1998	04	27	05	00	40.10	30.370	78.538	8.90
44	1998	05	22	01	54	28.20	30.574	78.075	28.20
45	1998	06	07	21	07	30.70	30.685	78.586	12.70
46	1998	06	13	23	01	11.00	30.305	78.176	29.80
47	2000	03	19	08	08	53.70	30.736	78.084	14.70
48	2000	05	02	22	57	4.80	30.084	78.759	23.10
49	2000	06	05	21	15	5.30	30.801	78.167	13.10
50	2000	07	02	01	37	25.20	30.692	78.320	12.30
51	2000	07	24	04	53	23.50	30.824	78.236	21.20
52	2000	07	29	19	08	56.80	30.504	78.311	11.90
53	2000	08	17	00	05	53.30	30.794	78.383	9.80
54	2000	09	22	23	04	2.10	30.789	78.206	14.50
55	2000	10	01	11	44	20.00	30.429	78.959	14.30
56	2000	10	05	19	58	9.70	30.614	78.494	14.00
57	2000	11	20	21	17	39.50	31.070	78.090	8.50
58	2000	12	22	02	51	48.70	30.125	78.160	31.70
59	2000	12	22	07	16	9.20	30.648	78.623	11.80
60	2001	01	04	11	45	14.60	30.370	78.577	7.00
61	2001	01	05	05	54	2.80	30.575	78.728	9.90
62	2001	01	06	04	58	28.30	30.494	79.159	10.70
63	2001	01	07	20	12	34.30	30.809	78.317	12.20
64	2001	01	24	04	18	7.20	30.544	78.275	9.10
65	2001	02	19	15	34	40.40	30.300	78.245	13.60
66	2001	03	02	20	18	20.20	30.487	79.086	11.70
67	2001	03	12	04	16	21.50	30.564	78.803	14.60
68	2001	03	19	04	28	40.00	30.667	78.620	13.90
69	2001	04	03	11	31	27.90	30.598	78.813	17.50
70	2001	04	14	16	26	0.40	30.789	78.397	14.50

Sl. No.	Origin -time						Latitude (° N)	Longitude (° E)	Depth (km)
	Y	M	D	Hr	Min	Sec			
71	2001	04	26	09	02	6.50	30.512	79.068	14.50
72	2001	05	28	09	02	9.80	30.871	78.213	27.10
73	2001	06	02	00	20	33.20	30.499	78.916	16.60
74	2001	06	02	23	56	14.40	30.275	78.638	15.40
75	2001	06	07	23	50	44.50	30.254	78.557	18.30
76	2001	06	08	04	36	16.90	30.637	78.753	14.20
77	2001	06	29	10	19	4.30	30.315	78.557	6.90
78	2001	07	12	06	34	46.10	30.704	78.408	12.60
79	2001	07	23	05	24	33.40	30.682	78.899	40.40
80	2001	07	26	00	31	56.70	29.827	79.794	27.60
81	2001	07	27	20	56	11.20	30.740	78.417	11.20
82	2001	07	29	19	49	12.00	30.403	77.999	21.10
83	2001	08	02	03	24	46.10	30.535	78.988	15.40
84	2001	09	18	03	34	47.20	30.646	78.611	8.70
85	2001	10	05	09	04	18.30	30.365	78.473	8.40
86	2001	10	20	01	09	6.70	30.062	78.741	22.90
87	2001	10	23	12	12	54.60	30.303	78.061	29.80
88	2001	11	09	20	46	22.20	30.819	78.351	13.10
89	2001	12	08	05	39	37.80	30.602	78.741	13.00
90	2001	12	15	20	32	28.00	30.338	78.563	14.20
91	2001	12	22	15	38	50.80	30.309	78.320	30.60
92	2002	01	02	18	40	9.20	30.698	78.343	8.70
93	2002	01	12	00	59	28.50	30.481	78.195	13.10
94	2002	01	14	22	06	55.40	30.813	78.351	13.90
95	2002	01	17	03	45	9.30	30.778	78.379	14.20
96	2002	01	26	19	56	24.90	30.449	79.413	42.90
97	2002	02	12	04	02	16.10	30.855	78.139	12.40
98	2002	02	23	19	54	42.40	30.450	79.204	24.20
99	2002	03	31	02	06	15.50	30.664	78.619	9.80
100	2002	04	13	22	10	43.10	31.000	78.173	12.40
101	2002	04	20	12	33	59.00	30.535	79.117	12.30
102	2002	07	15	05	10	56.10	30.638	78.511	32.10
103	2002	08	11	18	05	7.90	30.805	78.376	14.00
104	2002	08	12	03	46	57.50	30.451	78.092	22.40
105	2002	10	09	22	30	31.40	30.610	78.841	16.90
106	2003	01	19	20	46	47.60	30.578	78.676	18.40

Sl. No.	Origin -time						Latitude (° N)	Longitude (° E)	Depth (km)
	Y	M	D	Hr	Min	Sec			
107	2003	01	21	23	16	4.90	30.247	78.519	26.50
108	2003	01	25	05	35	59.20	30.577	78.795	16.20
109	2003	02	03	03	51	3.20	30.828	78.307	12.40
110	2003	02	13	06	57	7.00	30.361	78.466	7.20
111	2003	05	05	17	23	57.70	30.221	78.310	17.10
112	2003	11	05	02	58	35.10	30.775	78.417	14.60
113	2004	01	01	19	39	17.70	30.399	78.597	8.30
114	2004	01	07	18	43	39.70	30.378	78.617	17.00
115	2004	01	17	23	06	29.10	30.257	78.596	14.00
116	2004	02	05	16	02	8.00	30.494	78.252	18.40
117	2004	02	09	20	35	22.70	30.386	78.601	13.00
118	2004	03	15	23	59	9.50	30.751	78.388	9.50
119	2004	03	20	19	42	34.20	30.373	78.607	1.30
120	2004	03	22	23	49	22.60	30.527	79.046	12.70
121	2004	03	30	07	33	6.60	30.302	78.480	13.60
122	2004	04	01	11	20	43.30	30.541	79.001	18.70
123	2004	04	01	23	31	49.60	30.540	78.973	14.10
124	2004	04	05	21	15	26.60	30.760	78.207	13.30
125	2004	06	03	22	56	23.30	30.642	78.791	11.10
126	2004	06	24	18	14	46.10	30.380	78.626	41.00
127	2006	02	06	05	03	13.80	30.453	79.078	12.10
128	2006	02	08	07	29	2.20	30.639	78.652	9.40
129	2006	02	14	15	26	37.60	30.427	78.749	24.90
130	2006	02	16	05	58	5.60	30.517	79.042	27.20
131	2006	03	25	10	51	40.80	30.751	78.287	14.50
132	2006	04	29	19	30	32.40	30.621	78.174	9.90
133	2006	07	01	09	19	46.10	30.594	78.367	9.00
134	2006	07	10	00	08	8.30	30.404	78.568	12.60
135	2006	07	16	19	08	34.90	30.663	78.594	22.80
136	2006	07	31	13	45	16.20	30.503	79.201	15.60
137	2006	11	23	15	43	26.20	30.464	78.939	18.10
138	2006	12	08	06	22	34.20	30.483	78.100	20.20
139	2006	12	09	02	51	16.30	29.923	77.694	4.00
140	2006	12	09	06	47	31.10	30.858	78.229	26.80
141	2006	12	10	22	14	7.20	30.776	78.287	17.30
142	2006	12	13	01	04	26.70	30.965	78.155	12.70

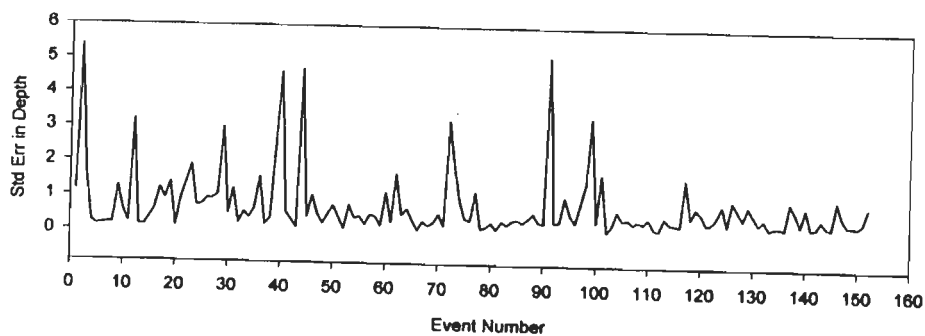
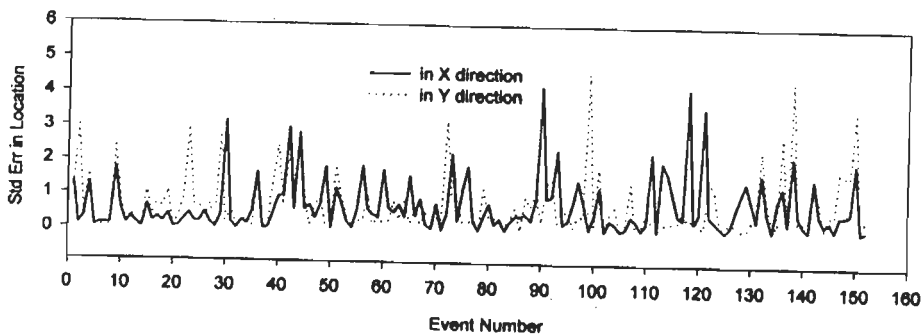
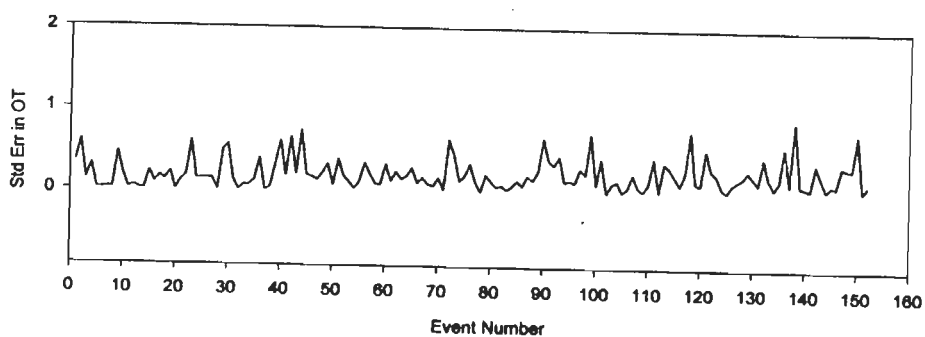
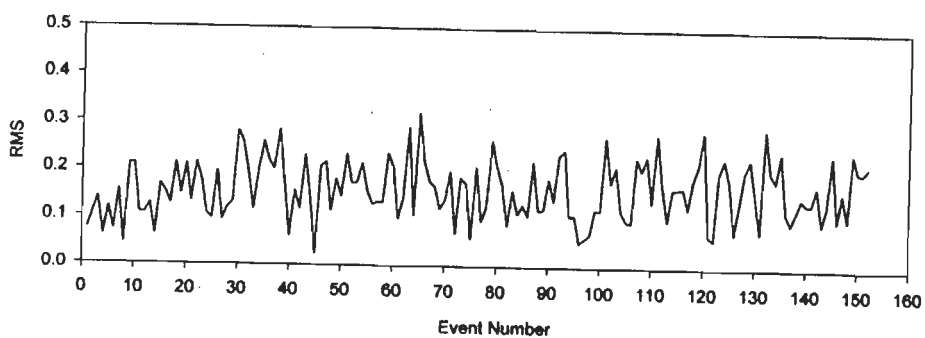
Sl. No.	Origin -time						Latitude (° N)	Longitude (° E)	Depth (km)
	Y	M	D	Hr	Min	Sec			
143	2007	01	10	00	22	6.60	30.873	78.197	13.80
144	2007	02	24	05	59	25.70	30.286	78.594	16.20
145	2007	02	28	05	38	45.40	30.524	78.937	15.20
146	2007	03	17	17	15	17.80	30.847	78.211	12.90
147	2007	03	23	23	14	37.60	30.624	78.648	24.70
148	2007	03	31	05	57	21.70	30.889	78.097	14.90
149	2007	04	11	16	57	52.80	30.601	78.782	13.40
150	2007	04	13	00	00	17.40	30.693	78.643	9.70
151	2007	04	13	14	49	47.50	30.250	78.566	11.80
152	2007	04	16	01	35	20.50	30.930	79.110	17.10
153	2007	04	20	12	51	33.70	30.909	78.240	16.20
154	2007	05	01	23	31	12.70	30.450	78.319	17.90
155	2007	05	08	03	07	21.20	30.765	78.298	14.90
156	2007	06	01	19	01	11.40	29.966	77.966	45.40
157	2007	06	30	22	29	16.40	30.716	78.506	11.30
158	2007	07	23	13	30	2.80	30.801	78.314	14.80
159	2007	07	28	20	35	15.40	30.813	78.309	10.90
160	2007	08	05	14	28	7.80	30.778	78.300	14.20
161	2007	08	07	17	57	53.90	30.752	78.185	13.30
162	2007	08	25	13	46	21.60	30.410	78.538	22.50
163	2007	09	14	00	20	10.40	30.707	78.531	21.30
164	2007	09	26	06	52	3.20	30.823	78.235	19.70

APPENDIX III

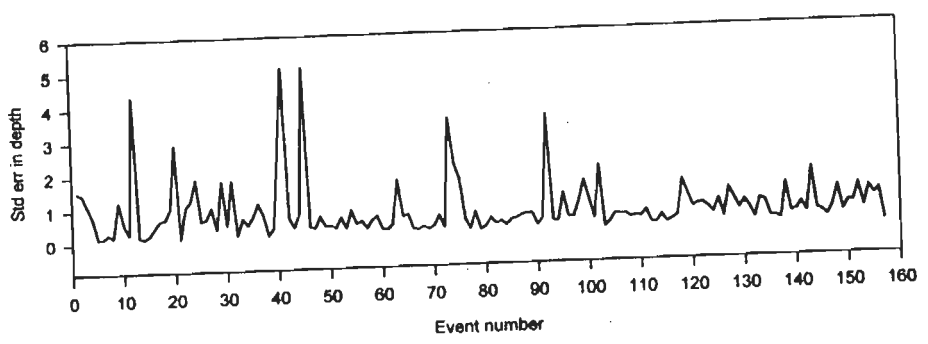
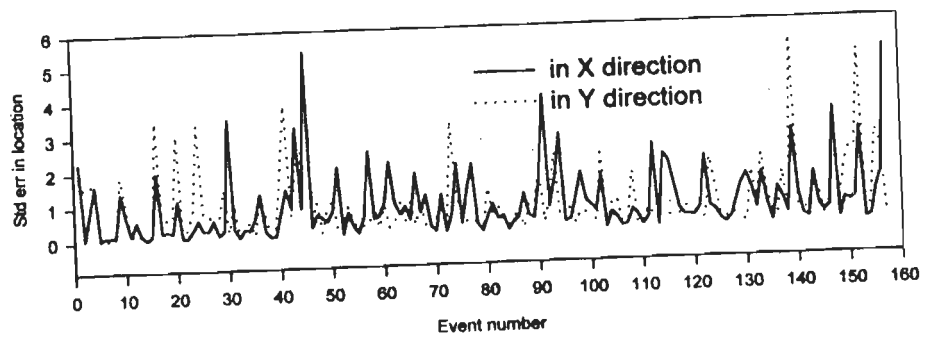
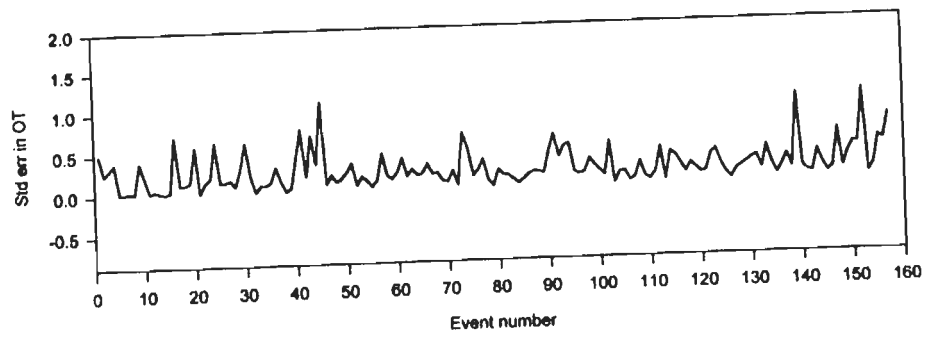
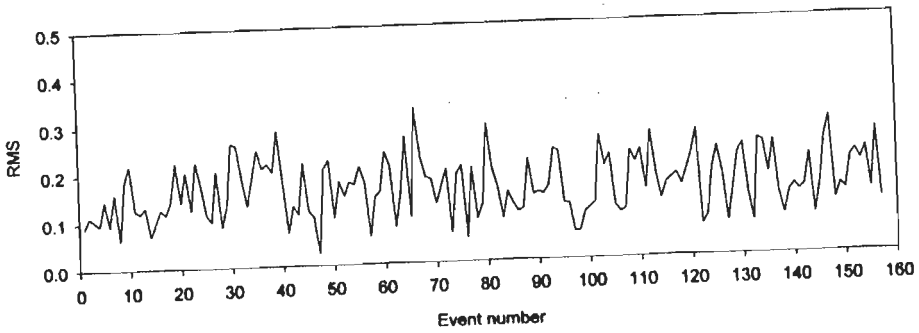
Appendix III presents the error in hypocentral parameters i.e. location of earthquake events (x, y and z); origin time and residuals. These errors were estimated while doing relocation of earthquakes during the process of 3-D analysis. The error gives the idea of the quality of the hypocenters located using the P and S arrivals and the 3-D structure estimated in last iteration. The appendix consists of the errors for Model I, Model II, Model III and Model IV using the east–west gridding and NE-SW gridding respectively.

Further, the parameters KHIT, DWS and RESOLUTION are also given in the same Appendix. These values are given for east–west gridding and NE-SW gridding respectively using all the four models.

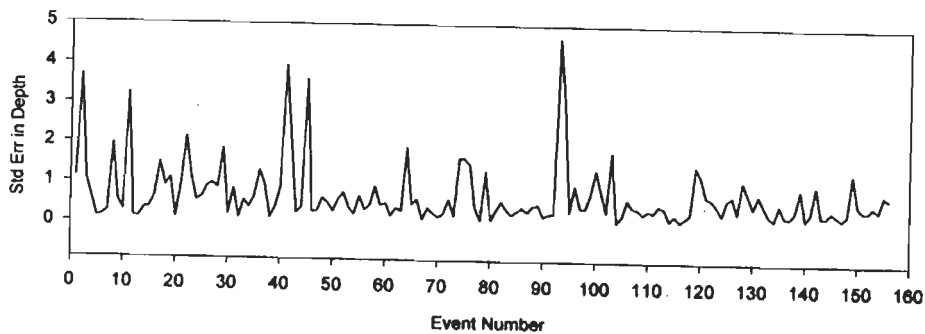
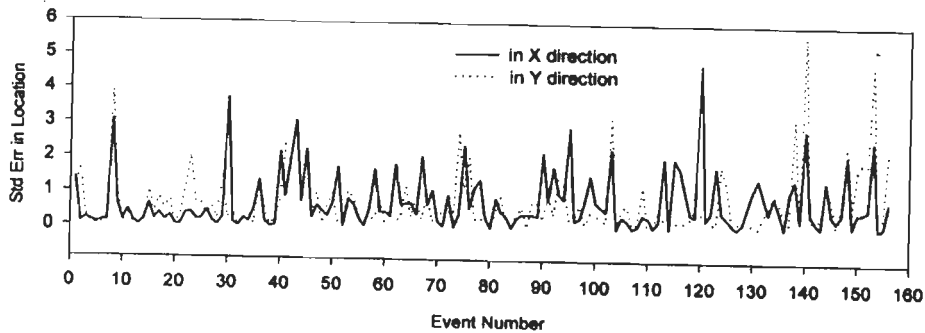
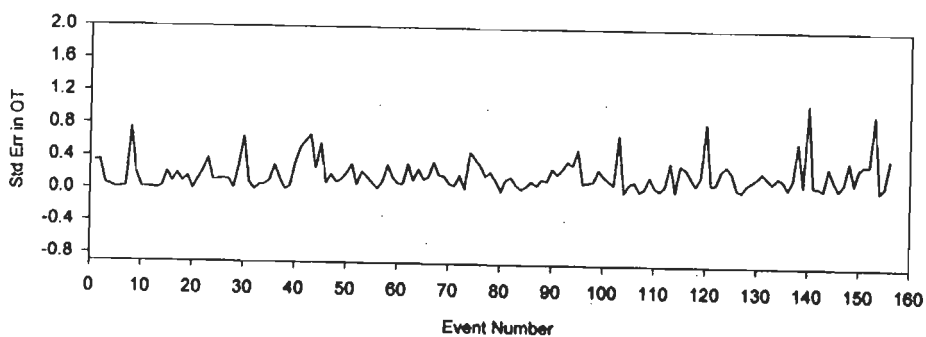
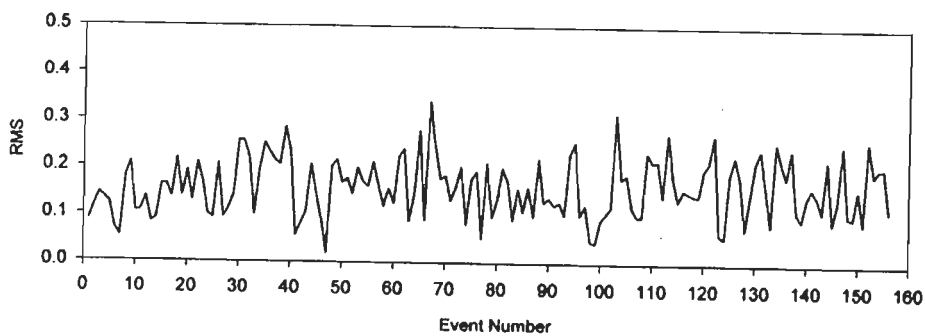
Model -I East West Gridding



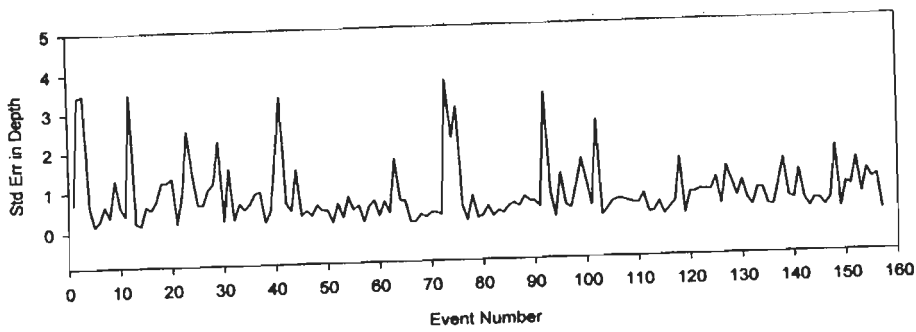
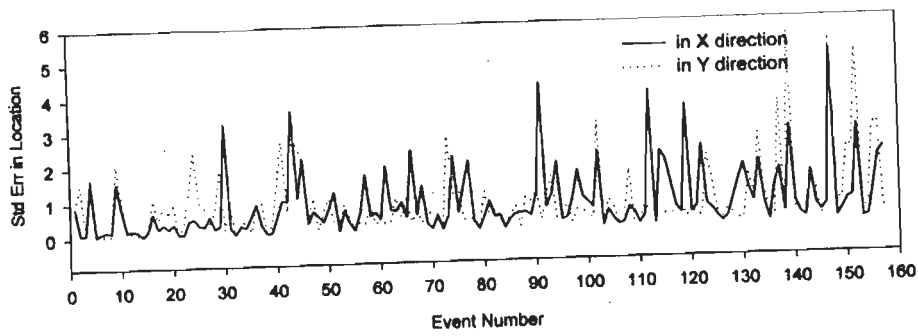
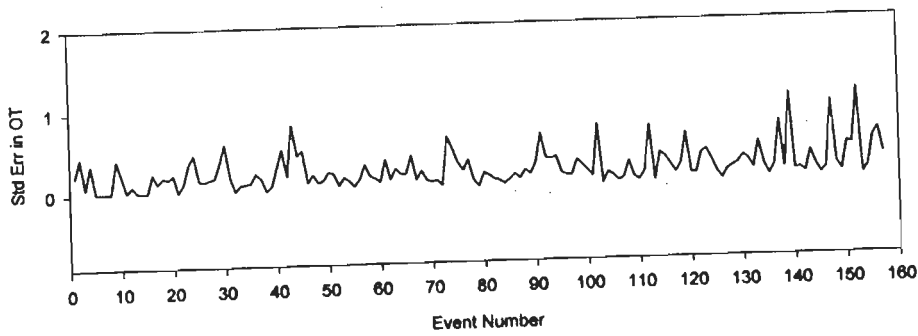
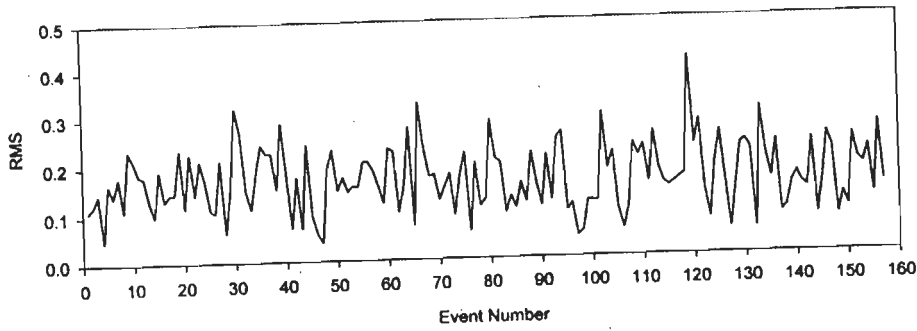
Model -II East West Gridding



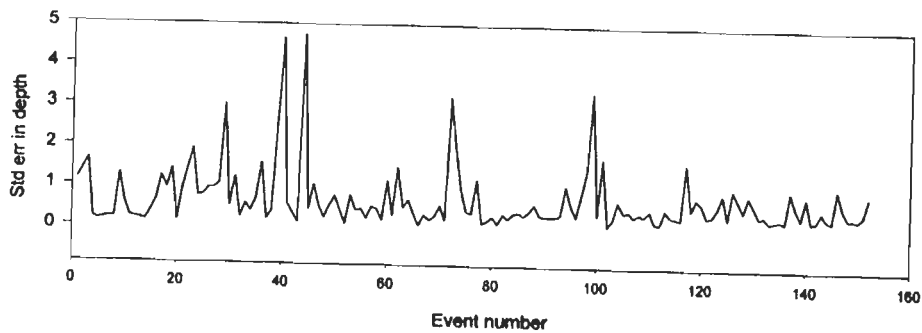
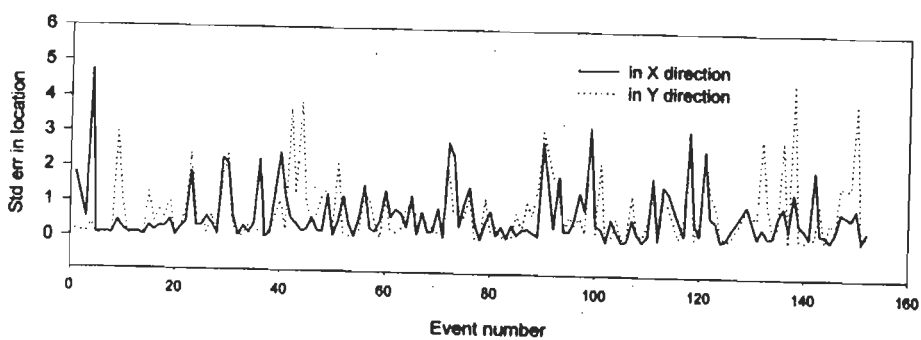
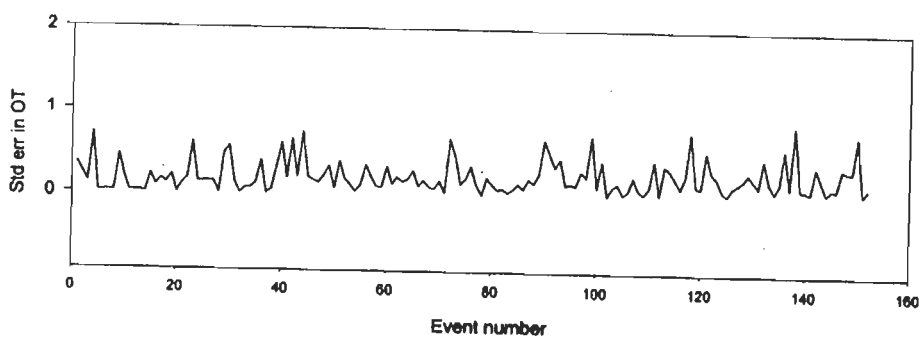
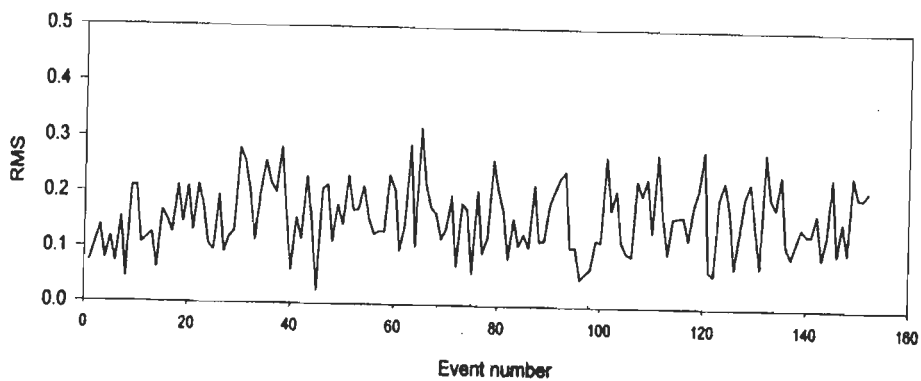
Model -III East West Gridding



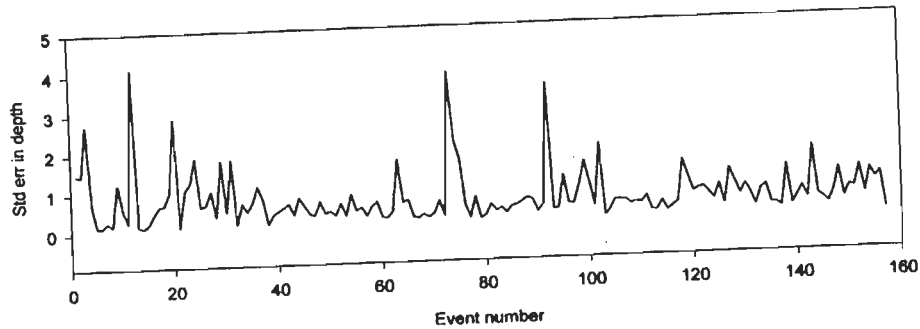
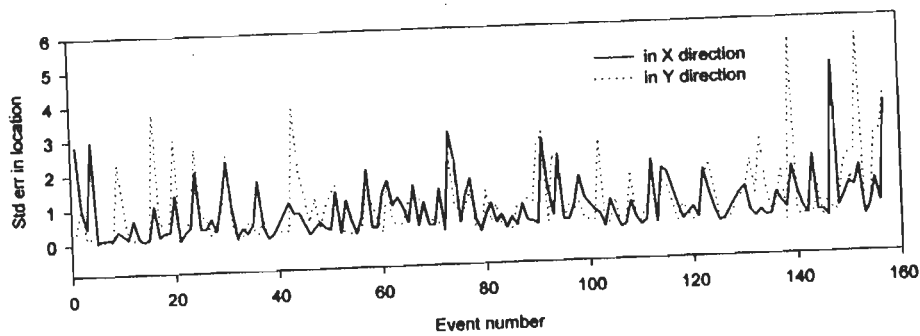
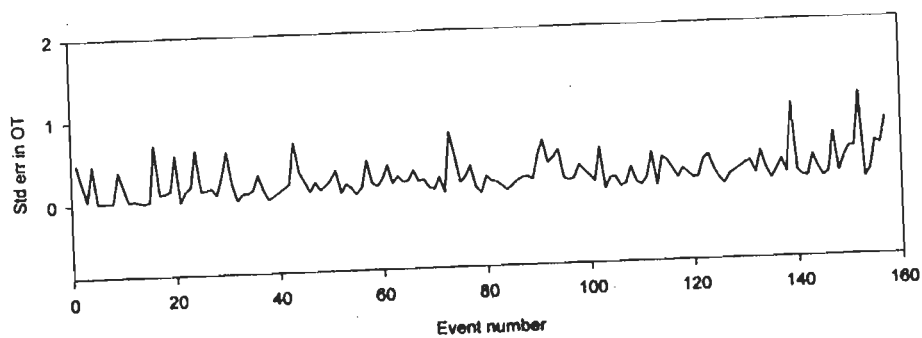
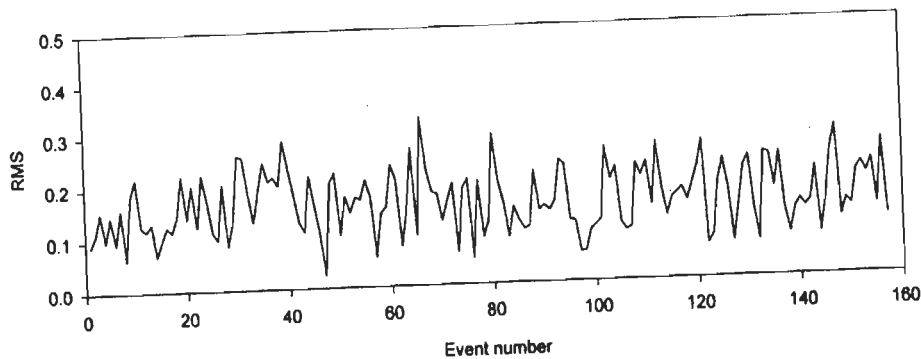
Model -IV East West Gridding



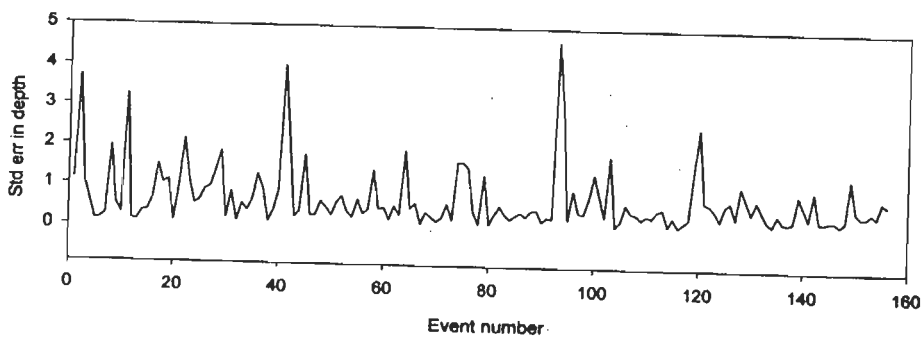
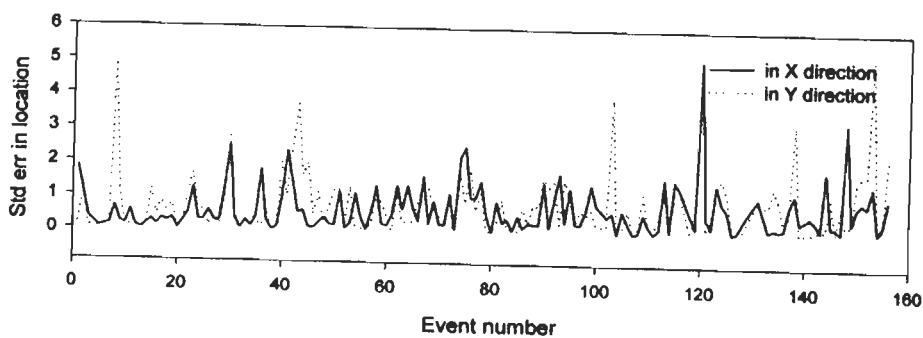
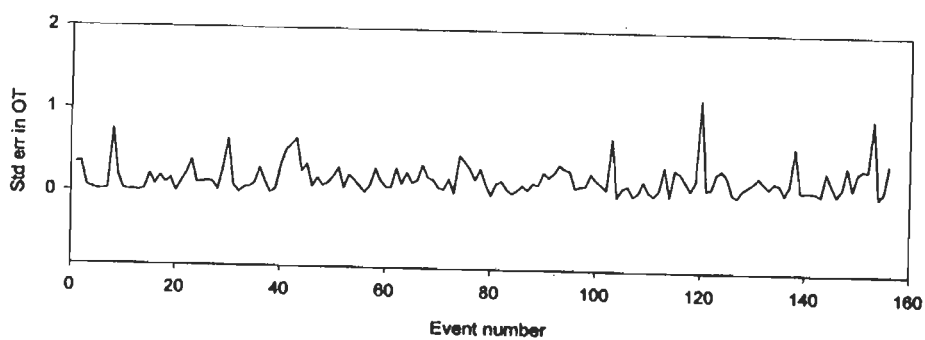
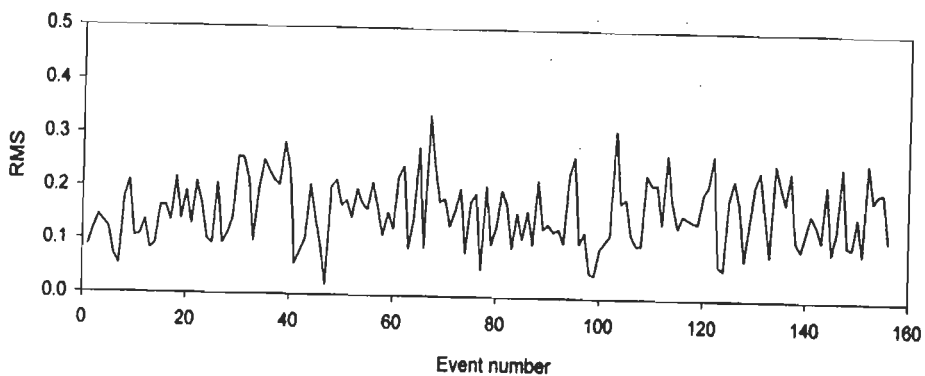
Model -I NE-SW Gridding



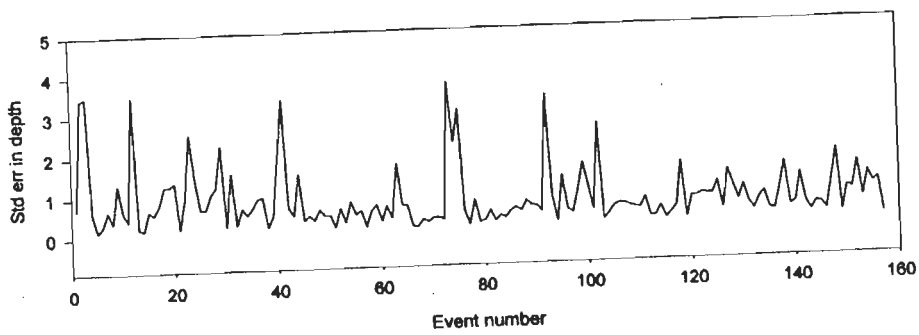
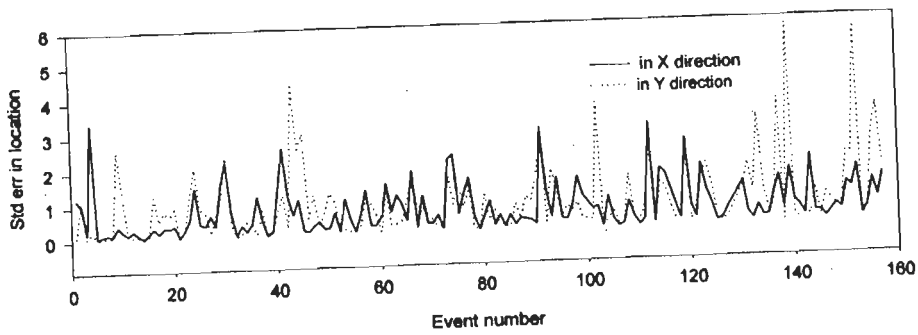
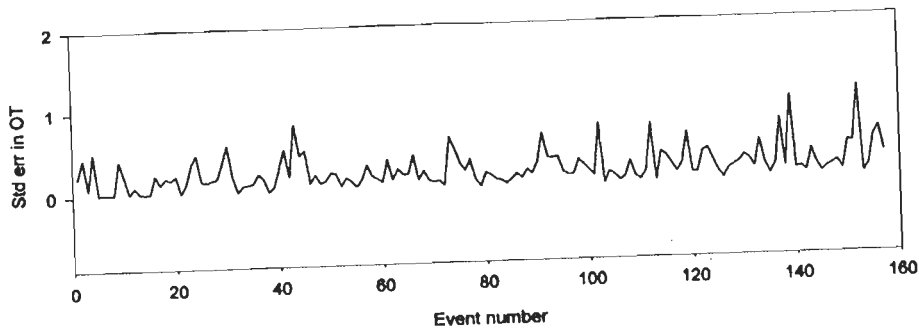
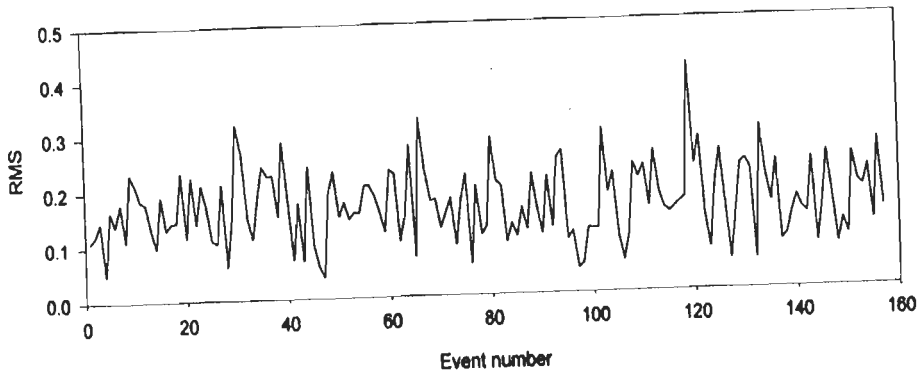
Model -II NE-SW Gridding



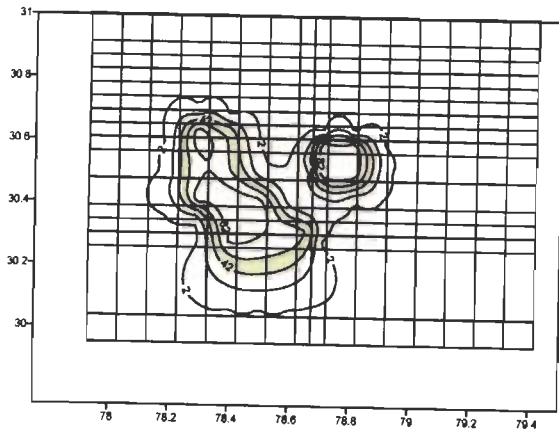
Model -III NE-SW Gridding



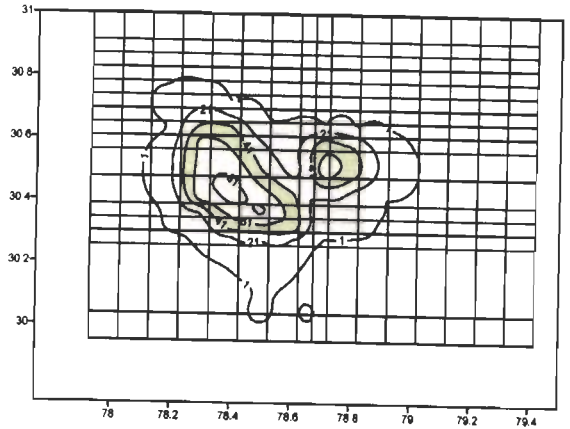
Model -IV NE-SW Gridding



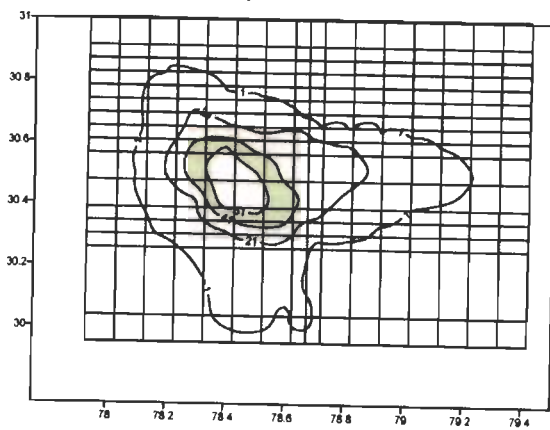
KHIT for 3-D Model-I



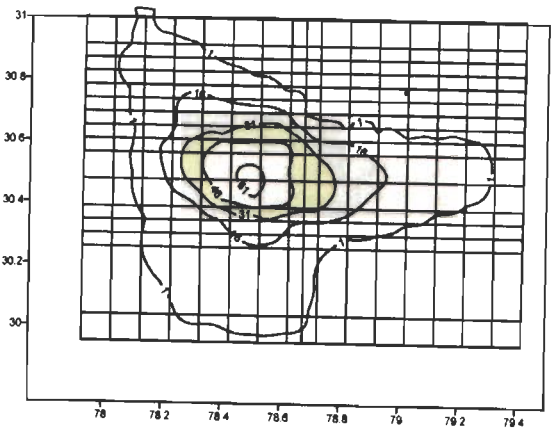
Depth 2 km



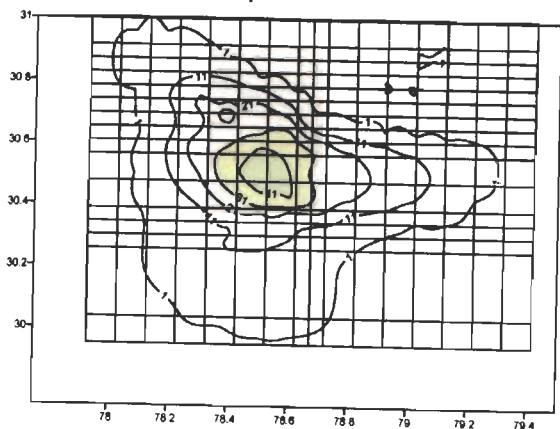
Depth 4 km



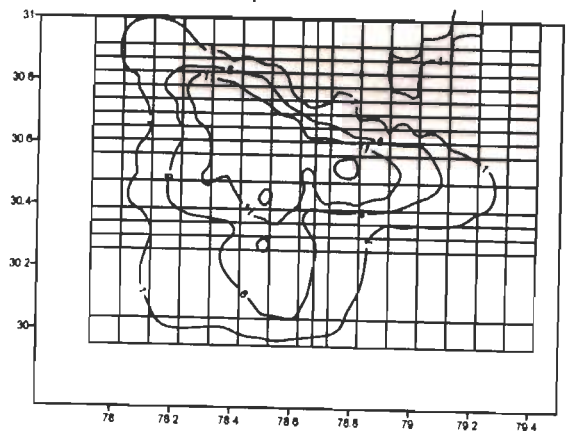
Depth 6 km



Depth 8 km

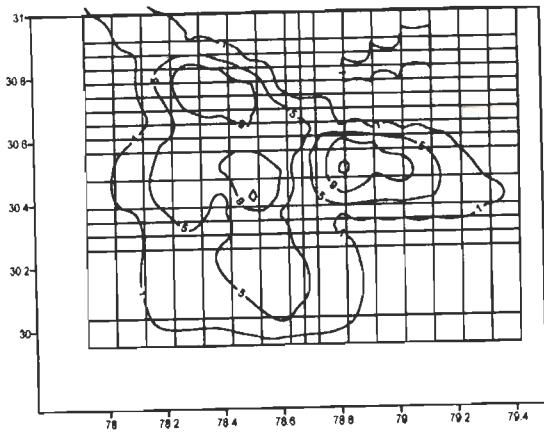


Depth 12 km

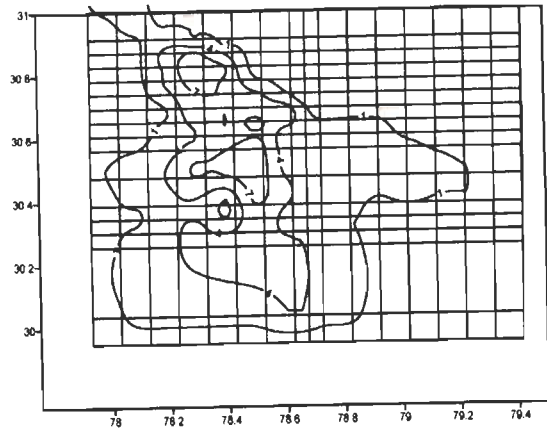


Depth 14 km

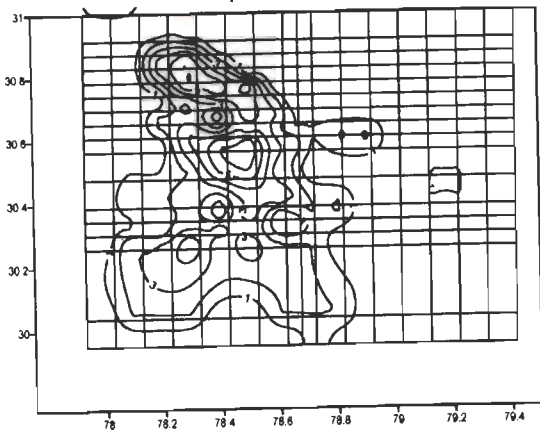
KHIT for 3-D Model-I



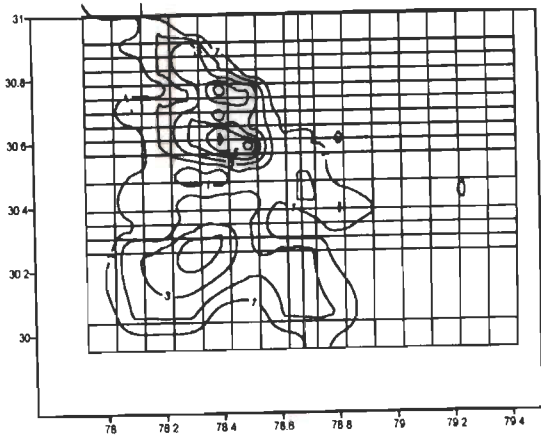
Depth 16 km



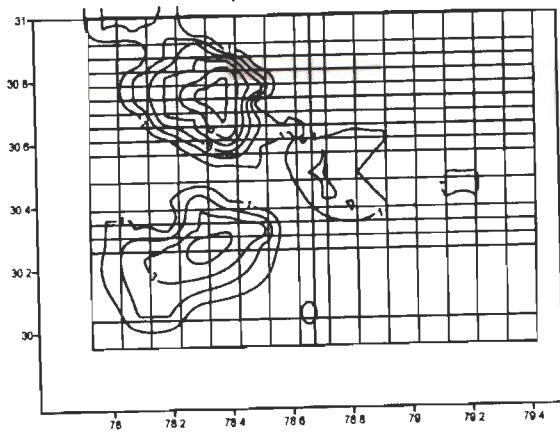
Depth 20 km



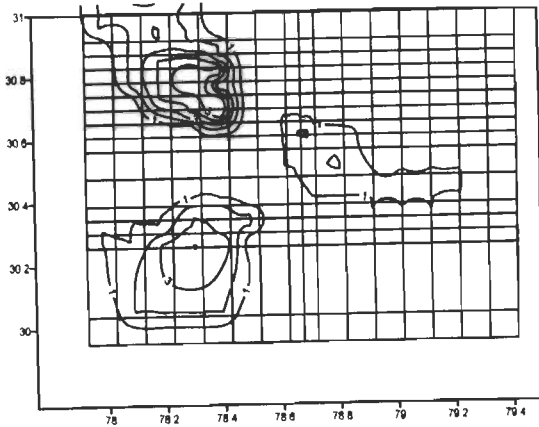
Depth 22 km



Depth 24 km

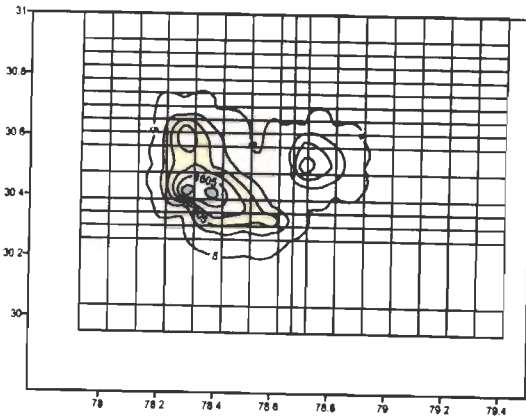


Depth 26 km

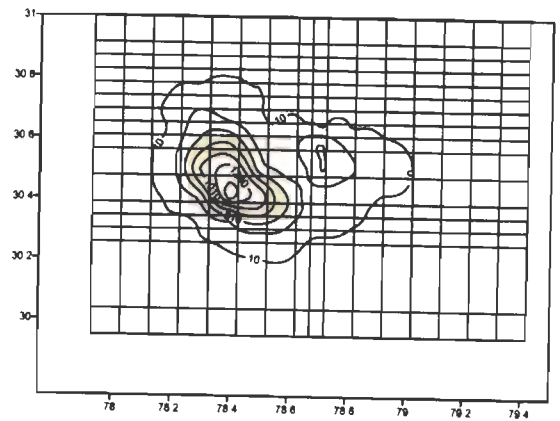


Depth 28 km

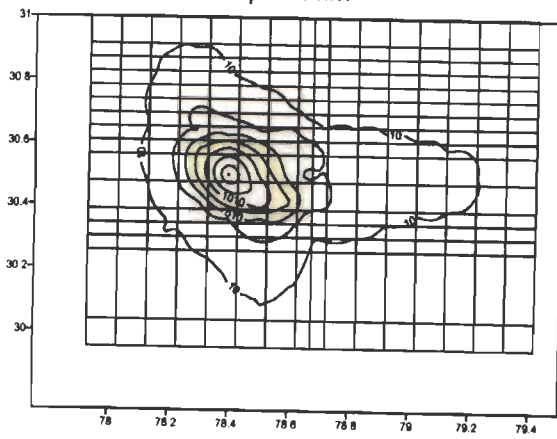
DWS for 3-D Model-I



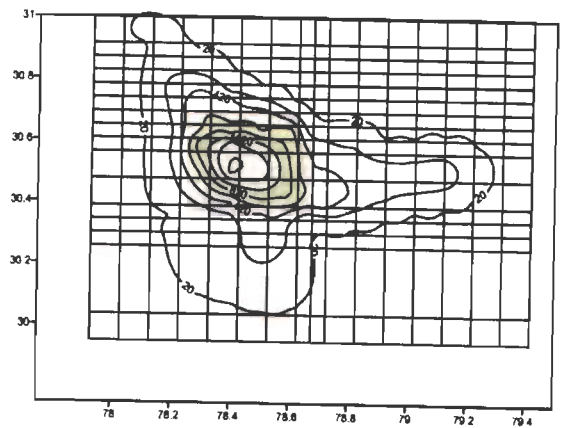
Depth 2 km



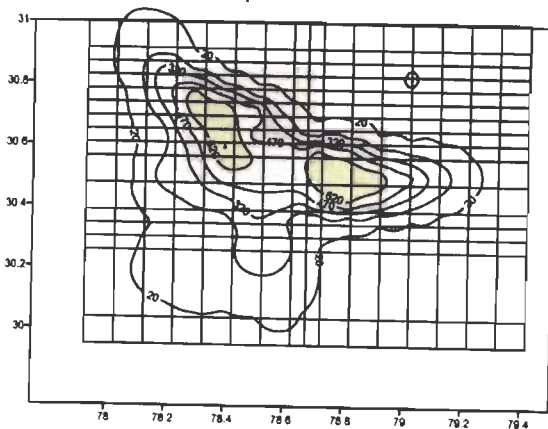
Depth 4 km



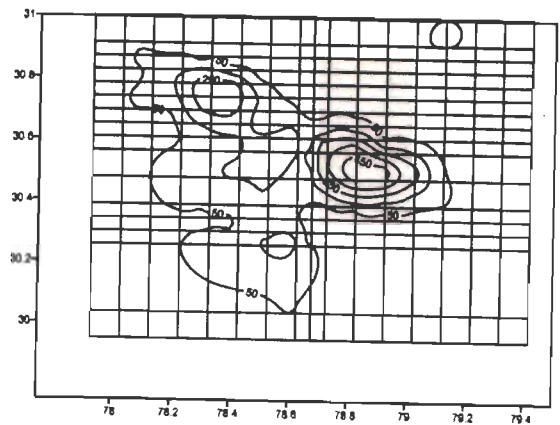
Depth 6 km



Depth 8 km

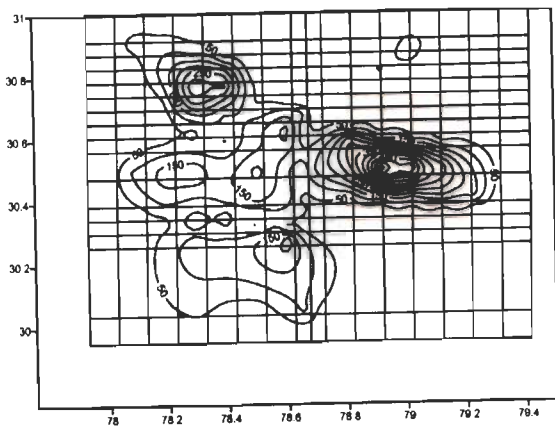


Depth 12 km

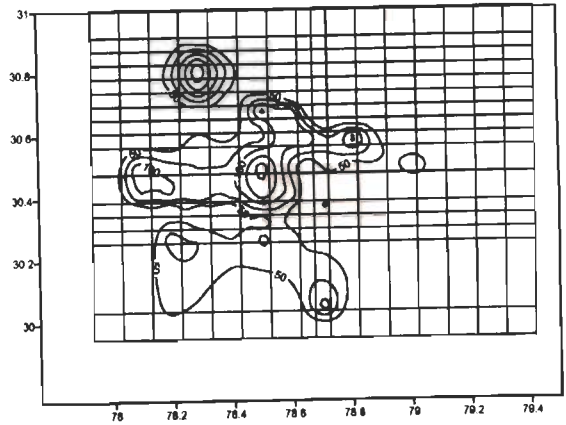


Depth 14 km

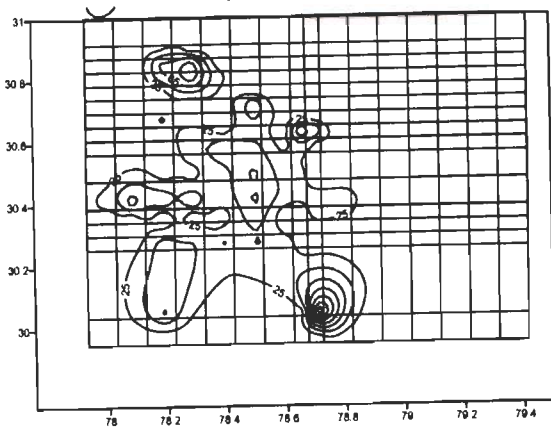
DWS for 3-D Model-I



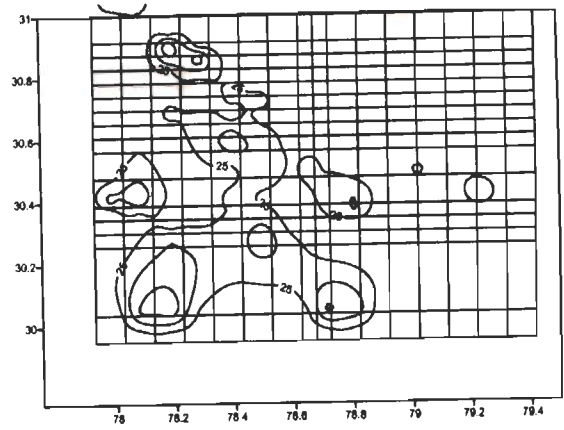
Depth 16 km



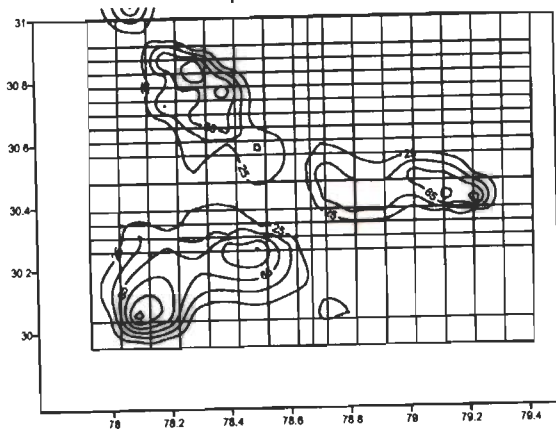
Depth 20 km



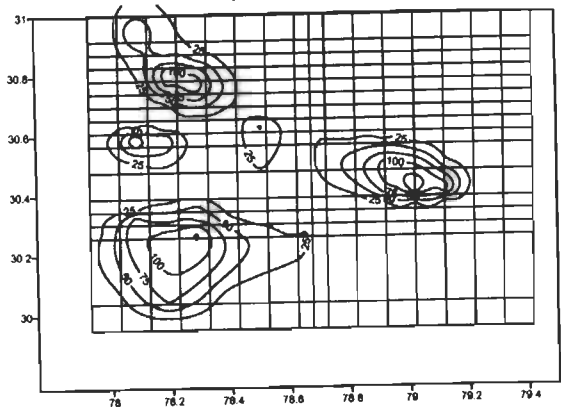
Depth 22 km



Depth 24 km

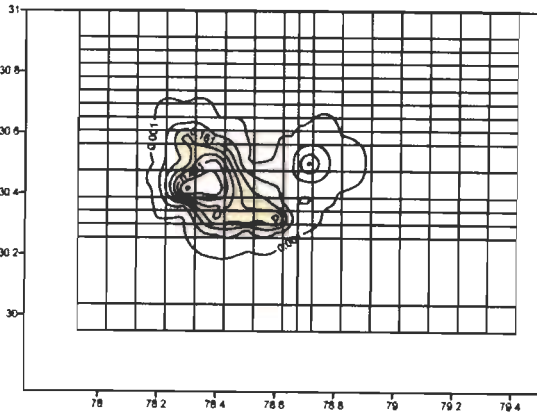


Depth 26 km

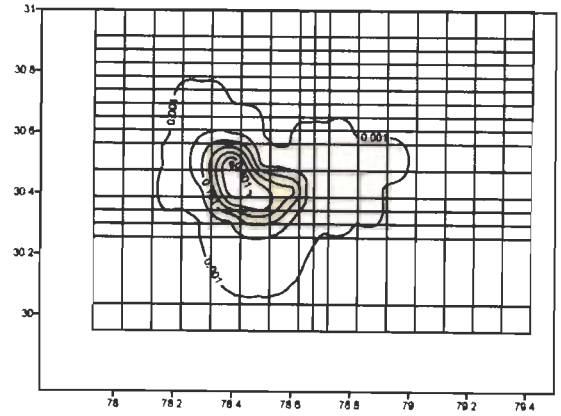


Depth 28 km

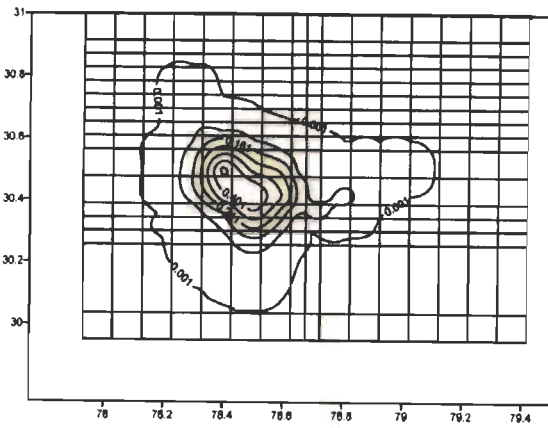
RESOLUTION for 3-D Model-I



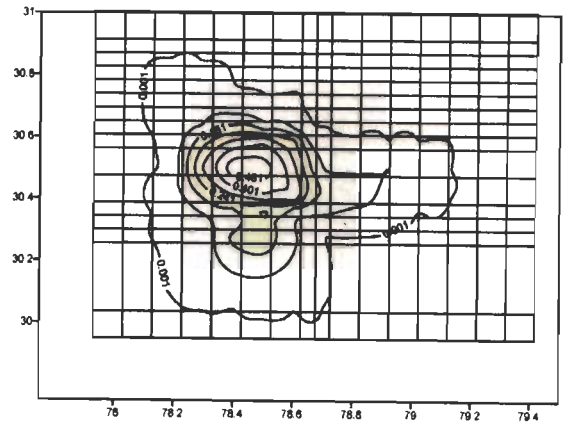
Depth 2 km



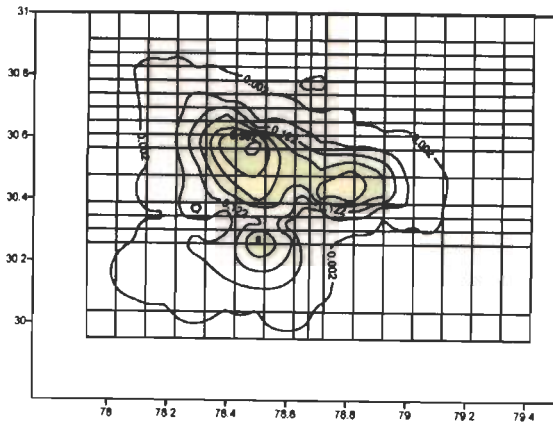
Depth 4 km



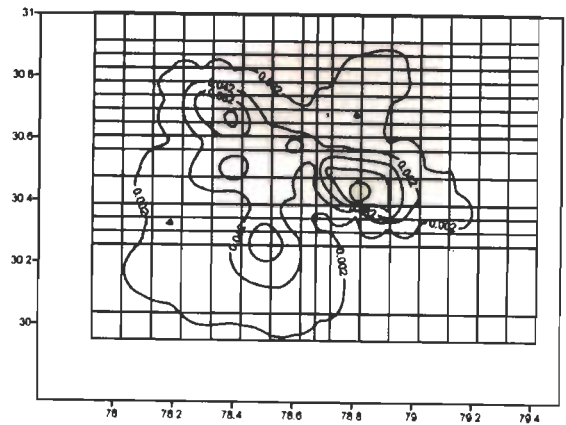
Depth 6 km



Depth 8 km

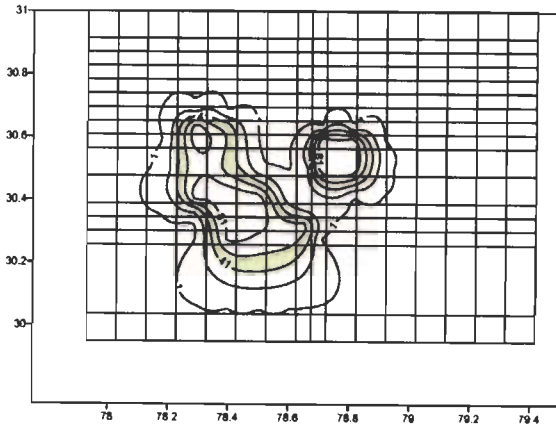


Depth 12 km

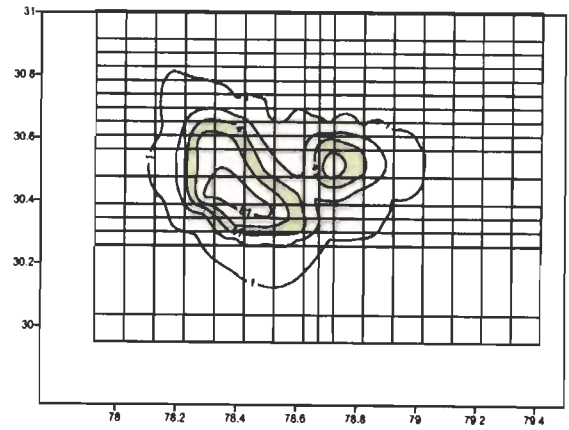


Depth 14 km

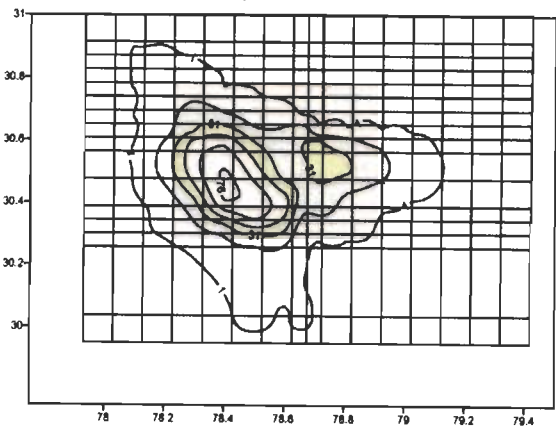
KHIT for 3-D Model-II



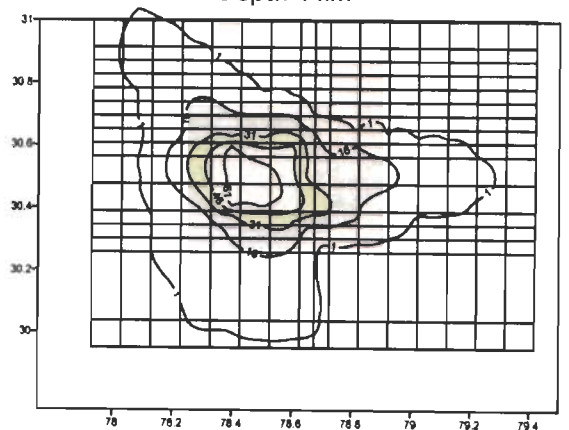
Depth 2 km



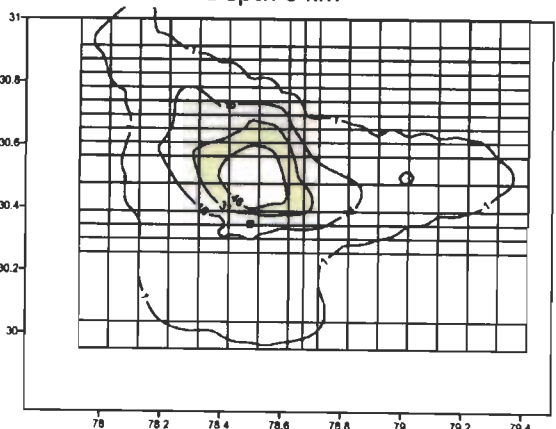
Depth 4 km



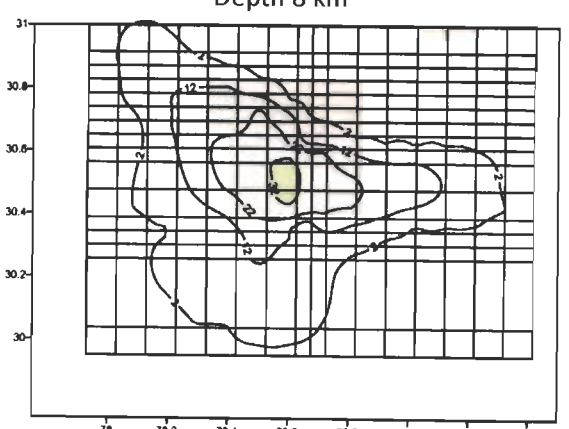
Depth 6 km



Depth 8 km

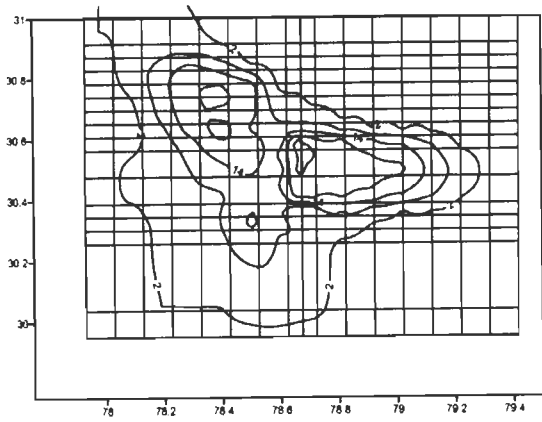


Depth 12 km

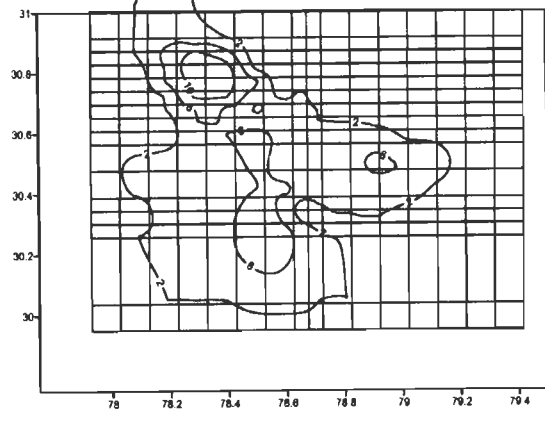


Depth 14 km

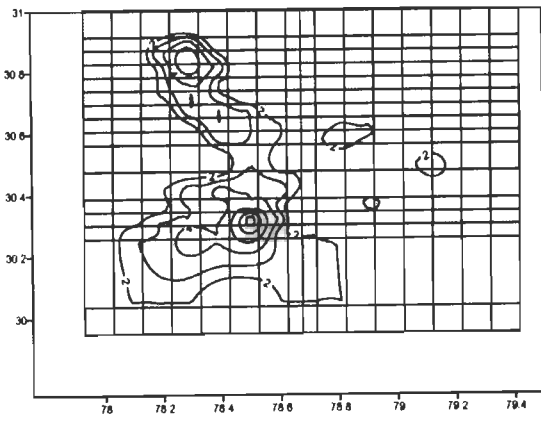
KHIT for 3-D Model-II



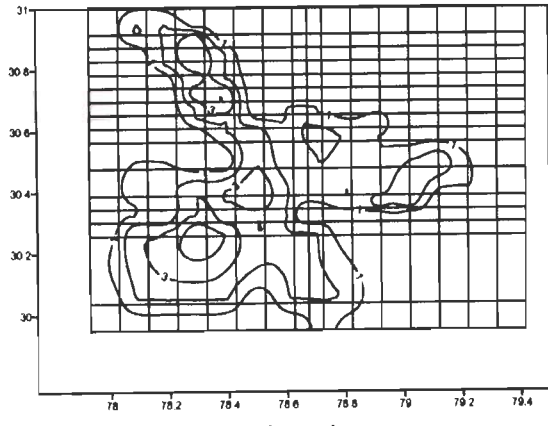
Depth 16 km



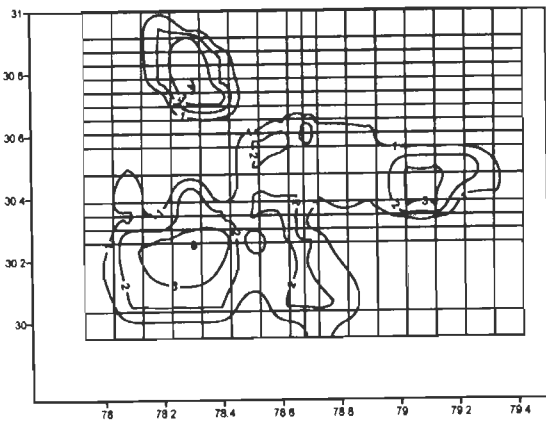
Depth 20 km



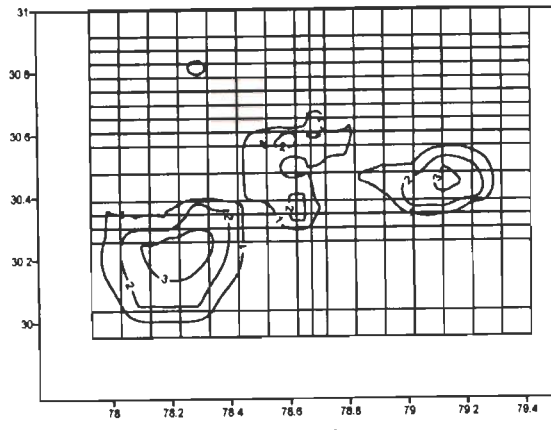
Depth 22 km



Depth 24 km

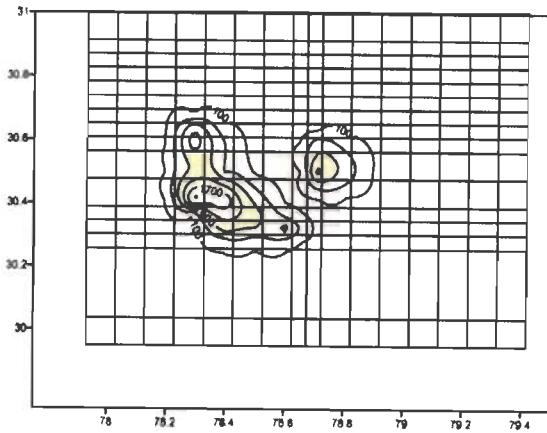


Depth 26 km

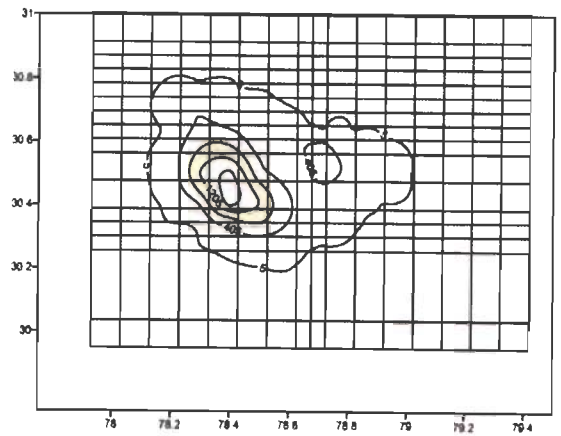


Depth 28 km

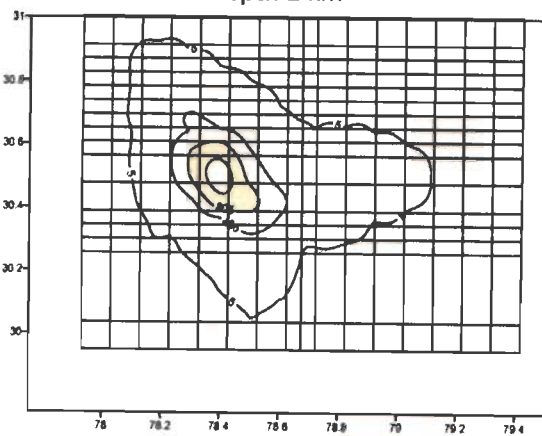
DWS for 3-D Model-II



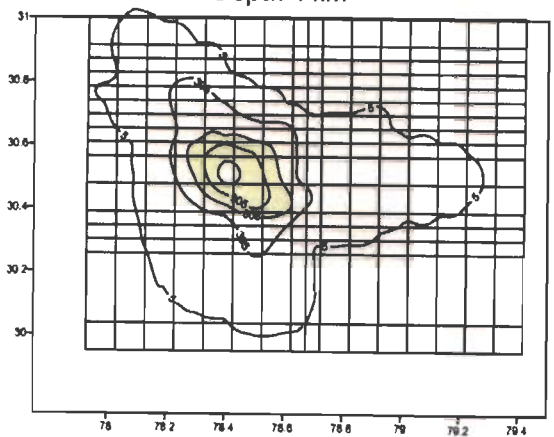
Depth 2 km



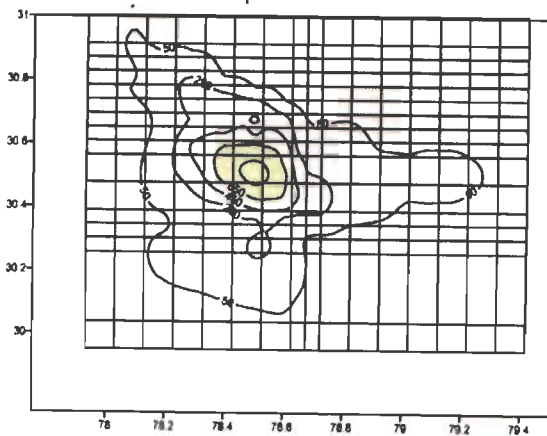
Depth 4 km



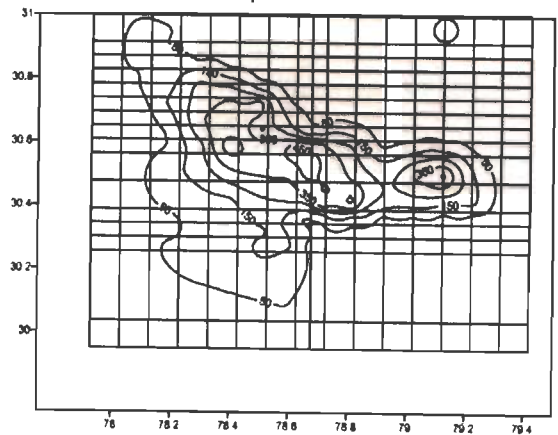
Depth 6 km



Depth 8 km

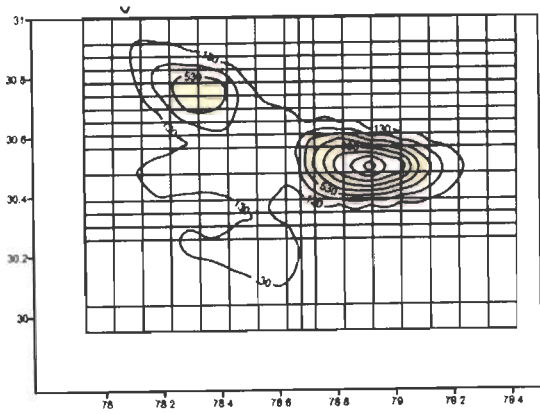


Depth 12 km

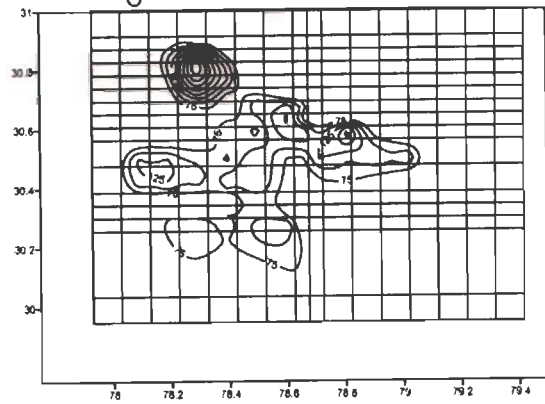


Depth 14 km

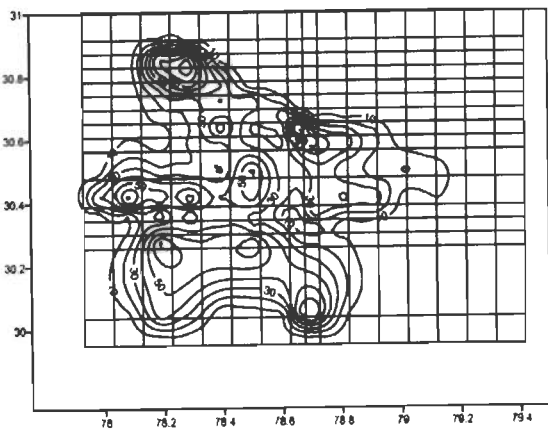
DWS for 3-D Model-II



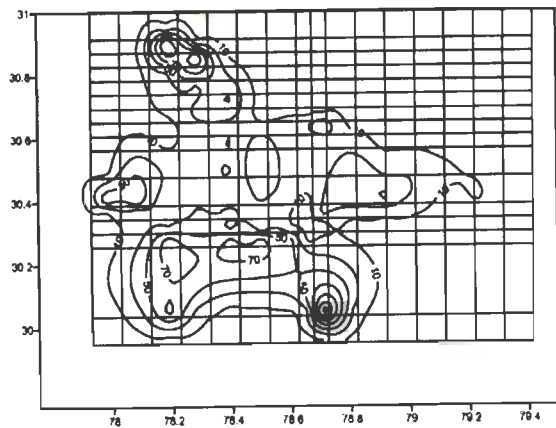
Depth 16 km



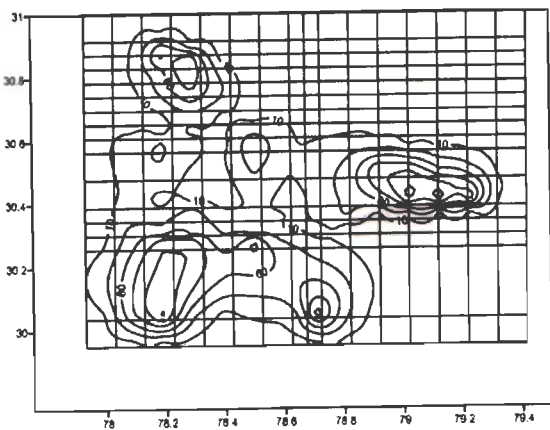
Depth 20 km



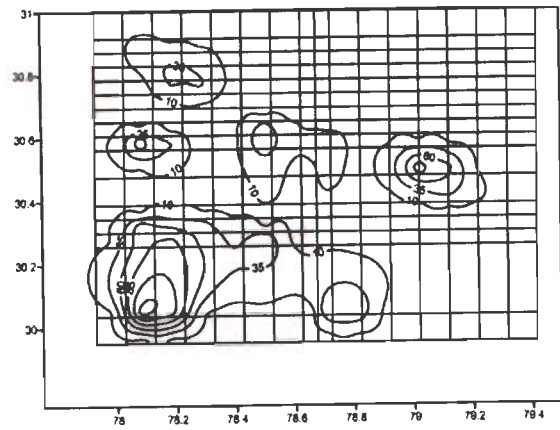
Depth 22 km



Depth 24 km

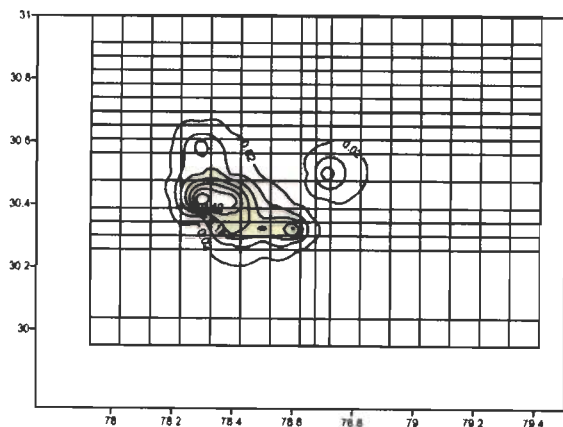


Depth 26 km

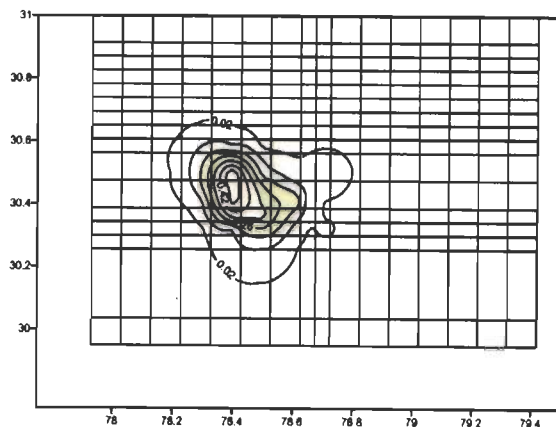


Depth 28 km

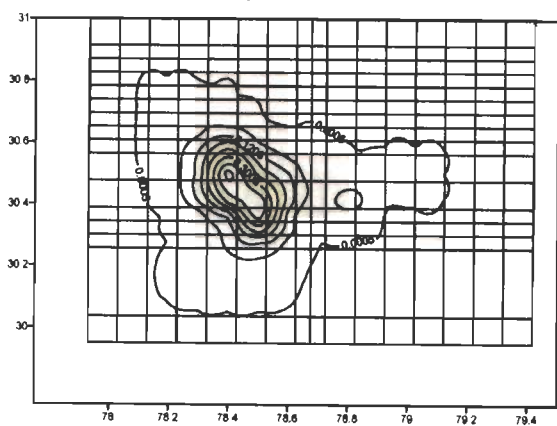
RESOLUTION for 3-D Model-II



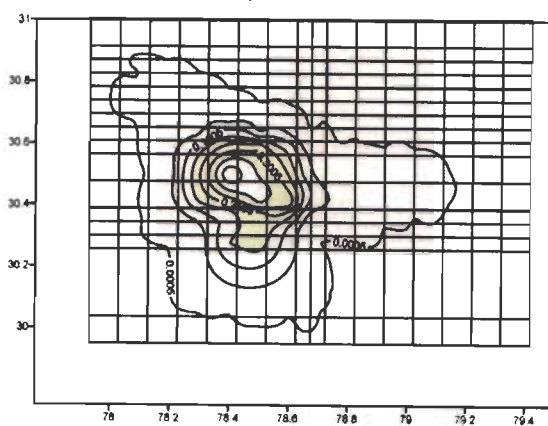
Depth 2 km



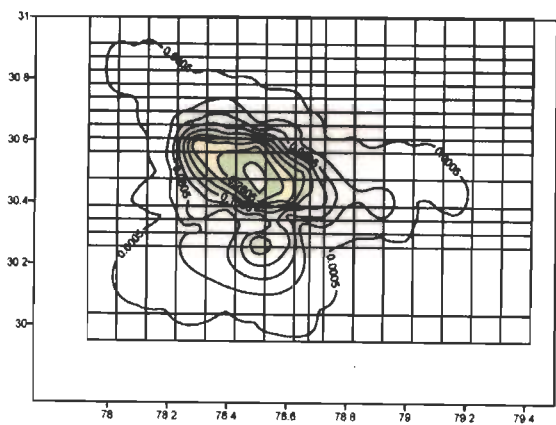
Depth 4 km



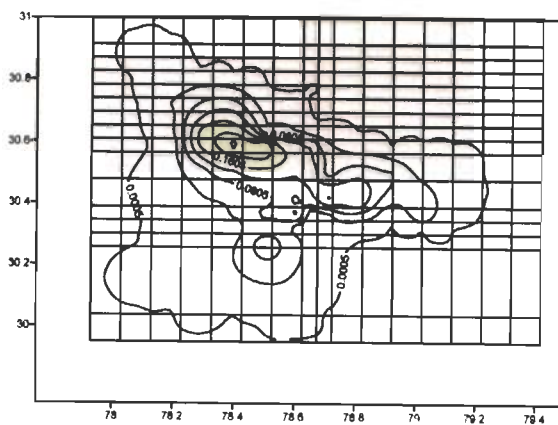
Depth 6 km



Depth 8 km

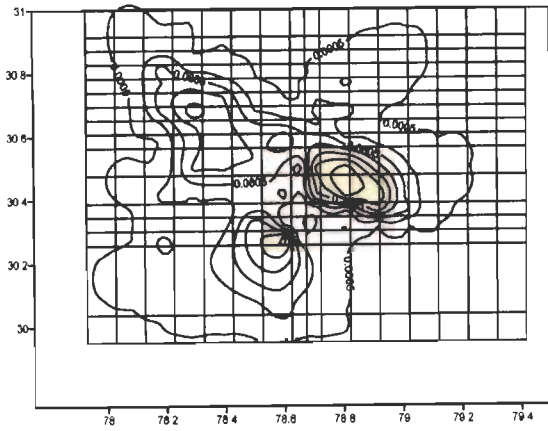


Depth 12 km

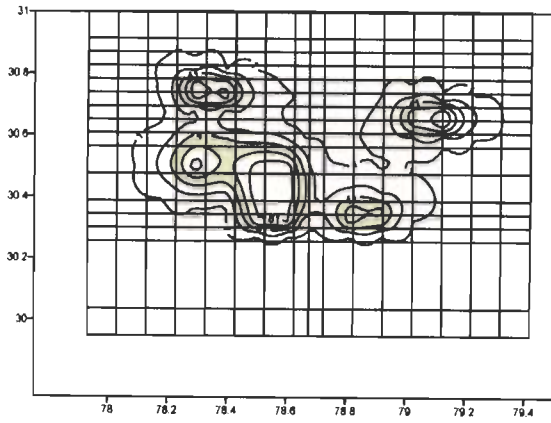


Depth 14 km

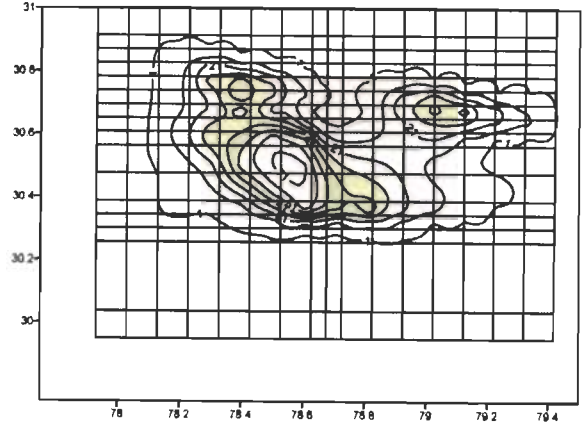
RESOLUTION for 3-D Model-II



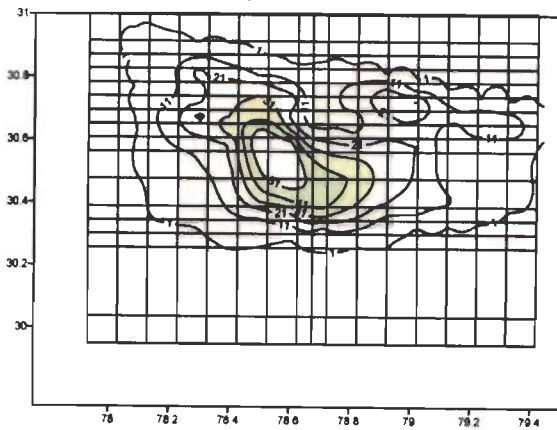
KHIT for 3-D Model-III



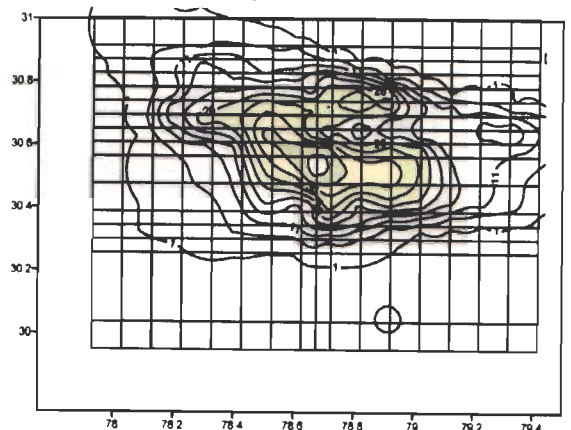
Depth 2 km



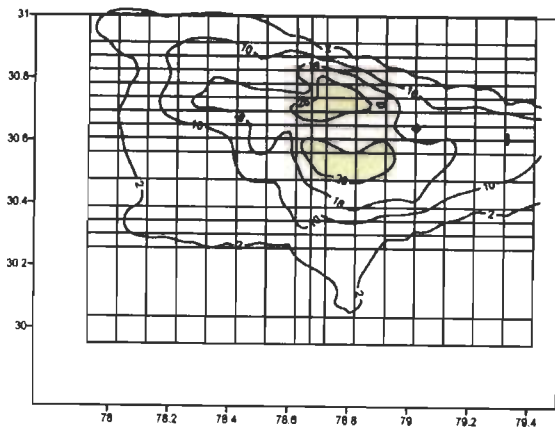
Depth 4 km



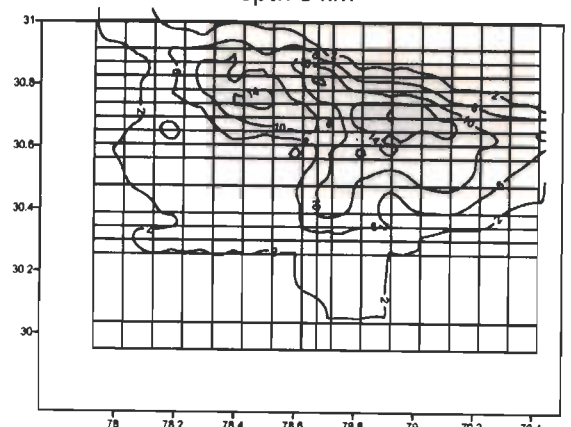
Depth 6 km



Depth 8 km

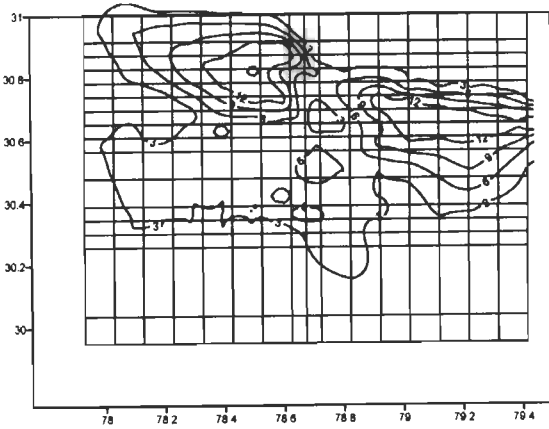


Depth 12 km

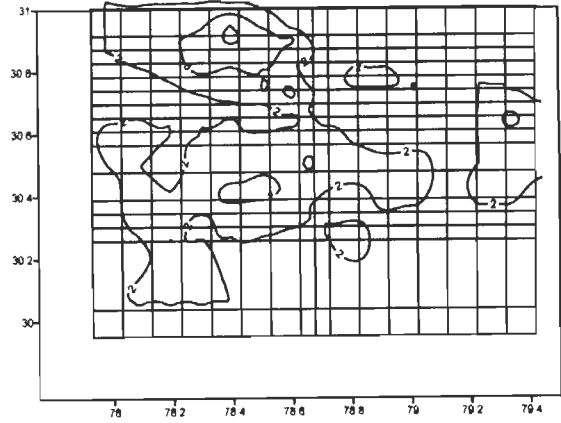


Depth 14 km

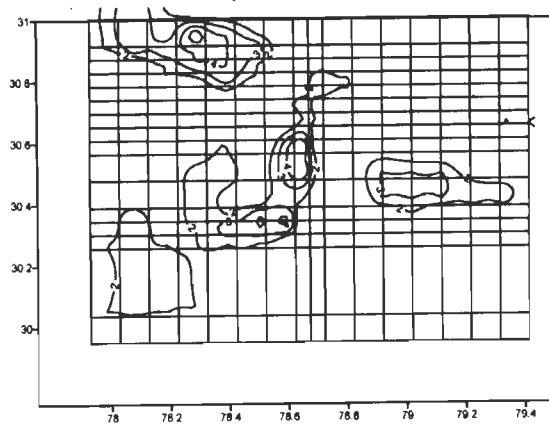
KHIT for 3-D Model-III



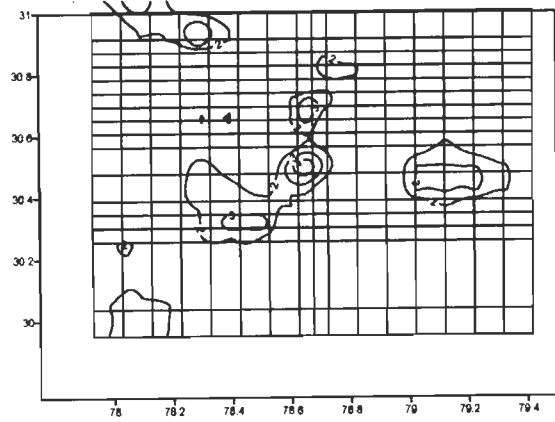
Depth 16 km



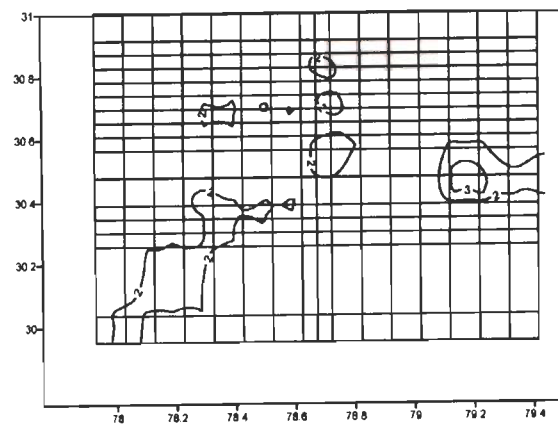
Depth 20 km



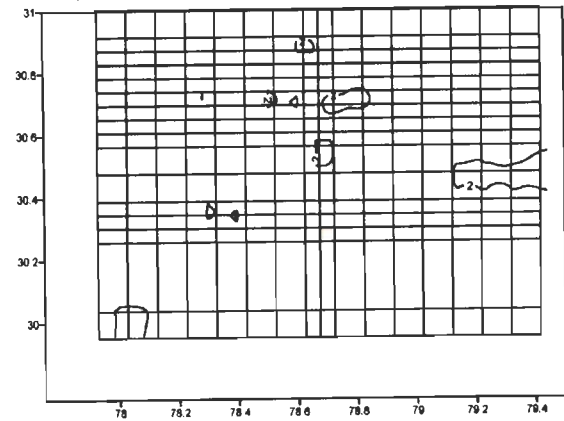
Depth 22 km



Depth 24 km

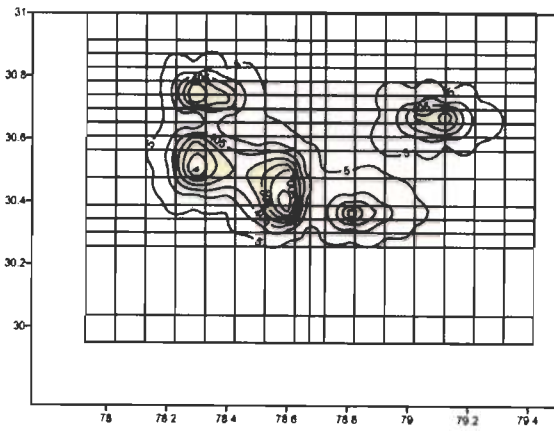


Depth 26 km

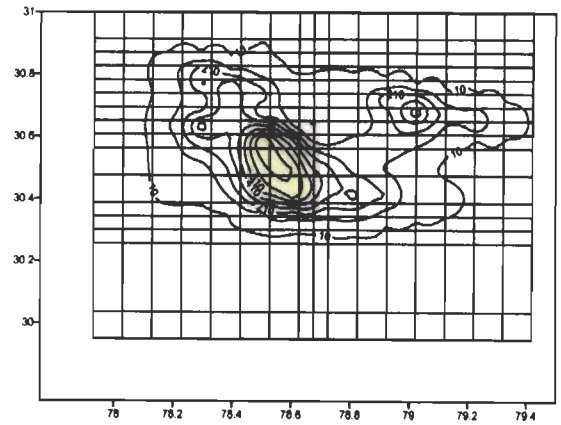


Depth 28 km

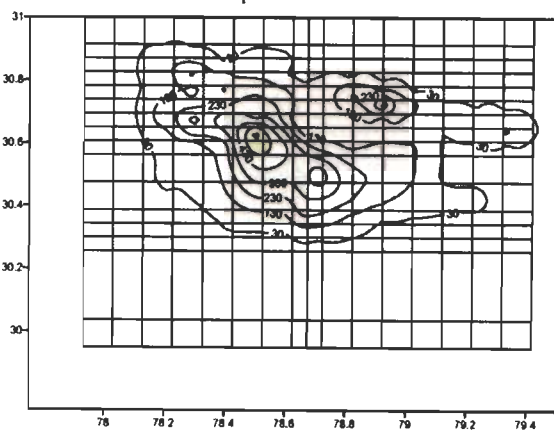
DWS for 3 D Model-III



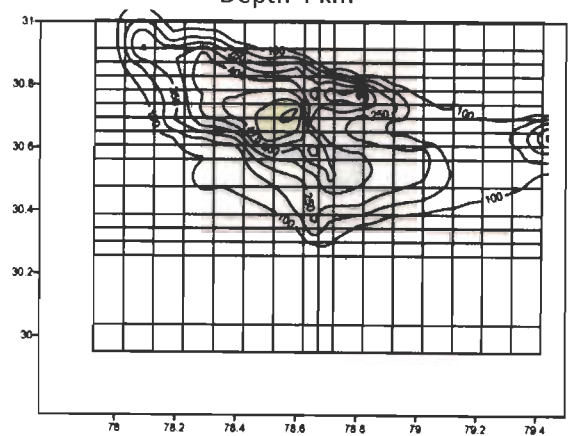
Depth 2 km



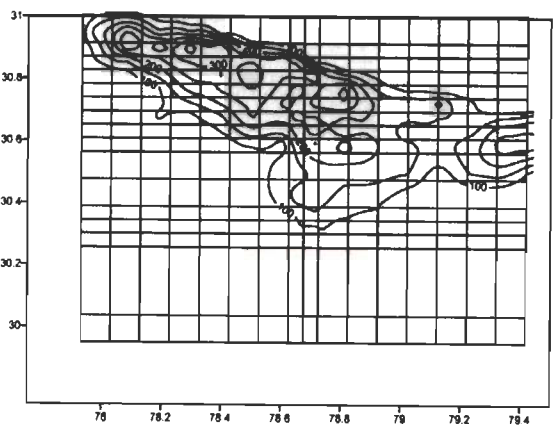
Depth 4 km



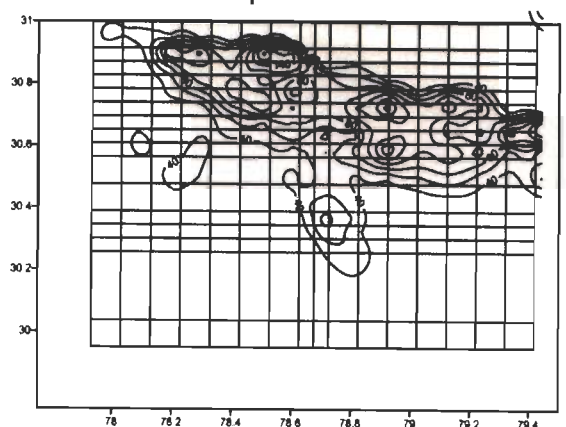
Depth 6 km



Depth 8 km

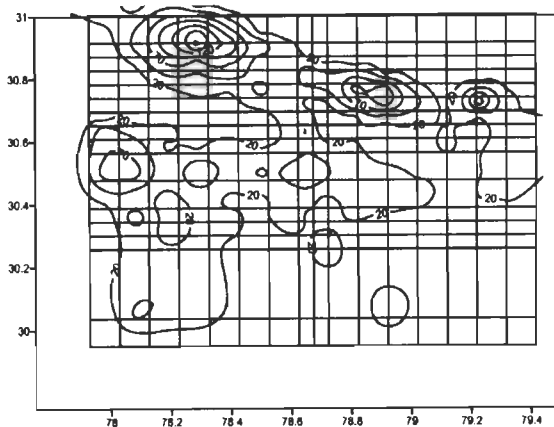
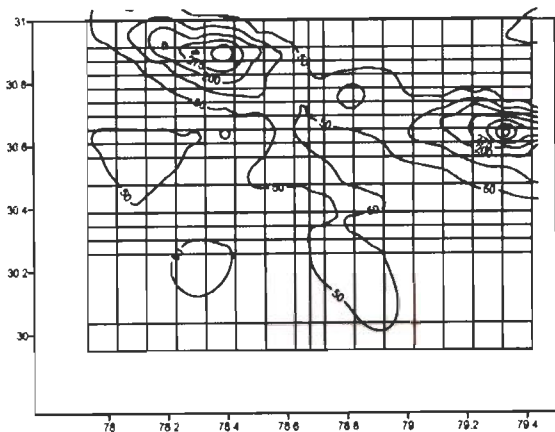


Depth 12 km

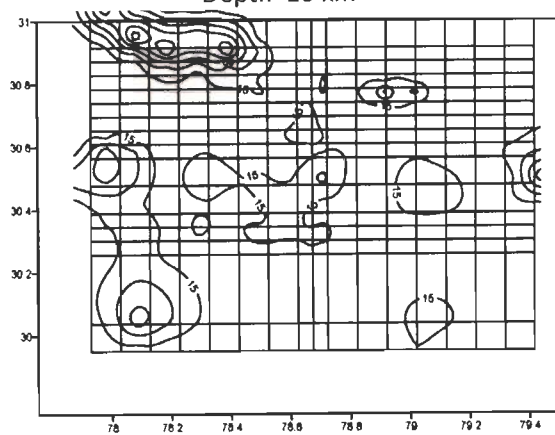


Depth 14 km

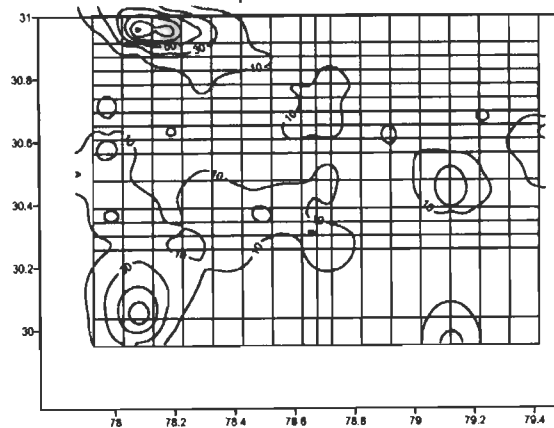
DWS for 3 D Model-III



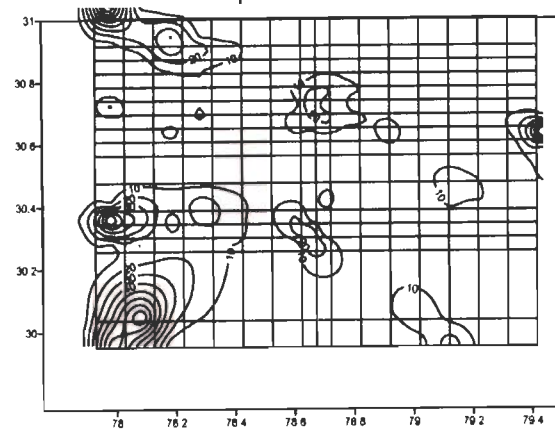
Depth 16 km



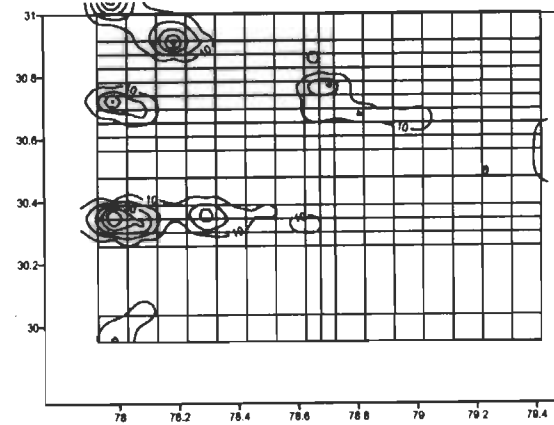
Depth 20 km



Depth 22 km

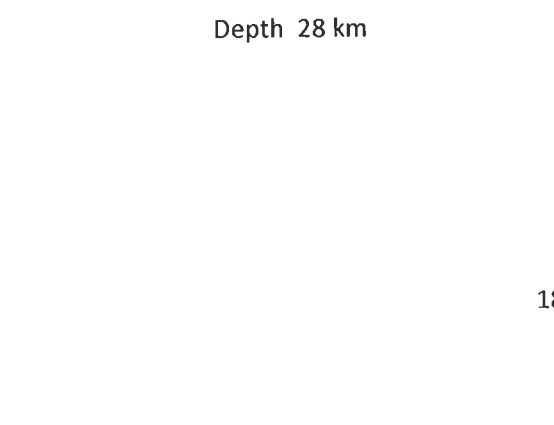


Depth 24 km

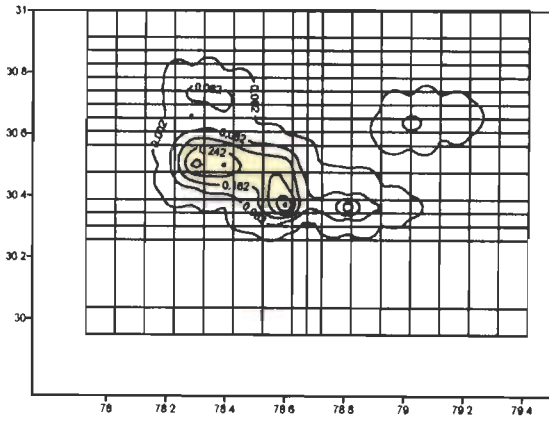


Depth 26 km

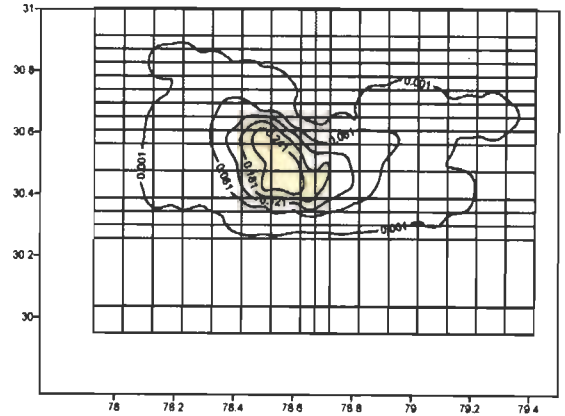
Depth 28 km



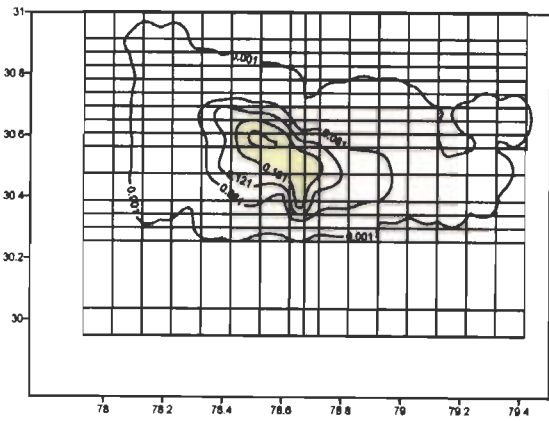
RESOLUTION for 3-D Model-III



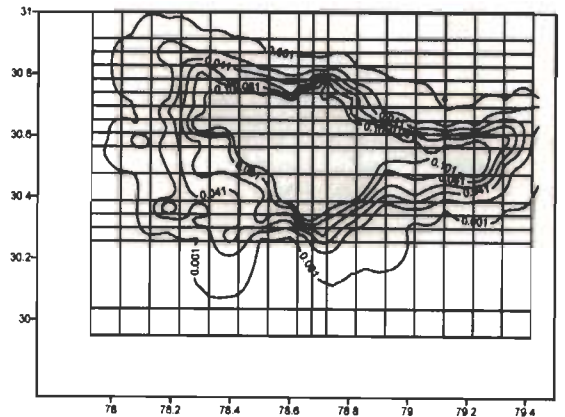
Depth 2 km



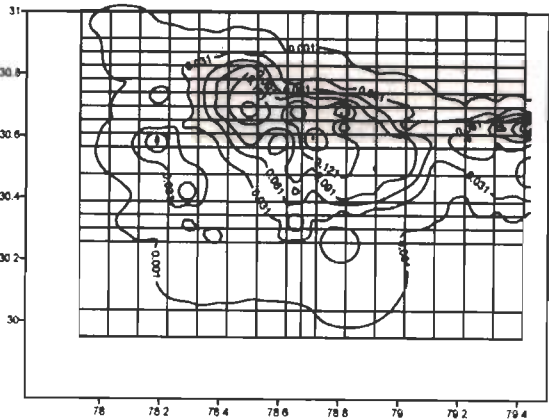
Depth 4 km



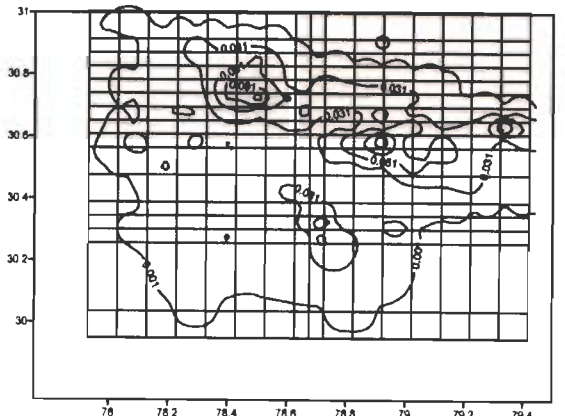
Depth 6 km



Depth 8 km

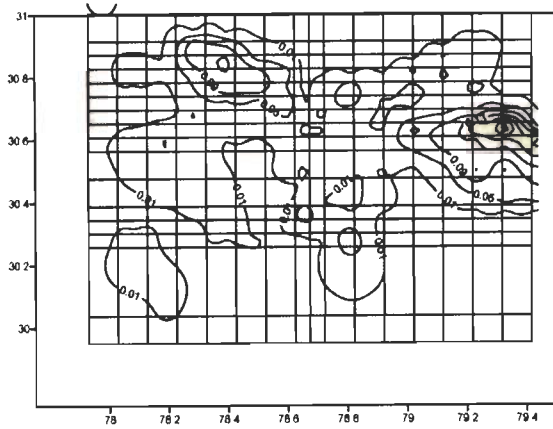


Depth 12 km

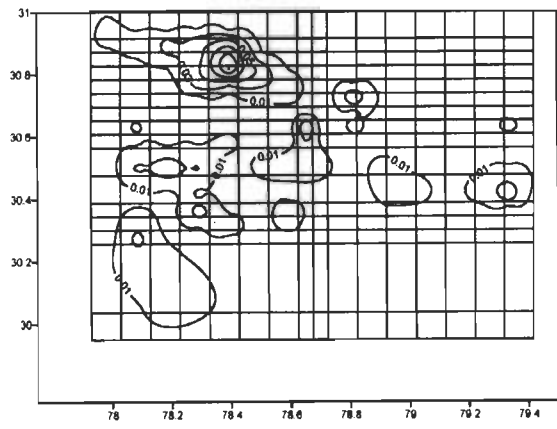


Depth 14 km

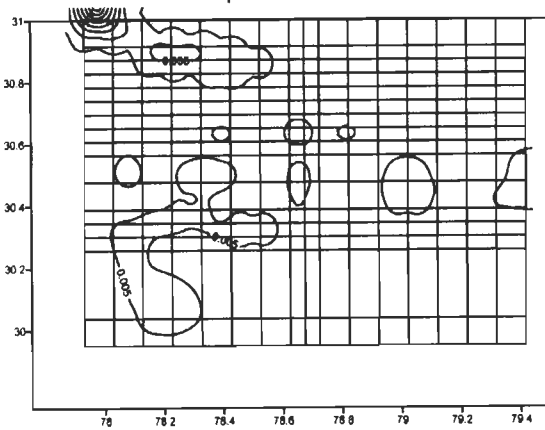
RESOLUTION for 3-D Model-III



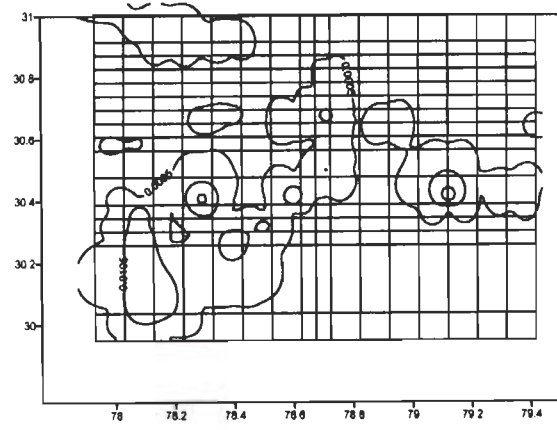
Depth 16 km



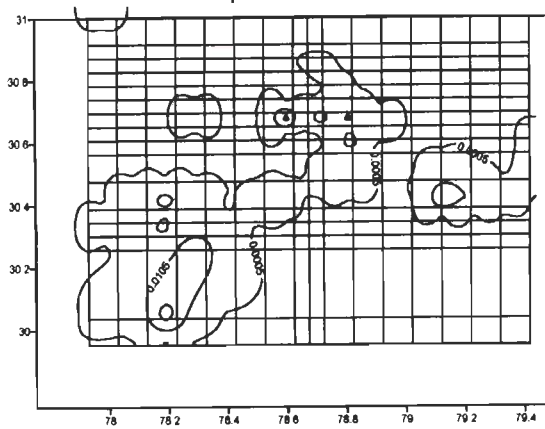
Depth 20 km



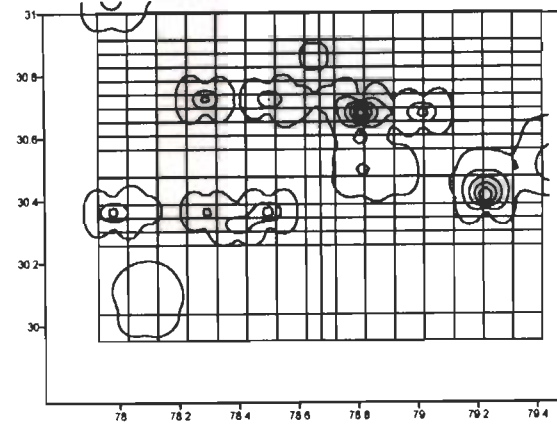
Depth 22 km



Depth 24 km

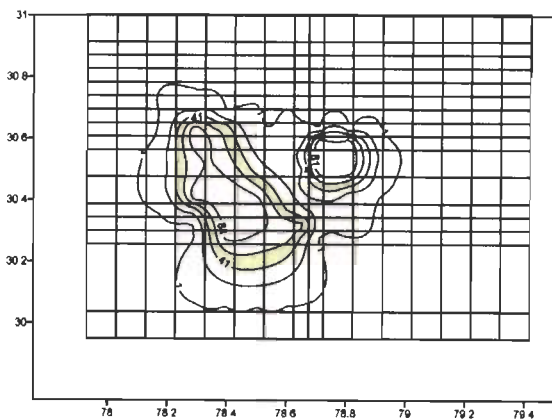


Depth 26 km

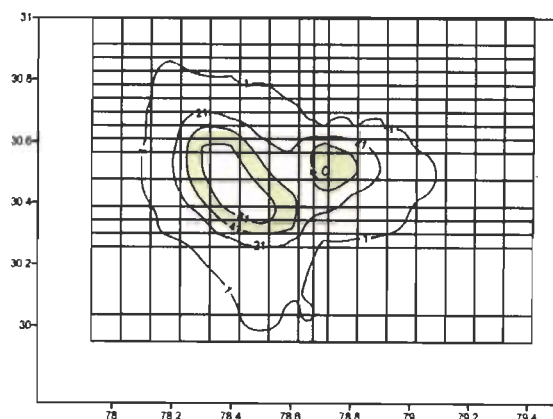


Depth 28 km

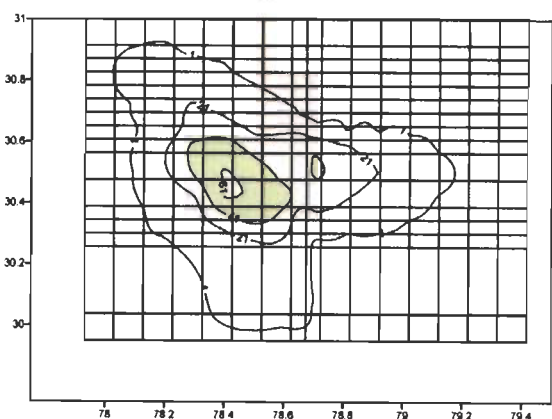
KHIT for 3-D Model-IV



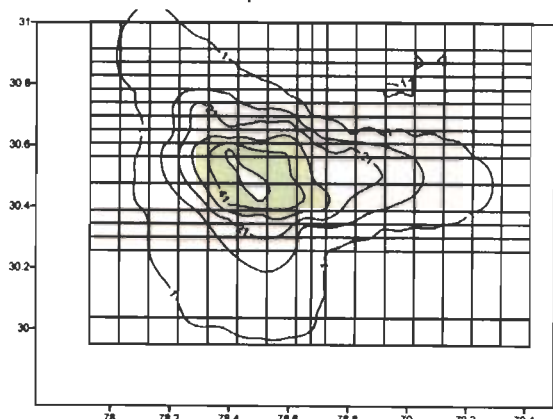
Depth 2 km



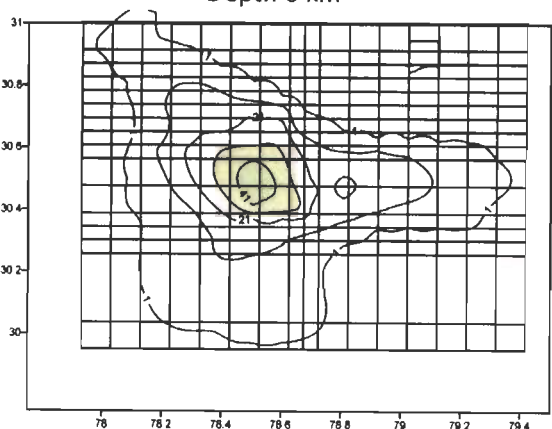
Depth 4 km



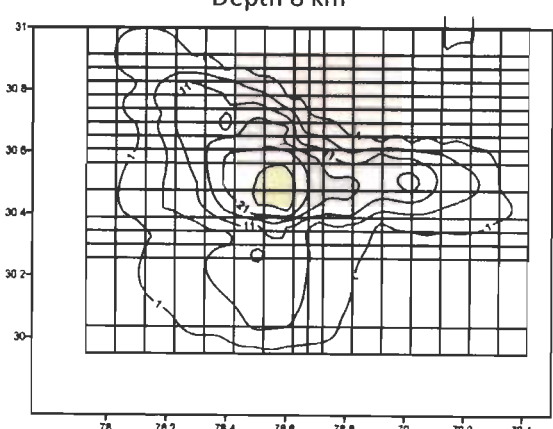
Depth 6 km



Depth 8 km

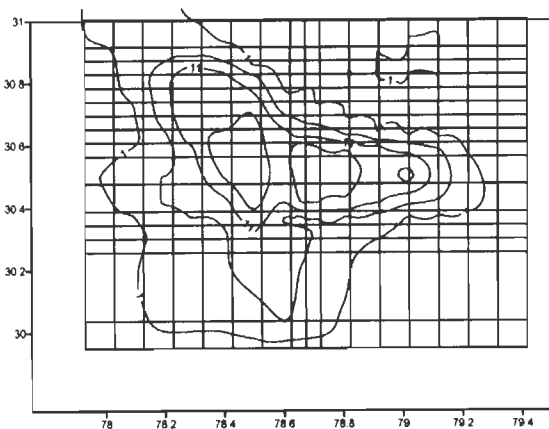


Depth 12 km

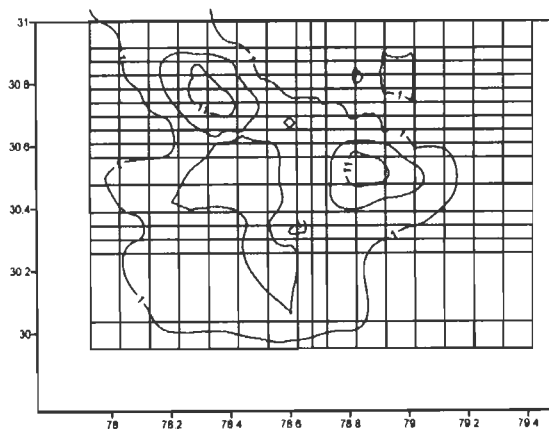


Depth 14 km

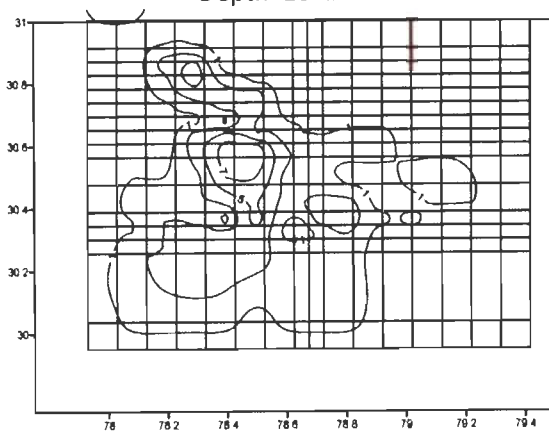
KHIT for 3-D Model-IV



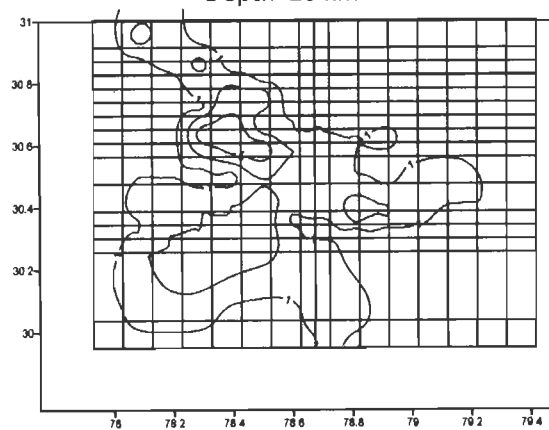
Depth 16 km



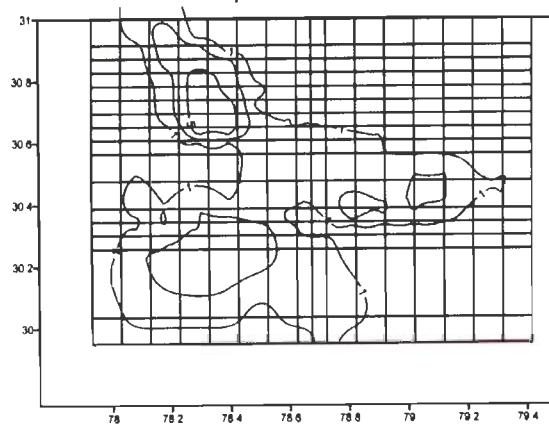
Depth 20 km



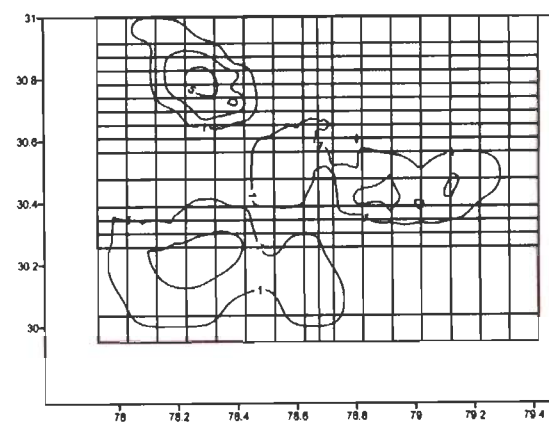
Depth 22 km



Depth 24 km

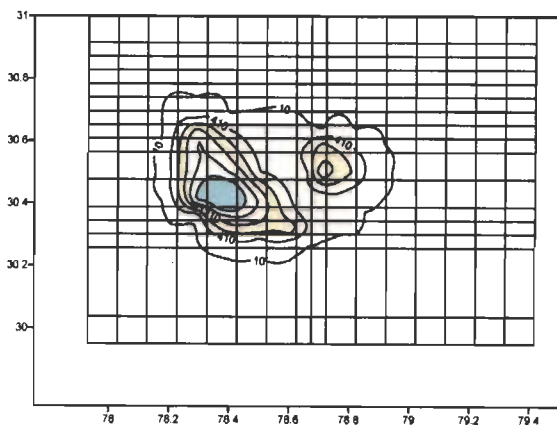


Depth 26 km

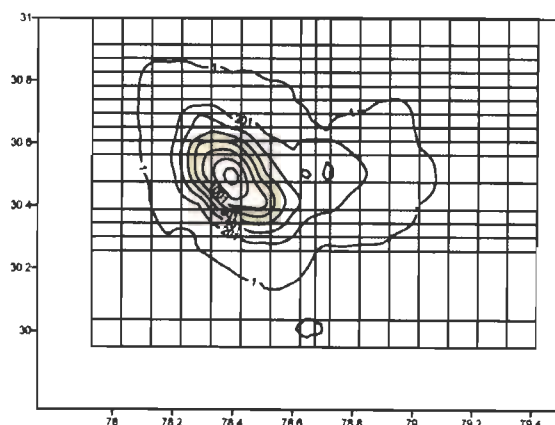


Depth 28 km

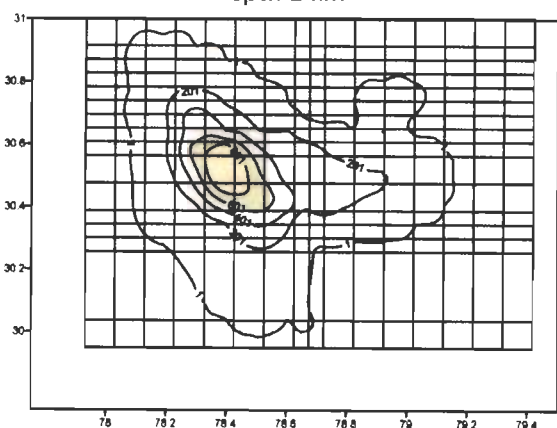
DWS for 3-D Model-IV



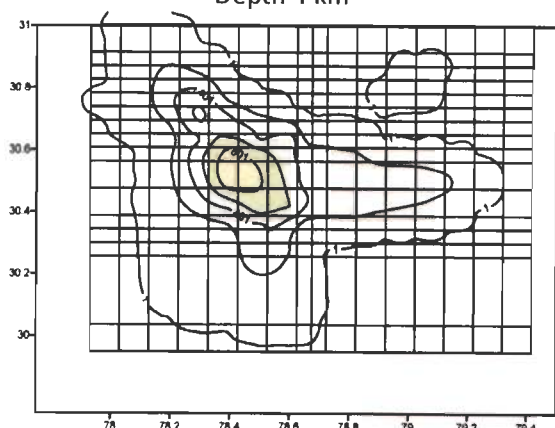
Depth 2 km



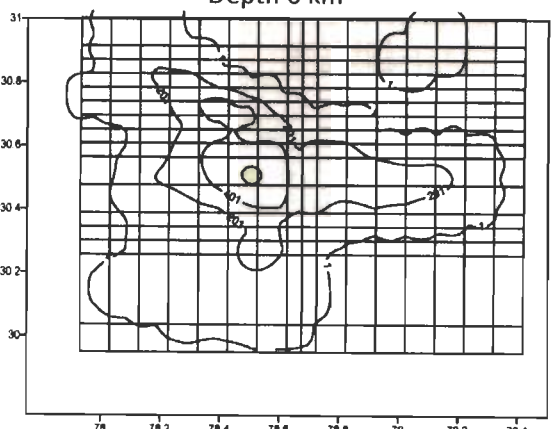
Depth 4 km



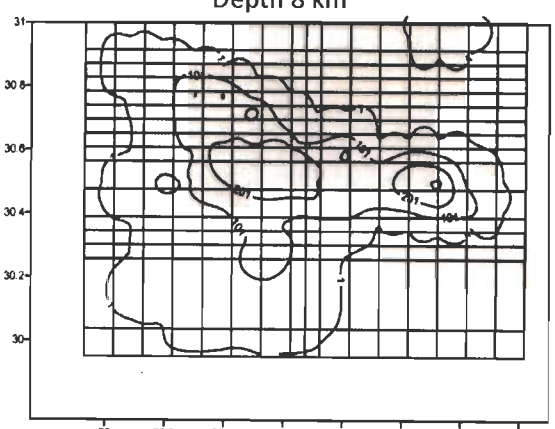
Depth 6 km



Depth 8 km

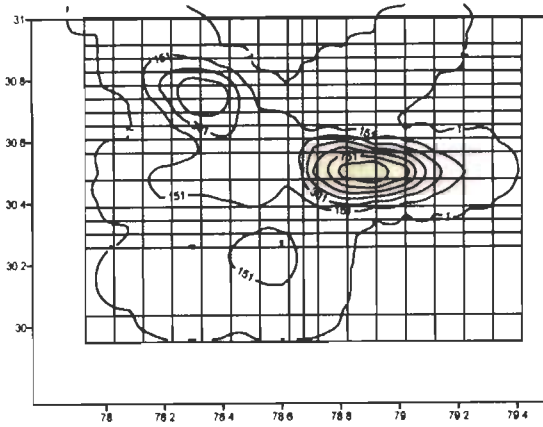


Depth 12 km

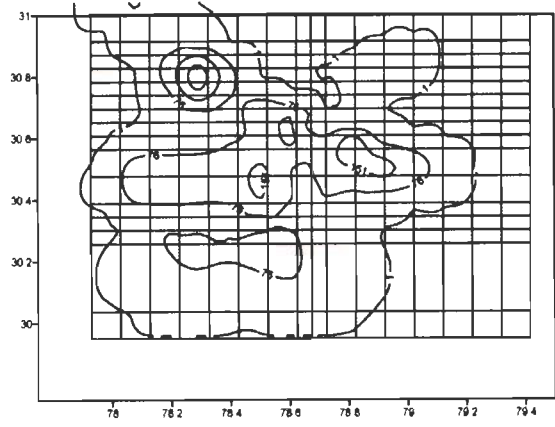


Depth 14 km

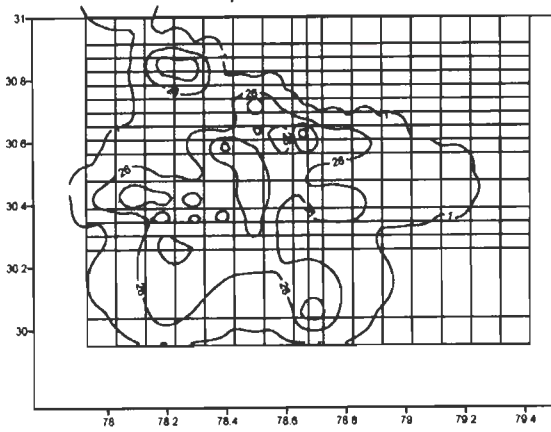
DWS for 3-D Model-IV



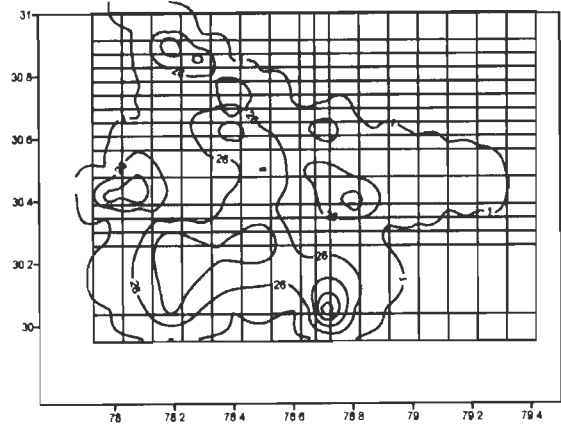
Depth 16 km



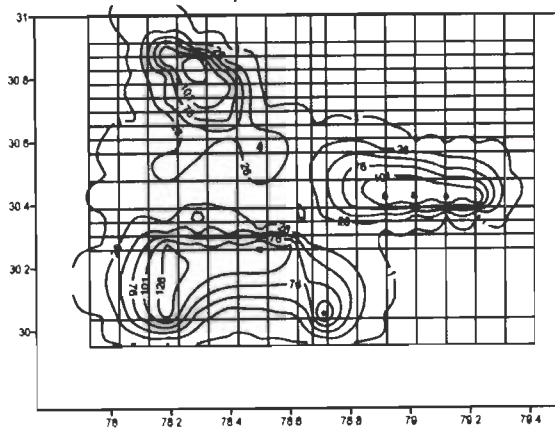
Depth 20 km



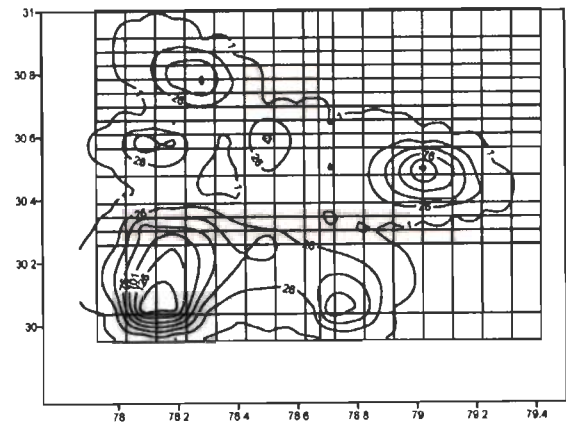
Depth 22 km



Depth 24 km

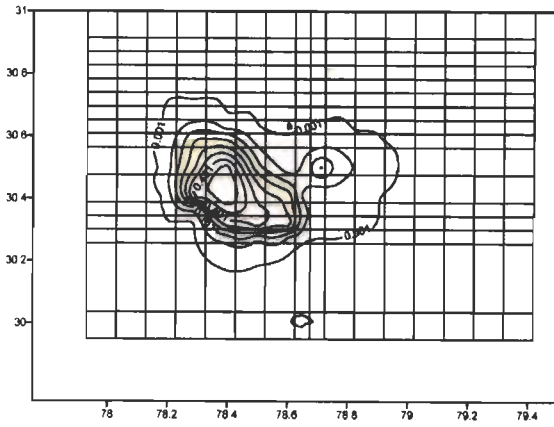


Depth 26 km

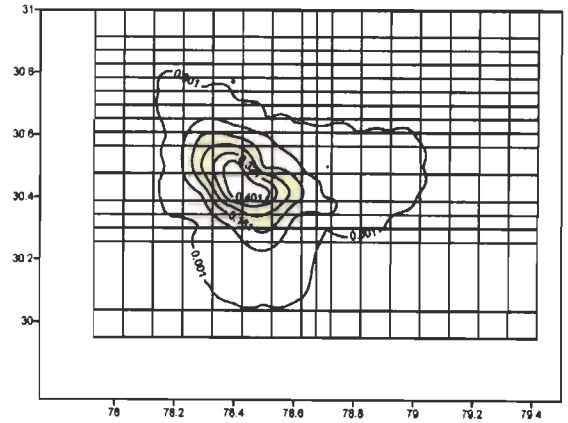


Depth 28 km

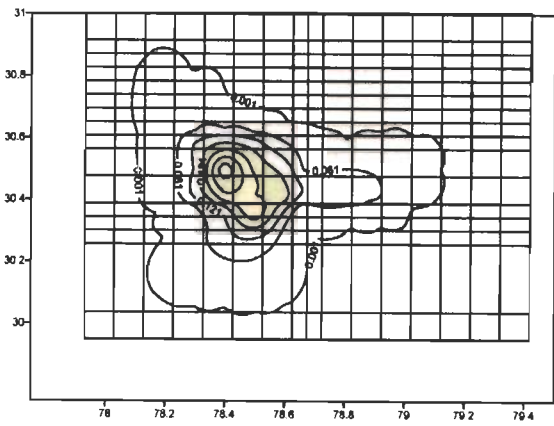
RESOLUTION for 3-D Model-IV



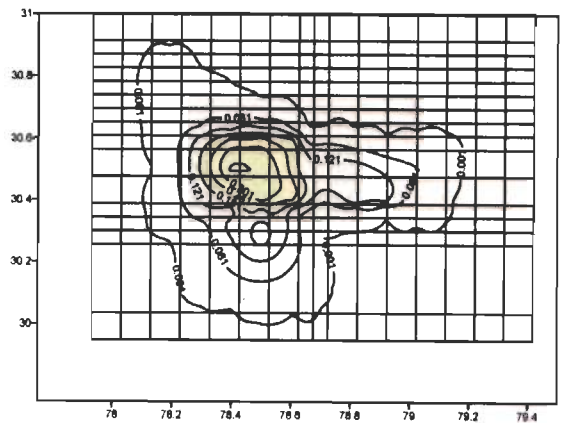
Depth 2 km



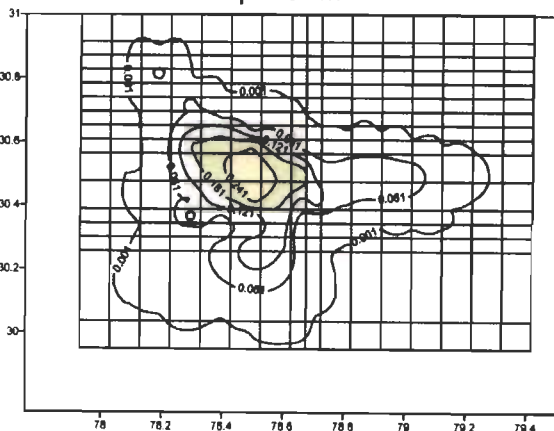
Depth 4 km



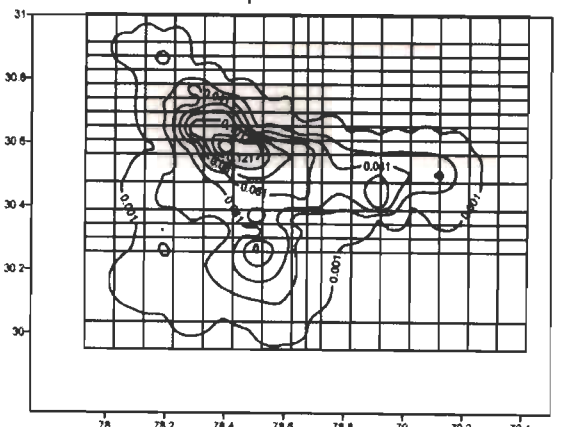
Depth 6 km



Depth 8 km

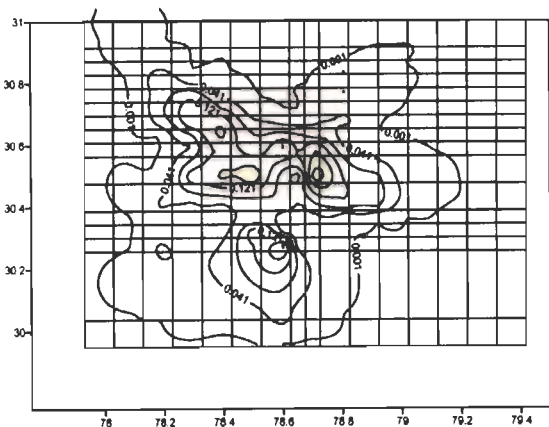


Depth 12 km

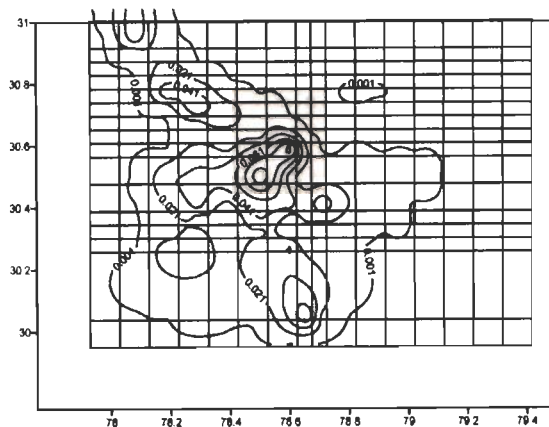


Depth 14 km

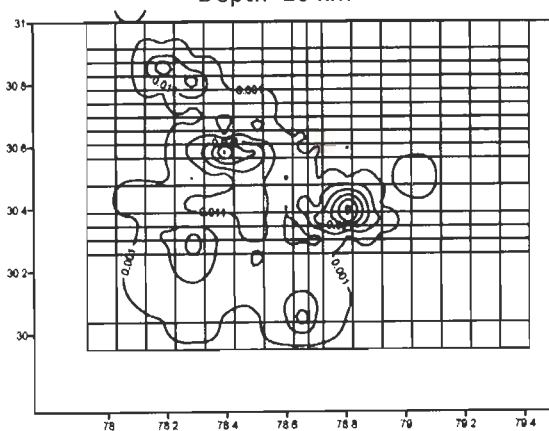
RESOLUTION for 3-D Model-IV



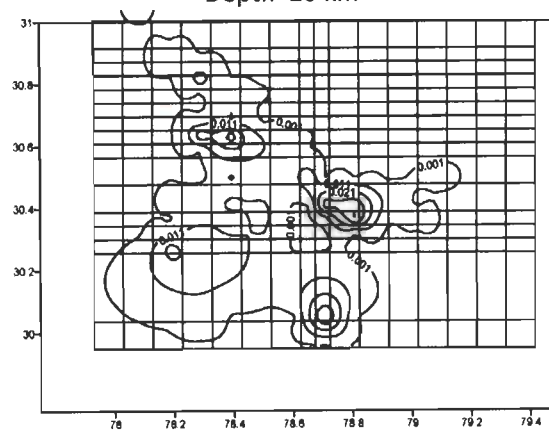
Depth 16 km



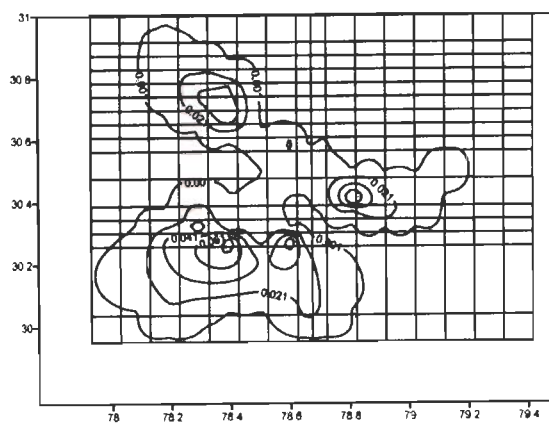
Depth 20 km



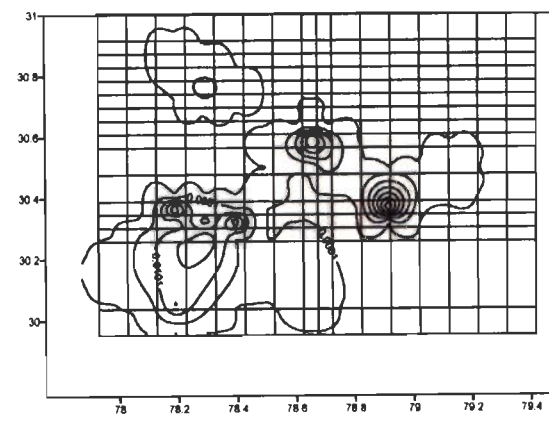
Depth 22 km



Depth 24 km

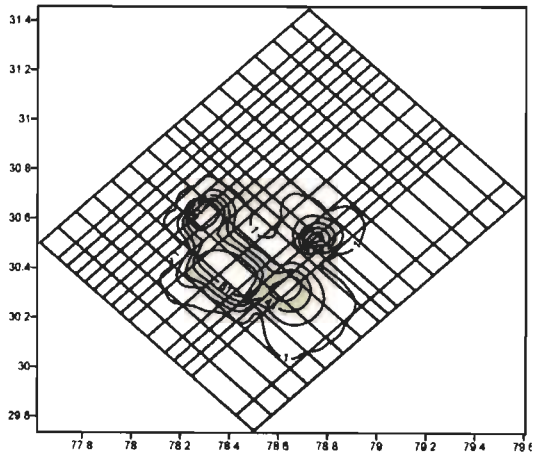


Depth 26 km

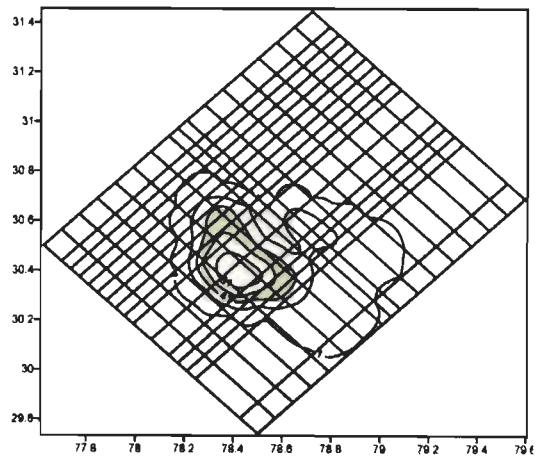


Depth 28 km

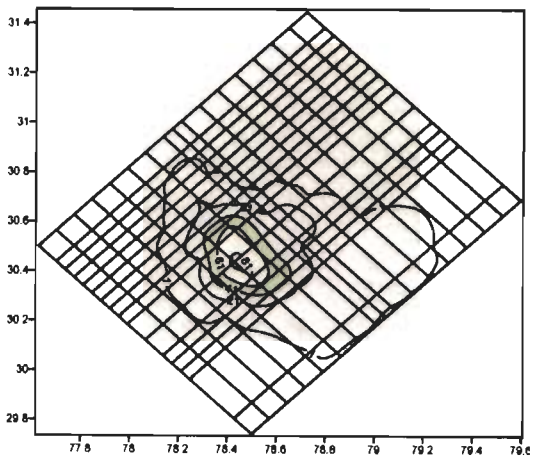
KHIT for 3-D Model-I



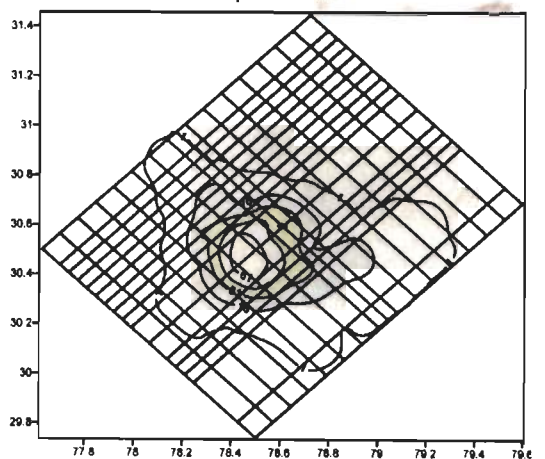
Depth 2 km



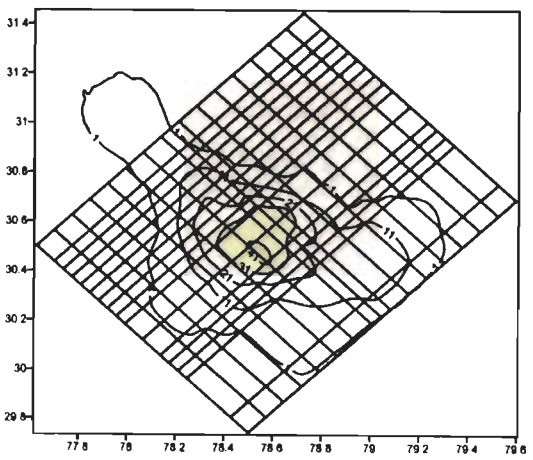
Depth 4 km



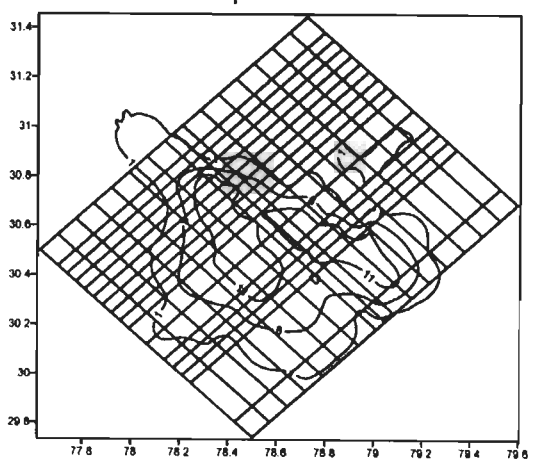
Depth 6 km



Depth 8 km

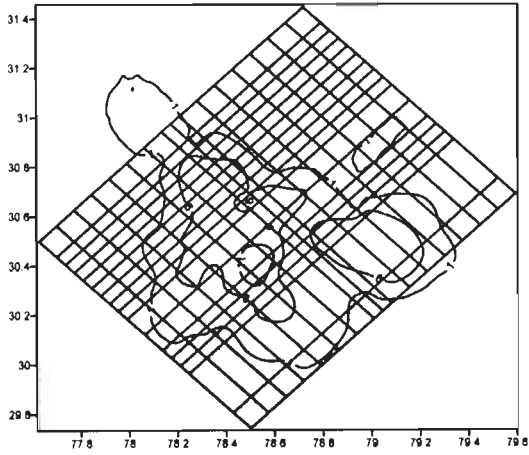


Depth 12 km

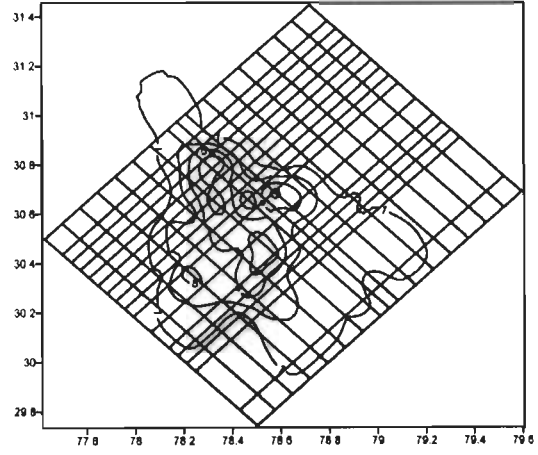


Depth 14 km

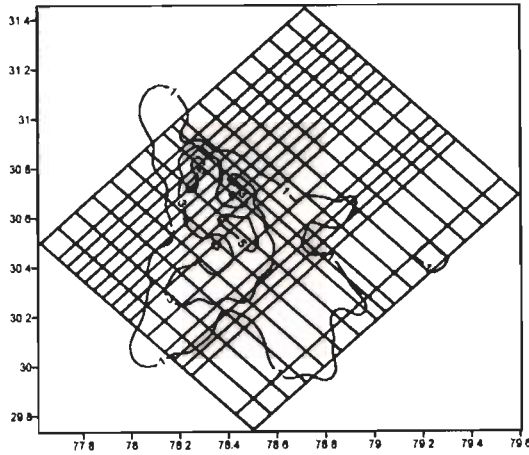
KHIT for 3-D Model-I



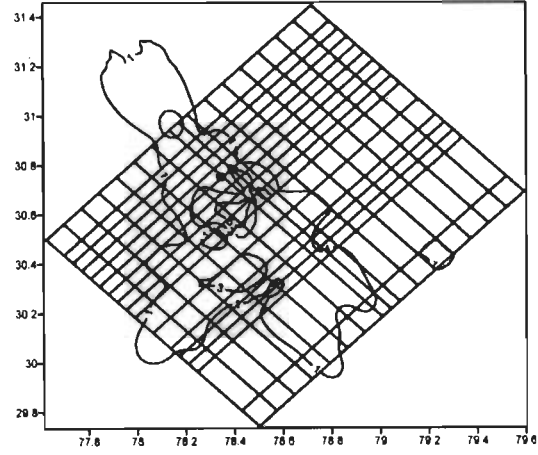
Depth 16 km



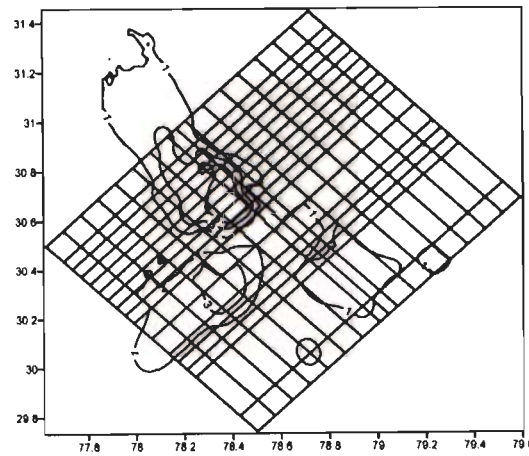
Depth 20 km



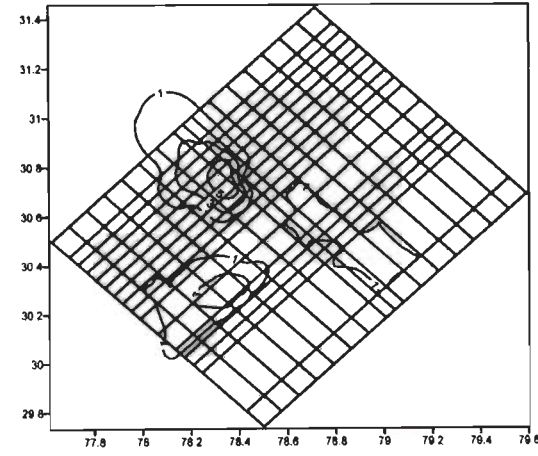
Depth 22 km



Depth 24 km

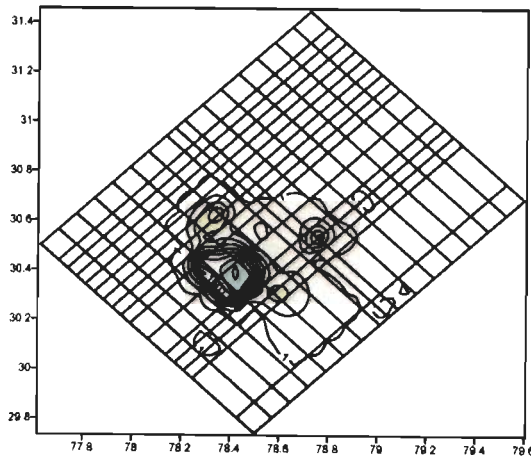


Depth 26 km

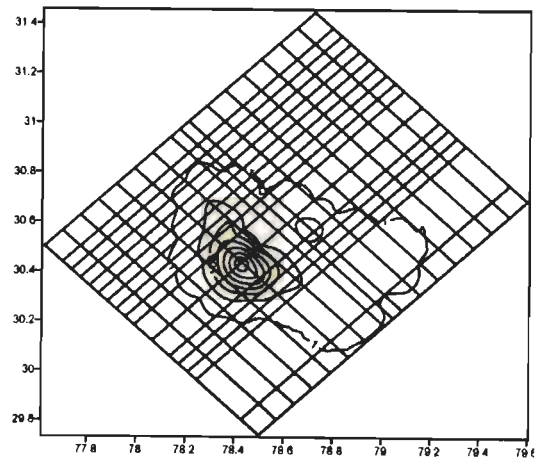


Depth 28 km

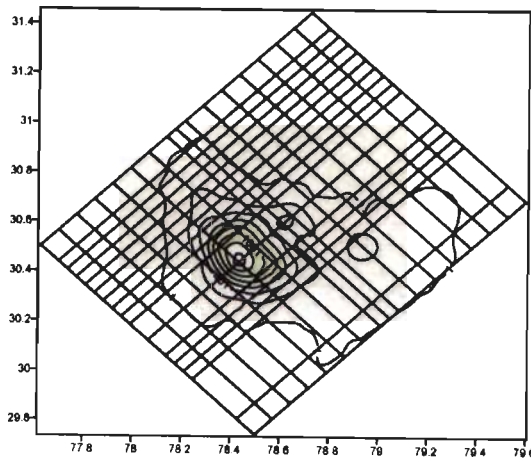
DWS for 3-D Model-I



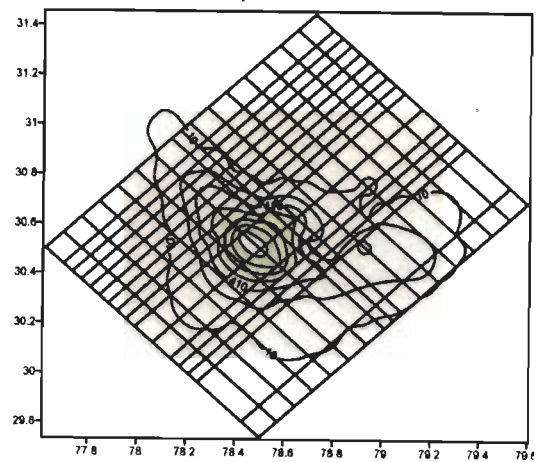
Depth 2 km



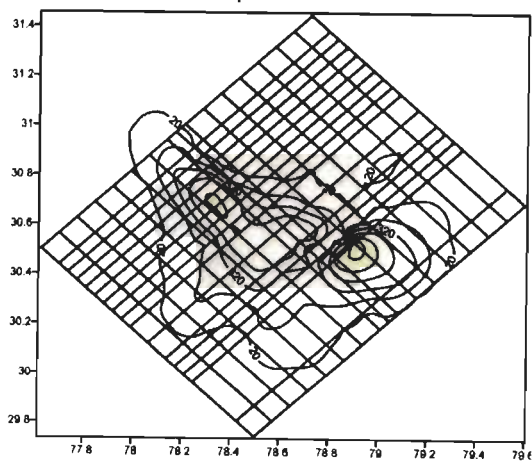
Depth 4 km



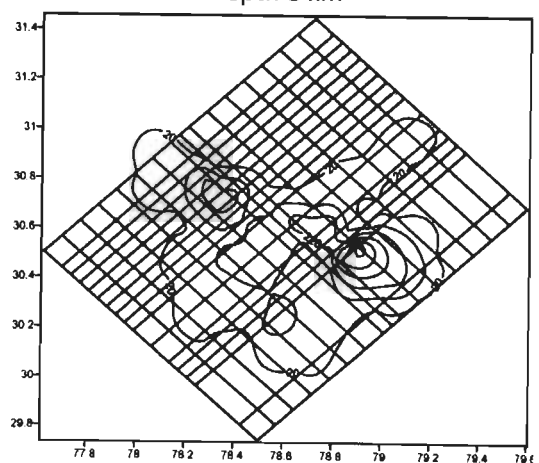
Depth 6 km



Depth 8 km

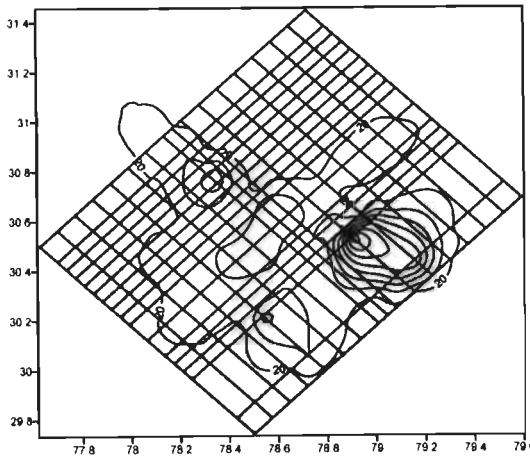


Depth 12 km

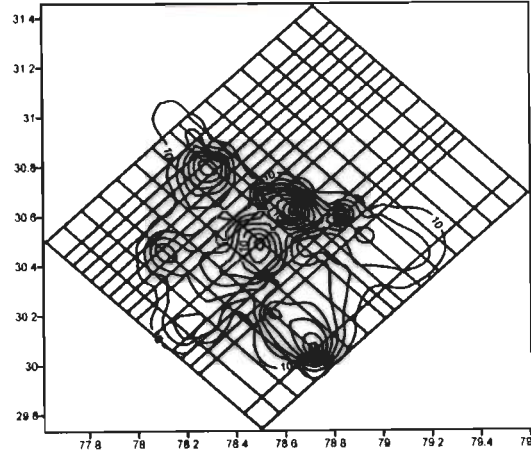


Depth 14 km

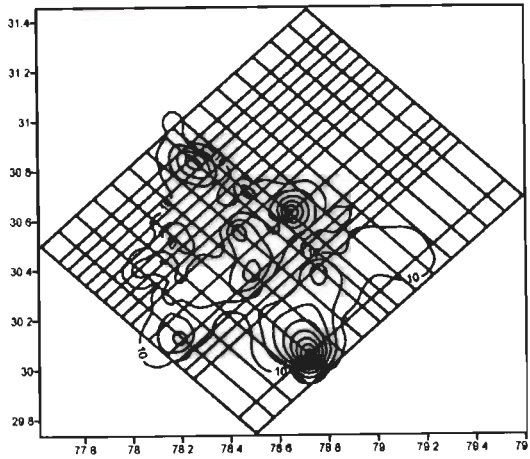
DWS for 3-D Model-I



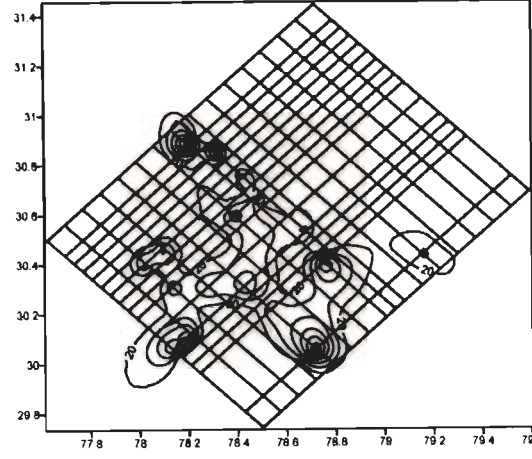
Depth 16 km



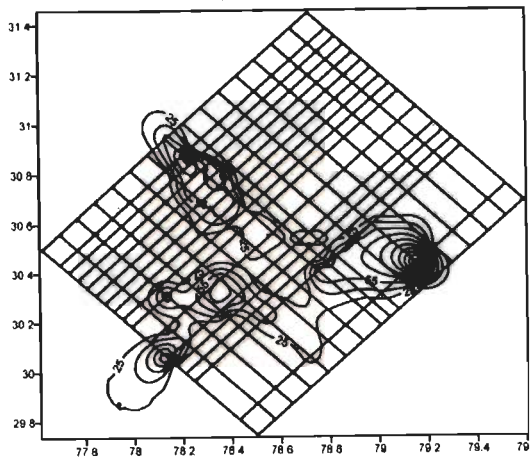
Depth 20 km



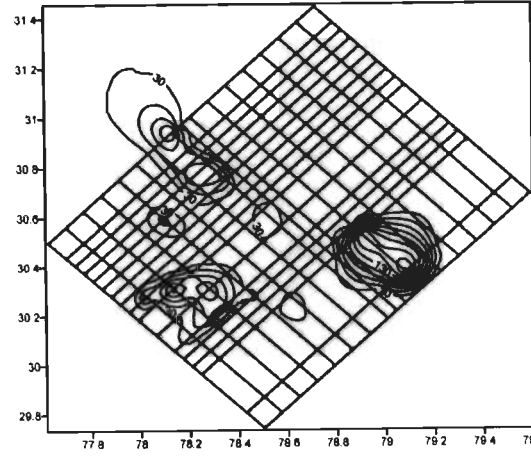
Depth 22 km



Depth 24 km

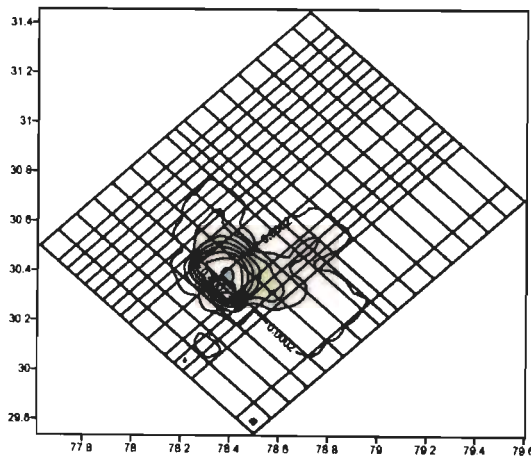


Depth 26 km

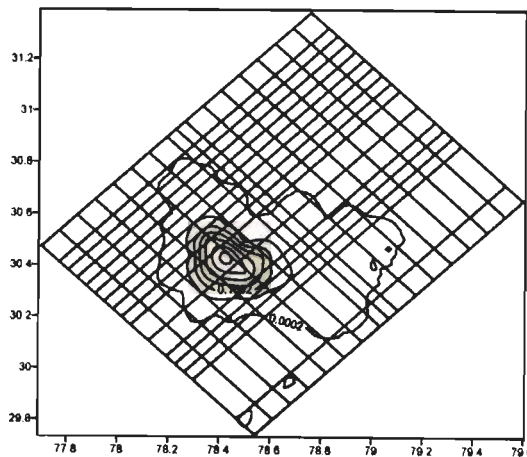


Depth 28 km

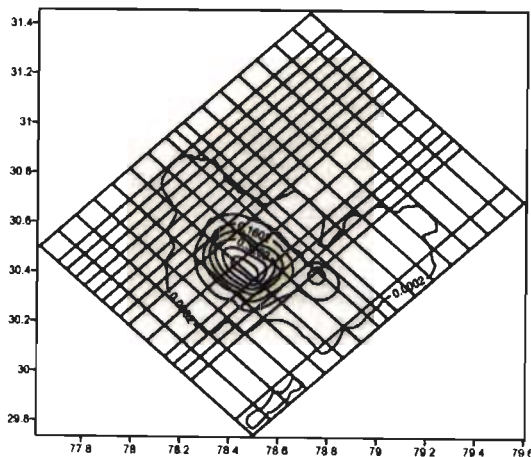
RESOLUTION for 3-D Model-I



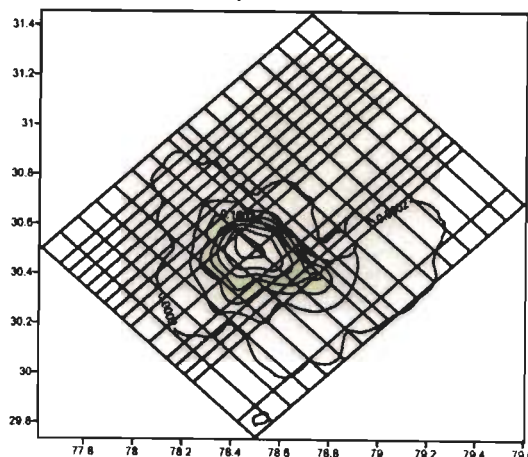
Depth 2 km



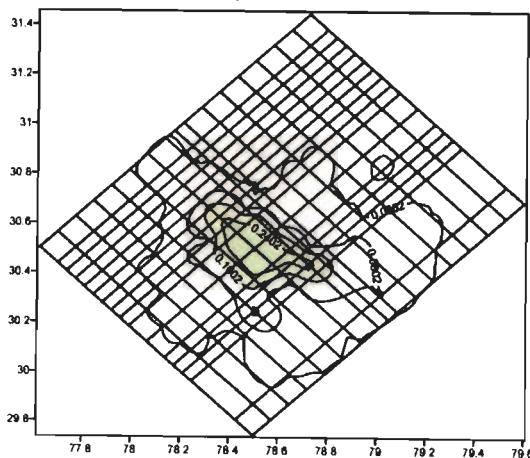
Depth 4 km



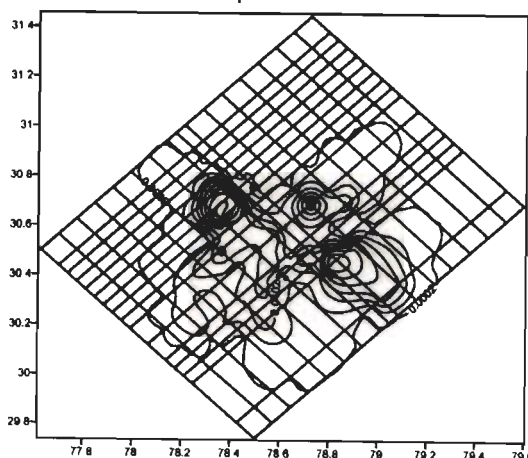
Depth 6 km



Depth 8 km

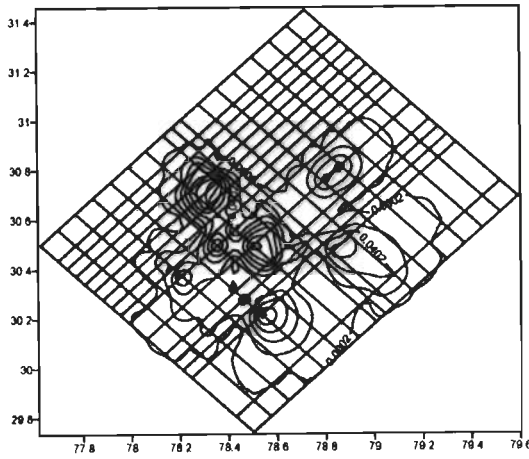


Depth 12 km

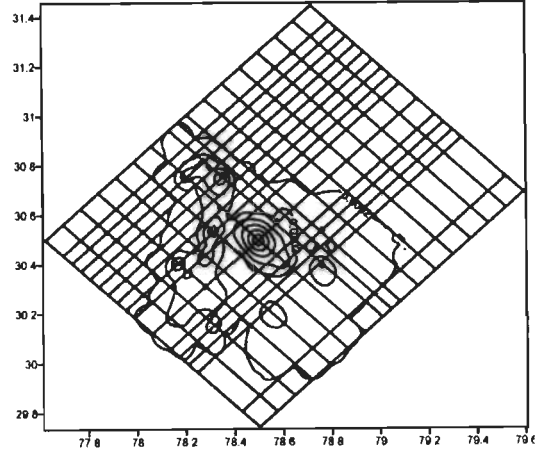


Depth 14 km

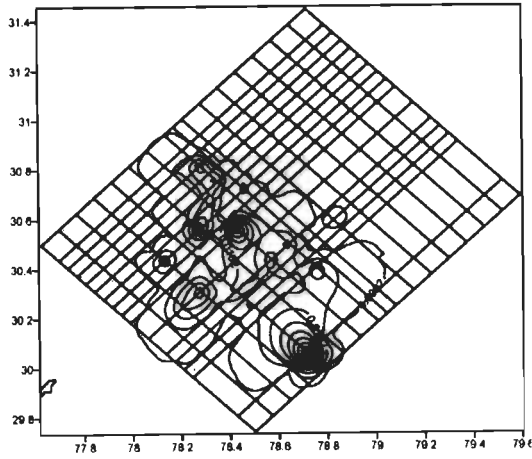
RESOLUTION for 3-D Model-I



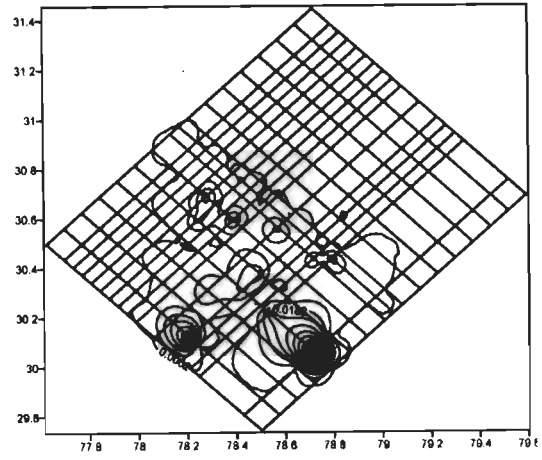
Depth 16 km



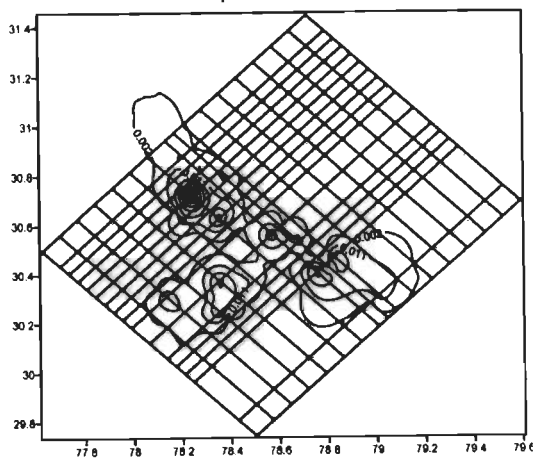
Depth 20 km



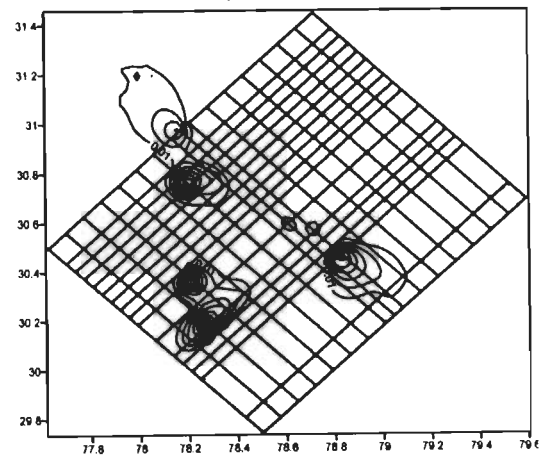
Depth 22 km



Depth 24 km

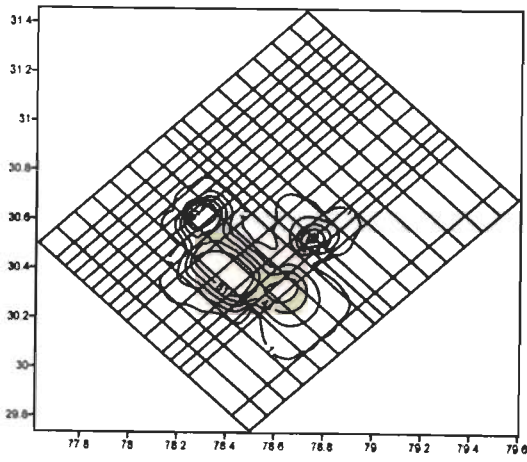


Depth 26 km

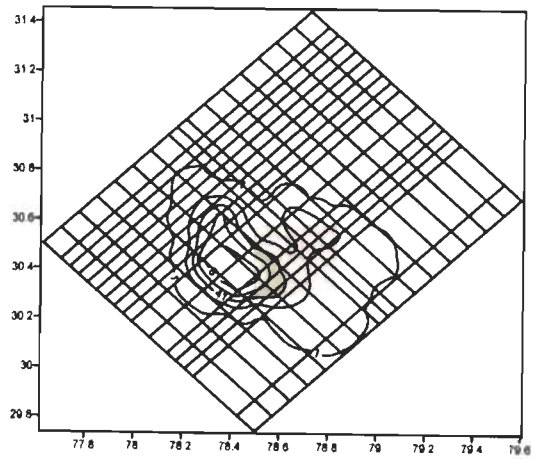


Depth 28 km

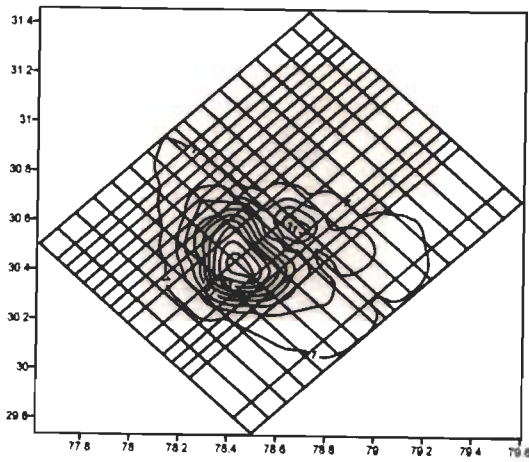
KHIT for 3-D Model-II



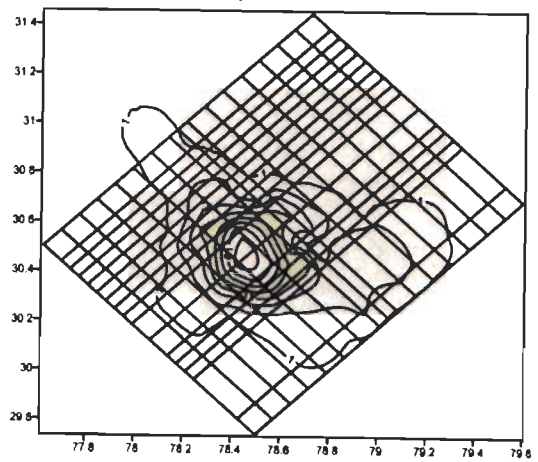
Depth 2 km



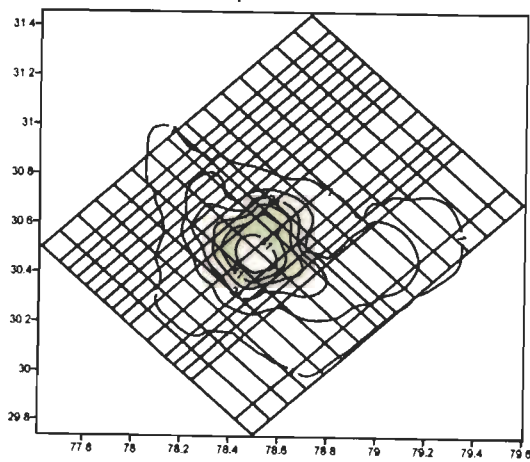
Depth 4 km



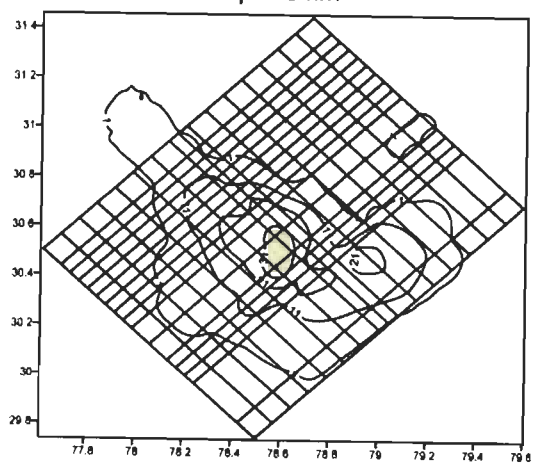
Depth 6 km



Depth 8 km

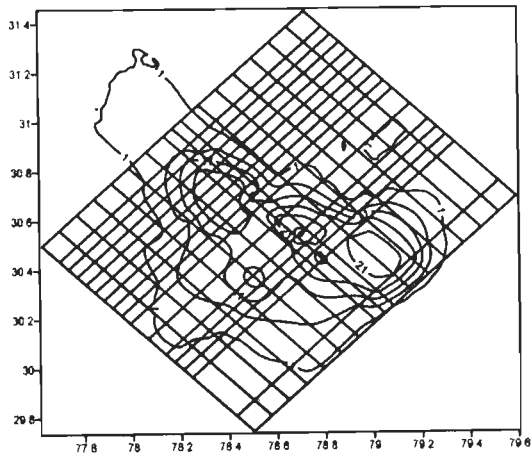


Depth 12 km

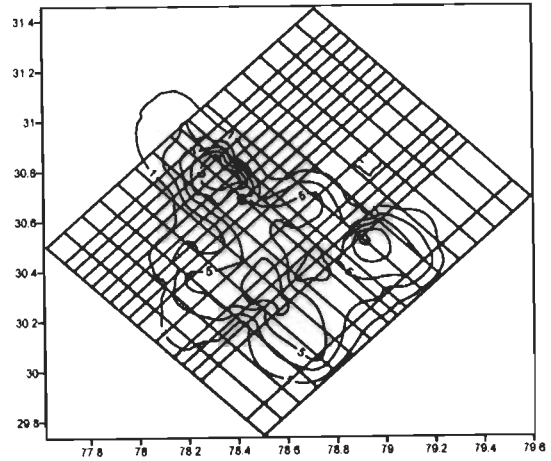


Depth 14 km

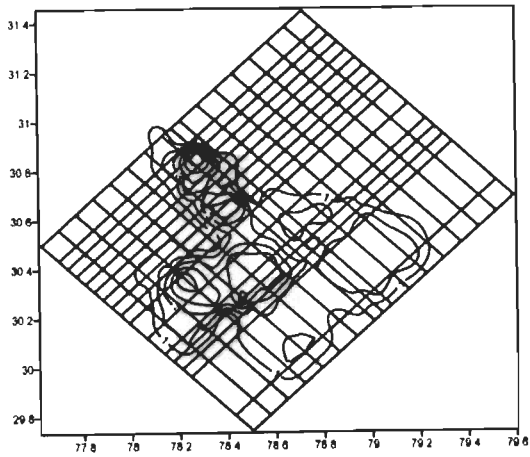
KHIT for 3-D Model-II



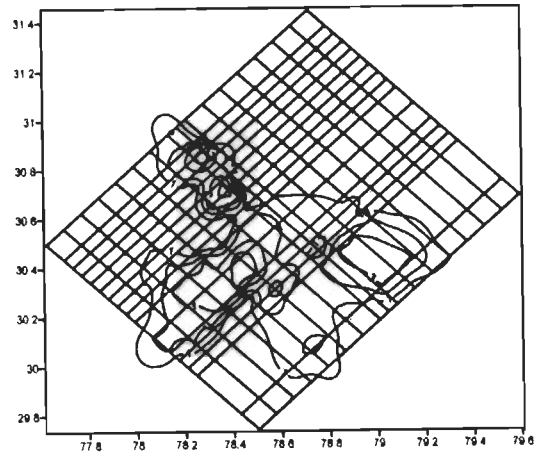
Depth 16 km



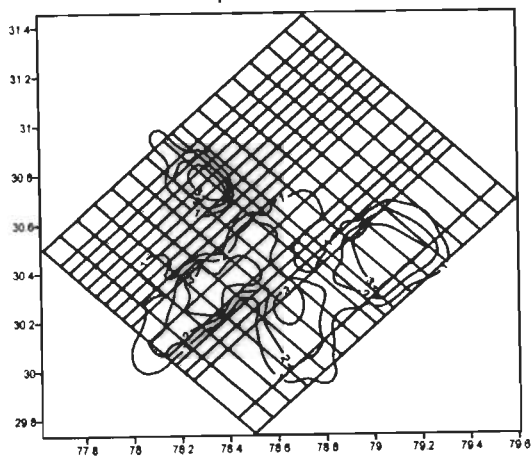
Depth 20 km



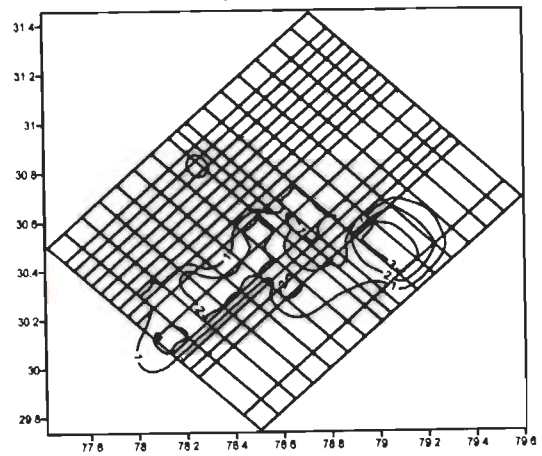
Depth 22 km



Depth 24 km

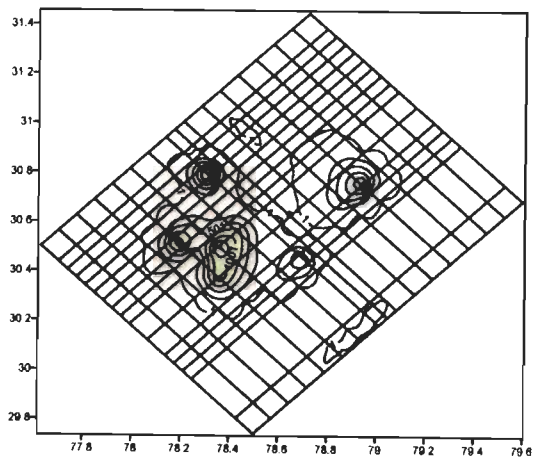


Depth 26 km

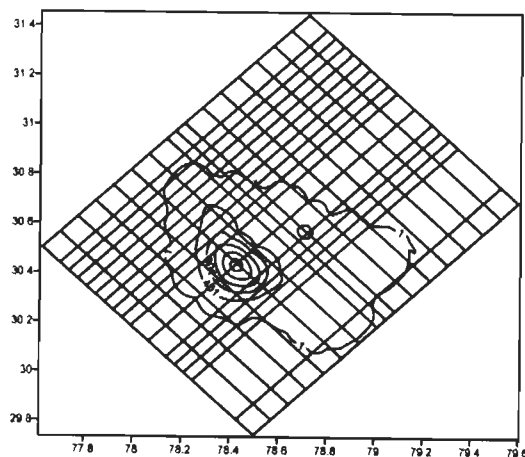


Depth 28 km

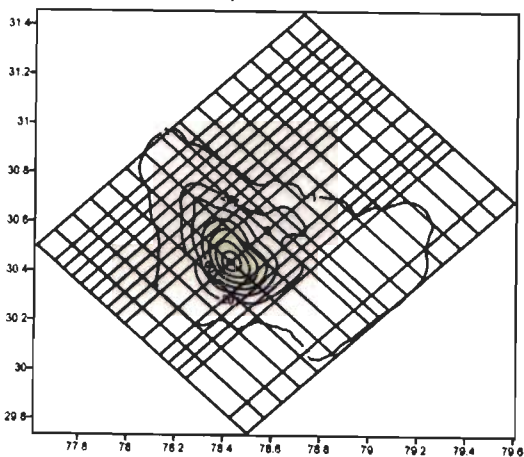
DWS for 3-D Model-II



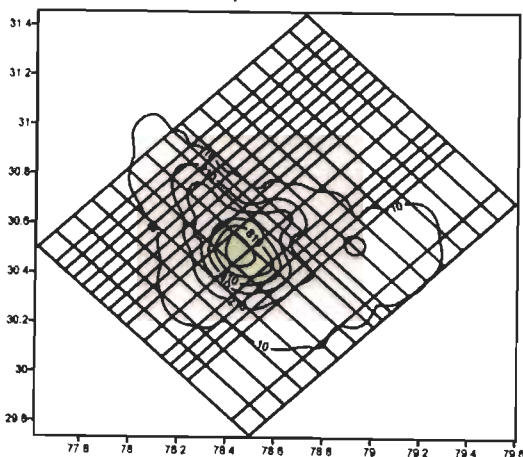
Depth 2 km



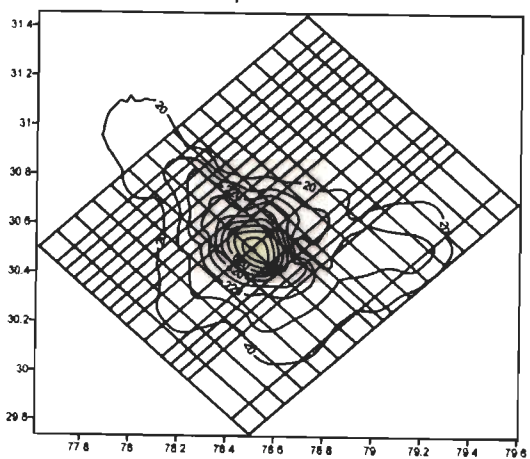
Depth 4 km



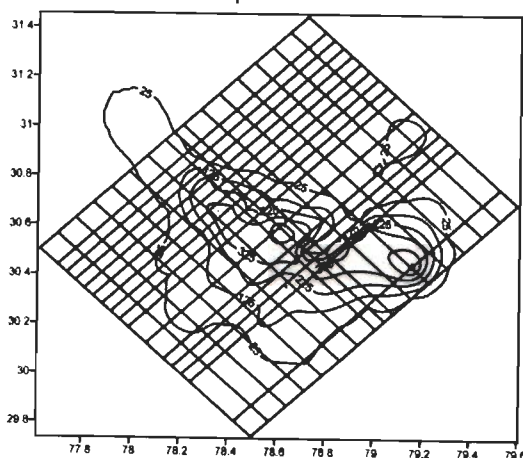
Depth 6 km



Depth 8 km

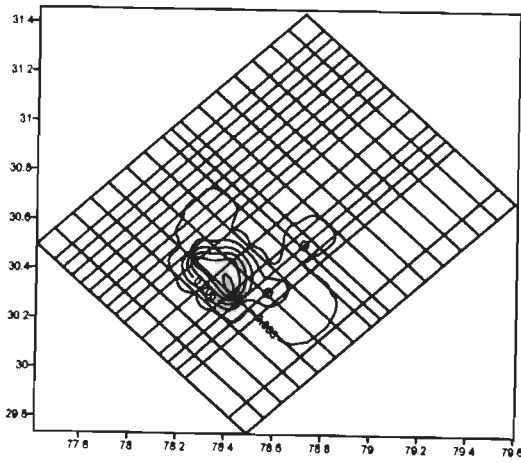


Depth 12 km

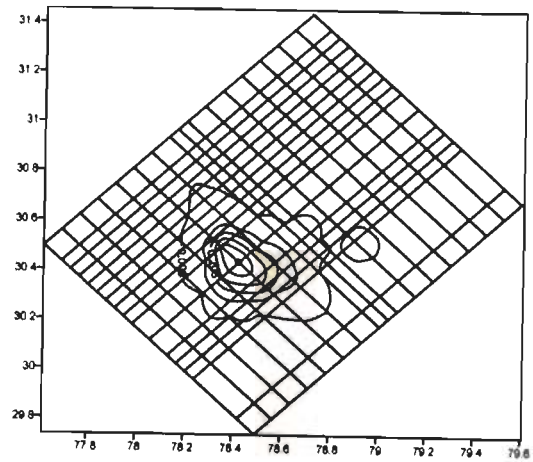


Depth 14 km

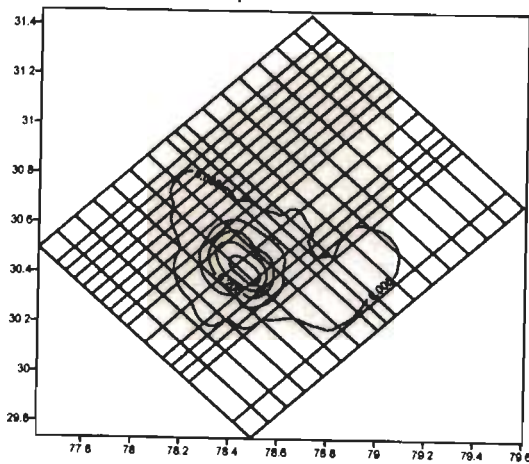
RESOLUTION for 3-D Model-II



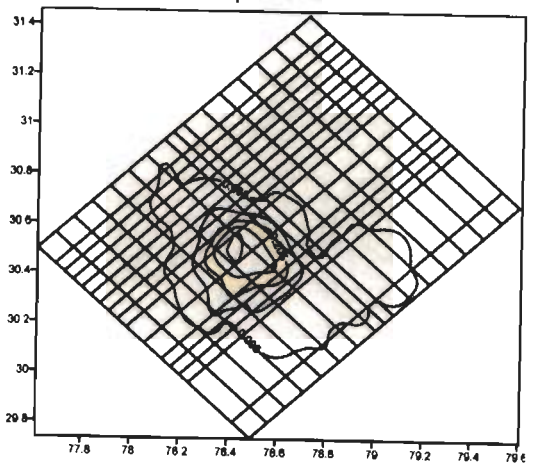
Depth 2 km



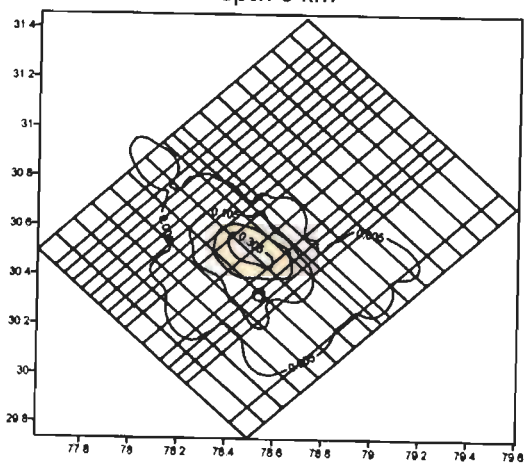
Depth 4 km



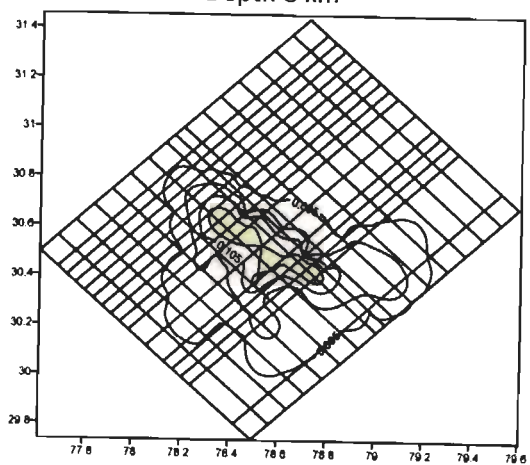
Depth 6 km



Depth 8 km

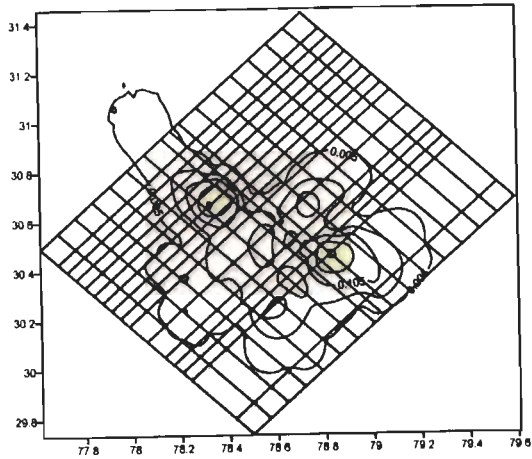


Depth 12 km

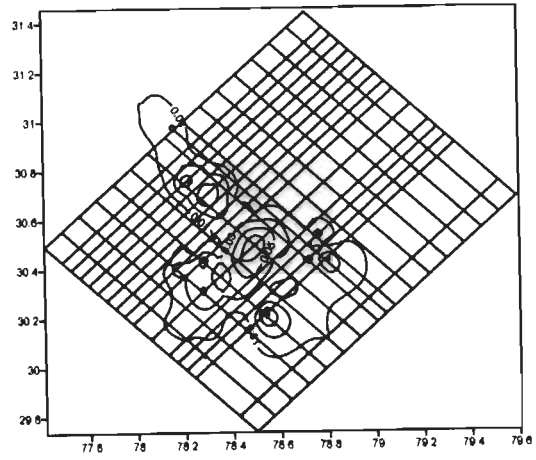


Depth 14 km

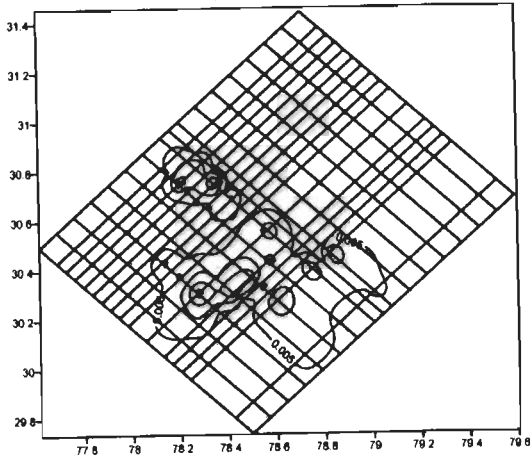
RESOLUTION for 3-D Model-II



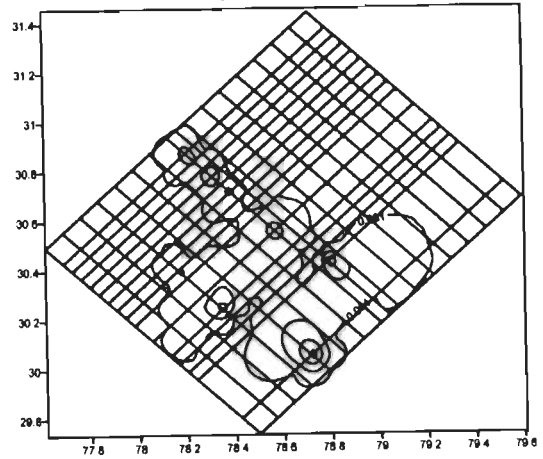
Depth 16 km



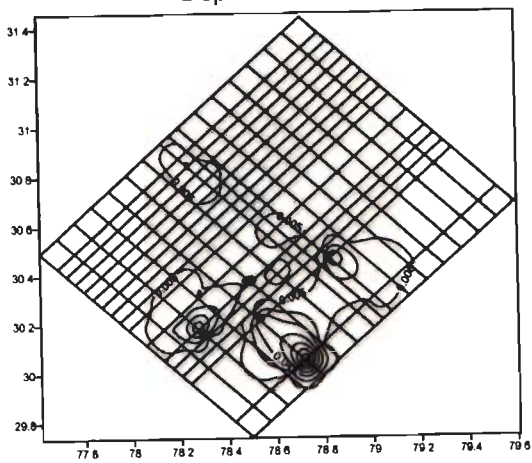
Depth 20 km



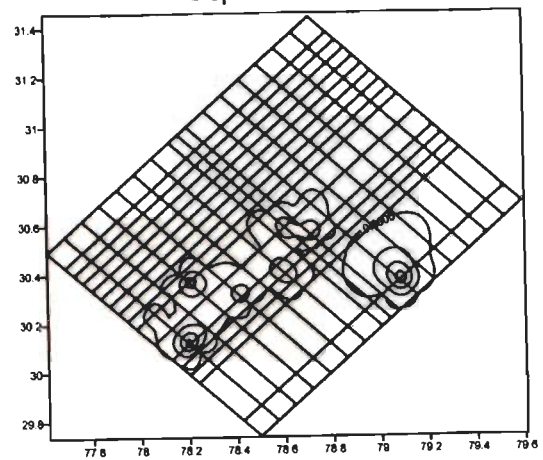
Depth 22 km



Depth 24 km

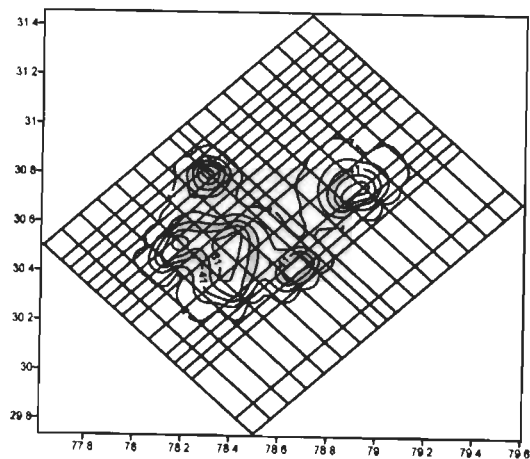


Depth 26 km

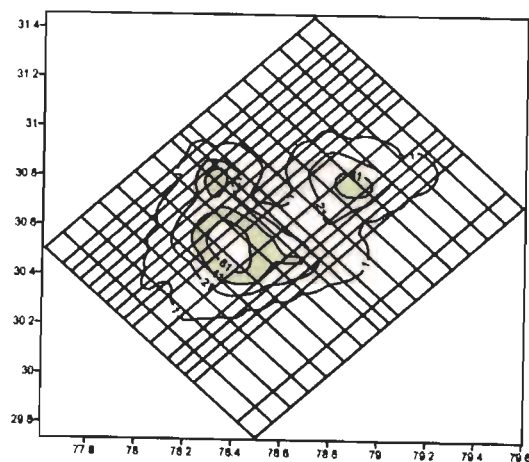


Depth 28 km

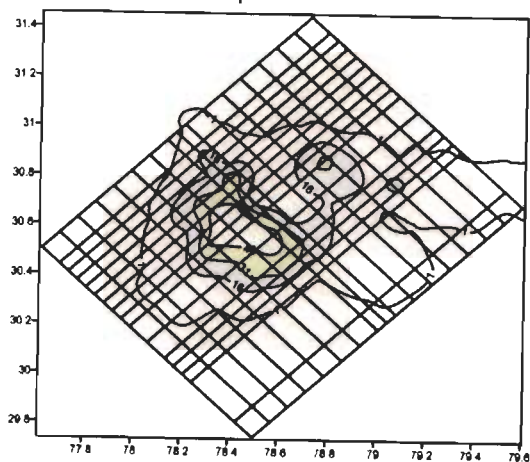
KHIT for 3-D Model-III



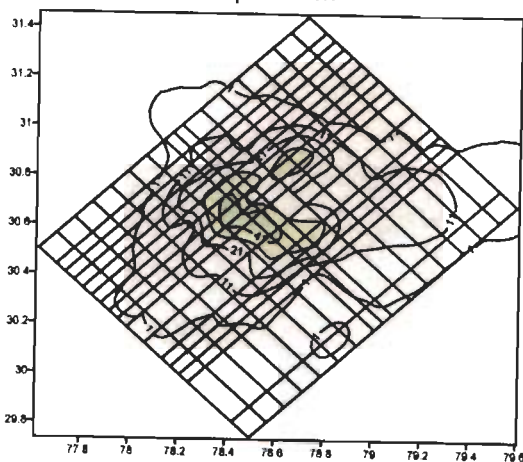
Depth 2 km



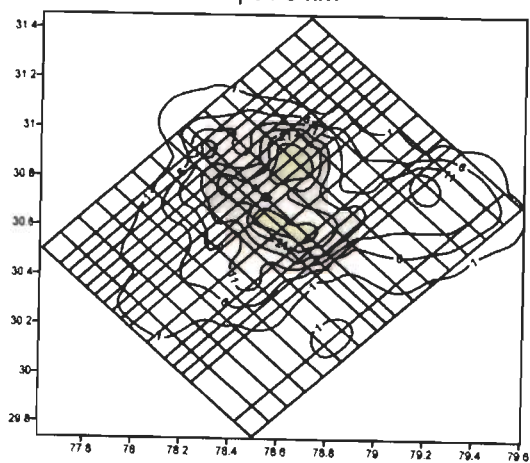
Depth 4 km



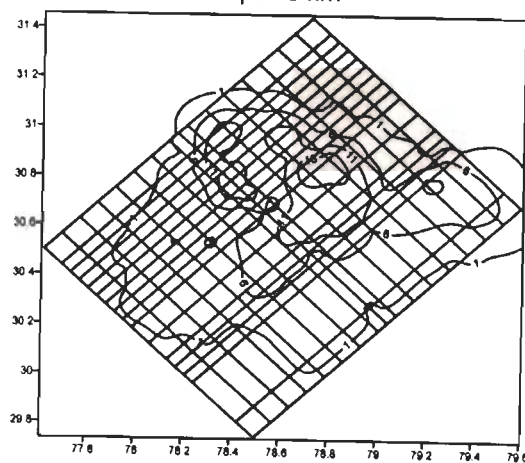
Depth 6 km



Depth 8 km

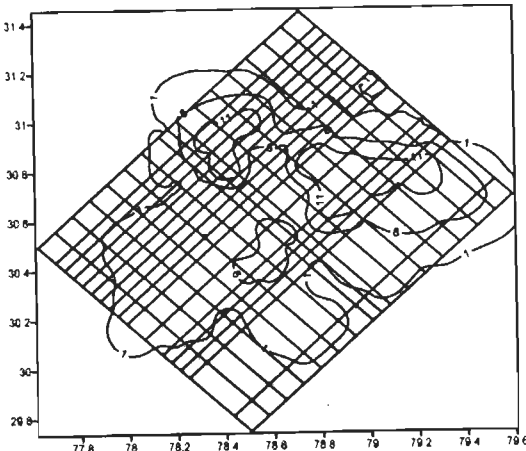


Depth 12 km

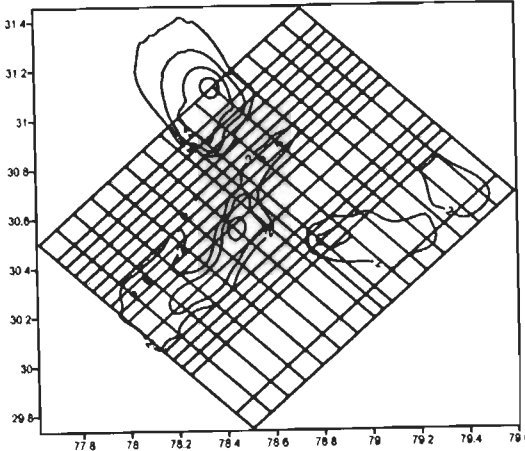


Depth 14 km

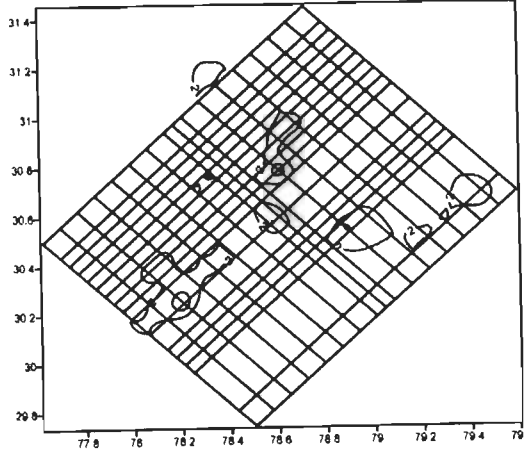
KHIT for 3-D Model-III



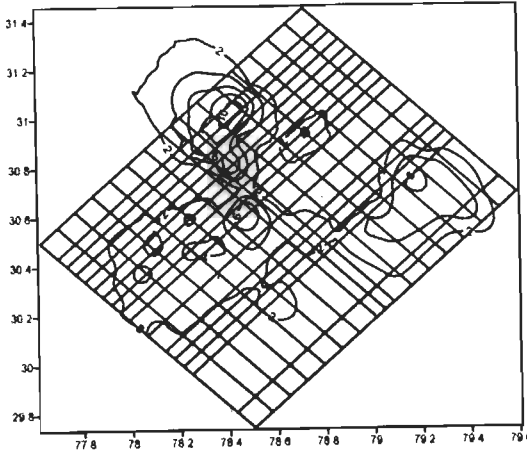
Depth 16 km



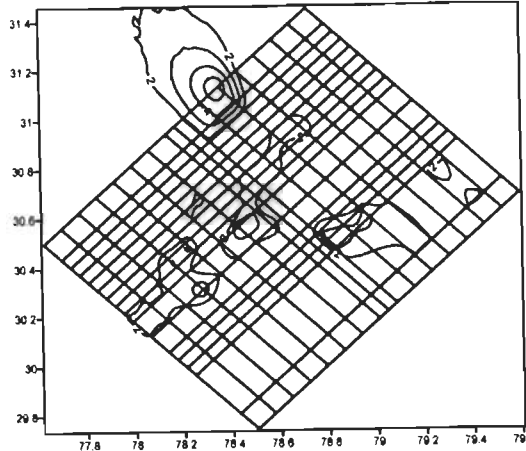
Depth 22 km



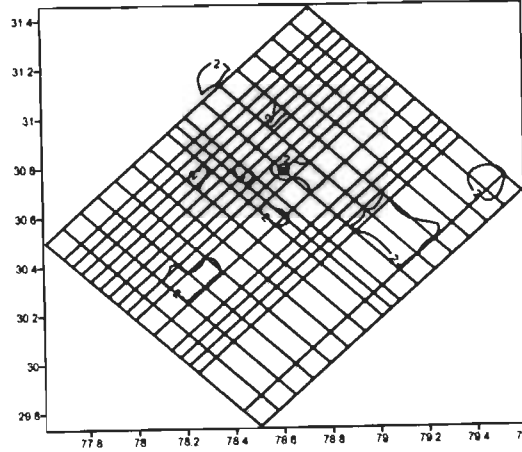
Depth 26 km



Depth 20 km

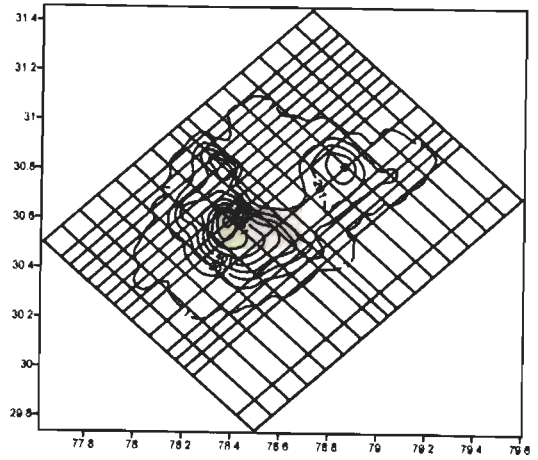
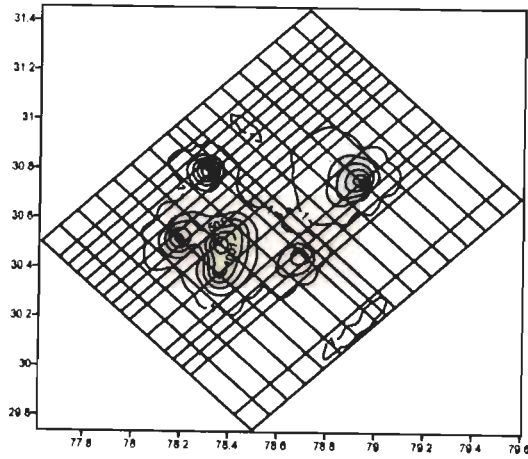


Depth 24 km



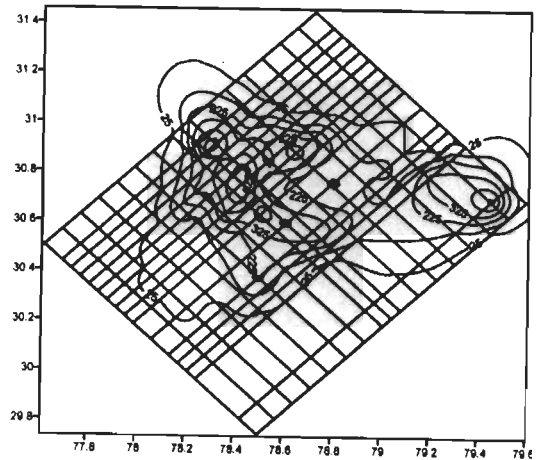
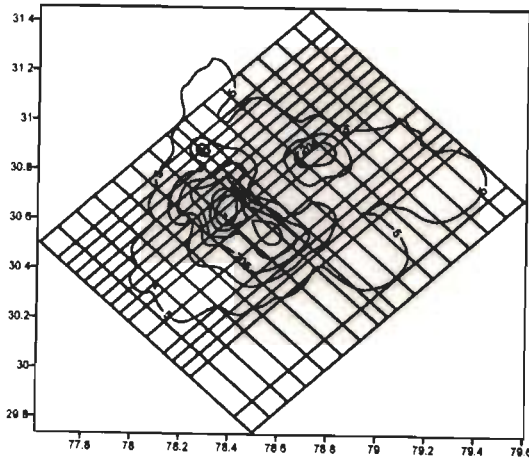
Depth 28 km

DWS for 3-D Model-III



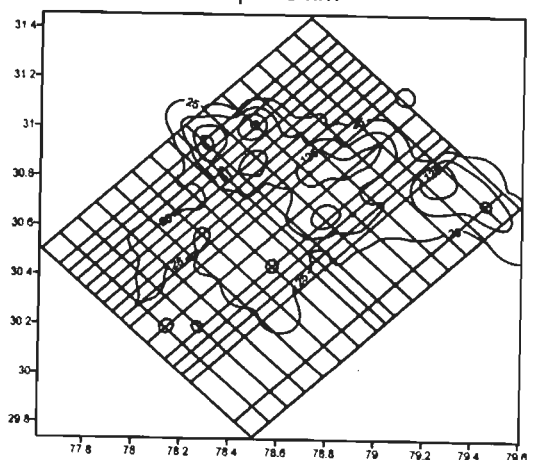
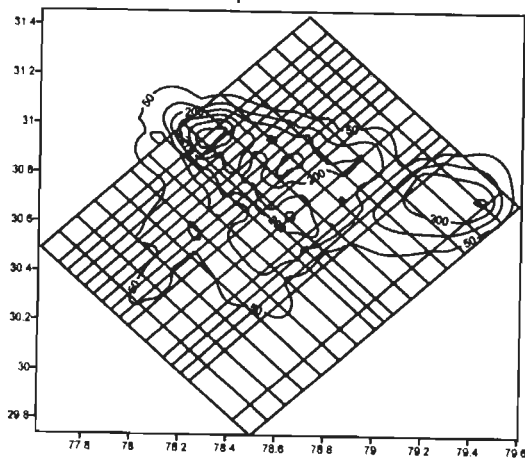
Depth 2 km

Depth 4 km



Depth 6 km

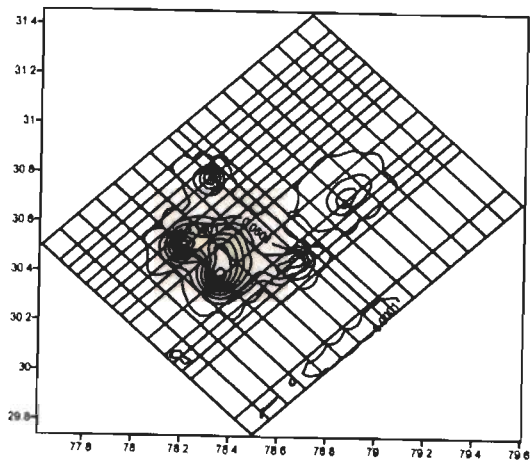
Depth 8 km



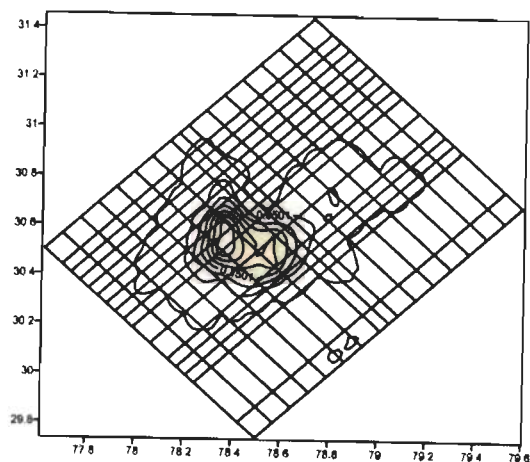
Depth 12 km

Depth 14 km

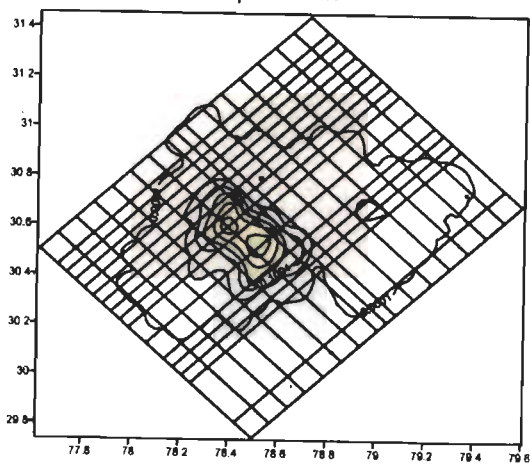
RESOLUTION for 3-D Model-III



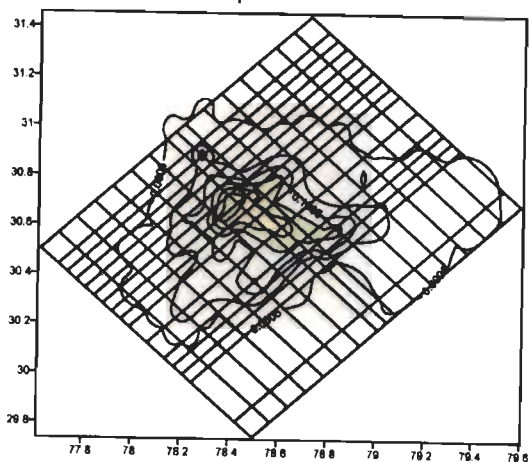
Depth 2 km



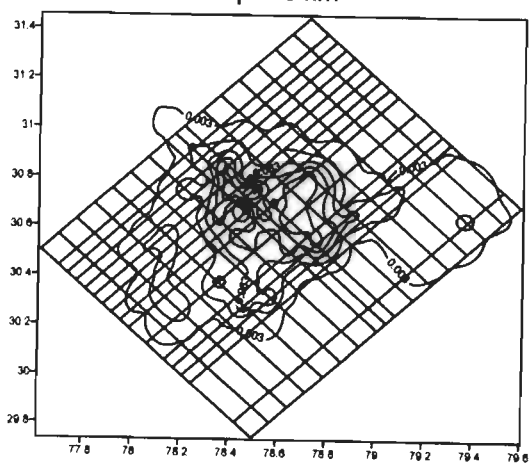
Depth 4 km



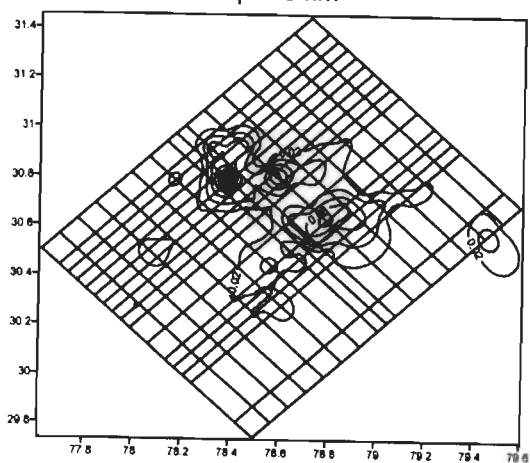
Depth 6 km



Depth 8 km

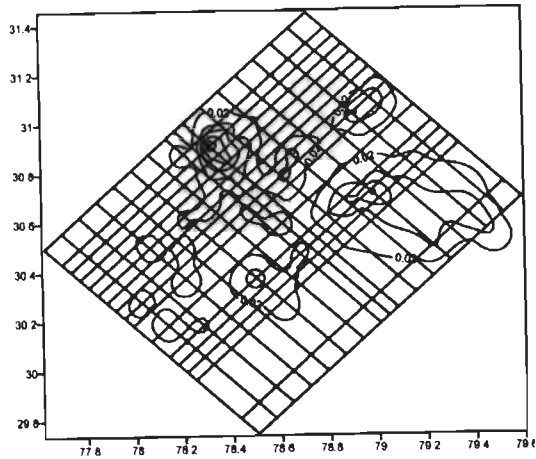


Depth 12 km

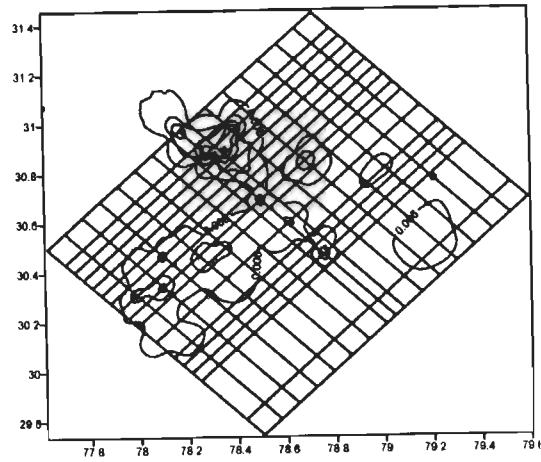


Depth 14 km

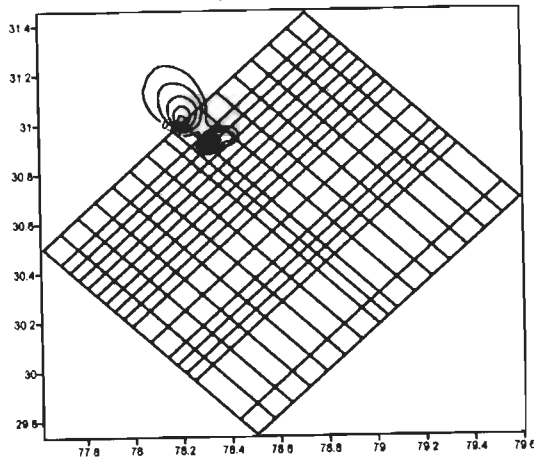
RESOLUTION for 3-D Model-III



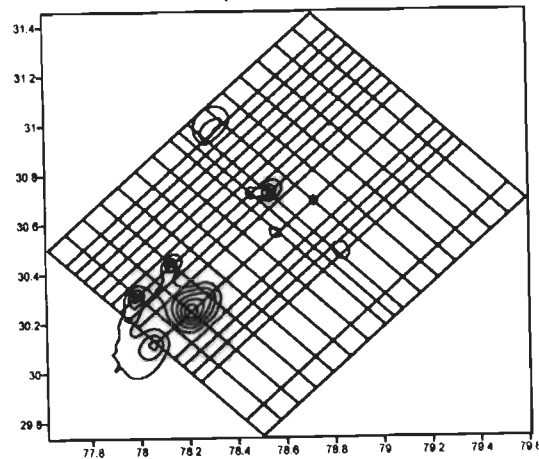
Depth 16 km



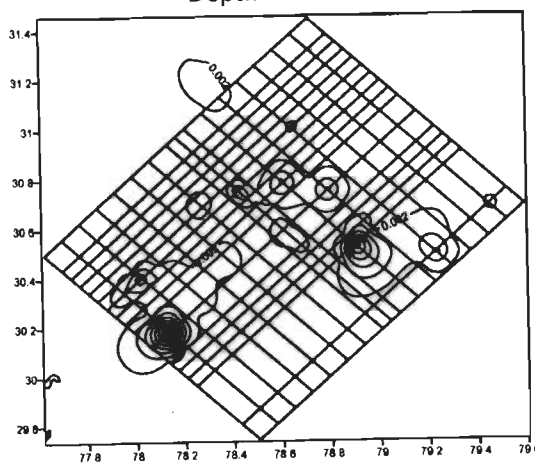
Depth 20 km



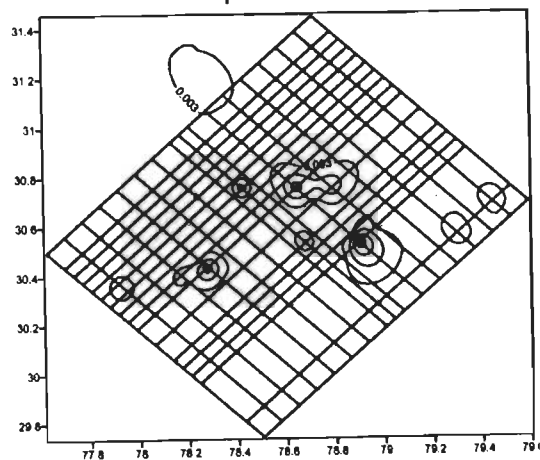
Depth 22 km



Depth 24 km

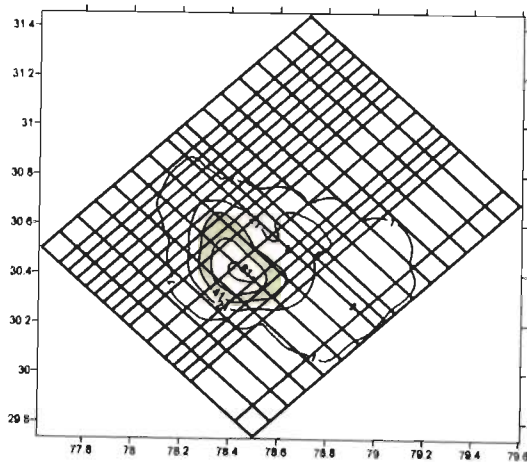
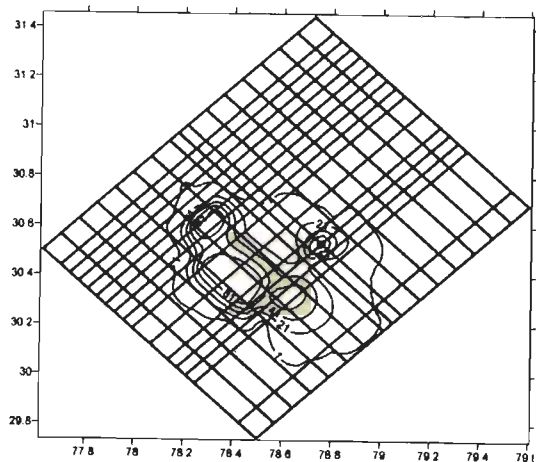


Depth 26 km



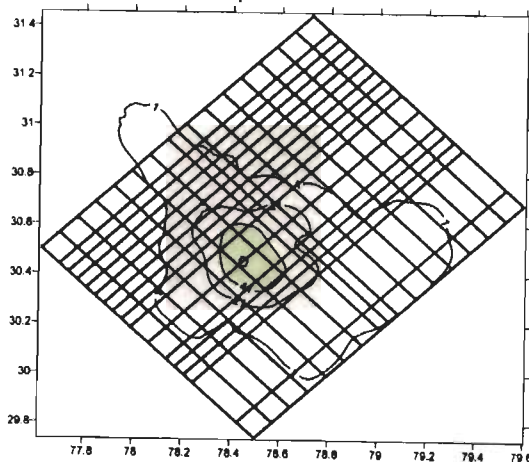
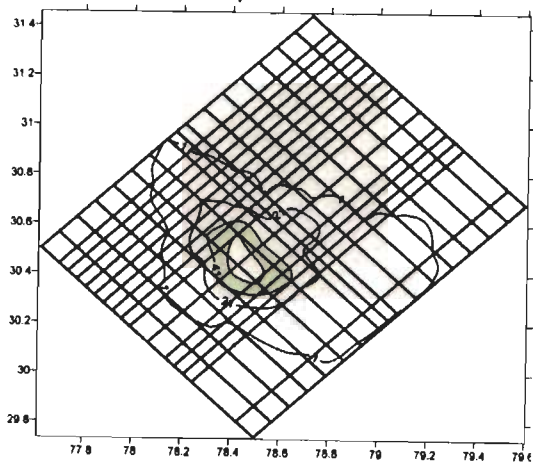
Depth 28 km

KHIT for 3-D Model-IV



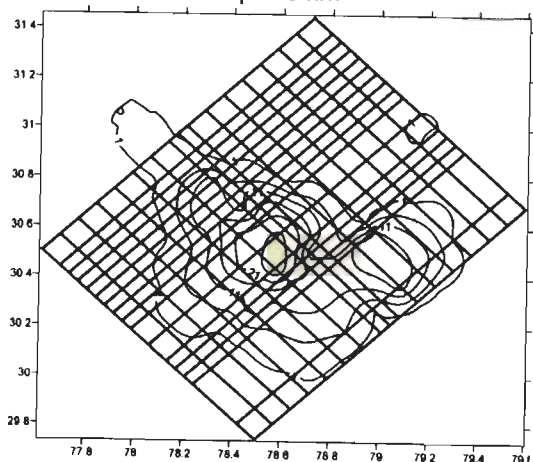
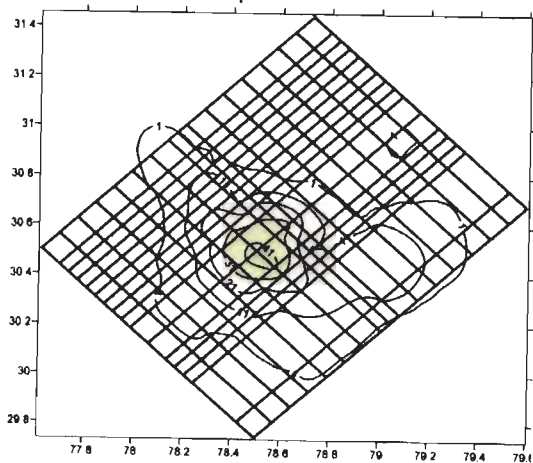
Depth 2 km

Depth 4 km



Depth 6 km

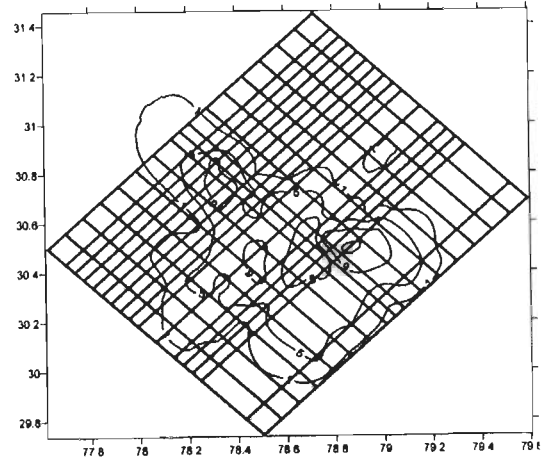
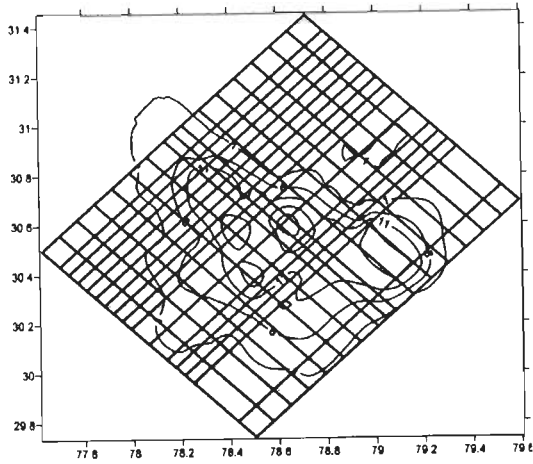
Depth 8 km



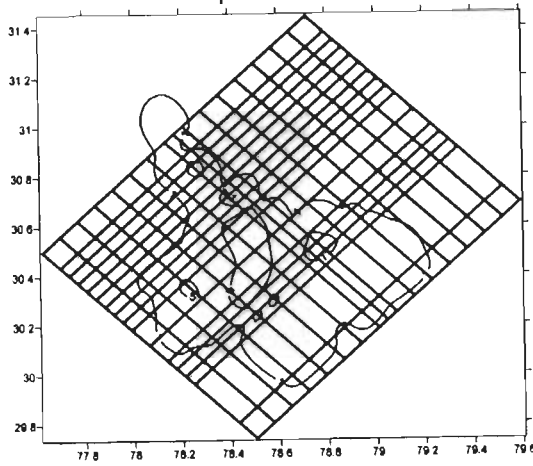
Depth 12 km

Depth 14 km

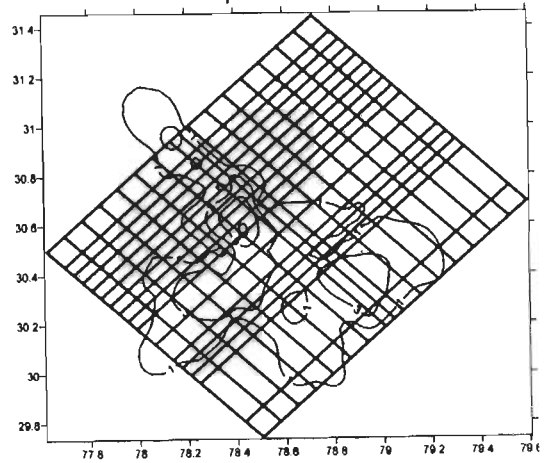
KHIT for 3-D Model-IV



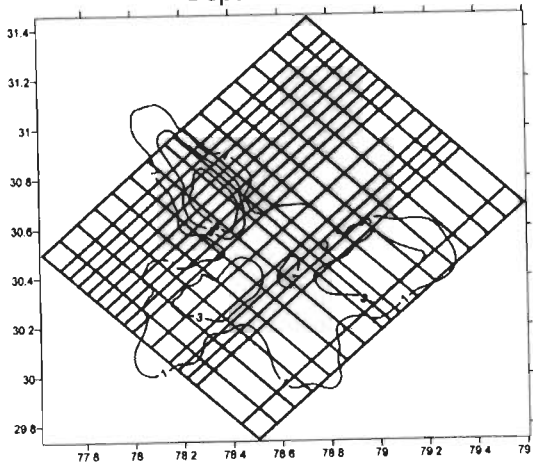
Depth 16 km



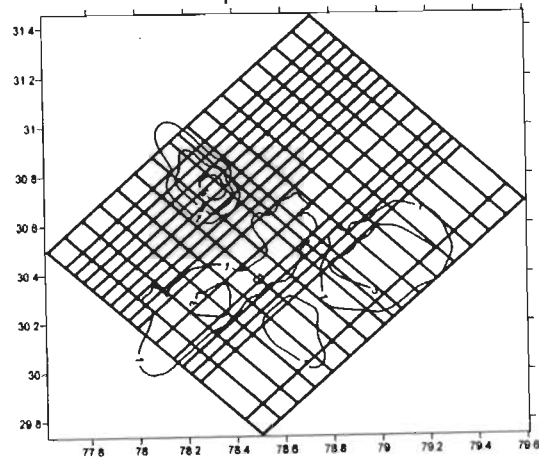
Depth 20 km



Depth 22 km



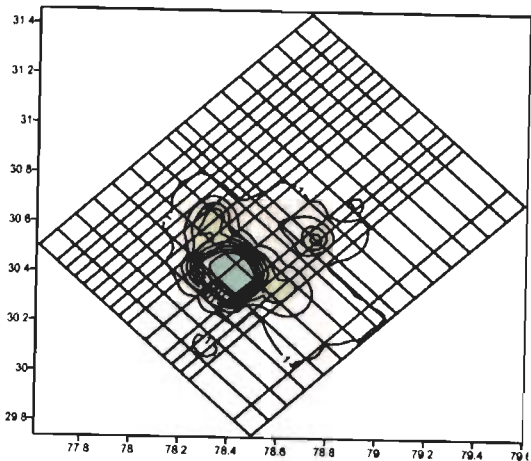
Depth 24 km



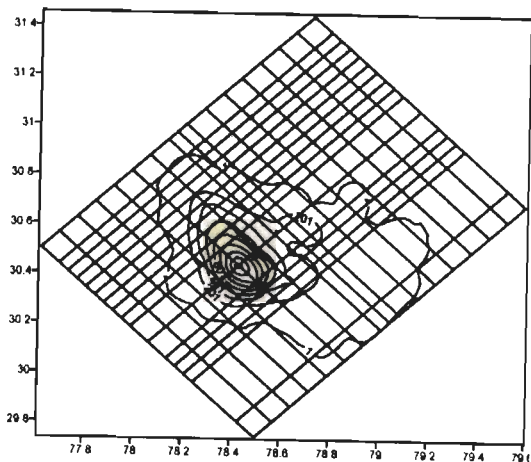
Depth 26 km

Depth 28 km

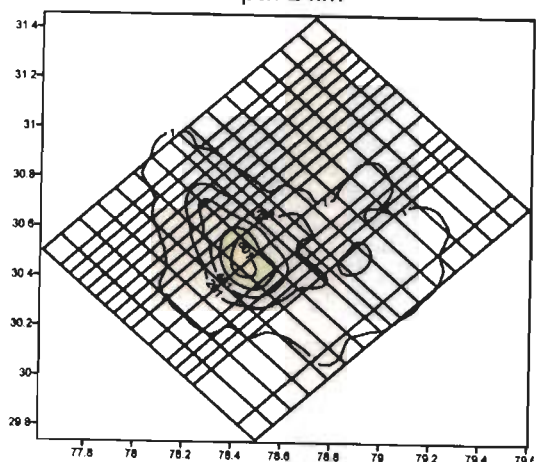
DWS for 3-D Model-IV



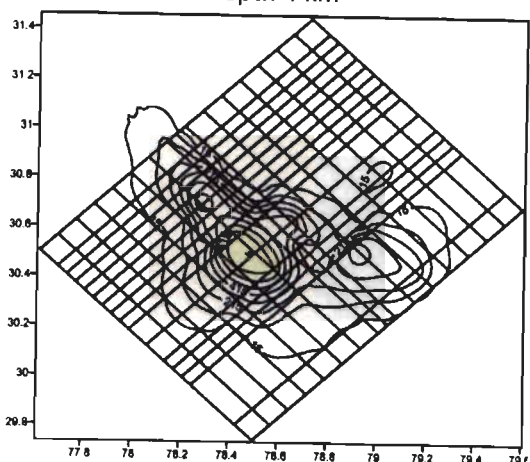
Depth 2 km



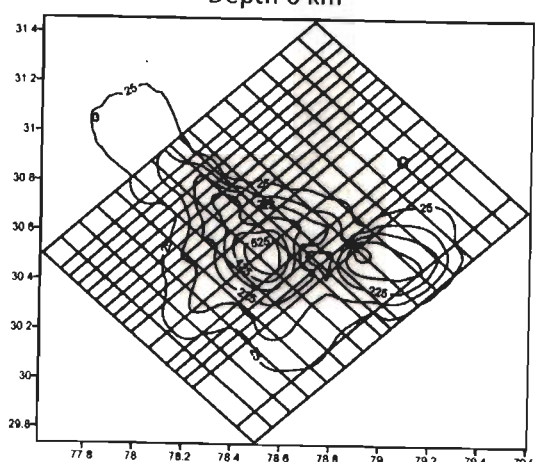
Depth 4 km



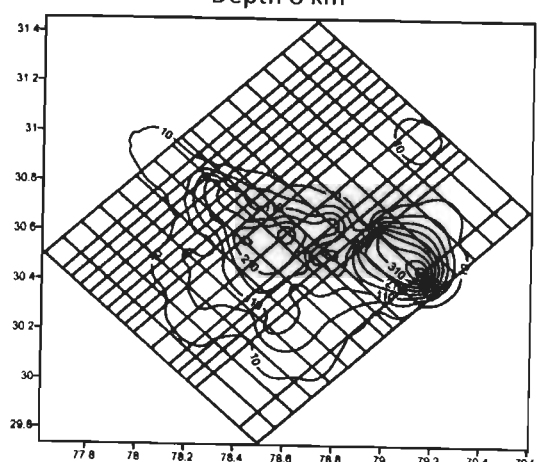
Depth 6 km



Depth 8 km

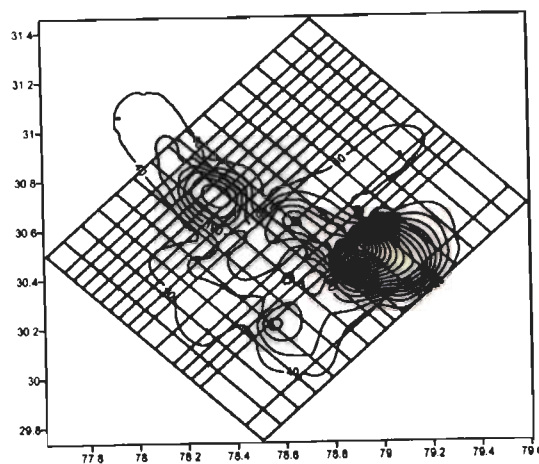


Depth 12 km

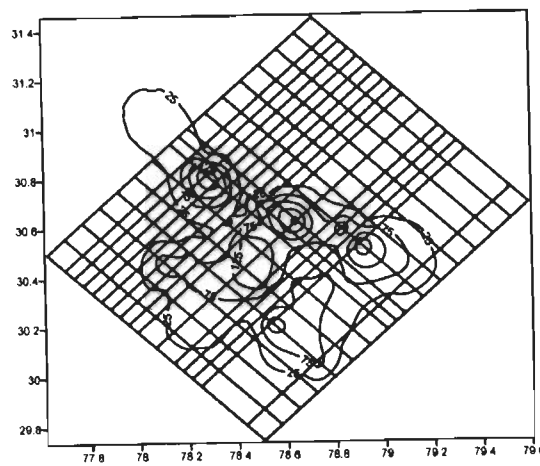


Depth 14 km

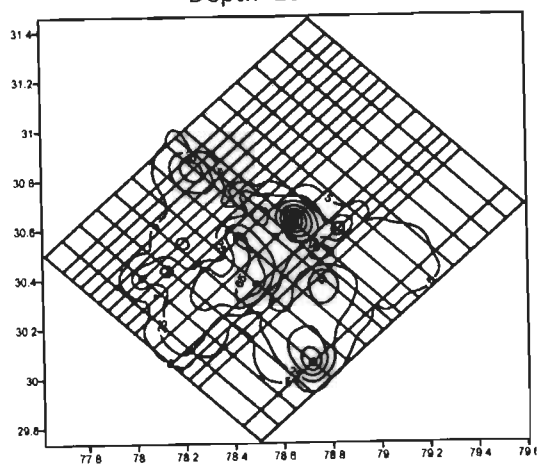
DWS for 3-D Model-IV



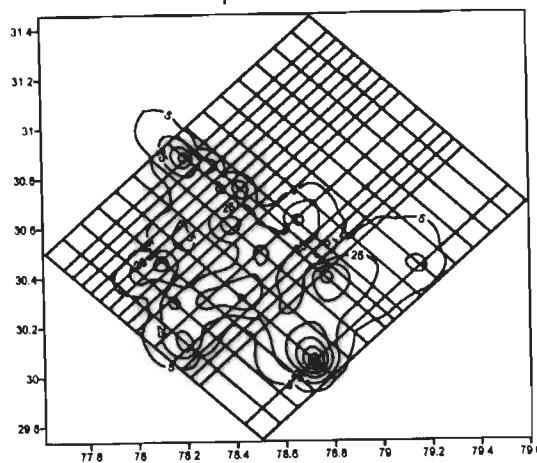
Depth 16 km



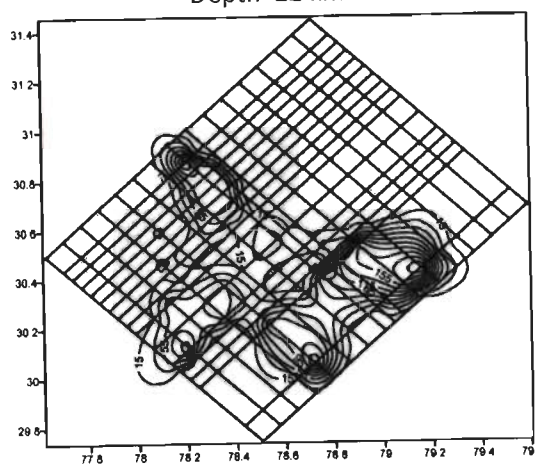
Depth 20 km



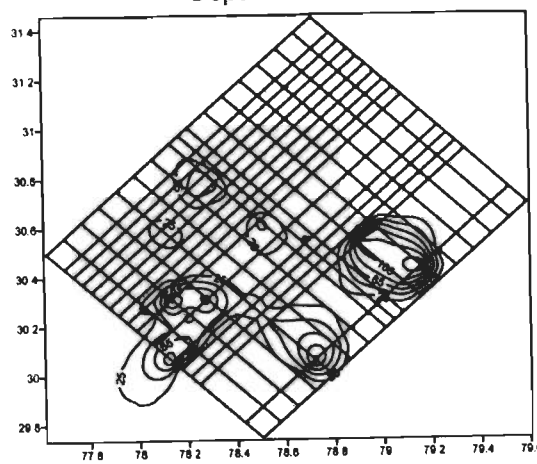
Depth 22 km



Depth 24 km

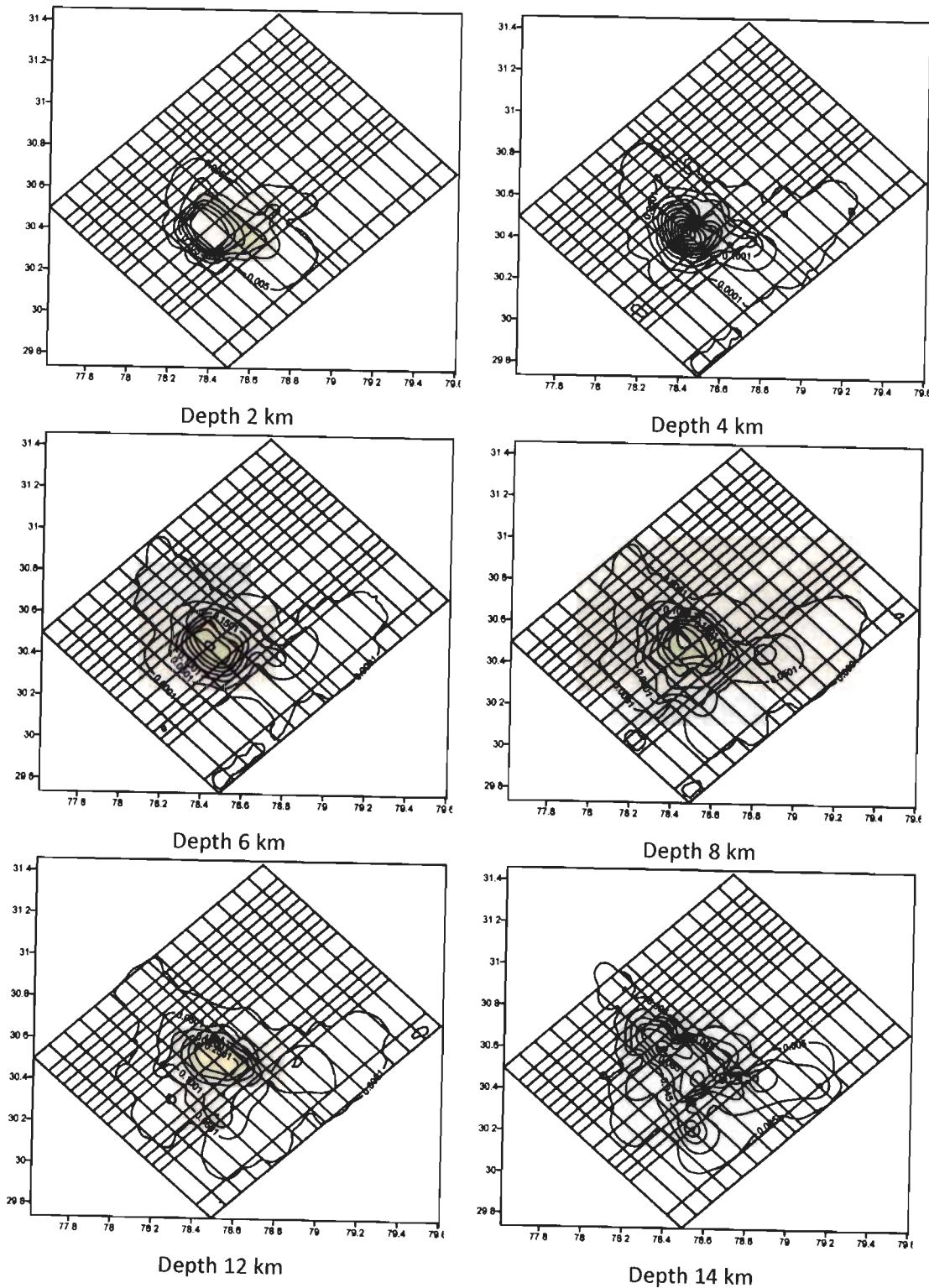


Depth 26 km

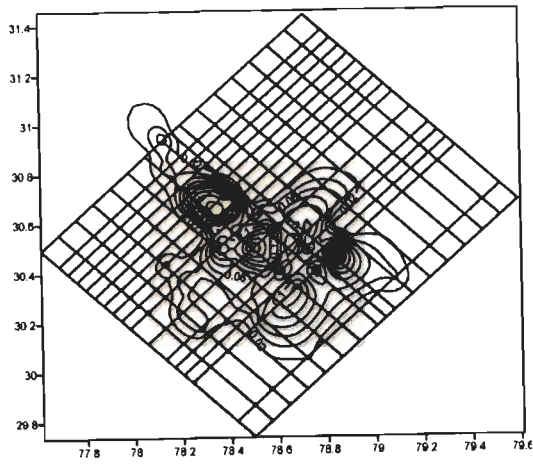


Depth 28 km

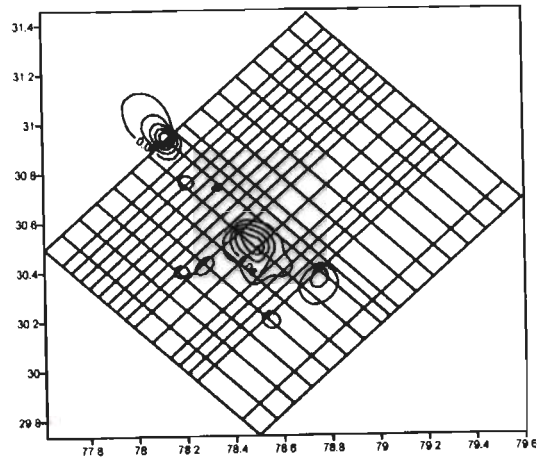
RESOLUTION for 3-D Model-IV



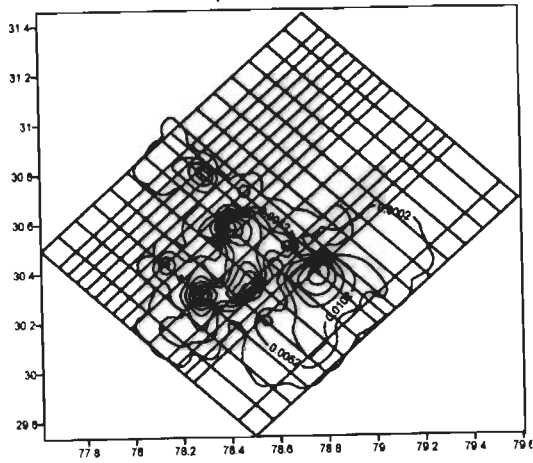
RESOLUTION for 3-D Model-IV



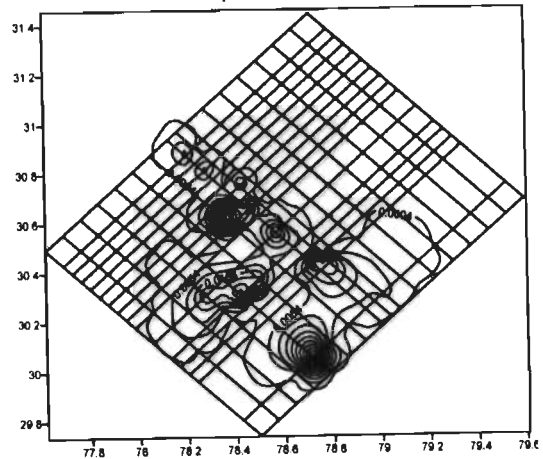
Depth 16 km



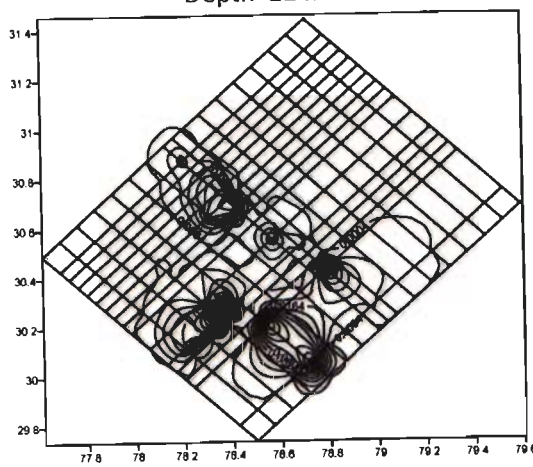
Depth 20 km



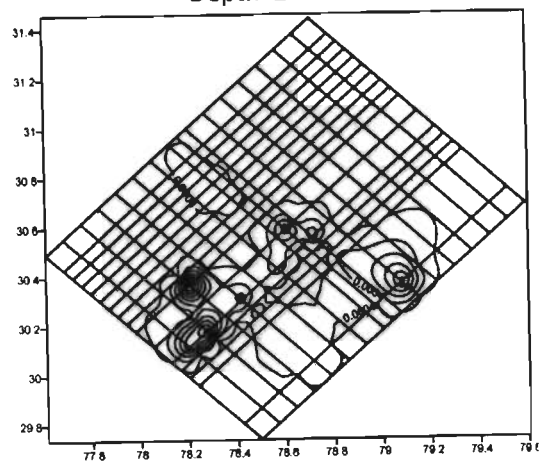
Depth 22 km



Depth 24 km



Depth 26 km

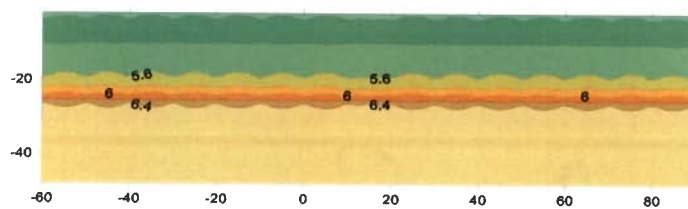


Depth 28 km

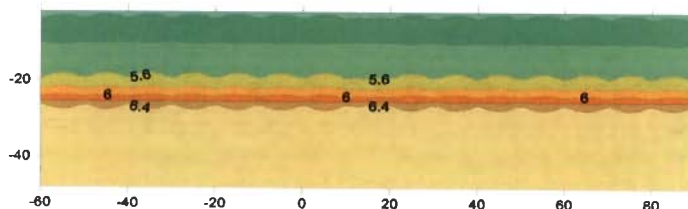
APPENDIX – IV

This appendix presents the vertical profiles of the 3-D Models obtained in the present study. It contains the vertical profiles for the four models namely, 3-D Model I, 3-D Model II, 3-D Model III and 3-D Model IV using east-west gridding and NE-SW gridding, respectively.

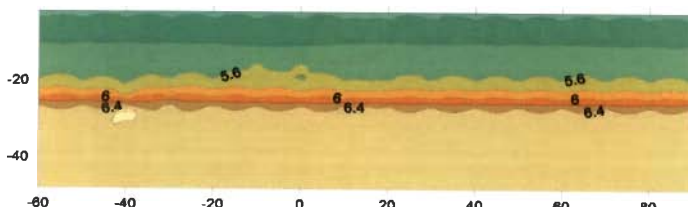
East-West gridding 3-D Model I



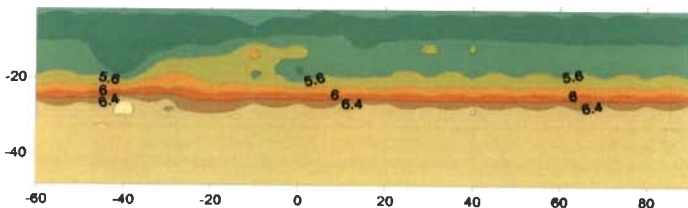
Profile 1



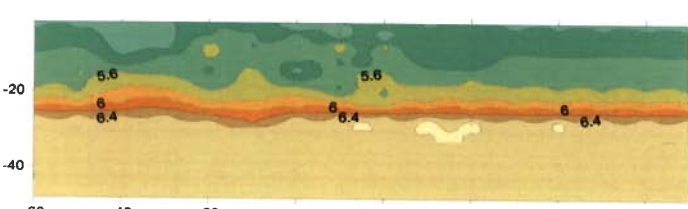
Profile 2



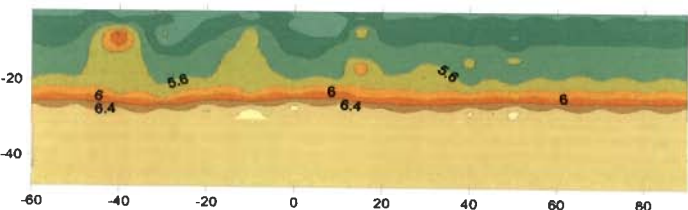
Profile 3



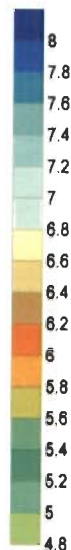
Profile 4



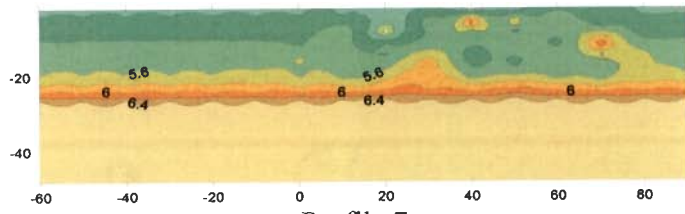
Profile 5



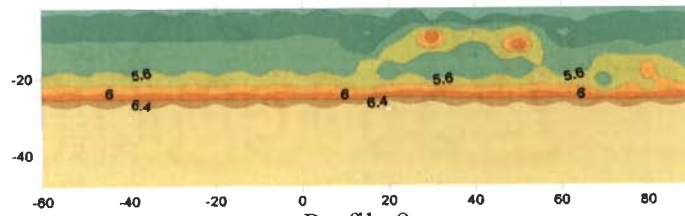
Profile 6



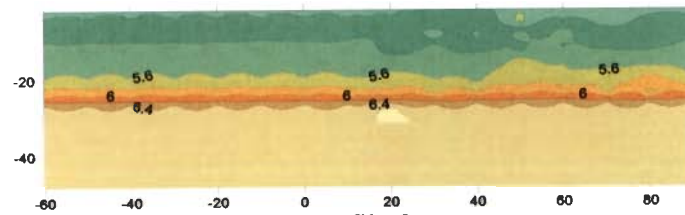
East-West gridding 3-D Model I



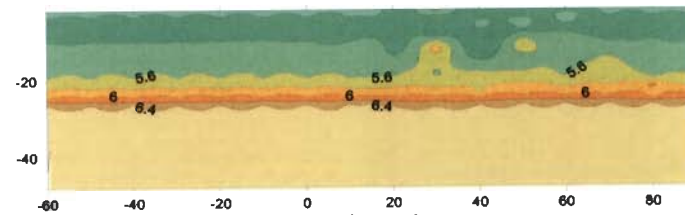
Profile 7



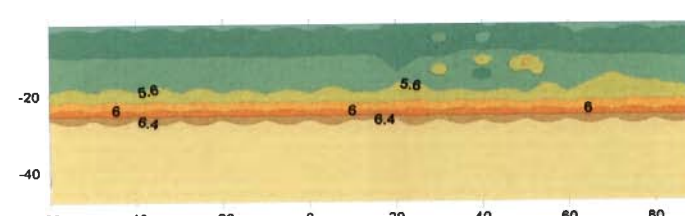
Profile 8



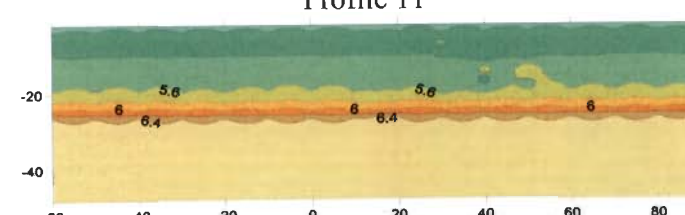
Profile 9



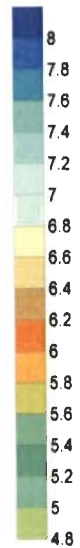
Profile 10



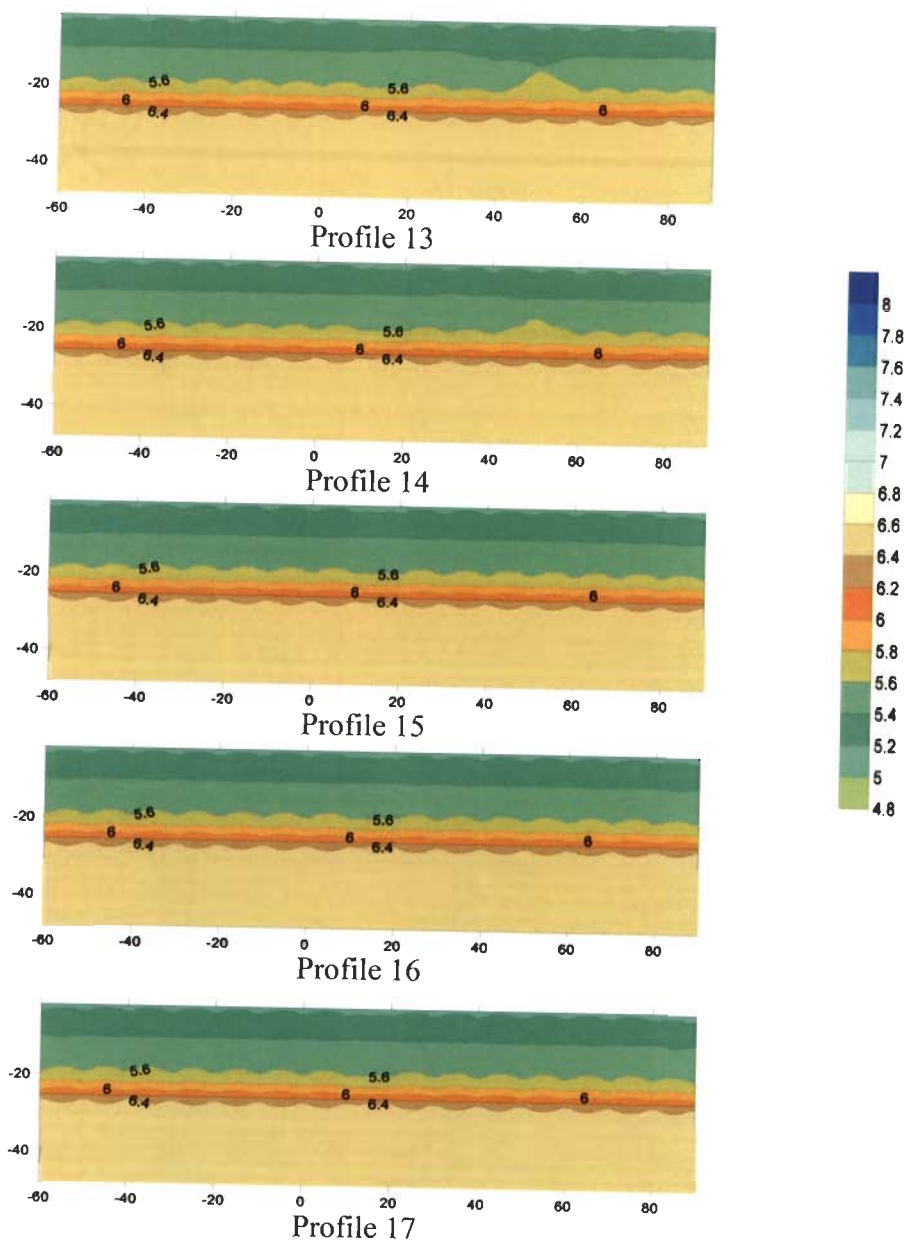
Profile 11



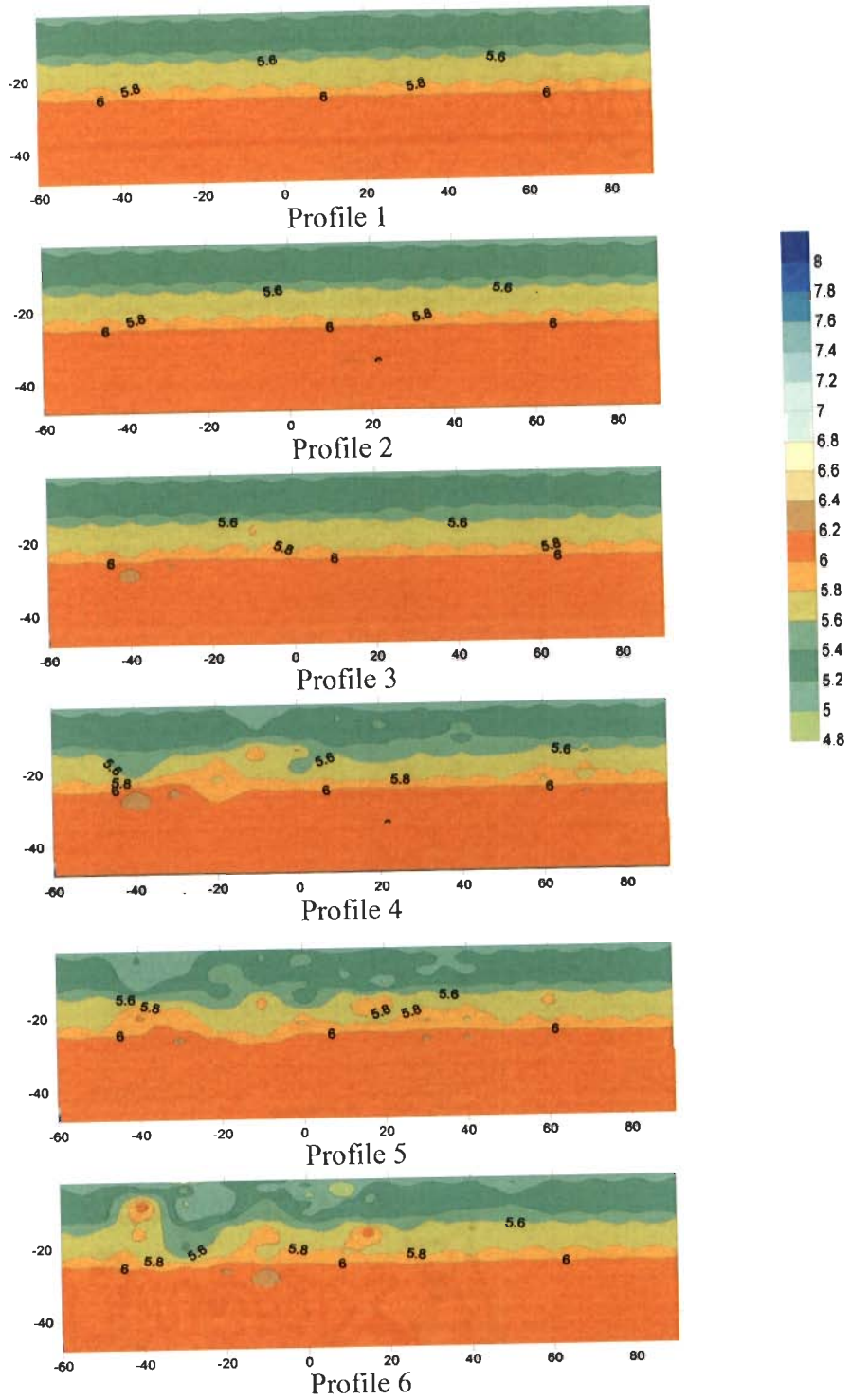
Profile 12



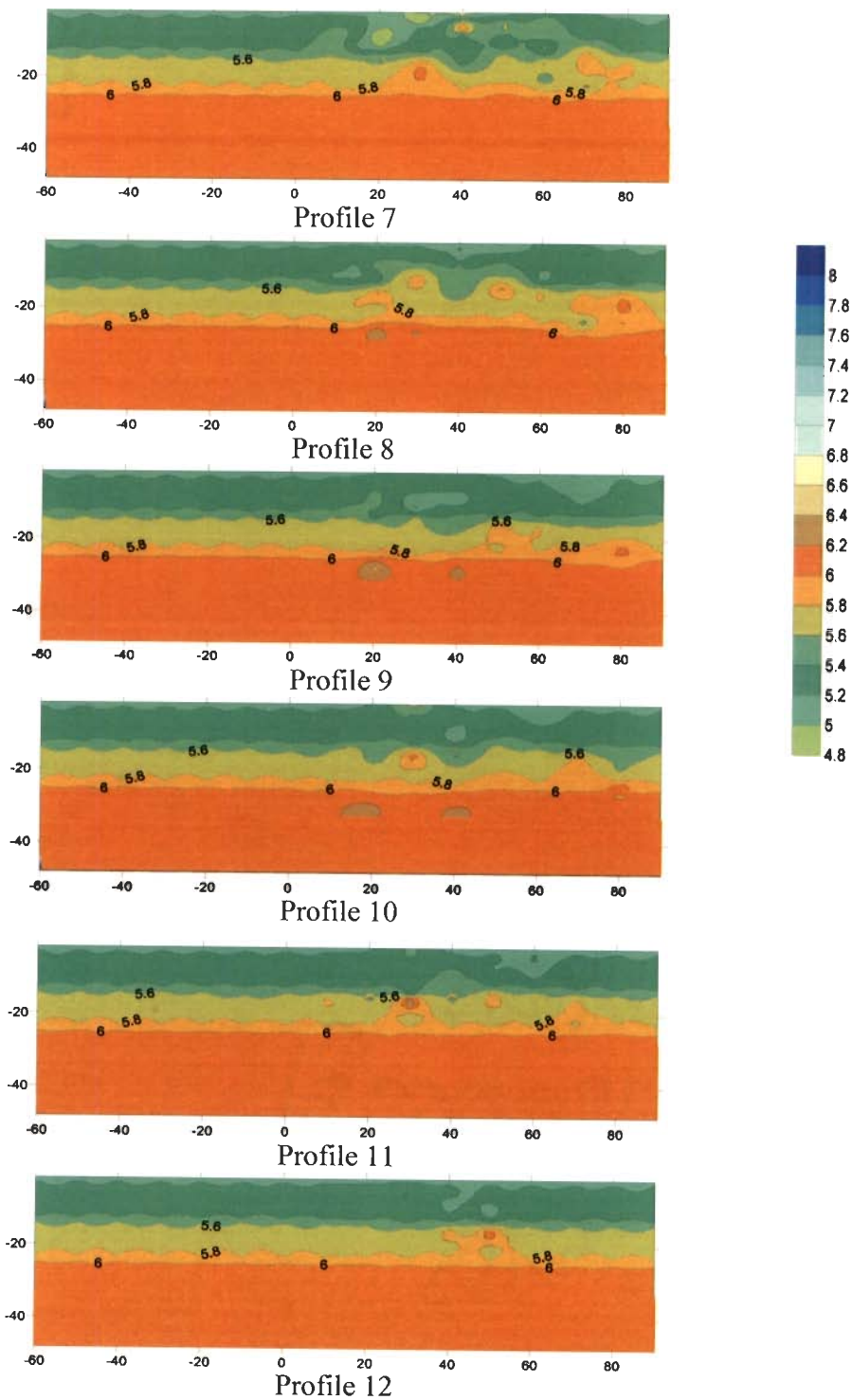
East-West gridding 3-D Model I



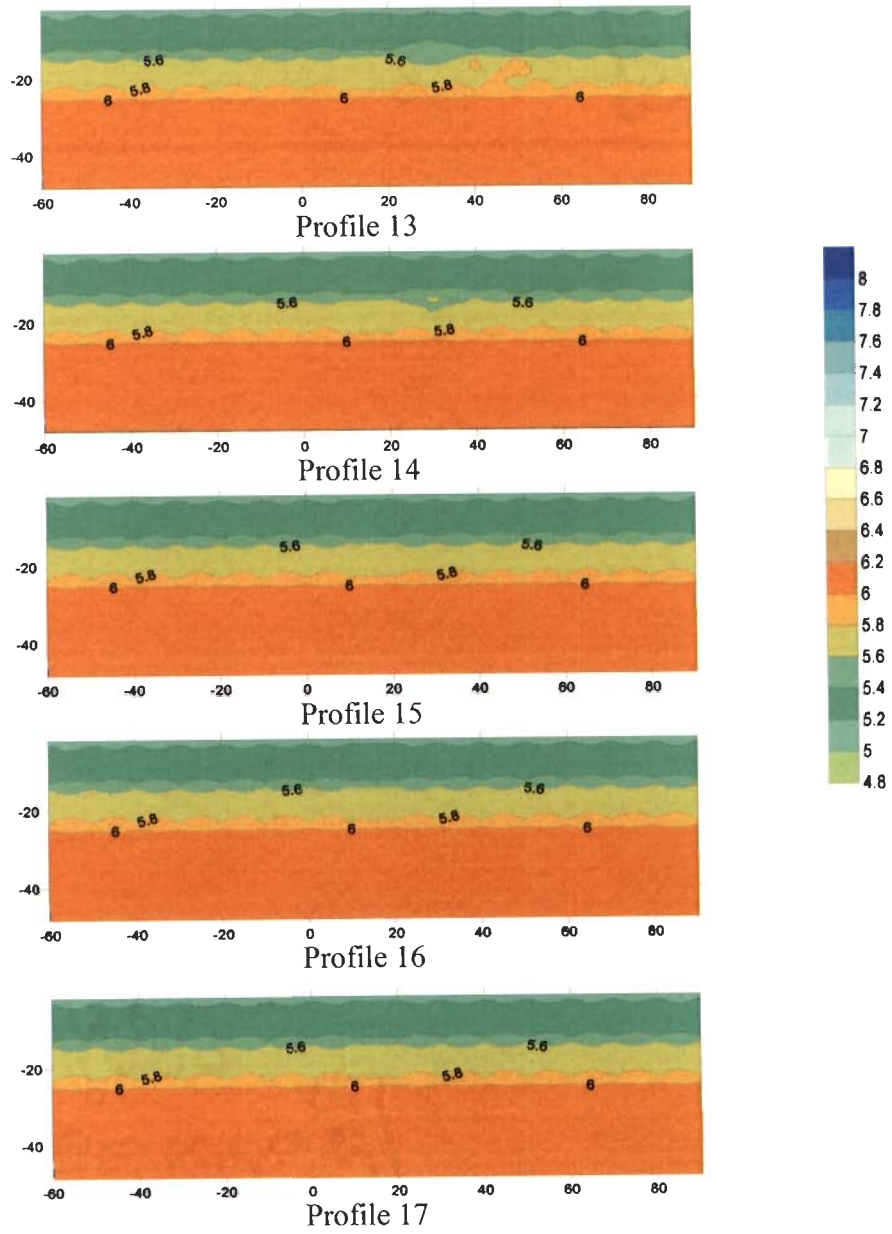
East-West gridding 3-D Model II



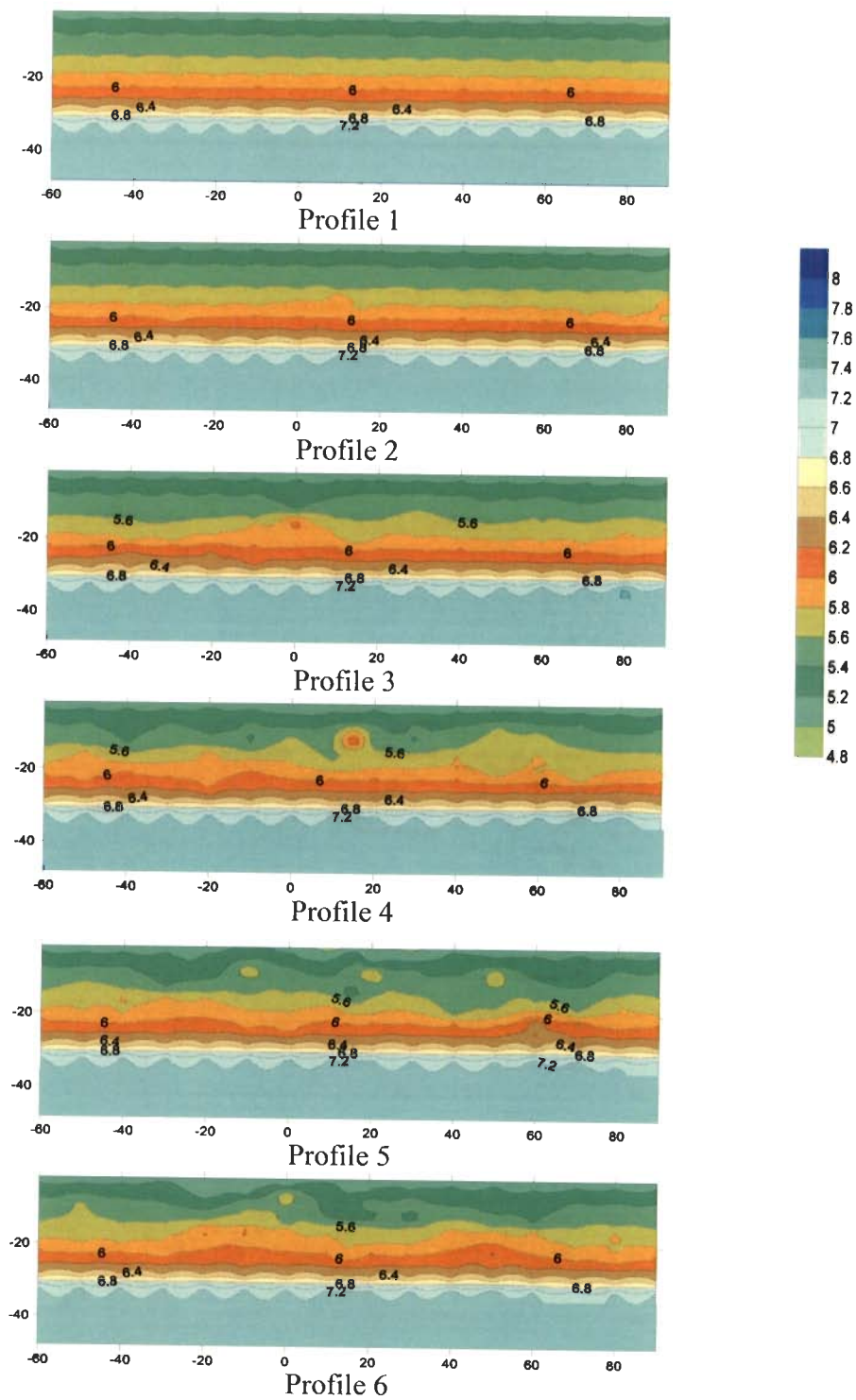
East-West gridding 3-D Model II



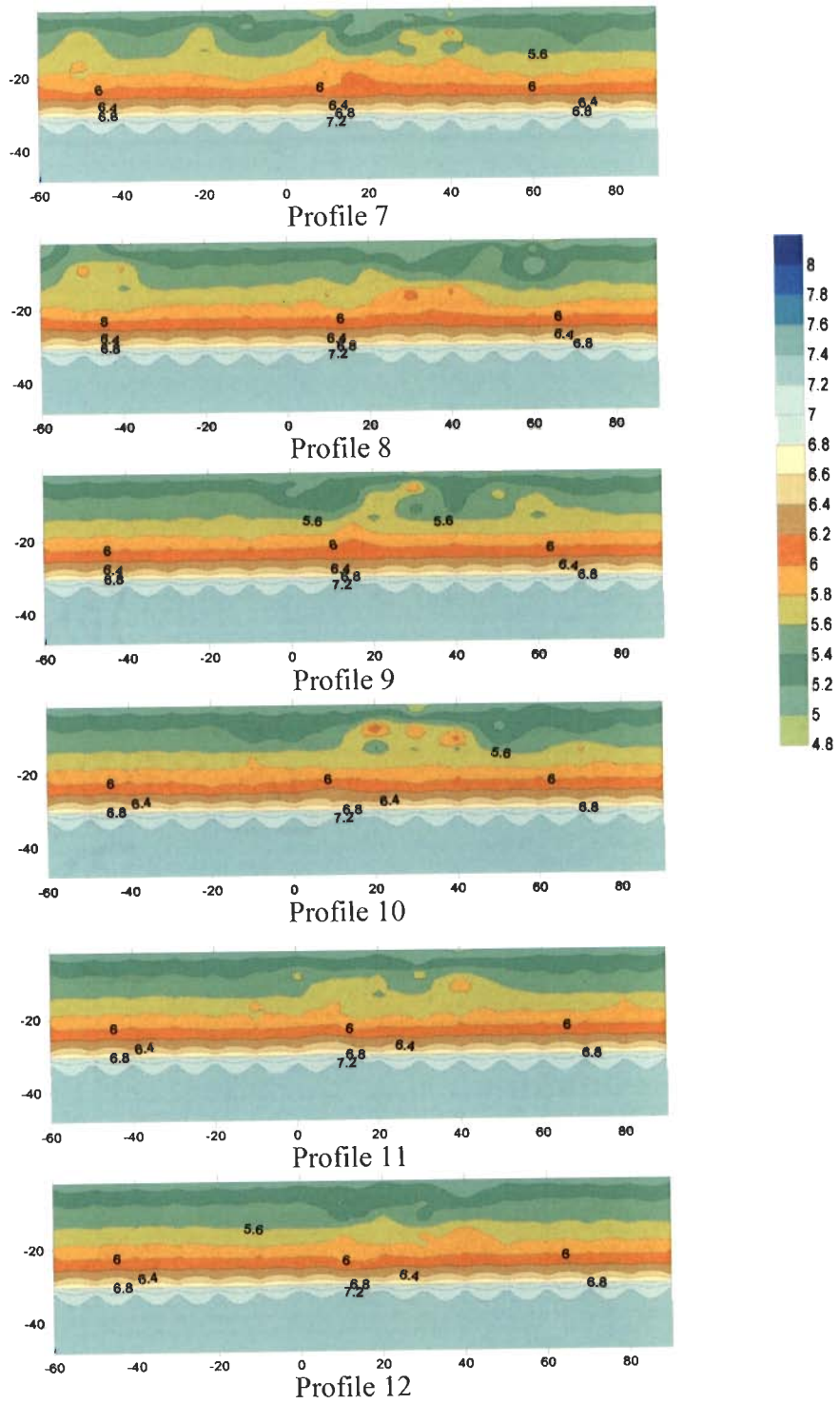
East-West gridding 3-D Model II



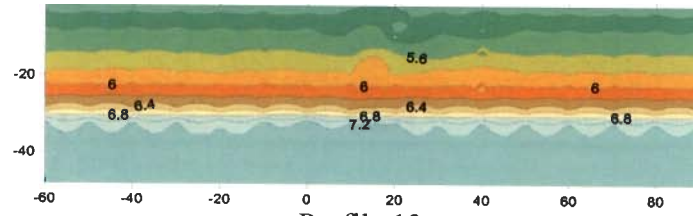
East-West gridding 3-D Model III



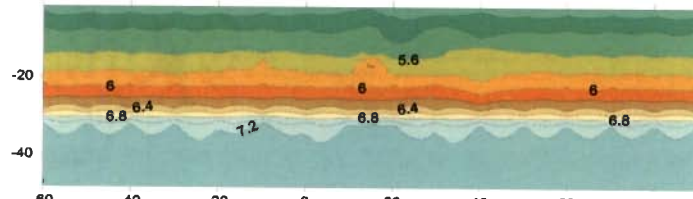
East-West gridding 3-D Model III



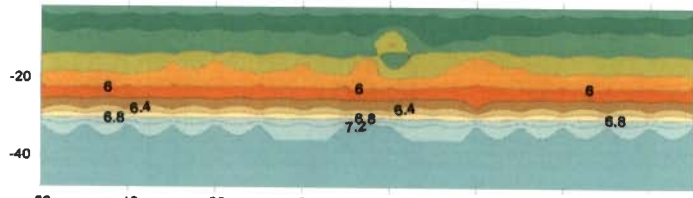
East-West gridding 3-D Model III



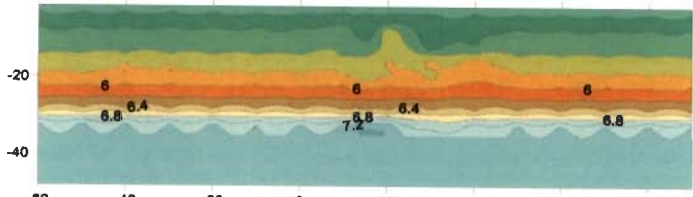
Profile 13



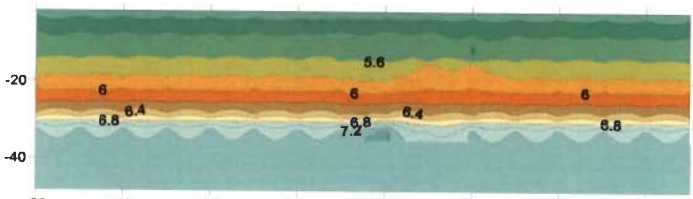
Profile 14



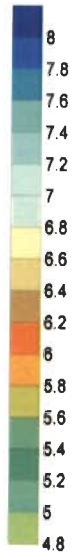
Profile 15



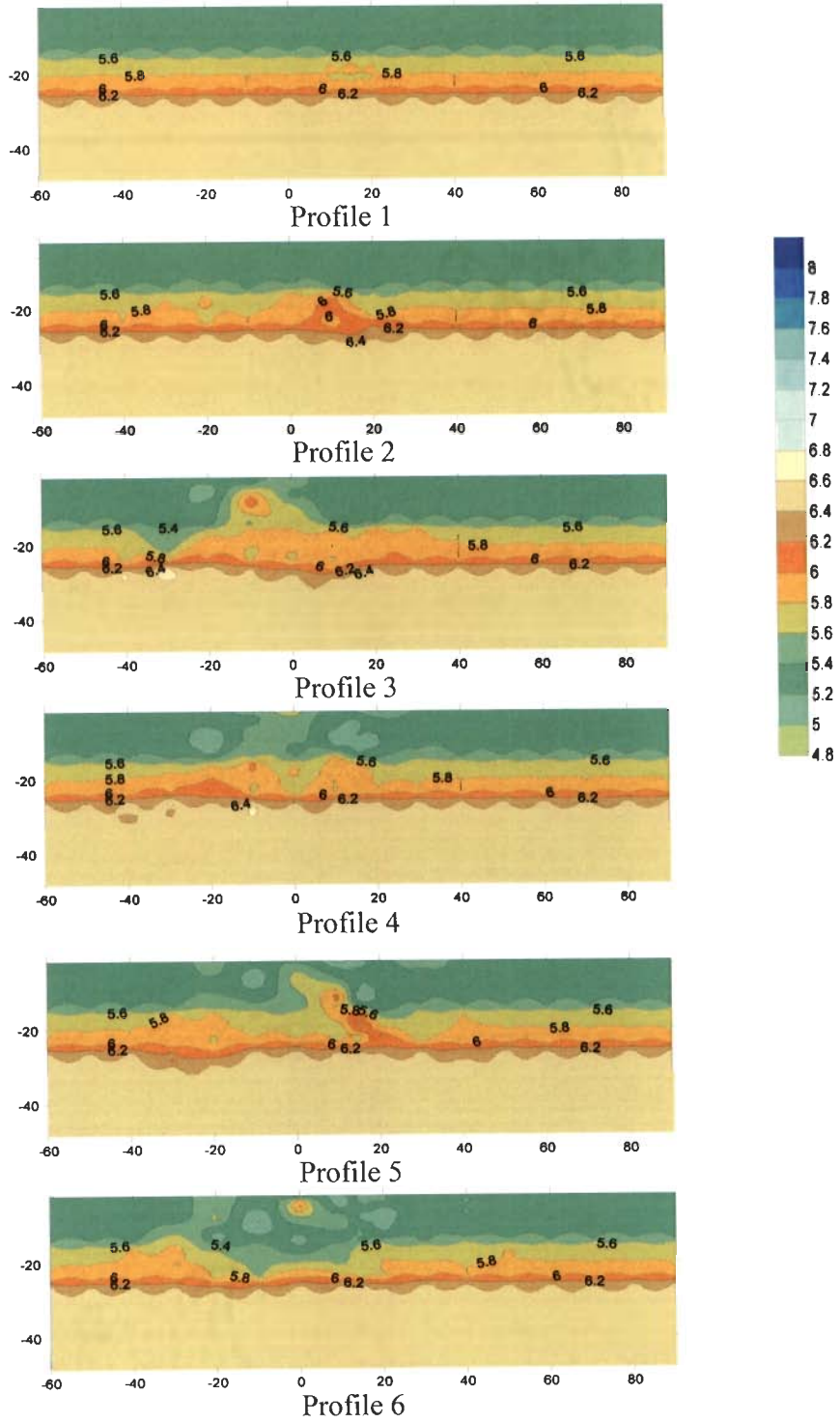
Profile 16



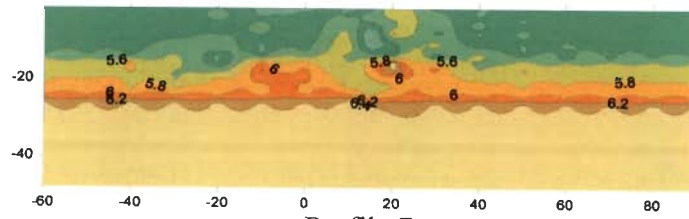
Profile 17



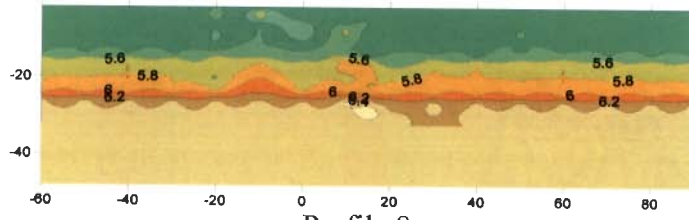
East-West gridding 3-D Model IV



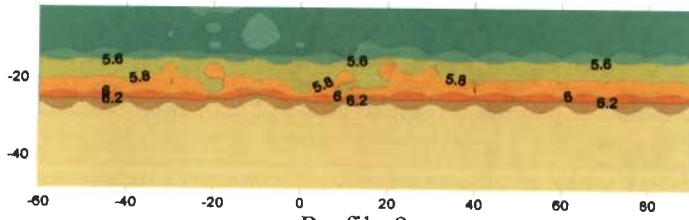
East-West gridding 3-D Model IV



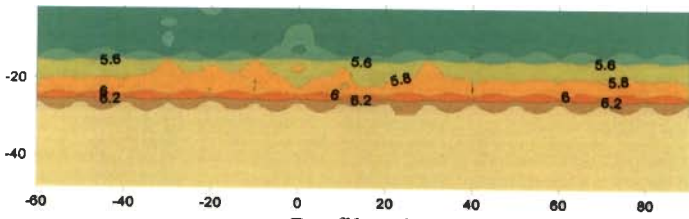
Profile 7



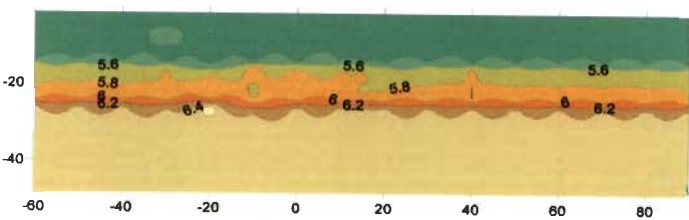
Profile 8



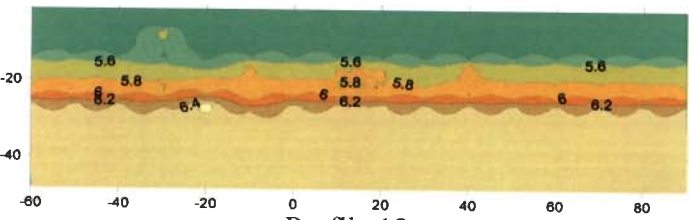
Profile 9



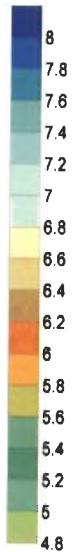
Profile 10



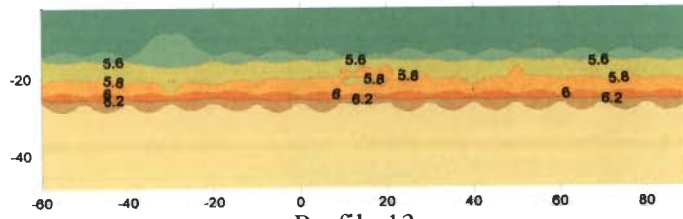
Profile 11



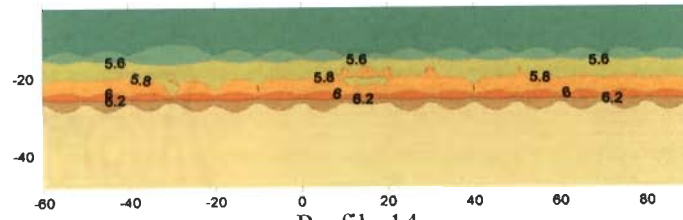
Profile 12



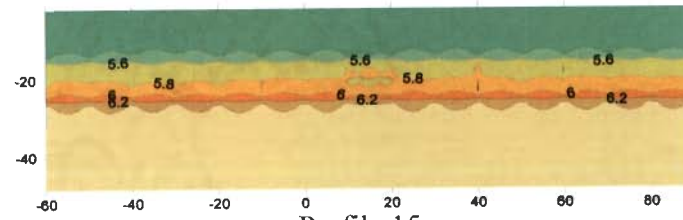
East-West gridding 3-D Model IV



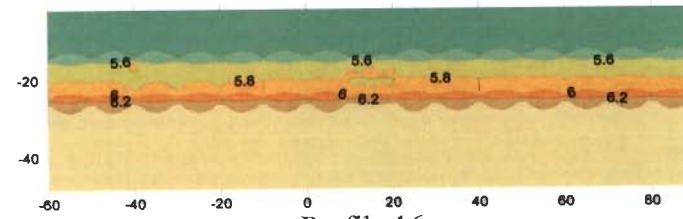
Profile 13



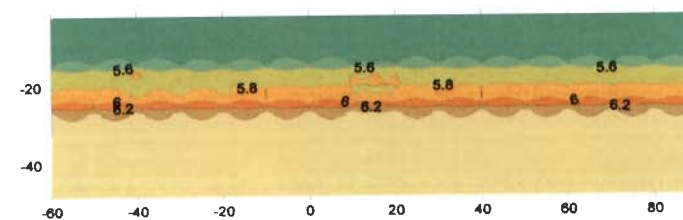
Profile 14



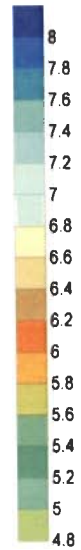
Profile 15



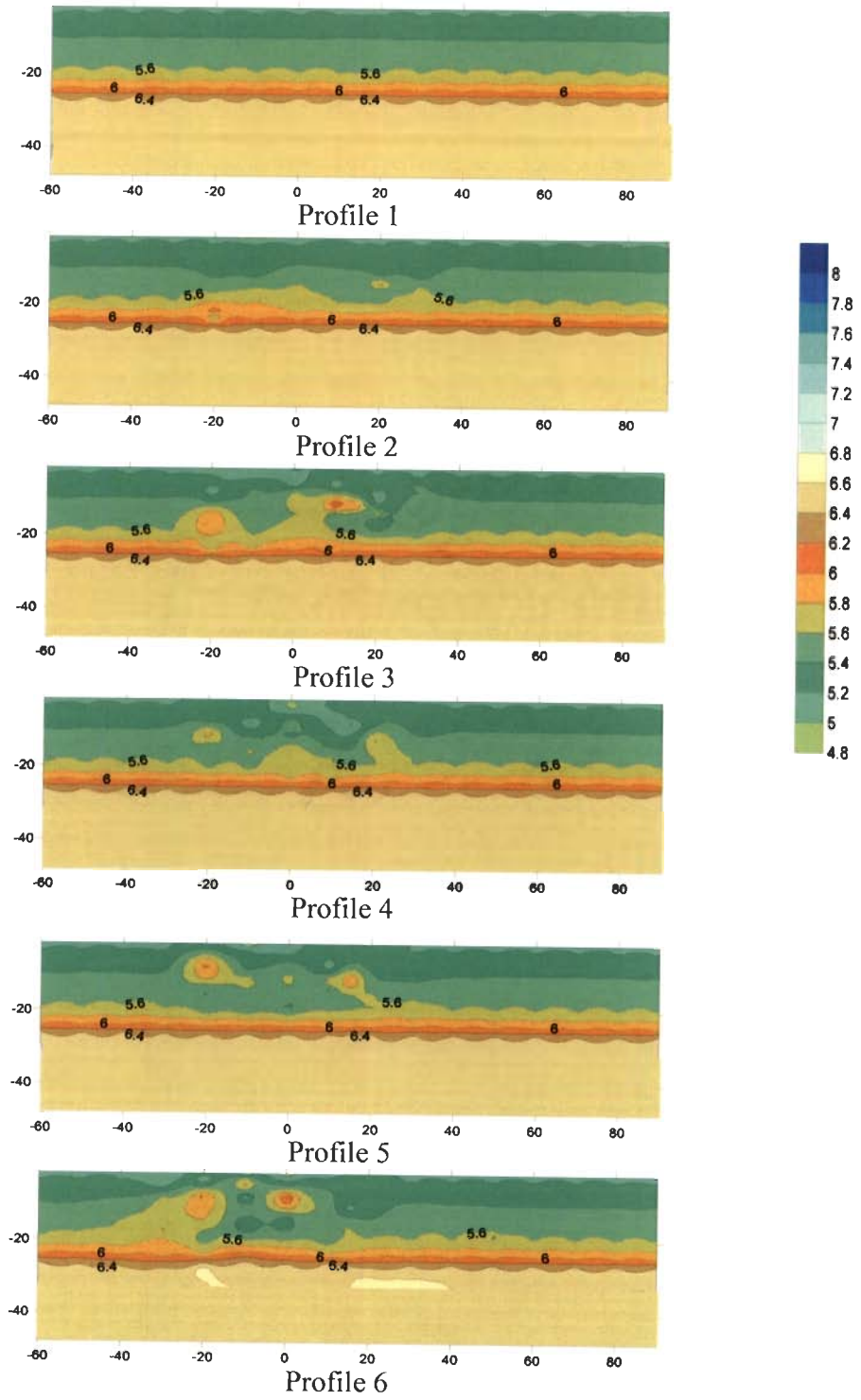
Profile 16



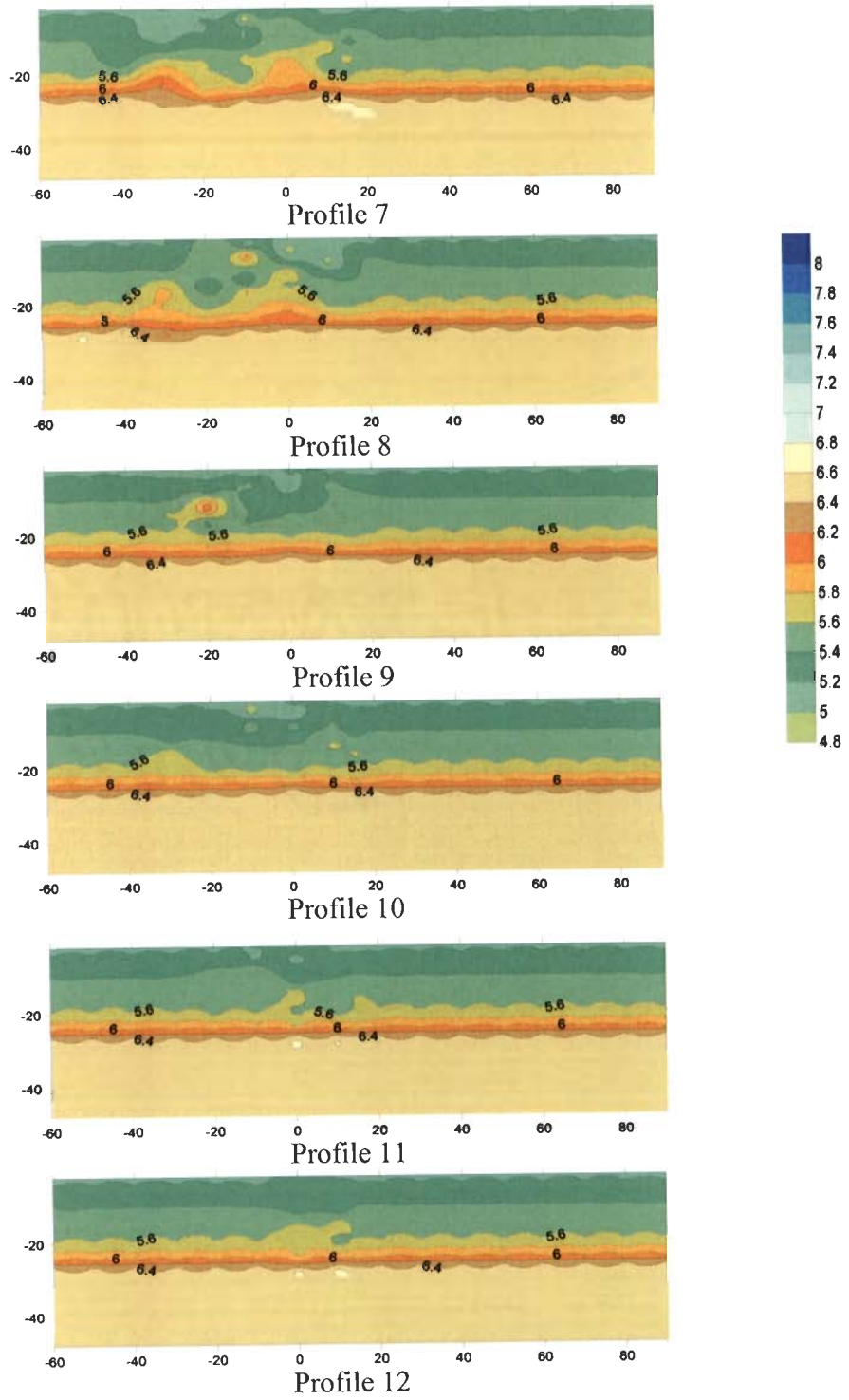
Profile 17



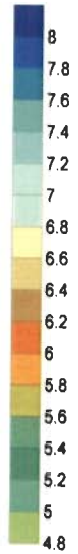
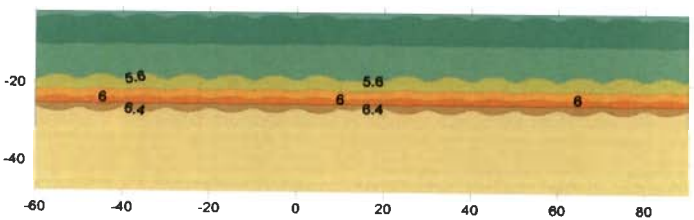
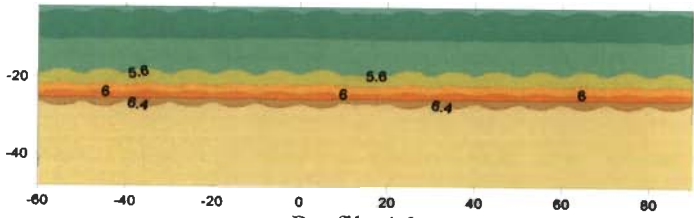
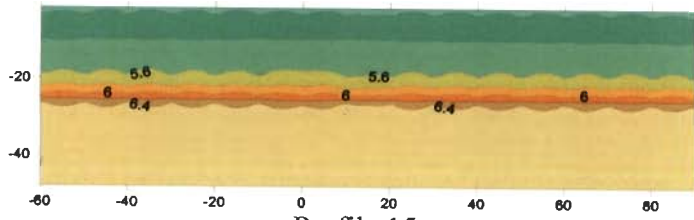
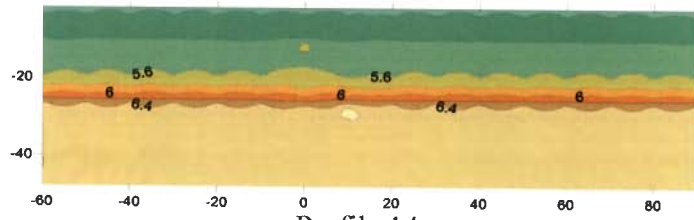
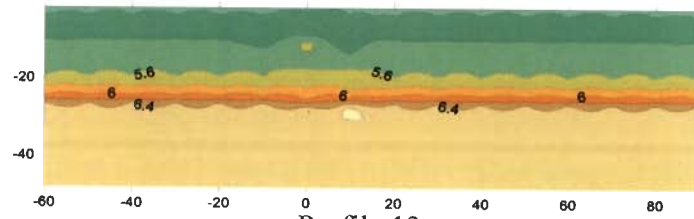
NE-SW gridding 3-D Model I



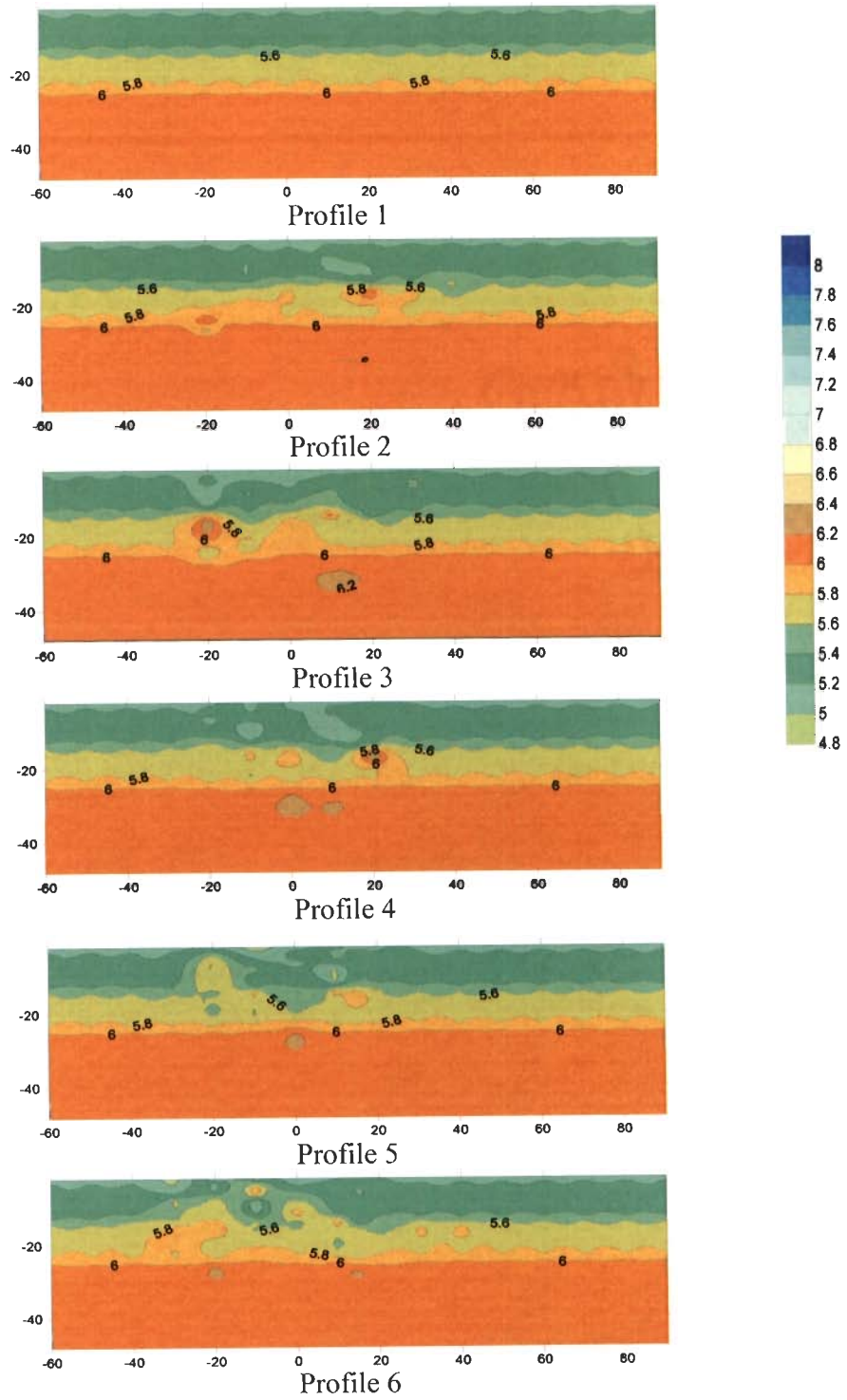
NE-SW gridding 3-D Model I



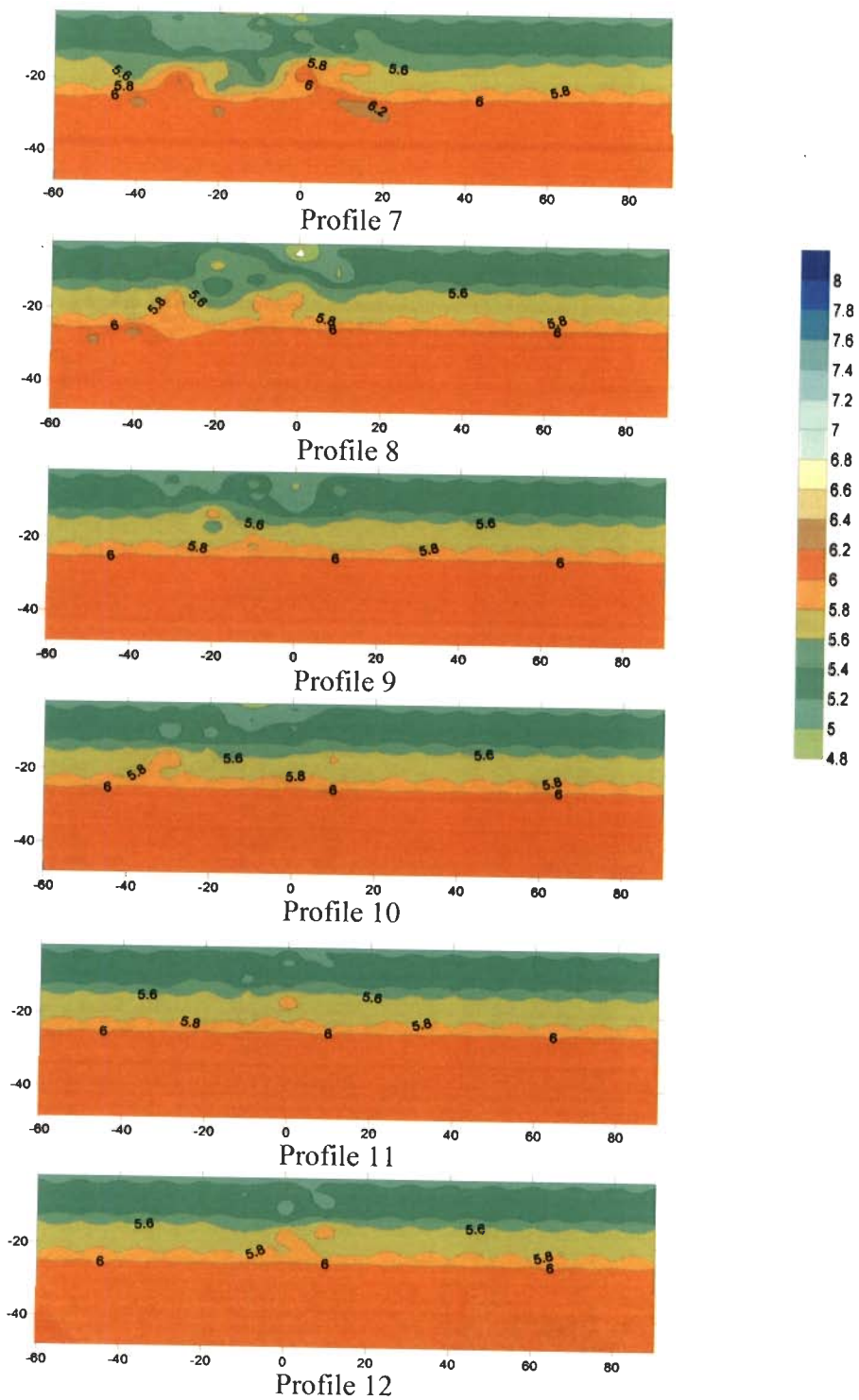
NE-SW gridding 3-D Model I



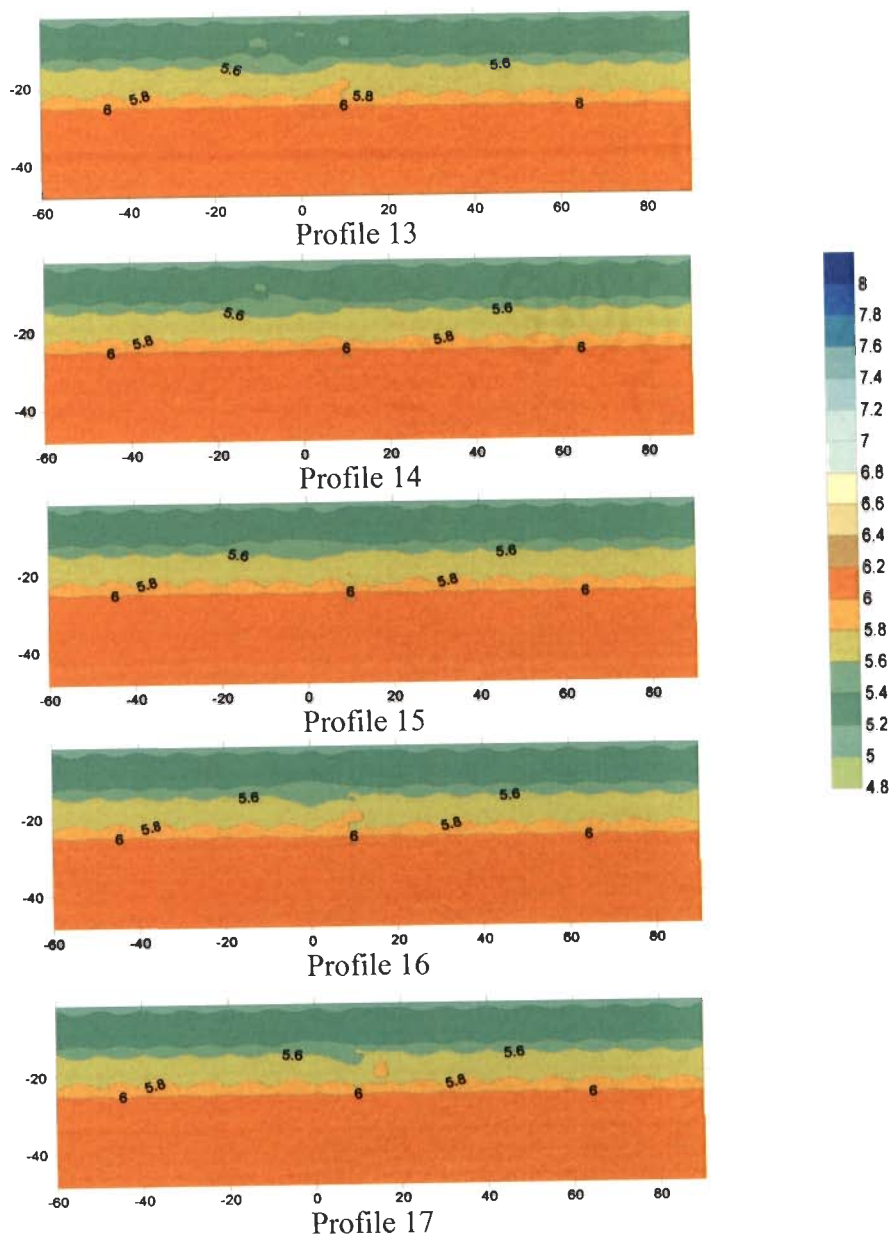
NE-SW gridding 3-D Model II



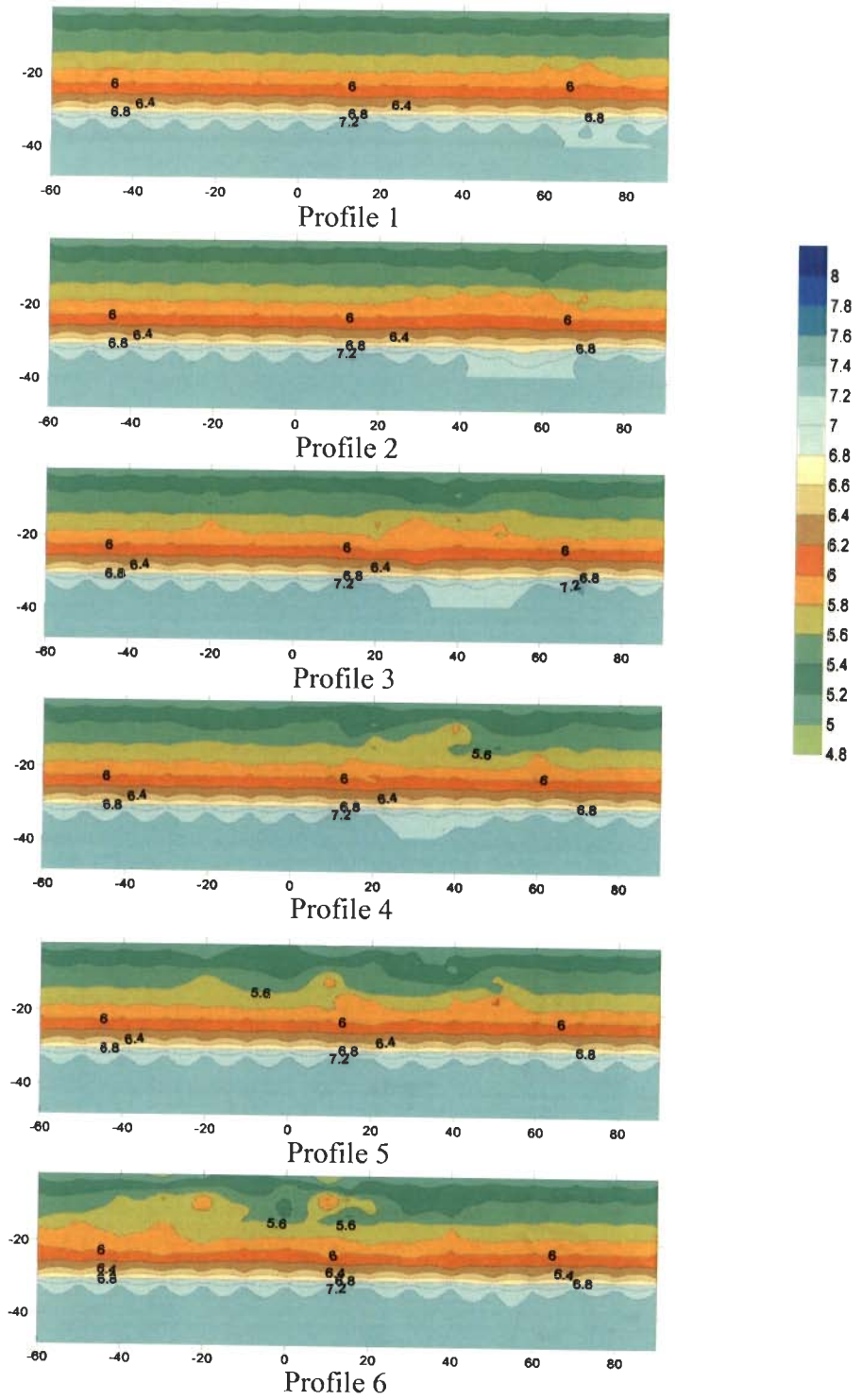
NE-SW gridding 3-D Model II



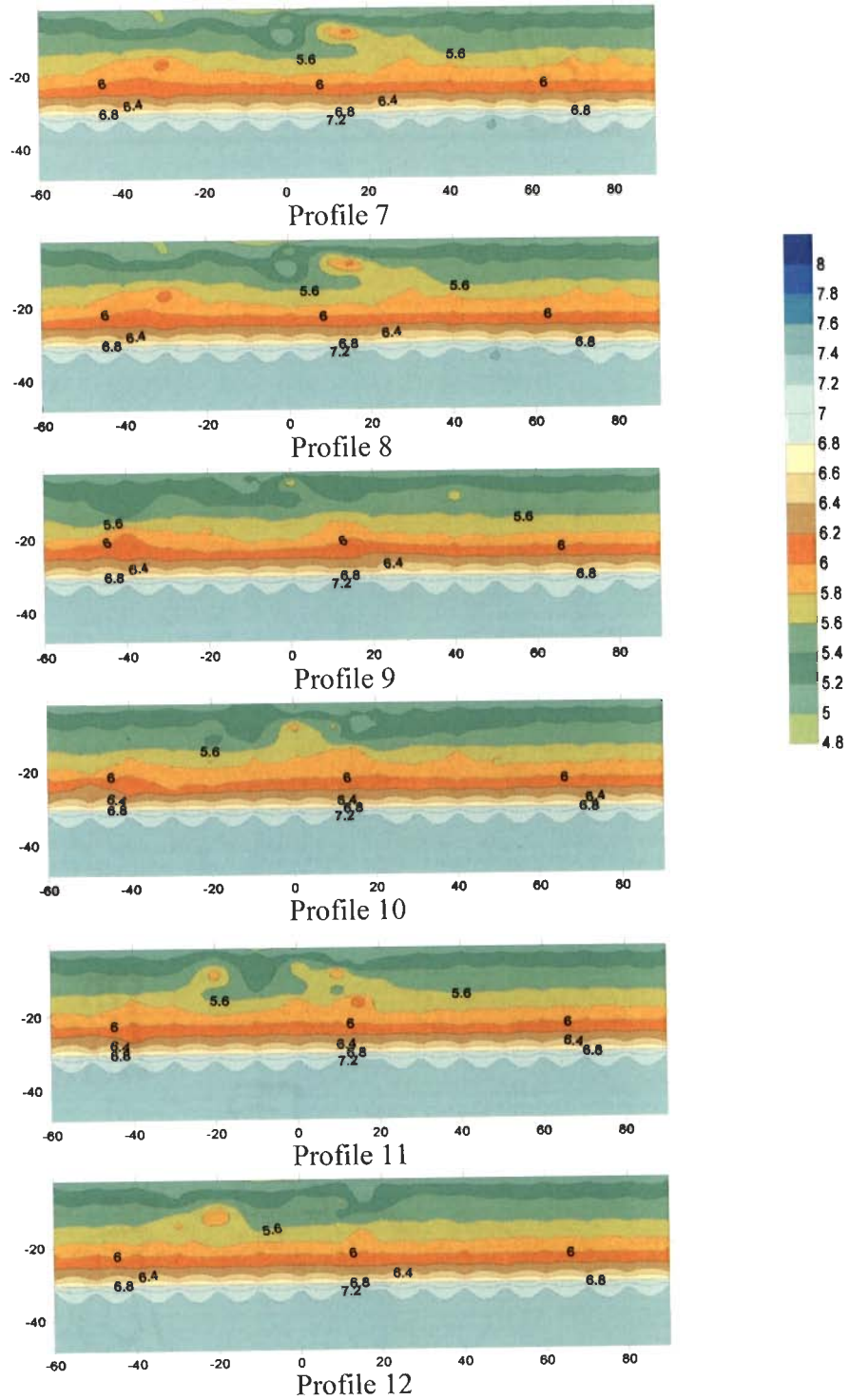
NE-SW gridding 3-D Model II



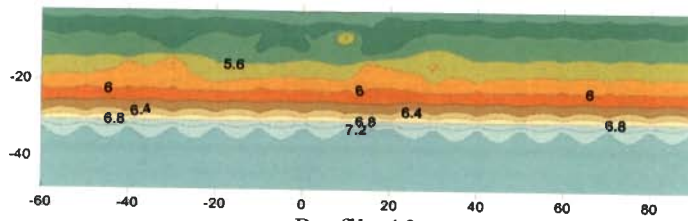
NE-SW gridding 3-D Model III



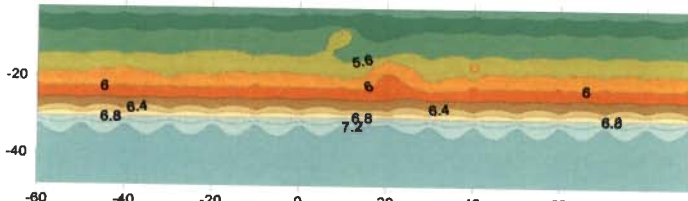
NE-SW gridding 3-D Model III



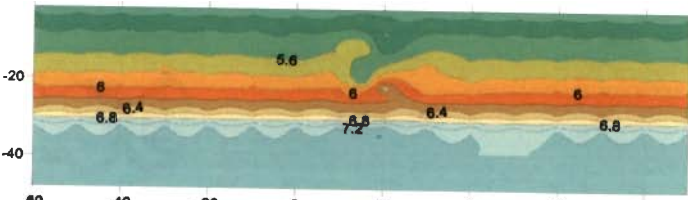
NE-SW gridding 3-D Model III



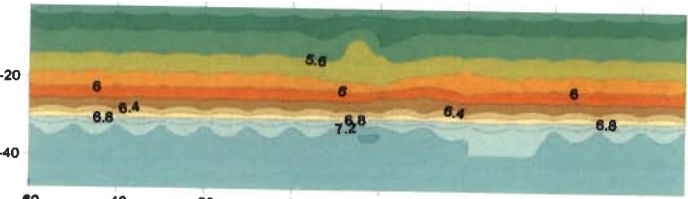
Profile 13



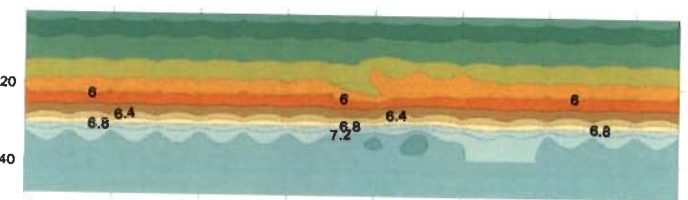
Profile 14



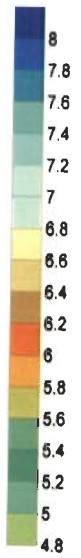
Profile 15



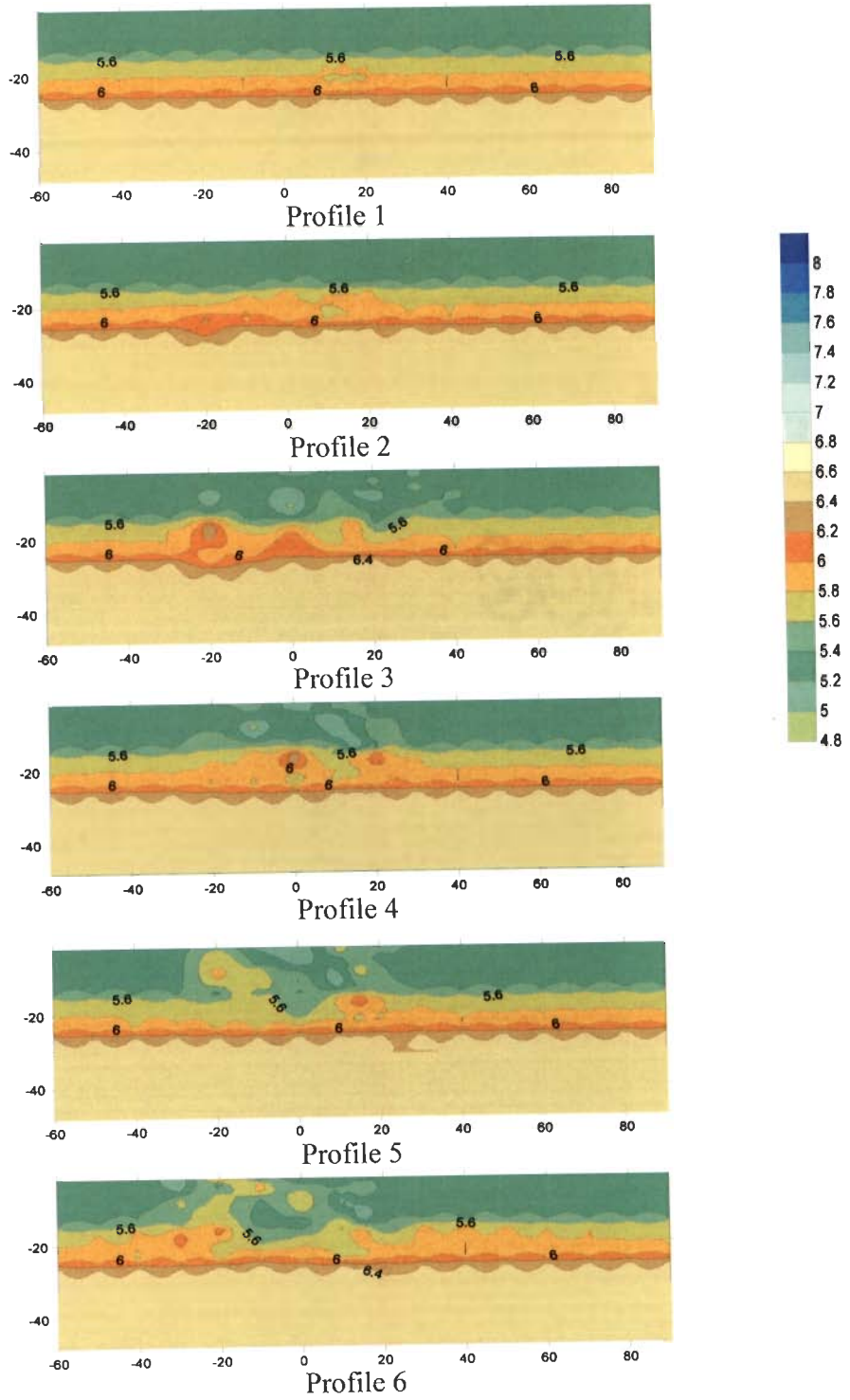
Profile 16



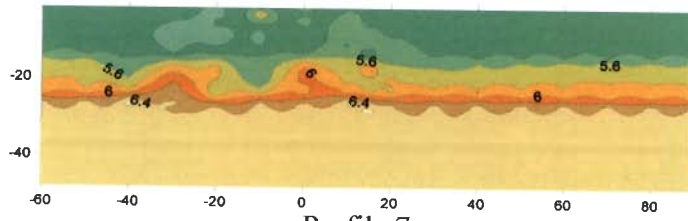
Profile 17



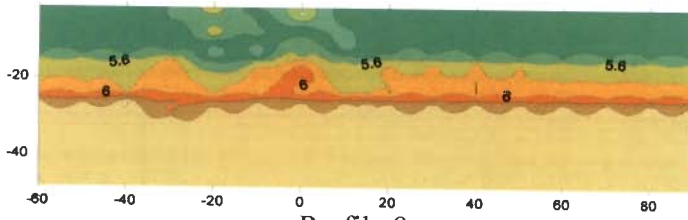
NE-SW gridding 3-D Model IV



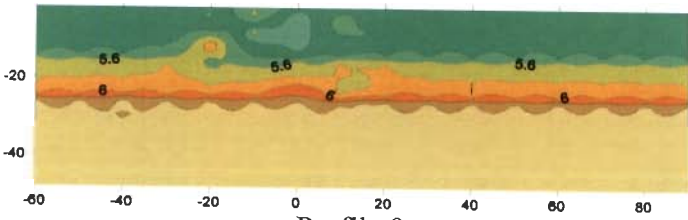
NE-SW gridding 3-D Model IV



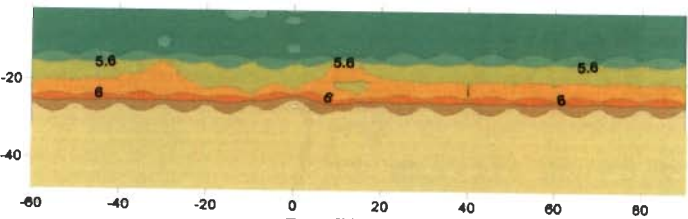
Profile 7



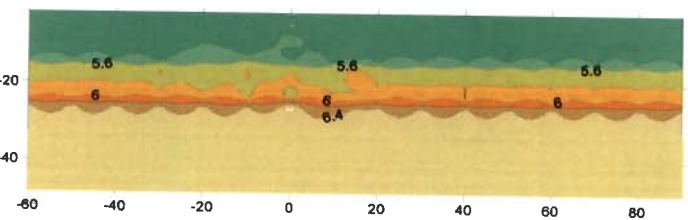
Profile 8



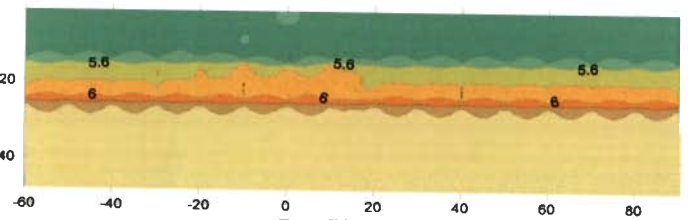
Profile 9



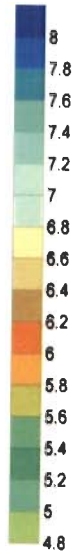
Profile 10



Profile 11



Profile 12



NE-SW gridding 3-D Model IV

